On the implementation of Hybridizable Discontinuous Galerkin discretization for linear anisotropic elastic wave equation: Voigt-notation and stabilization

Ha Pham, Florian Faucher, Hélène Barucq

On the implementation of Hybridizable Discontinuous Galerkin discretization for linear anisotropic elastic wave equation: Voigt-notation and stabilization

Ha Pham, Florian Faucher, and Hélène Barucq

RESEARCH REPORT
N° 9533
December 2023
Project-Team Makutu

ISSN 0249-6399 ISRN INRIA/RR--9533--ENG

On the implementation of Hybridizable Discontinuous Galerkin discretization for linear anisotropic elastic wave equation: Voigt-notation and stabilization

Ha Pham*, Florian Faucher*, and Hélène Barucq*

Project-Team Makutu

Research Report n° 9533 — December 2023 — 76 pages

Abstract:
This work is concerned with implementing the hybridizable discontinuous Galerkin (HDG) method to solve the linear anisotropic elastic equation in the frequency domain, focusing in particular on providing a compact description of the discrete problem and an optimal choice of stabilization in defining the HDG numerical traces. Voigt notation is employed in the description of the discrete problem in order to facilitate matrix operation and to provide efficient book-keeping of physical parameters. Additionally, a first-order formulation working with the compliance elasticity tensor is employed to allow for parameter variation within a mesh cell, for better representation of complex media. We determine an optimal choice of stabilization by constructing a hybridized Godunov-upwind flux for anisotropic elasticity possessing three distinct wavespeeds. This stabilization removes the need to choose judiciously scaling factors and can be used as a versatile choice for all materials. Its optimality is established by comparing with identity matrix-based stabilization in a wide range of values for the scaling factor. Numerical investigations are carried out in two and three dimensions, for isotropic elasticity and material with varying degree of anisotropy.

Key-words: Wave equations – anisotropic elasticity – time-harmonic waves – Hybridizable discontinuous Galerkin method – 3D wave propagation – Hybridized Godunov flux – Hybridized upwind flux – Stabilization – Voigt notation – Tilted transverse isotropy

* Project-Team Makutu, Inria, University of Pau and Pays de l'Adour, TotalEnergies, CNRS UMR 5142.

RESEARCH CENTRE
BORDEAUX – SUD-OUEST

200, avenue de la Vieille Tour
33405 Talence Cedex

Contents

1 Introduction

In this work, we implement Hybridizable Discontinuous Galerkin (HDG) method to solve the time-harmonic linear anisotropic elastic equation in two and three dimensions. This is carried out in the context of simulating wave propagation in the frequency domain for heterogeneous Earth subsurfaces ranging from local to global scale, and to be employed in full waveform inversion (FWI) algorithms. Such applications require discretization methods that can handle material heterogeneity and nonconforming meshes, while, at the same time, provide accurate and stable performance at tenable computational costs due to the large scale of the domain and high number of iterations employed in FWI. Finally, an ideal candidate also exploits efficiently advanced and parallel computing architecture. A method that can meet these requirements is the HDG method. The form employed in this work follows the original HDG method devised by Cockburn and co-authors [19, 21] for second-order elliptic equation, which was adapted and analyzed for Helmholtz equation in [39]. In implementing HDG method for elastic equation, the contributions of our work are centered around the following three main points.

1. Starting from a systematic formalism based on Voigt notation, our work writes the discretized problem in compact matrix form, which handles efficiently general anisotropy and facilitates numerical implementation.

2. A hybridized numerical flux for HDG method is constructed for anisotropy under the assumption of three distinct wave speeds, by extending the hybridization technique of upwind flux in [53].

3. In-depth numerical investigations are carried out to study the effect of stabilization operator in the definition of numerical trace for varying degrees of anisotropy. This is in terms of the form of the stabilization matrix-operator, that can be a multiple of the identity matrix or a symmetric matrix containing material parameters, or from hybridizing Godunov-upwind fluxes.

Before developing further discussion, we cite some description of HDG method and refer to [3, 21, 15, 52, 49, 34] and the recent survey [17] for more in-depth discussion. For a review of the implementation of HDG method for wave equation to fluid flow and continuum mechanics, in both time and frequency domain, we refer to [31] and [35, Section 2]. Other methods related to HDG are Weak Galerkin or Hybrid High Order, for elasticity, cf. [60] and [26, 18]. HDG method was initially introduced in [19, 21] to remedy a disadvantage in terms of computational cost of Discontinuous Galerkin (DG) approximations compared to standard Continuous Galerkin (CG) discretizations reinforced with static condensation. By relaxing continuity constraints of solution between mesh elements, DG family is able to capture 'physically relative' discontinuity without producing spurious oscillation[1], which forms one of the main advantages

[1] We refer to [23, 14] for an overview of the development of DG method since the seminal work of Reed and Hill in 1973 [48]. From its development in 1973 for the neural transport equation, a hyperbolic scalar equation, DG discretization was extended to time-dependent hyperbolic conservation law, computational fluid dynamics, and to elliptic equation. A unified treatment of DG methods for elliptic equation is given in [2], cf. in particular Table 3.1.

of DG methods compared to Finite Difference and Finite Volume ones, in addition to their flexibility to handle complicated geometries (CG method as well), adaptive strategies, and being highly parallelizable, [23]. However relaxing continuity constraints is obtained by doubling degrees of freedom at interior edges, which leads to high computational cost. While static condensation presents a strategy to reduce this cost, it is not applicable to all DG methods, in particular those containing coupling of interior nodes of an element with neighboring ones. As described in [15, 16], an HDG method is a DG method amenable to hybridization and thus static condensation.

In more recent literature, HDG method is directly defined as a two-staged process in which the original problem is written as a union of local boundary problems on each mesh cell whose boundary data are the hybrid variables, and the local problems are linked by transmission conditions which together with inversion of local problem results in a global problem in the hybrid variable defined on the skeleton of the mesh, [15]. HDG method retains the attractive features of the DG family, being locally conservative, flexible with h-p adaptivity strategy and thus unstructured nonconforming meshes, and highly parallelizable, e.g., [62, Section 4]. Additionally, HDG method allows for unified treatment of boundary condition and numerical flux [45], and is amenable to hybrid computing architecture, cf., e.g., [28]. In simple formulations using L^2-based approximation, which are non-conforming bases employing polynomial functions, HDG method provides optimal convergence which is also observed even when the primal variable and its gradient are approximated with polynomials of the same degree, see further discussion in Remark 10. In comparing with CG method, HDG method is also observed to be more stable for convection-dominated problems, cf. [31], while numerical results in [43, 52] for elastostatics show higher convergence rate for HDG using the same mesh and degree of approximation. For in-depth comparison of HDG with CG and other DG methods, we further refer to [41, 36, 62] and [46] in the context of incompressible fluid flow with high-order elements; see also [32] for sparsity comparison. In the context of seismology in frequency domain, for local or regional seismology, Finite Difference method can outperform Finite Element method; however it requires structured grids, which impedes taking into consideration strong background variation, topography (roughness of boundary) and implementation about boundary conditions, cf. [58, Section 4.2].

Works implementing HDG for elasticity are e.g., [7] for time-harmonic elasticity, [49] for static isotropic elasticity, [52, 33, 24, 27] for static elasticity allowing anisotropy, [53, 44, 31] in time-domain isotropic elasticity. In [49, 34], authors employ HDG-Voigt in their formulation, in addition to curved mesh feature in [34]. In [52, 33, 24], authors work with general form of the elastic equation thus allow for anisotropy, however their numerical investigation only consider isotropy. While [53] hybridizes the Godunov-upwind flux employed by [61] for DG method in time-domain problem, other works use multiple of identity stabilization, with the exception of [52, 33, 24] which propose stabilization in terms of the Kelvin–Christoffel matrix. In comparison to these references, our work contains the following new aspects (references are also discussed and compared in more details in Appendix C with respect to the choice of primal and mixed variables, and stabilization operators used to define the numerical traces).

1. While Voigt notations are also used with HDG method in [49], referred to as the HDG-Voigt method, we employ it in a more systematic way to provide a compact treatment of the discretized problem with anisotropic elasticity, and of the construction of hybridized Godunov-upwind flux. Our formalism, cf. Section 3, starts from the introduction of Voigt notation in [11], and offers a matrix-block alternative to the brute-force component-wise description which lists each component of the discretized problems. This latter approach can quickly become cumbersome not only in formal writing, but also renders code building daunting, especially for general anisotropy in 3D, cf. [7, Appendix B, Sections 5.4.1 and 5.4.2]. Voigt formalism offers better organization not only in writing but also in coding, bringing out block-structure pattern, which enables matrix operations and thus optimization of the direct solver. Additionally, good book-keeping of physical materials will be indispensable in the second stage which is inversion.

2. We extend to anisotropy the method employed by [53] to hybridize the upwind flux constructed in [61] for DG formulation in time domain. The main ingredients in hybridization are the exact solution of the Riemann problem and the fact that they satisfy the Rankine–Huguniot jump condition. The HDG numerical trace constructed in this way, despite having a more complicated form, arises

naturally in the sense that it is rigorously derived, rather than being simply proposed, as remarked in [8]. The ingredients for anisotropy case remain the same as in isotropy: exact solution of the Riemann problem and Rankine–Hugoniot jump conditions[2]. The name 'Godunov-upwind' is adopted from [8, 9, 10], in which hybridization was carried out following different approaches; however that employing Rankine–Hugoniot jump condition is recognized in sequel work [9, 10] (where the hybridized flux is also called 'Rankine–Hugoniot' flux) to be more natural and direct. Also employing notion of Riemann problem to devise HDG scheme are, e.g., [59, 43] and the references therein, in the context of compressible fluid flow (in [59], hybridization is carried out with Lax-Friedrichs, Roe and Harten-Lax-Van Leer approximate Riemann solver).

3. As mentioned above, most implementations with HDG method for elasticity employ multiple of identity stabilization ($\tau\mathbb{I}_d$, with $\mathbb{I}_d$ the identity matrix and τ a scalar coefficient) with the exception of [52, 33, 24] and [53] that use the Kelvin–Christoffel (KC) matrix and hybridizing Godunov-upwind flux, respectively. It is commented in [31] that for linear elasticity, the choice of the stabilization matrix-operator has slight effect on the accuracy of the approximation[3], allowing for a wide range of choices, and that the multiple of identity stability is as effective as more complicated ones. Regarding the effect of the scaling factor in multiple of identity stabilization, numerical investigation for Helmholtz equation has been carried out in [38] with τ in the complex plane, and for static isotropic elasticity in [49]. For static isotropic elasticity, numerical results in [52, 33] compare between multiple of identity stabilization and one with KC matrix. We note that for elastodynamics, even for isotropy, there are no numerical investigations comparing between multiple of identity stabilization and other more complicated forms. We extend the numerical investigation in these references to dynamic elasticity for both isotropy and anisotropy. We investigate whether the stabilization matrix-operator should contain the anisotropy of the material. Intuitively, multiple of identity stabilization performs well with the condition that the scaling factor τ is chosen appropriately in terms of sign and magnitude, while without additional choosing, the Godunov flux offers a reference optimal performance. We also extend the investigation in [38] to elasticity with scaling factor τ taking value in the complex plane.

4. Our formulation of the wave equations in linear elasticity is written in terms of the compliance tensor $\boldsymbol{S}$ instead of the usual stiffness tensor $\boldsymbol{C} = \boldsymbol{S}^{-1}$. This allows us to easily treat physical properties that vary within the cell avoiding having to derive these properties, see Subsection 6.3. Firstly, it allows us to treat highly varying properties while keeping large-cell discretization, hence keeping high-order polynomial discretization, which is critical for the efficiency of the HDG method compared to CG one, [28]. Secondly, it allows us to have a flexible representation of the physical properties on the discretized domain, which is a key-ingredient for inversion, [30].

The organization of this report is as follows. We first introduce the first-order formulation for the elastic equation and its HDG formulation in Section 2. In order to prepare for discretization and construction of the Godunov flux, we develop a formalism based on Voigt notation in Section 3. The discretized problem in matrix form is developed in Section 4. A summary of the stabilization investigated in this paper is given in Subsection 4.4 together with a detailed discussion of literature in Appendix C. In Section 5, the basic ingredients of the Riemann problem are given in Subsections 5.1 and 5.2, and the construction for anisotropy is carried out in Subsection 5.4. Finally, we carry out numerical experiments in Sections 6 and 7, respectively for isotropic and anisotropic media.

[2] These are also employed in [56, 55, 63] to construct upwind flux for DG implementation in time domain. Although constructed from the same ingredients, the DG numerical flux in [61, 56, 55, 63] depends on information both from left and right of the interface, while the hybridized HDG numerical fluxes in [53] and in our work are defined from one-sided data.

[3] It is beyond our scope to consider nonlinear-elasticity. However it is interesting to note the remark in [31, Section 4.2.4] that a complicate form of stabilization matrix containing information of the stiffness tensor is not suitable for nonlinear elasticity in time. They cite in specific the stabilization in [52], i.e., the Kelvin–Christoffel stabilization which was proposed for linear electrostatics. The question is whether this remark pertains to the hybridized Godunov form in [53], i.e, M_{Godunov} (4.63) derived for linear isotropic elasticity.

2 HDG Formulations for time-harmonic linear elasticity

As mentioned in the introduction, in order to reduce the computational cost due to the doubling of degrees of freedom at an interior edge in a DG method, HDG formulation employs two strategies: the *hybridization* of mixed method, and static condensation. Firstly, the original problem is written as a union of local boundary-valued problems defined for each mesh cell with boundary data a hybrid variable. Secondly, local problems are introduced and are linked by transmission conditions (or jump conditions) which constrain weakly the continuity of the solutions through numerical flux. With HDG method, the local problems are solved in mixed formulation with a pair of unknowns made up of the original unknown (also called primal), a mixed unknown (usually the derivatives of the primal), and the boundary data given by the hybrid variable for Dirichlet problem, that is, the trace of the primal unknown. The global problem is written only in terms of the hybrid variables defined only on the skeleton of the mesh, then the primal and mixed unknowns are found via the inversion of local problems which can be carried out in a parallel manner as they are independent on each element of the discretized domain.

Remark 1 (On hybrid, hybridization and mixed methods)**.** *We cite here some explanation from [21, 15] on the origins of the name of the HDG method. As explained in [21], the name 'hybrid' comes from p.421 in the book of Ciarlet (1978) [13] and designates any finite-element methods whose set of unknowns consist of a primal unknown, a mixed unknown (usually a derivative of the primal one) and the trace of the primal unknown, usually denoted by λ along the skeleton. This is also called Lagrange multiplier in the work [2] (1985) associated with the continuity of the mixed unknown, specifically jump of the flux. As explained in [15, Section 2.3] and [21, Section 1.2], hybridization is what allows a mixed method to undergo static condensation. Commonly, a mixed method corresponds to a first-order formulation, solving simultaneously for the primal/original unknown and a mixed unknown (usually a derivative of the primal one). For instance for the Poisson equation $\Delta w = f$, the unknowns are $(\mathbf{q} := \nabla w, w)$. In mixed methods, the left-hand side is written as a system* $\begin{pmatrix} A & B \\ B^t & 0 \end{pmatrix} \begin{pmatrix} \mathbf{q}_h \\ w_h \end{pmatrix}$*, where A is not block-diagonal due to the requirement of strong continuity of $\mathbf{q}_h$, therefore static condensation cannot be performed to eliminate $\mathbf{q}_h$. This problem is remedied by introducing an approximation of $\mathbf{q}$ which allows discontinuity from one element to another, and a hybrid unknown $\widehat{w}$ approximating the trace of w on the skeleton of the mesh. DG methods amenable to the hybridization approach in [21] are those whose globally coupled unknowns are the numerical trace, cf. [21, Section 1.3]. Additionally, as explained in the same reference, examples of DG methods that are not hybridizable are those presented in [3] with the exception of some local DG (LDG) methods, since they involve no dependency between the numerical trace and the mixed unknown. For original article on hybridization of mixed method, we further refer to [20].*

2.1 Notations

We list here the operations on tensors employed, working with the following objects,

- fourth-order tensor $\boldsymbol{S} = (S_{ijkl})_{i,j,k,l=1}^{3}$,
- matrix $\boldsymbol{\chi} = (\chi_{kl})_{k,l=1}^{3}$, and $\tilde{\boldsymbol{\chi}} = (\tilde{\chi}_{kl})_{k,l=1}^{3}$,
- vector $\mathbf{v} = (v_i)_{i=1}^{3}$, $\mathbf{w} = (w_i)_{i=1}^{3}$.

Tensor-valued functions whose components taking value in a function space $\mathcal{V}$ are written as,

$$\text{vector-valued} \quad \mathcal{V}^n\,, \qquad \text{matrix-valued} \quad \mathcal{V}^{n\times n}\,, \qquad \begin{matrix}\text{symmetric}\\ \text{matrix-valued}\end{matrix} \quad \mathcal{V}^{n\times n}_{\text{sym}}\,. \tag{2.1}$$

Tensor operations We have the standard dot product

$$\begin{matrix}\text{Vector dot}\\ \text{product}\end{matrix} \quad \mathbf{v}\cdot\mathbf{w} = \sum_{j=1}^{3} v_j w_j \tag{2.2a}$$

$$\begin{matrix}\text{fourth-order tensor}\\ \text{matrix product}\end{matrix} \quad (\boldsymbol{S}\boldsymbol{\chi})_{ij} = \sum_{k,l} S_{ijkl}\,\chi_{kl} \tag{2.2b}$$

$$\begin{matrix}\text{Matrix-vector}\\ \text{product}\end{matrix} \quad \boldsymbol{\chi}\mathbf{v} = \sum_{j=1}^{3} \chi_{ij}\,v_j \tag{2.2c}$$

$$\begin{matrix}\text{Matrix}\\ \text{contraction}\end{matrix} \quad \boldsymbol{\chi} : \tilde{\boldsymbol{\chi}} = \sum_{i,j=1}^{3} \chi_{ij}\,\tilde{\chi}_{ij}\,. \tag{2.2d}$$

The tensor product vector between two vectors $\mathbf{v}$ and $\mathbf{w}$ is written as $\mathbf{v} \otimes \mathbf{w}$ and defines a matrix whose components in Cartesian basis are

$$(\mathbf{v} \otimes \mathbf{w})_{ij} = v_i \, w_j \, . \tag{2.3}$$

Denote the bilinear form between two vectors $\mathbf{v}$, $\mathbf{w}$ with matrix $\boldsymbol{\chi}$ such as,

$$\mathbf{v} \cdot \boldsymbol{\chi} \cdot \mathbf{w} = \sum_{i,j=1}^{3} v_i \, \chi_{ij} \, w_j \, . \tag{2.4}$$

Differential operations Gradient of vector is given by matrix with rows indexed by i and columns by j,

$$(\nabla \mathbf{w})_{ij} = \partial_j w_i \tag{2.5}$$

We denote by $\nabla^{\mathfrak{s}}$ the symmetric gradient for a vector $\mathbf{w}$, with t denoting matrix transpose,

$$\nabla^{\mathfrak{s}} \mathbf{w} := \frac{\nabla \mathbf{w} + (\nabla \mathbf{w})^t}{2} \, . \tag{2.6}$$

The divergence of a matrix $\boldsymbol{\chi}$ is given by a vector whose components are given by,

$$(\nabla \cdot \boldsymbol{\chi})_i = \sum_{j=1}^{3} \partial_j \chi_{ij} \, . \tag{2.7}$$

2.2 First-order systems of wave equations in linear elasticity

We consider the propagation of time-harmonic waves in linear elasticity, given in terms of the displacement $\mathbf{u}$ or velocity $\mathbf{v}$ defined such that $\mathbf{v} := -\mathrm{i}\omega \, \mathbf{u}$. We therefore work with the following two variants (which are equivalent) of the elastic wave equation. Considering a domain Ω and an interior source $\mathbf{f}$, the wave equations are given by (e.g., [11]),

$$\text{Formulation } (\mathbf{u}, \boldsymbol{\sigma})_{\boldsymbol{S}} \quad \begin{cases} -\omega^2 \, \rho(\mathbf{x}) \, \mathbf{u}(\mathbf{x}, \omega) \, - \, \nabla \cdot \boldsymbol{\sigma}(\mathbf{x}, \omega) \, = \, \mathbf{f}(\mathbf{x}, \omega) \, , & \text{(2.8a)} \\ \boldsymbol{S}(\mathbf{x}) \boldsymbol{\sigma}(\mathbf{x}, \omega) = \nabla^{\mathfrak{s}} \mathbf{u}(\mathbf{x}, \omega) \, . & \text{(2.8b)} \end{cases}$$

$$\text{Formulation } (\mathbf{v}, \boldsymbol{\sigma})_{\boldsymbol{S}} \quad \begin{cases} -\mathrm{i}\omega \, \rho(\mathbf{x}) \, \mathbf{v}(\mathbf{x}, \omega) \, - \, \nabla \cdot \boldsymbol{\sigma}(\mathbf{x}, \omega) \, = \, \mathbf{f}(\mathbf{x}, \omega) \, , & \text{(2.9a)} \\ \mathrm{i}\omega \, \boldsymbol{S}(\mathbf{x}) \boldsymbol{\sigma}(\mathbf{x}, \omega) = -\nabla^{\mathfrak{s}} \mathbf{v}(\mathbf{x}, \omega) \, . & \text{(2.9b)} \end{cases}$$

Here, $\boldsymbol{\sigma}$ is the stress tensor, ρ is the density, $\boldsymbol{S}$ is the compliance tensor which is the inverse of the stiffness tensor $\boldsymbol{S} := \boldsymbol{C}^{-1}$.

Remark 2. *The two variants in (2.8) and (2.9) are analogous to those for the Helmholtz equation (acoustic wave) with a first or second-order in ω, cf., [39, 30] and [25] respectively. We note that only the variant $(\mathbf{u}, \boldsymbol{\sigma})_{\boldsymbol{S}}$ gives the formulation for elastostatics as $\omega \to 0$. Other formulations equivalent to (2.8) and (2.9) are also discussed in [42, Section 6], cf. continued discussion in Appendix C focusing on the form of stabilization operator. For instance, variants found in literature include,*

$$(\mathbf{u}, \boldsymbol{\sigma})_{\boldsymbol{C}} \begin{cases} -\omega^2 \, \rho \, \mathbf{u} \, - \, \nabla \cdot \boldsymbol{\sigma} \, = \, \mathbf{f} \, , & \text{(2.10a)} \\ \boldsymbol{\sigma} \, = \, \boldsymbol{C} \, (\nabla^{\mathfrak{s}} \mathbf{u}) \, , & \text{(2.10b)} \end{cases} \qquad (\mathbf{v}, \boldsymbol{\sigma})_{\boldsymbol{C}} \begin{cases} -\mathrm{i}\omega \, \rho \, \mathbf{v} \, - \, \nabla \cdot \boldsymbol{\sigma} \, = \, \mathbf{f} \, , & \text{(2.10c)} \\ \mathrm{i}\omega \, \boldsymbol{\sigma} \, = \, -\boldsymbol{C} (\nabla^{\mathfrak{s}} \mathbf{v}) \, , & \text{(2.10d)} \end{cases}$$

$$(\mathbf{u}, \boldsymbol{\epsilon})_{\boldsymbol{C}} \begin{cases} -\omega^2 \rho \, \mathbf{u} \, - \, \nabla \cdot (\boldsymbol{C} \boldsymbol{\epsilon}) \, = \, \mathbf{f} \, , & \text{(2.10e)} \\ \boldsymbol{\epsilon} = \nabla^{\mathfrak{s}} \mathbf{u} \, , & \text{(2.10f)} \end{cases} \qquad (\mathbf{v}, \boldsymbol{\epsilon})_{\boldsymbol{C}} \begin{cases} -\mathrm{i}\omega \rho \mathbf{v} \, - \, \nabla \cdot (\boldsymbol{C} \boldsymbol{\epsilon}) \, = \, \mathbf{f} \, , & \text{(2.10g)} \\ \mathrm{i}\omega \boldsymbol{\epsilon} \, = \, -\nabla^{\mathfrak{s}} \mathbf{v} \, . & \text{(2.10h)} \end{cases}$$

The strain tensor is $\boldsymbol{\epsilon} := \nabla^{\mathfrak{s}} \mathbf{u}$. Note that our choice of working with the compliance tensor $\boldsymbol{S}$ rather than the stiffness tensor $\boldsymbol{C}$ is motivated as it is more convenient to allow for physical properties that vary within each element of the discretized domain, see Subsection 6.3.

2.3 Discretization domain

To solve numerically the elastic wave problem, the domain Ω is discretized with an ordered set $\mathcal{T}_h$ (also referred to as the *mesh*) of non-overlapping elements K^e, $1 \le e \le |\mathcal{T}_h|$, providing a partition of Ω:

$$\mathcal{T}_h = \{K^e \big| 1 \le e \le |\mathcal{T}_h|\}\,, \qquad \Omega = \bigcup_{e=1}^{|\mathcal{T}_h|} K^e := \Omega_h\,. \tag{2.11}$$

For simplicity, we have assumed that the domain used for numerical computation Ω_h is exactly the original physical domain Ω. Notation e is the index of element K^e in the set $\mathcal{T}_h$, the size of which is $|\mathcal{T}_h|$. In our numerical implementation, we exclusively work with simplexes, thus K is a tetrahedron in 3D and a triangle in 2D.

The set of faces in the mesh $\mathcal{T}_h$ is denoted by Σ_h. It consists of the union of the faces F which also form the boundary of all element K in $\mathcal{T}_h$,

$$\Sigma_h = \bigcup_{e=1}^{|\mathcal{T}_h|} \partial K^e = \overline{\Omega_h} \setminus \bigcup_{e=1}^{|\mathcal{T}_h|} \overset{\circ}{K}{}^e = \{\mathsf{F}^k \big| 1 \le k \le |\Sigma_h|\}\,. \tag{2.12}$$

Here, for a domain K, we have written $\overset{\circ}{K}$ to denote its interior, that is,

$$\overset{\circ}{K} = \overline{K} \setminus \partial K\,. \tag{2.13}$$

Index k is the global index of the face F in Σ_h, each of which has also a local index with respect to the element K that contains it, cf. discussion in Subsection 4.1, in particular (4.1). We distinguish between the interior faces, also called *interfaces*, and boundary ones which forms the boundary of Ω_h,

$$\Sigma = \Sigma_{\text{int}} \cup \Sigma_\partial, \quad \Sigma_\partial = \partial\Omega_h = \Sigma_{\text{N}} \cup \Sigma_{\text{D}} \cup \Sigma_\infty\,. \tag{2.14}$$

Here, the boundary of the domain, Σ_∂ consists of non-overlapping regions where Neumann, Dirichlet, and Robin boundary conditions are imposed, respectively Σ_{N}, Σ_{D} and Σ_∞.

Jump operator For a scalar quantity f regular enough defined on the interior of domain K, to denote its zero-th order trace operator along ∂K, we write

$$f|_{\partial K} := \lim_{h \to 0^+} f(\mathbf{x} - h\boldsymbol{\nu})\,, \qquad \boldsymbol{\nu} \text{ the outward-pointing normal}\,. \tag{2.15}$$

Consider an interface F shared between elements K^+ and K^- i.e., $\mathsf{F} = \partial K^+ \cap \partial K^-$. Denote by $\boldsymbol{\nu}^\pm$ the outward-pointing normal vector defined on $\partial K^\pm$. At interface F, the jumps $[\![\,\cdot\,]\!]$ of a vector $\mathbf{v}$ and of the traction of a matrix $\boldsymbol{w}$ defined on $\overset{\circ}{K}{}^+ \cup \overset{\circ}{K}{}^-$ are respectively defined as

$$[\![\mathbf{v}]\!] := \mathbf{v}|_{K^+} - \mathbf{v}\big|_{K^-}\,, \qquad [\![\boldsymbol{w}\,\boldsymbol{\nu}]\!] := \boldsymbol{w}|_{K^+}\boldsymbol{\nu}^+ + \boldsymbol{w}|_{K^-}\boldsymbol{\nu}^-\,. \tag{2.16}$$

2.4 Statement of HDG problem for formulation $(\mathbf{v}, \boldsymbol{\sigma})_{\boldsymbol{S}}$

Strong form The HDG method comprises of local problems defined on each cell $K \in \mathcal{T}_h$, for formulation $(\mathbf{v}, \boldsymbol{\sigma})_{\boldsymbol{S}}$ of (2.9), we have

$$\begin{cases} \mathrm{i}\omega\,\rho\,\mathbf{v} - \nabla\cdot\boldsymbol{\sigma} = \mathbf{f}\,, & \text{on } K\,, & \text{(2.17a)} \\ \mathrm{i}\omega\,\mathbf{S}\boldsymbol{\sigma} = -\nabla^{\mathrm{s}}\mathbf{v}\,, & \text{on } K\,, & \text{(2.17b)} \\ \mathbf{v} = \boldsymbol{\lambda}_{\mathbf{v}}\,, & \text{on } \partial K\,. & \text{(2.17c)} \end{cases}$$

We note that the local problem is a boundary value problem with prescribed Dirichlet condition $\boldsymbol{\lambda}_{\mathbf{v}} \in L^2(\partial K)$. The trace $\boldsymbol{\lambda}_{\mathbf{v}}$ is determined by the conservativity condition[4],

$$[\![\boldsymbol{\sigma}\boldsymbol{\nu}]\!] = 0 \quad \text{on} \quad \mathsf{F} \in \Sigma_{\text{int}}. \tag{2.18}$$

[4]Originally, the continuity of the global solution is given by $[\![\mathbf{v}]\!] = 0$ and $[\![\boldsymbol{\sigma}\boldsymbol{\nu}]\!] = 0$ along Σ_{int}. The first one is satisfied automatically by Dirichlet condition (2.17c) which obliges $\mathbf{v}|_{K^+} = \mathbf{v}|_{K^-}$ on interface $\mathsf{F} \in \overline{K^+} \cap \overline{K^-}$. In another word, $[\![\mathbf{v}]\!] = 0$ for all $\mathsf{F} \in \Sigma_{\text{int}}$.

On the boundary of the domain Σ_∂, the three types of boundary conditions are as follow,

$$\begin{aligned} &\boldsymbol{\lambda}_{\mathbf{v}} = 0 && \text{on } \Sigma_{\mathrm{D}}\,, && \text{Dirichlet boundary,}\\ &\boldsymbol{\sigma\nu} = 0 && \text{on } \Sigma_{\mathrm{N}}\,, && \text{Neumann boundary,}\\ &\boldsymbol{\sigma\nu} = \mathcal{Z}\,\boldsymbol{\lambda}_{\mathbf{v}} && \text{on } \Sigma_{\infty}\,, && \text{Robin boundary.} \end{aligned} \tag{2.19}$$

The last condition represents a low order absorbing boundary condition with impedance-like matrix $\mathcal{Z}$.

Weak form To state the weak form, in addition to convention listed in (2.1), we also introduce the space:

$$\begin{aligned} \boldsymbol{\mathcal{H}}(K) := \Big\{\, A = \big(a_{ij}\big)_{i,j=1}^{3} \;|\; A = A^t, \quad \mathbf{a}_i \in L^2(K)^3 \;\text{ and }\; \nabla\cdot\mathbf{a}_i \in L^2(K)\,,\\ \text{where }\; \mathbf{a}_i := (a_{ij})_{j=1}^{3}\,, \quad i=1,2,3 \,\Big\}\,. \end{aligned} \tag{2.20}$$

On ∂K, given $\widehat{\mathbf{v}} = \boldsymbol{\lambda}_{\mathbf{v}}$ and a definition of $\widehat{\boldsymbol{\sigma\nu}}$ in terms of $\boldsymbol{\lambda}_{\mathbf{v}}$ and $(\mathbf{v},\boldsymbol{\sigma})|_{\overset{\circ}{K}}$, the weak form consists in finding $(\mathbf{v},\boldsymbol{\sigma},\boldsymbol{\lambda}_{\mathbf{v}})$ that solve

1. The local problems on each $K \in \mathcal{T}_h$: for all test-functions $(\boldsymbol{\phi},\Psi) \in H^1(K)^3 \times \boldsymbol{\mathcal{H}}(K)$,

$$\begin{cases} -\,\mathrm{i}\omega \displaystyle\int_K \rho\,\mathbf{v}\cdot\overline{\boldsymbol{\phi}}\,\mathrm{d}\mathbf{x} + \int_K \boldsymbol{\sigma} : \nabla\overline{\boldsymbol{\phi}}\,\mathrm{d}\mathbf{x} - \int_{\partial K} \overline{\boldsymbol{\phi}}\cdot\widehat{\boldsymbol{\sigma\nu}}\,\mathrm{d}s_{\mathbf{x}} = \int_K \mathbf{f}\cdot\overline{\boldsymbol{\phi}}\,\mathrm{d}\mathbf{x}\,, & \text{(2.21a)}\\ \mathrm{i}\omega \displaystyle\int_K \mathbf{S}\boldsymbol{\sigma} : \overline{\Psi}\,\mathrm{d}\mathbf{x} = \int_K \mathbf{v}\cdot\big(\nabla\cdot\overline{\Psi}\big)\,\mathrm{d}\mathbf{x} - \int_{\partial K} \boldsymbol{\nu}\cdot\overline{\Psi}\cdot\widehat{\mathbf{v}}\,\mathrm{d}s_{\mathbf{x}}\,; & \text{(2.21b)} \end{cases}$$

2. The global problem is given by conservativity condition on Σ_{int}: for $\boldsymbol{\xi} \in L^2(\Sigma_{\mathrm{int}})$,

$$\int_{\Sigma_{\mathrm{int}}} [\![\widehat{\boldsymbol{\sigma\nu}}]\!]\cdot\overline{\boldsymbol{\xi}}\,\mathrm{d}s_{\mathbf{x}} = 0\,, \tag{2.22}$$

and boundary conditions (2.19) write as,

$$\begin{cases} \boldsymbol{\lambda}_{\mathbf{v}} = 0 \text{ on } \Sigma_{\mathrm{D}}\,; \qquad \displaystyle\int_{\Sigma_{\mathrm{N}}} \widehat{\boldsymbol{\sigma\nu}}\cdot\overline{\boldsymbol{\xi}}\,\mathrm{d}s_{\mathbf{x}} = 0\,, \quad \forall\boldsymbol{\xi} \in L^2(\Sigma_{\mathrm{N}})\,;\\ \displaystyle\int_{\Sigma_\infty} (\mathrm{i}\omega\,\widehat{\boldsymbol{\sigma\nu}} - \mathcal{Z}\,\boldsymbol{\lambda}_{\mathbf{v}})\cdot\overline{\boldsymbol{\xi}}\,\mathrm{d}s_{\mathbf{x}} = 0\,, \quad \forall\boldsymbol{\xi} \in L^2(\Sigma_\infty)\,. \end{cases} \tag{2.23}$$

Finite element spaces Below we write $L^2(\Omega_h)^{3\times3}_{\mathrm{sym}}$ to denote the space of symmetric 3×3 matrices (thus $\boldsymbol{w} = (w_{IJ})_{I,J=x,y,z}$ with $w_{IJ} = w_{JI}$). Introduce the global finite element spaces

$$\begin{aligned} U_h &= \{\mathbf{u} = (u_I)_{I=x,y,z} \in L^2(\Omega_h)^3 \;\;:\;\; u_I|_K \in U_h(K),\ \forall K \in \mathcal{T}_h\}\,;\\ V_h &= \{\boldsymbol{v} = (v_{IJ})_{I,J=x,y,z} \in L^2(\Omega_h)^{3\times3}_{\mathrm{sym}} \;:\;\; v_{IJ}|_K \in V_h(K),\ \forall K \in \mathcal{T}_h\}\,;\\ M_h &= \{\boldsymbol{w} = (w_I)_{I=x,y,z} \in L^2(\Sigma_h)^3 \;\;:\;\; \mu_I|_{\mathsf{F}} \in M_h(\mathsf{F}),\ \forall \mathsf{F} \in \Sigma_h\}\,. \end{aligned} \tag{2.24}$$

The local function spaces $U_h(K)$, $V_h(K)$ and $M_h(\mathsf{F})$ are generally spaces of polynomials of finite degree on the corresponding domain. Denote $\mathcal{P}^{\mathsf{k}}(D)$ the space of polynomials of degree k defined on domain $D \subset \mathbb{R}^3$. As common choice[5] for elasticity using nonconformal spaces (L^2 space), same degrees are chosen for all three spaces, e.g., [52, 7, 31],

$$U_h(K) \;=\; V_h(K) \;=\; \mathcal{P}^{\mathsf{k}}(K)\,, \qquad M_h(\mathsf{F}) = \mathcal{P}^{\mathsf{k}}(\mathsf{F})\,. \tag{2.25}$$

[5] The local function spaces can also be allowed to have different degrees. In [47, p.2 and Table 1],

$$U_h(K) = \mathcal{P}^{\mathsf{k}+1}(K)\,, \quad V_h = \mathcal{P}^{\mathsf{k}}\,, \quad M_h(\mathsf{F}) = \mathcal{P}^{\mathsf{k}}(\mathsf{F})\,.$$

Numerical trace of traction The numerical trace of the traction is defined as

$$\widehat{\boldsymbol{\sigma}\boldsymbol{\nu}} = \boldsymbol{\sigma}_h \boldsymbol{\nu} - \boldsymbol{\tau}_{\mathbf{v}} (\mathbf{v}_h - \boldsymbol{\lambda}_{\mathbf{v}h}) . \tag{2.26}$$

In the current form, the stabilization operator $\boldsymbol{\tau}_{\mathbf{v}}$ is usually a symmetric definite positive matrix, a list of the variants considered in our work is further detailed in Subsection 4.4. We next substitute this into (2.21)–(2.23) to obtain the approximate problem below.

Approximate problem Find $(\mathbf{v}_h, \boldsymbol{\sigma}_h, \boldsymbol{\lambda}_{\mathbf{v}h}) \in U_h \times V_h \times M_h$ that solve,

1. **Local problems** on each element $K^e \in \mathcal{T}_h$, for all test functions $(\boldsymbol{\phi}, \Psi) \in U_h \times V_h$,

$$\begin{cases} -\mathrm{i}\omega \displaystyle\int_K \rho\, \mathbf{v}_h \cdot \overline{\boldsymbol{\phi}}\, \mathrm{d}\mathbf{x} - \int_K (\nabla \cdot \boldsymbol{\sigma}_h) \cdot \overline{\boldsymbol{\phi}}\, \mathrm{d}\mathbf{x} + \int_{\partial K} \overline{\boldsymbol{\phi}} \cdot \boldsymbol{\tau}_{\mathbf{v}} \cdot (\mathbf{v}_h - \boldsymbol{\lambda}_{\mathbf{v}h})\, \mathrm{d}s_{\mathbf{x}} = \displaystyle\int_K \mathbf{f} \cdot \overline{\boldsymbol{\phi}}\, \mathrm{d}\mathbf{x} , & \text{(2.27a)} \\ \mathrm{i}\omega \displaystyle\int_K \boldsymbol{\sigma}_h : \mathbf{S} : \overline{\Psi}\, \mathrm{d}\mathbf{x} = \int_K \mathbf{v}_h \cdot \big(\nabla \cdot \overline{\Psi}\big)\, \mathrm{d}\mathbf{x} - \displaystyle\int_{\partial K} \boldsymbol{\nu} \cdot \overline{\Psi} \cdot \boldsymbol{\lambda}_{\mathbf{v}h}\, \mathrm{d}s_{\mathbf{x}} , & \text{(2.27b)} \end{cases}$$

2. **Interface and boundary problems** Conservativity and Neumann conditions give,

$$\sum_{e=1}^{|\mathcal{T}_h|} \int_{\partial K^e \cap (\Sigma_{\mathrm{int}} \cup \Sigma_{\mathrm{N}})} \big(\overline{\boldsymbol{\xi}} \cdot \boldsymbol{\sigma}_h \cdot \boldsymbol{\nu} - \overline{\boldsymbol{\xi}} \cdot \boldsymbol{\tau}_{\mathbf{v}} \cdot (\boldsymbol{v}_h - \boldsymbol{\lambda}_{\mathbf{v}h}) \big)\, \mathrm{d}s_{\mathbf{x}} = 0 , \quad \forall \boldsymbol{\xi} \in \mathbf{M}_h(\Sigma_{\mathrm{int}} \cup \Sigma_{\mathrm{N}}) . \tag{2.28}$$

The Robin boundary condition (2.19) gives, $\forall \boldsymbol{\xi} \in \mathbf{M}_h(\Sigma_\infty)$,

$$\sum_{e=1}^{|\mathcal{T}_h|} \int_{\partial K^e \cap \Sigma_\infty} \big(\overline{\boldsymbol{\xi}} \cdot \boldsymbol{\sigma}_h \cdot \boldsymbol{\nu} - \overline{\boldsymbol{\xi}} \cdot \boldsymbol{\tau}_{\mathbf{v}} \cdot (\boldsymbol{v}_h - \boldsymbol{\lambda}_{\mathbf{v}h}) - \overline{\boldsymbol{\xi}} \cdot \mathcal{Z} \cdot \boldsymbol{\lambda}_{\mathbf{v}h} \big)\, \mathrm{d}s_{\mathbf{x}} = 0 , \tag{2.29}$$

The Dirichlet condition is imposed strongly such that,

$$\boldsymbol{\lambda}_{\mathbf{v}h} = 0 , \quad \text{on} \quad \Sigma_{\mathrm{D}} . \tag{2.30}$$

2.5 Statement of HDG problem for formulation $(\mathbf{u}, \boldsymbol{\sigma})_{\boldsymbol{S}}$

The HDG problem associated with formulation $(\mathbf{u}, \boldsymbol{\sigma})_{\boldsymbol{S}}$ follows the same step as above. The strong form associated with (2.8) is

$$\begin{cases} -\omega^2 \rho\, \mathbf{u} - \nabla \cdot \boldsymbol{\sigma} = \mathbf{f} , & \text{on } K , & \text{(2.31a)} \\ \mathbf{S}\boldsymbol{\sigma} = \nabla^{\mathrm{s}} \mathbf{u} , & \text{on } K , & \text{(2.31b)} \\ \mathbf{u} = \boldsymbol{\lambda}_{\mathbf{u}} , & \text{on } \partial K . & \text{(2.31c)} \end{cases}$$

We now use $\widehat{\mathbf{u}} = \boldsymbol{\lambda}_{\mathbf{u}}$ on ∂K, and a definition of $\widehat{\boldsymbol{\sigma}}$ in terms of $\boldsymbol{\lambda}_{\mathbf{u}}$ and $(\mathbf{u}, \boldsymbol{\sigma})|_{\overset{\circ}{K}}$. The weak form is to find $(\mathbf{u}, \boldsymbol{\sigma}, \boldsymbol{\lambda}_{\mathbf{u}})$ that solve

1. The local problems on each $K \in \mathcal{T}_h$, for all $(\boldsymbol{\phi}, \Psi) \in H^1(K)^3 \times H^1(K)^6$, are,

$$\begin{cases} -\omega^2 \displaystyle\int_K \rho\, \mathbf{u} \cdot \overline{\boldsymbol{\phi}}\, \mathrm{d}\mathbf{x} + \int_K \boldsymbol{\sigma} : \nabla \overline{\boldsymbol{\phi}}\, \mathrm{d}\mathbf{x} - \displaystyle\int_{\partial K} \overline{\boldsymbol{\phi}} \cdot \widehat{\boldsymbol{\sigma}} \cdot \boldsymbol{\nu}\, \mathrm{d}s_{\mathbf{x}} = \int_K \mathbf{f} \cdot \overline{\boldsymbol{\phi}}\, \mathrm{d}\mathbf{x} , & \text{(2.32a)} \\ \displaystyle\int_K \boldsymbol{\sigma} : \mathbf{S} : \overline{\Psi}\, \mathrm{d}\mathbf{x} = - \int_K \mathbf{u} \cdot \big[\nabla \cdot \overline{\Psi}\big]\, \mathrm{d}\mathbf{x} + \int_{\partial K} \boldsymbol{\nu} \cdot \overline{\Psi} \cdot \widehat{\mathbf{u}}\, \mathrm{d}s_{\mathbf{x}} . & \text{(2.32b)} \end{cases}$$

2. The global problem is given by conservativity condition on Σ_{int}: for $\boldsymbol{\xi} \in L^2(\Sigma_{\mathrm{int}})$,

$$\int_{\Sigma_{\mathrm{int}}} [\![\widehat{\boldsymbol{\sigma}} \boldsymbol{\nu}]\!] \cdot \overline{\boldsymbol{\xi}}\, \mathrm{d}s_{\mathbf{x}} = 0 \tag{2.33}$$

and boundary conditions (2.19),

$$\begin{cases} \boldsymbol{\lambda}_{\mathbf{u}} = 0 \text{ on } \Sigma_{\mathrm{D}}\,; & \displaystyle\int_{\Sigma_{\mathrm{N}}} \widehat{\boldsymbol{\sigma\nu}} \cdot \overline{\boldsymbol{\xi}}\, \mathrm{d}s_{\mathbf{x}} = 0\,, \quad \forall \boldsymbol{\xi} \in L^2(\Sigma_{\mathrm{N}})\,, \\ \displaystyle\int_{\Sigma_\infty} (\widehat{\boldsymbol{\sigma\nu}} - \mathcal{Z}\,\boldsymbol{\lambda}_{\mathbf{u}}) \cdot \overline{\boldsymbol{\xi}}\, \mathrm{d}s_{\mathbf{x}} = 0\,, \quad \forall \boldsymbol{\xi} \in L^2(\Sigma_\infty)\,. \end{cases} \tag{2.34}$$

The numerical trace of the traction is now defined (with a list of variants for $\boldsymbol{\tau}_{\mathbf{u}}$ given in Subsection 4.4)

$$\widehat{\boldsymbol{\sigma\nu}} \;=\; \boldsymbol{\sigma}_h\boldsymbol{\nu} - \boldsymbol{\tau}_{\mathbf{u}}(\mathbf{u}_h - \boldsymbol{\lambda}_{\mathbf{u}h})\,. \tag{2.35}$$

Substitute this into (2.32)–(2.34) to obtain the approximate HDG problem:

Approximate problem Find $(\mathbf{u}_h, \boldsymbol{\sigma}_h, \boldsymbol{\lambda}_{\mathbf{u}h}) \in U_h \times V_h \times M_h$ that solve,

1. **Local problems** on element $K^e \in \mathcal{T}_h$, for all test functions $(\boldsymbol{\phi}, \Psi) \in U_h \times V_h$,

$$\begin{cases} -\omega^2 \displaystyle\int_K \rho \mathbf{u}_h \cdot \overline{\boldsymbol{\phi}}\, \mathrm{d}\mathbf{x} - \int_K (\nabla \cdot \boldsymbol{\sigma}_h) \cdot \overline{\boldsymbol{\phi}}\, \mathrm{d}\mathbf{x} + \int_{\partial K} \overline{\boldsymbol{\phi}} \cdot \boldsymbol{\tau}_{\mathbf{u}}(\mathbf{u}_h - \boldsymbol{\lambda}_{\mathbf{u}h})\, \mathrm{d}s_{\mathbf{x}} = \int_K \mathbf{f} \cdot \overline{\boldsymbol{\phi}}\, \mathrm{d}\mathbf{x}, & \text{(2.36a)} \\ \displaystyle\int_K \boldsymbol{\sigma}_h : \mathbf{S} : \overline{\Psi}\, \mathrm{d}\mathbf{x} = -\int_K \mathbf{u}_h \cdot \nabla \cdot \overline{\Psi} \mathrm{d}\mathbf{x} + \int_{\partial K} \boldsymbol{\nu} \cdot \overline{\Psi} \cdot \boldsymbol{\lambda}_h\, \mathrm{d}s_{\mathbf{x}}\,. & \text{(2.36b)} \end{cases}$$

2. **Interface and boundary problems** Conservativity and Neumann conditions give,

$$\sum_{e=1}^{|\mathcal{T}_h|} \int_{\partial K^e \cap (\Sigma_{\mathrm{int}} \cup \Sigma_{\mathrm{N}})} \left(\boldsymbol{\nu} \cdot \boldsymbol{\sigma}_h \cdot \overline{\boldsymbol{\xi}} - \overline{\boldsymbol{\xi}} \cdot \boldsymbol{\tau}_{\mathbf{u}} \cdot (\mathbf{u}_h - \boldsymbol{\lambda}_{\mathbf{u}h})\right) \mathrm{d}s_{\mathbf{x}} \;=\; 0\,, \quad \forall \boldsymbol{\xi} \in \mathbf{M}_h(\Sigma_{\mathrm{int}} \cup \Sigma_{\mathrm{N}})\,. \tag{2.37}$$

The Robin boundary conditions (2.19) give, $\forall \boldsymbol{\xi} \in \mathbf{M}_h(\Sigma_\infty)$,

$$\sum_{e=1}^{|\mathcal{T}_h|} \int_{\partial K^e \cap \Sigma_\infty} \left(\boldsymbol{\nu} \cdot \boldsymbol{\sigma}_h \cdot \overline{\boldsymbol{\xi}} \;-\; \overline{\boldsymbol{\xi}} \cdot \boldsymbol{\tau}_{\mathbf{u}} \cdot (\mathbf{u}_h - \boldsymbol{\lambda}_{\mathbf{u}h}) \;-\; \overline{\boldsymbol{\xi}} \cdot \mathcal{Z} \cdot \boldsymbol{\lambda}_{\mathbf{u}h}\right) \mathrm{d}s_{\mathbf{x}} \;=\; 0\,. \tag{2.38}$$

The Dirichlet condition is imposed strongly,

$$\boldsymbol{\lambda}_{\mathbf{u}h} \;=\; 0\,, \quad \text{on } \Sigma_{\mathrm{D}}\,. \tag{2.39}$$

3 Voigt notations

Streamlined and compact writing of the discretized problem is useful for clear writing but also indispensable in view of building direct solver that can maximize efficient matrix operations and block storage. The Voigt notation (e.g., [11]), is employed to represent not only the tensors, but also operations on them including differential operators in Subsections 3.2 and 3.3. One obtains explicit expression for the Kelvin–Christoffel matrix Subsection 3.4.2 for general anisotropy which is an important object characterizing anisotropy in terms of wavespeeds. The notations and results of this section, in particular Subsection 3.4, will be used for the discretization in Section 4 and to derive the hybridized Godunov-upwind flux in Section 5.

3.1 Definitions

We denote by $\mathbf{e}_I$ with $I = x, y, z$ the unit vectors in Cartesian basis in three dimensions. A vector $\mathbf{u}$ in $\mathbb{C}^3$ is written as

$$\mathbf{u} = u_x\mathbf{e}_x + u_y\mathbf{e}_y + u_z\mathbf{e}_z\,. \tag{3.1}$$

We denote by $\mathcal{S}_2$ the set of symmetric matrices and $\mathcal{S}_4$ the set of fourth order tensors which have the same symmetry as the stiffness tensor $\boldsymbol{C}$:

$$\begin{aligned} \mathcal{S}_2 &:= \{\boldsymbol{w} = (w_{ij})_{i,j=x,y,z} \in \mathbb{C}^{3\times 3} \,\big|\, w_{ij} = w_{ji}\}\,, \\ \mathcal{S}_4 &:= \left\{\mathbf{T} = (t_{ijkl})_{i,j,k,l=x,y,z} \in \mathbb{C}^{3\times3\times3\times3} \,\big|\, t_{ijkl} = t_{jikl} = t_{ijlk} = t_{klij}\right\}\,. \end{aligned} \tag{3.2}$$

Index sets of symmetric matrices and tensors Denote by $\mathcal{I}_{\rm sm}$ the *ordered* set consisting of diagonal and upper-diagonal indices of a symmetric matrix. These are identified with diagonal and lower-diagonal indices, referred to as $1,\dots,6$,

$$\begin{aligned}\mathcal{I}_{\rm sm} &:= (\text{ 'xx' }, \text{ 'yy'}, \text{ 'zz'}, \text{ 'yz'}, \text{ 'xz'}, \text{ 'xy'}) \\ &= (\text{ 'xx' }, \text{ 'yy'}, \text{ 'zz'}, \text{ 'zy'}, \text{ 'zx'}, \text{ 'yx'})\end{aligned} \quad \begin{matrix}\text{identified}\\ \leftrightarrow \\ \text{with}\end{matrix} \quad (1,\dots,6)\,. \tag{3.3}$$

We further define the constant arrays $\mathfrak{c}_{\mathfrak{J}}$, $\mathfrak{J} \in \mathcal{I}_{\rm sm}$ and diagonal matrix $D^\dagger$ such that,

$$\mathfrak{c}_{\mathfrak{J}} = \begin{cases} 1\,, & \text{for } \mathfrak{J} = \text{'xx','yy','zz'} \\ 2\,, & \text{for } \mathfrak{J} = \text{ 'yz', 'xz', 'xy'} \end{cases}, \quad D^\dagger := \begin{pmatrix} \mathbb{Id}_{3\times 3} & \mathbf{0}_{3\times 3} \\ \mathbf{0}_{3\times 3} & 2\,\mathbb{Id}_{3\times 3} \end{pmatrix}, \tag{3.4}$$

hence $D^\dagger = \operatorname{diag}(\mathfrak{c}_1,\dots,\mathfrak{c}_6)$.

Voigt and Kelvin identifications for symmetric matrices A symmetric 3×3 matrix $\boldsymbol{w} \in S_2$ is identified with a vector of length 6 in Voigt and Kelvin notation, that we refer to as $\overrightarrow{\boldsymbol{w}}$ and $\overrightarrow{\boldsymbol{w}}^\dagger$ respectively, such that

$$S_2 \ni \boldsymbol{w} = \begin{pmatrix} w_{xx} & w_{xy} & w_{xz} \\ w_{yx} & w_{yy} & w_{yz} \\ w_{zx} & w_{zy} & w_{zz} \end{pmatrix} \underset{\text{Voigt identification}}{\longleftrightarrow} \overrightarrow{\boldsymbol{w}} = (w_{xx}\,,\, w_{yy}\,,\, w_{zz}\,,\, w_{yz}\,,\, w_{xz}\,,\, w_{xy})^t\,, \tag{3.5a}$$

$$\underset{\text{Kelvin identification}}{\longleftrightarrow} \overrightarrow{\boldsymbol{w}}^\dagger = (w_{xx}\,,\, w_{yy}\,,\, w_{zz}\,,\, 2\,w_{yz}\,,\, 2\,w_{xz}\,,\, 2\,w_{xy})^t\,. \tag{3.5b}$$

The relation between the two representations is given using $D^\dagger$ (3.4):

$$\overrightarrow{\boldsymbol{w}}^\dagger = D^\dagger\, \overrightarrow{\boldsymbol{w}}\,. \tag{3.6}$$

Voigt identification for symmetric tensor A fourth order symmetric tensor in S_4 is identified with a symmetric matrix of size 6×6 as

$$\begin{aligned} \mathbf{T} \in S_4 \quad &\underset{\text{Voigt identification}}{\leftrightarrow} \quad \overline{\overline{\mathbf{T}}} = (\mathsf{t}_{\mathfrak{J}\mathfrak{J}'})_{\mathfrak{J},\mathfrak{J}'\in\mathcal{I}_{\rm sm}}\,, \\ &\underset{\text{Kelvin identification}}{\leftrightarrow} \quad \overline{\overline{\mathbf{T}}}^\dagger = \left(\mathsf{t}^\dagger_{\mathfrak{J}\mathfrak{J}'}\right)_{\mathfrak{J},\mathfrak{J}'\in\mathcal{I}_{\rm sm}}\,, \end{aligned} \tag{3.7}$$

with[6]

$$\overline{\overline{\mathbf{T}}} := \begin{pmatrix} \mathsf{c}_{11} & \mathsf{c}_{12} & \mathsf{c}_{13} & \mathsf{c}_{14} & \mathsf{c}_{15} & \mathsf{c}_{16} \\ \mathsf{c}_{21} & \mathsf{c}_{22} & \mathsf{c}_{23} & \mathsf{c}_{24} & \mathsf{c}_{25} & \mathsf{c}_{26} \\ \mathsf{c}_{31} & \mathsf{c}_{32} & \mathsf{c}_{33} & \mathsf{c}_{34} & \mathsf{c}_{35} & \mathsf{c}_{36} \\ \mathsf{c}_{41} & \mathsf{c}_{42} & \mathsf{c}_{43} & \mathsf{c}_{44} & \mathsf{c}_{45} & \mathsf{c}_{46} \\ \mathsf{c}_{51} & \mathsf{c}_{52} & \mathsf{c}_{53} & \mathsf{c}_{54} & \mathsf{c}_{55} & \mathsf{c}_{56} \\ \mathsf{c}_{61} & \mathsf{c}_{62} & \mathsf{c}_{63} & \mathsf{c}_{64} & \mathsf{c}_{65} & \mathsf{c}_{66} \end{pmatrix}, \quad \overline{\overline{\mathbf{T}}}^\dagger := \begin{pmatrix} \mathsf{c}_{11} & \mathsf{c}_{12} & \mathsf{c}_{13} & 2\,\mathsf{c}_{14} & 2\,\mathsf{c}_{15} & 2\,\mathsf{c}_{16} \\ \mathsf{c}_{21} & \mathsf{c}_{22} & \mathsf{c}_{23} & 2\,\mathsf{c}_{24} & 2\,\mathsf{c}_{25} & 2\,\mathsf{c}_{26} \\ \mathsf{c}_{31} & \mathsf{c}_{32} & \mathsf{c}_{33} & 2\,\mathsf{c}_{34} & 2\,\mathsf{c}_{35} & 2\,\mathsf{c}_{36} \\ \mathsf{c}_{41} & \mathsf{c}_{42} & \mathsf{c}_{43} & 2\,\mathsf{c}_{44} & 2\,\mathsf{c}_{45} & 2\,\mathsf{c}_{46} \\ \mathsf{c}_{51} & \mathsf{c}_{52} & \mathsf{c}_{53} & 2\,\mathsf{c}_{54} & 2\,\mathsf{c}_{55} & 2\,\mathsf{c}_{56} \\ \mathsf{c}_{61} & \mathsf{c}_{62} & \mathsf{c}_{63} & 2\,\mathsf{c}_{64} & 2\,\mathsf{c}_{65} & 2\,\mathsf{c}_{66} \end{pmatrix}. \tag{3.8}$$

The above representations are related by,

$$\overline{\overline{\mathbf{T}}}^\dagger = \overline{\overline{\mathbf{T}}}\, D^\dagger\,. \tag{3.9}$$

It is also useful to define,

$$^\dagger\overline{\overline{\mathbf{T}}}^\dagger := D^\dagger \overline{\overline{\mathbf{T}}}\, D^\dagger\,. \tag{3.10}$$

[6] In the above expression, identification (3.3) is used to label the components of a symmetric tensor in $\mathcal{S}_4$. In original indices, $\overline{\overline{\mathbf{T}}} = \begin{pmatrix} t_{xxxx} & t_{xxyy} & t_{xxzz} & t_{xxxy} & t_{xxxz} & t_{xxyz} \\ t_{yyxx} & t_{yyyy} & t_{yyzz} & t_{yyxy} & t_{yyxz} & t_{yyyz} \\ t_{zzxx} & t_{zzyy} & t_{zzzz} & t_{zzxy} & t_{zzxz} & t_{zzyz} \\ t_{xyxx} & t_{xyyy} & t_{xyzz} & t_{xyxy} & t_{xyxz} & t_{xyyz} \\ t_{xzxx} & t_{xzyy} & t_{xzzz} & t_{xzxy} & t_{xzxz} & t_{xzyz} \\ t_{yzxx} & t_{yzyy} & t_{yzzz} & t_{yzxy} & t_{yzxz} & t_{yzyz} \end{pmatrix}$.

3.2 Operations in Voigt notation

We define the following matrices:

$$\mathbb{A}_x = \begin{pmatrix} 1 & 0 & 0 & 0 & 0 & 0 \\ 0 & 0 & 0 & 0 & 0 & \frac{1}{2} \\ 0 & 0 & 0 & 0 & \frac{1}{2} & 0 \end{pmatrix}, \quad \mathbb{A}_y = \begin{pmatrix} 0 & 0 & 0 & 0 & 0 & \frac{1}{2} \\ 0 & 1 & 0 & 0 & 0 & 0 \\ 0 & 0 & 0 & \frac{1}{2} & 0 & 0 \end{pmatrix}, \quad \mathbb{A}_z = \begin{pmatrix} 0 & 0 & 0 & 0 & \frac{1}{2} & 0 \\ 0 & 0 & 0 & \frac{1}{2} & 0 & 0 \\ 0 & 0 & 1 & 0 & 0 & 0 \end{pmatrix}; \tag{3.11a}$$

$$\mathbb{A}_x^\dagger = \begin{pmatrix} 1 & 0 & 0 & 0 & 0 & 0 \\ 0 & 0 & 0 & 0 & 0 & 1 \\ 0 & 0 & 0 & 0 & 1 & 0 \end{pmatrix}, \quad \mathbb{A}_y^\dagger = \begin{pmatrix} 1 & 0 & 0 & 0 & 0 & 1 \\ 0 & 0 & 0 & 0 & 0 & 0 \\ 0 & 0 & 0 & 1 & 0 & 0 \end{pmatrix}, \quad \mathbb{A}_z^\dagger = \begin{pmatrix} 0 & 0 & 0 & 0 & 1 & 0 \\ 0 & 0 & 0 & 1 & 0 & 0 \\ 0 & 0 & 1 & 0 & 0 & 0 \end{pmatrix}. \tag{3.11b}$$

With matrix $D^\dagger$ defined in (3.4), the two identifications $\mathbb{A}_I^\dagger$ and $\mathbb{A}_I$ are related by

$$\mathbb{A}_I^\dagger = \mathbb{A}_I \, D^\dagger \,, \quad \text{where } I = x, y, z \,. \tag{3.12}$$

For a vector $\boldsymbol{\xi} \in \mathbb{C}^3$, we define

$$\mathbb{A}^\dagger(\boldsymbol{\xi}) := \sum_{I=x,y,z} \xi_I \, \mathbb{A}_I^\dagger \,, \qquad \mathbb{A}(\boldsymbol{\xi}) := \sum_{I=x,y,z} \xi_I \, \mathbb{A}_I \,. \tag{3.13}$$

They are related by,

$$\mathbb{A}^\dagger(\boldsymbol{\xi}) = \mathbb{A}(\boldsymbol{\xi}) \, D^\dagger \,. \tag{3.14}$$

Symmetric tensor product between two vectors We denote by $\odot$ the symmetric tensor product: for two vectors $\mathbf{v} = (v_I)_{I=x,y,z}$ and $\mathbf{w} = (w_I)_{I=x,y,z}$

$$\mathbf{w} \odot \mathbf{v} = \frac{\mathbf{w} \otimes \mathbf{v} + \mathbf{v} \otimes \mathbf{w}}{2} = \frac{1}{2} \begin{pmatrix} 2\, w_x v_x & w_x v_y + w_y v_x & w_x v_z + w_z v_x \\ w_y v_x + w_x v_y & 2\, w_y v_y & w_y v_z + w_z v_y \\ w_z v_x + w_x v_z & w_z v_y + w_y v_z & 2\, w_z v_z \end{pmatrix} . \tag{3.15}$$

We can further represent the symmetric tensor product between two vectors $\mathbf{w}$ and $\mathbf{v}$ of length 3, as a vector of length 6 in Voigt and Kelvin notations:

$$\begin{aligned} \overrightarrow{\mathbf{w} \odot \mathbf{u}} &= \begin{pmatrix} w_x u_x \\ w_y u_y \\ w_z u_z \\ \frac{1}{2}(w_y u_z + w_z u_y) \\ \frac{1}{2}(w_x u_z + w_z u_x) \\ \frac{1}{2}(w_x u_y + w_y u_x) \end{pmatrix} = w_x \begin{pmatrix} u_x \\ 0 \\ 0 \\ 0 \\ \frac{1}{2}u_z \\ \frac{1}{2}u_y \end{pmatrix} + w_y \begin{pmatrix} 0 \\ u_y \\ 0 \\ \frac{1}{2}u_z \\ 0 \\ \frac{1}{2}u_x \end{pmatrix} + w_z \begin{pmatrix} 0 \\ 0 \\ u_z \\ \frac{1}{2}u_y \\ \frac{1}{2}u_x \\ 0 \end{pmatrix}, \\ \overrightarrow{\mathbf{w} \odot \mathbf{u}}^\dagger &= \begin{pmatrix} w_x u_x \\ w_y u_y \\ w_z u_z \\ w_y u_z + w_z u_y \\ w_x u_z + w_z u_x \\ w_x u_y + w_y u_x \end{pmatrix} = w_x \begin{pmatrix} u_x \\ 0 \\ 0 \\ 0 \\ u_z \\ u_y \end{pmatrix} + w_y \begin{pmatrix} 0 \\ u_y \\ 0 \\ u_z \\ 0 \\ u_x \end{pmatrix} + w_z \begin{pmatrix} 0 \\ 0 \\ u_z \\ u_y \\ u_x \\ 0 \end{pmatrix} . \end{aligned} \tag{3.16}$$

Additionally, we have

$$\overrightarrow{\boldsymbol{\xi} \odot \mathbf{w}} = \mathbb{A}(\boldsymbol{\xi})^t \, \mathbf{w} \,, \qquad \overrightarrow{\boldsymbol{\xi} \odot \mathbf{w}}^\dagger = \mathbb{A}^\dagger(\boldsymbol{\xi})^t \, \mathbf{w} \,. \tag{3.17}$$

Symmetric matrix-vector product The dot product between a 3×3 symmetric matrix $\boldsymbol{\chi}$ and a 3×1 vector $\mathbf{w}$ can be written as, using identity (3.24),

$$\boldsymbol{\chi} \, \mathbf{w} = \mathbb{A}^\dagger(\mathbf{w}) \overrightarrow{\boldsymbol{\chi}} \,, \tag{3.18}$$

$$\boldsymbol{\chi}\mathbf{w} = w_x \begin{pmatrix} \chi_{xx} \\ \chi_{xy} \\ \chi_{xz} \end{pmatrix} + w_y \begin{pmatrix} \chi_{yx} \\ \chi_{yy} \\ \chi_{yz} \end{pmatrix} + w_z \begin{pmatrix} \chi_{zx} \\ \chi_{zy} \\ \chi_{zz} \end{pmatrix} = \left(\sum_I w_I \mathbb{A}_I^\dagger \right) \overrightarrow{\boldsymbol{\chi}} = \left(\sum_I w_I \mathbb{A}_I \right) \overrightarrow{\boldsymbol{\chi}}^\dagger \,. \tag{3.19}$$

Contraction For the contraction of two symmetric matrices $\boldsymbol{\tau_1}, \boldsymbol{\tau_2} \in S_2$,

$$\boldsymbol{\tau_1} : \boldsymbol{\tau_2} = \overrightarrow{\boldsymbol{\tau_1}} \cdot \overrightarrow{\boldsymbol{\tau_2}}^\dagger = \overrightarrow{\boldsymbol{\tau_1}}^\dagger \cdot \overrightarrow{\boldsymbol{\tau_2}} = \overrightarrow{\boldsymbol{\tau_1}} \cdot D^\dagger \cdot \overrightarrow{\boldsymbol{\tau_2}} \tag{3.20}$$

Here the operation in the second and third expressions are vector dot products, while the last one is a bilinear form between two vectors and matrix, cf. Subsection 2.1.

Symmetric tensor-matrix product For symmetric tensor $\boldsymbol{C} \in S_4$ and matrix $\boldsymbol{\chi} \in S_2$,

$$\overrightarrow{\boldsymbol{C}\boldsymbol{\chi}} \;=\; \overline{\overline{\boldsymbol{C}}}\, D^\dagger \overrightarrow{\boldsymbol{\chi}} \;=\; \overline{\overline{\boldsymbol{C}}}^\dagger \overrightarrow{\boldsymbol{\chi}} \;=\; \overline{\overline{\boldsymbol{C}}} \overrightarrow{\boldsymbol{\chi}}^\dagger ; \tag{3.21a}$$

$$\overrightarrow{\boldsymbol{C}\boldsymbol{\chi}^\dagger} \;=\; D^\dagger \overline{\overline{\boldsymbol{C}}}\, D^\dagger \overrightarrow{\boldsymbol{\chi}} \;\overset{(3.10)}{=}\; {}^\dagger\overline{\overline{\boldsymbol{C}}}^\dagger \overrightarrow{\boldsymbol{\chi}} \;=\; D^\dagger \overline{\overline{\boldsymbol{C}}} \overrightarrow{\boldsymbol{\chi}}^\dagger . \tag{3.21b}$$

Useful identities For a 4^{th}-order tensor $\mathbf{T} \in S_4$ and symmetric matrices $\boldsymbol{\tau}, \boldsymbol{w} \in S_2$,

$$\begin{aligned} (\boldsymbol{S}\boldsymbol{\tau}) : \boldsymbol{w} \;&=\; \overrightarrow{\boldsymbol{S}\boldsymbol{\tau}}^\dagger \cdot \overrightarrow{\boldsymbol{w}} \;=\; \overrightarrow{\boldsymbol{w}} \cdot (D^\dagger \overline{\overline{\boldsymbol{S}}} D^\dagger) \cdot \overrightarrow{\tau} \\ &=\; \overrightarrow{\boldsymbol{w}} \cdot {}^\dagger\overline{\overline{\boldsymbol{S}}}^\dagger \cdot \overrightarrow{\tau} \;=\; \overrightarrow{\boldsymbol{w}}^\dagger \cdot \overline{\overline{\boldsymbol{S}}} \cdot \overrightarrow{\tau}^\dagger . \end{aligned} \tag{3.22}$$

For two vectors $\boldsymbol{v}, \boldsymbol{w}$ and a symmetric matrix $\boldsymbol{\tau} \in S_2$,

$$\boldsymbol{\tau}\boldsymbol{v} = \mathbb{A}^\dagger(\boldsymbol{v})\overrightarrow{\boldsymbol{\tau}} \;\;\Rightarrow\;\; \boldsymbol{\tau}\boldsymbol{v} \cdot \boldsymbol{w} = \boldsymbol{w} \cdot \boldsymbol{\tau} \cdot \boldsymbol{v} = \boldsymbol{w} \cdot \mathbb{A}^\dagger(\boldsymbol{v}) \cdot \overrightarrow{\boldsymbol{\tau}} . \tag{3.23}$$

3.3 Differential operators in Voigt notation

We first note that the three columns of symmetric matrix $\boldsymbol{\chi}$ can be given by

$$\begin{pmatrix} \chi_{xI} \\ \chi_{yI} \\ \chi_{zI} \end{pmatrix} = \mathbb{A}_I^\dagger \overrightarrow{\boldsymbol{\chi}} = \mathbb{A}_I \, \overrightarrow{\boldsymbol{\chi}}^\dagger , \quad I = x, y, z . \tag{3.24}$$

Using notation of the vector-valued differential operator $\partial_{\mathbf{x}} = (\partial_x, \partial_y, \partial_z)^t$, we define the operators acting on length 3 vector functions,

$$\begin{aligned} \mathbb{A}(\partial_{\mathbf{x}}) &:= \sum_{I=x,y,z} \partial_I \, \mathbb{A}_I = \begin{pmatrix} \partial_x & 0 & 0 & 0 & \frac{1}{2}\partial_z & \frac{1}{2}\partial_y \\ 0 & \partial_y & 0 & \frac{1}{2}\partial_z & 0 & \frac{1}{2}\partial_x \\ 0 & 0 & \partial_z & \frac{1}{2}\partial_y & \frac{1}{2}\partial_x & 0 \end{pmatrix} , \\ \mathbb{A}^\dagger(\partial_{\mathbf{x}}) &:= \sum_{I=x,y,z} \partial_I \, \mathbb{A}_I^\dagger = \begin{pmatrix} \partial_x & 0 & 0 & 0 & \partial_z & \partial_y \\ 0 & \partial_y & 0 & \partial_z & 0 & \partial_x \\ 0 & 0 & \partial_z & \partial_y & \partial_x & 0 \end{pmatrix} . \end{aligned} \tag{3.25}$$

Using their transpose[7], we also define

$$\mathbb{A}(\partial_{\mathbf{x}})^t = \sum_I \partial_I \mathbb{A}_I^t = \sum_I \mathbb{A}_I^t \partial_I , \qquad \mathbb{A}^\dagger(\partial_{\mathbf{x}})^t = \sum_I \partial_I \mathbb{A}_I^{\dagger t} = \sum_I \mathbb{A}_I^{\dagger t} \partial_I . \tag{3.26}$$

It is useful to note that for a constant vector $\mathbf{v}$ and scalar function ϕ, with $\mathbb{A}(\nabla\phi)$ defined using (3.13) (with $\boldsymbol{\xi} = \nabla\mathbf{v}$), we have

$$\mathbb{A}(\partial_{\mathbf{x}})(\phi\mathbf{v}) \;=\; \mathbb{A}(\nabla\phi)\,\mathbf{v} . \tag{3.27}$$

[7] For matter of completeness, we list here their explicit expressions.

$$\mathbb{A}_x^t = \begin{pmatrix} 1 & 0 & 0 \\ 0 & 0 & 0 \\ 0 & 0 & 0 \\ 0 & 0 & 0 \\ 0 & 0 & 1/2 \\ 0 & 1/2 & 0 \end{pmatrix}, \quad \mathbb{A}_y^t = \begin{pmatrix} 0 & 0 & 0 \\ 0 & 1 & 0 \\ 0 & 0 & 0 \\ 0 & 0 & 1/2 \\ 0 & 0 & 0 \\ 1/2 & 0 & 0 \end{pmatrix}, \quad \mathbb{A}_y^t = \begin{pmatrix} 0 & 0 & 0 \\ 0 & 0 & 0 \\ 0 & 0 & 1 \\ 0 & 1/2 & 0 \\ 1/2 & 0 & 0 \\ 0 & 0 & 0 \end{pmatrix}, \quad \mathbb{A}_x^{\dagger t} = \begin{pmatrix} 1 & 0 & 0 \\ 0 & 0 & 0 \\ 0 & 0 & 0 \\ 0 & 0 & 0 \\ 0 & 0 & 1 \\ 0 & 1 & 0 \end{pmatrix}, \quad \mathbb{A}_y^{\dagger t} = \begin{pmatrix} 0 & 0 & 0 \\ 0 & 1 & 0 \\ 0 & 0 & 0 \\ 0 & 0 & 1 \\ 0 & 0 & 0 \\ 1 & 0 & 0 \end{pmatrix}, \quad \mathbb{A}_z^{\dagger t} = \begin{pmatrix} 0 & 0 & 0 \\ 0 & 0 & 0 \\ 0 & 0 & 1 \\ 0 & 1 & 0 \\ 1 & 0 & 0 \\ 0 & 0 & 0 \end{pmatrix} .$$

Symmetrized gradient of a vector The symmetrized gradient (2.6) in Voigt notation is

$$\overrightarrow{\nabla^{\mathfrak{s}}\mathbf{w}} = \begin{pmatrix} \partial_x u_x \\ \partial_y u_y \\ \partial_z u_z \\ \frac{1}{2}\left(\partial_y w_z + \partial_z w_y\right) \\ \frac{1}{2}\left(\partial_x w_z + \partial_z w_x\right) \\ \frac{1}{2}\left(\partial_x w_y + \partial_y w_x\right) \end{pmatrix} = \partial_x \begin{pmatrix} w_x \\ 0 \\ 0 \\ 0 \\ \frac{1}{2}w_z \\ \frac{1}{2}w_y \end{pmatrix} + \partial_y \begin{pmatrix} 0 \\ w_y \\ 0 \\ \frac{1}{2}w_z \\ 0 \\ \frac{1}{2}w_x \end{pmatrix} + \partial_z \begin{pmatrix} 0 \\ 0 \\ w_z \\ \frac{1}{2}w_y \\ \frac{1}{2}w_x \\ 0 \end{pmatrix} . \tag{3.28}$$

Using the transpose of the matrices $\mathbb{A}$, we can further write the Voigt notation:

$$\overrightarrow{\nabla^{\mathfrak{s}}\mathbf{w}} = \left(\sum_{I=x,y,z} \partial_I \, \mathbb{A}_I^t \right) \begin{pmatrix} w_x \\ w_y \\ w_z \end{pmatrix} . \tag{3.29}$$

Similarly, the Kelvin representation of $\nabla^{\mathfrak{s}}\mathbf{w}$, using the transpose of $\mathbb{A}_\bullet^\dagger$ is

$$\overrightarrow{\nabla^{\mathfrak{s}}\mathbf{w}}^{\,\dagger} = \begin{pmatrix} \partial_x u_x \\ \partial_y u_y \\ \partial_z u_z \\ \partial_y w_z + \partial_z w_y \\ \partial_x w_z + \partial_z w_x \\ \partial_x w_y + \partial_y w_x \end{pmatrix} = \left(\sum_{I=x,y,z} \partial_I \, \mathbb{A}_I^{\dagger\, t} \right) \begin{pmatrix} w_x \\ w_y \\ w_z \end{pmatrix} . \tag{3.30}$$

We thus obtain the following identities,

$$\overrightarrow{\nabla^{\mathfrak{s}}\mathbf{w}} = \mathbb{A}(\partial_{\mathbf{x}})^t \mathbf{w} \,, \qquad \overrightarrow{\nabla^{\mathfrak{s}}\mathbf{w}^\dagger} = \mathbb{A}^\dagger(\partial_{\mathbf{x}})^t \mathbf{w} \,. \tag{3.31}$$

Divergence of a symmetric matrix The divergence of a symmetric matrix $\boldsymbol{\chi}$ is rewritten as

$$\nabla \cdot \boldsymbol{\chi} \, = \, \mathbb{A}^\dagger(\partial_{\mathbf{x}}) \overrightarrow{\boldsymbol{\chi}} \, = \, \mathbb{A}(\partial_{\mathbf{x}}) \overrightarrow{\boldsymbol{\chi}}^\dagger \,. \tag{3.32}$$

This is seen by using identity (3.24),

$$\nabla \cdot \boldsymbol{\chi} = \partial_x \begin{pmatrix} \chi_{xx} \\ \chi_{xy} \\ \chi_{xz} \end{pmatrix} + \partial_y \begin{pmatrix} \chi_{yx} \\ \chi_{yy} \\ \chi_{yz} \end{pmatrix} + \partial_z \begin{pmatrix} \chi_{zx} \\ \chi_{zy} \\ \chi_{zz} \end{pmatrix} = \left(\sum_I \partial_I \mathbb{A}_I^\dagger \right) \overrightarrow{\boldsymbol{\chi}} = \left(\sum_I \partial_I \mathbb{A}_I \right) \overrightarrow{\boldsymbol{\chi}}^{\,\dagger} \,. \tag{3.33}$$

3.4 Useful examples and identities

3.4.1 Basis for symmetric matrices

The following matrices form a basis for S_2:

$$\begin{aligned} &\mathbf{e}_x \odot \mathbf{e}_x = \left(\begin{smallmatrix} 1 & 0 & 0 \\ 0 & 0 & 0 \\ 0 & 0 & 0 \end{smallmatrix}\right), \quad \mathbf{e}_y \odot \mathbf{e}_y = \left(\begin{smallmatrix} 0 & 0 & 0 \\ 0 & 1 & 0 \\ 0 & 0 & 0 \end{smallmatrix}\right), \quad \mathbf{e}_z \odot \mathbf{e}_z = \left(\begin{smallmatrix} 0 & 0 & 0 \\ 0 & 0 & 0 \\ 0 & 0 & 1 \end{smallmatrix}\right) \\ &\mathbf{e}_y \odot \mathbf{e}_z = \begin{pmatrix} 0 & 0 & 0 \\ 0 & 0 & \frac{1}{2} \\ 0 & \frac{1}{2} & 0 \end{pmatrix}, \quad \mathbf{e}_x \odot \mathbf{e}_z = \begin{pmatrix} 0 & 0 & \frac{1}{2} \\ 0 & 0 & 0 \\ \frac{1}{2} & 0 & 0 \end{pmatrix}, \quad \mathbf{e}_x \odot \mathbf{e}_y = \begin{pmatrix} 0 & \frac{1}{2} & 0 \\ \frac{1}{2} & 0 & 0 \\ 0 & 0 & 0 \end{pmatrix}. \end{aligned} \tag{3.34}$$

In particular, for the stress tensor $\boldsymbol{\sigma}$, we have,

$$\boldsymbol{\sigma} \, = \, \sum_{I=x,y,z} \sigma_{II} \, \mathbf{e}_I \odot \mathbf{e}_I + 2 \left(\sigma_{yz} \, \mathbf{e}_y \odot \mathbf{e}_z + \sigma_{xz} \, \mathbf{e}_x \odot \mathbf{e}_z + \sigma_{xy} \, \mathbf{e}_x \odot \mathbf{e}_y \right) . \tag{3.35}$$

With $\mathcal{I}_{\rm sm}$ the ordered set (3.3), we write the unit Cartesian vectors in $\mathbb{R}^6$ as,

$$\hat{\mathbf{e}}_{\mathfrak{J}}, \qquad \mathfrak{J} \in \mathcal{I}_{\rm sm} \,. \tag{3.36}$$

The unit basis vector $\hat{\mathsf{E}}_{\mathfrak{J}}$ in $\mathbb{R}^6$ is (inversely) identified with the symmetric matrix[8] given in (3.34),

$$\overline{\overline{\mathfrak{e}}}_{\mathfrak{J}} := \begin{cases} \mathbf{e}_I \odot \mathbf{e}_J\,, & I = J \\ 2\,\mathbf{e}_I \odot \mathbf{e}_J\,, & I \neq J \end{cases} \quad \Rightarrow \quad \overrightarrow{\overline{\overline{\mathfrak{e}}}}_{\mathfrak{J}} = \hat{\mathfrak{e}}_{\mathfrak{J}}\,. \tag{3.37}$$

where the explicit expression of $\overline{\overline{\mathfrak{e}}}_{\mathfrak{J}}$ is obtained from definition (3.34),

$$\begin{aligned} &\overline{\overline{\mathfrak{e}}}_{xx} = \begin{pmatrix} 1&0&0\\0&0&0\\0&0&0 \end{pmatrix}, \quad \overline{\overline{\mathfrak{e}}}_{yy} = \begin{pmatrix} 0&0&0\\0&1&0\\0&0&0 \end{pmatrix}, \quad \overline{\overline{\mathfrak{e}}}_{zz} = \begin{pmatrix} 0&0&0\\0&0&0\\0&0&1 \end{pmatrix}, \\ &\overline{\overline{\mathfrak{e}}}_{yz} = \begin{pmatrix} 0&0&0\\0&0&1\\0&1&0 \end{pmatrix}, \quad \overline{\overline{\mathfrak{e}}}_{xz} = \begin{pmatrix} 0&0&1\\0&0&0\\1&0&0 \end{pmatrix}, \quad \overline{\overline{\mathfrak{e}}}_{xy} = \begin{pmatrix} 0&1&0\\1&0&0\\0&0&0 \end{pmatrix}. \end{aligned} \tag{3.38}$$

In particular, a symmetric matrix $\boldsymbol{\sigma} \in S_2$ can be written in the basis $\overline{\overline{\mathfrak{e}}}_{\mathfrak{J}}$, or in Voigt notation in terms of the basis $\mathfrak{e}_{\mathfrak{J}}$ such that,

$$\boldsymbol{\sigma} = \sum_{\mathfrak{J}\in\mathcal{I}_{\rm sm}} \sigma_{\mathfrak{J}}\, \overline{\overline{\mathfrak{e}}}_{\mathfrak{J}}\,, \qquad \overrightarrow{\boldsymbol{\sigma}} = \sum_{\mathfrak{J}\in\mathcal{I}_{\rm sm}} \sigma_{\mathfrak{J}}\, \hat{\mathfrak{e}}_{\mathfrak{J}}\,. \tag{3.39}$$

Its divergence is

$$\nabla\cdot\boldsymbol{\sigma} = \sum_{\mathfrak{J}\in\mathcal{I}_{\rm sm}} \mathbb{A}^{\dagger}(\nabla\sigma_{\mathfrak{J}})\,\hat{\mathfrak{e}}_{\mathfrak{J}}\,, \qquad (\nabla\cdot\boldsymbol{\sigma})\cdot\mathbf{e}_I = \sum_{\mathfrak{J}\in\mathcal{I}_{\rm sm}} \mathbf{e}_I\cdot\mathbb{A}^{\dagger}(\nabla\sigma_{\mathfrak{J}})\cdot\hat{\mathfrak{e}}_{\mathfrak{J}}\,. \tag{3.40}$$

3.4.2 Kelvin–Christoffel matrix

We first recall the definition of the Kelvin–Christoffel matrix, see, for instance, [11].

Definition 1 (Kelvin–Christoffel matrix)**.** *With normalized vector $\boldsymbol{\nu}$ and fourth-order elasticity tensor $\boldsymbol{C}$, the Kelvin–Christoffel matrix is,*

$$\boldsymbol{\Gamma}(\boldsymbol{\nu}) := \boldsymbol{\nu}\cdot\boldsymbol{C}\cdot\boldsymbol{\nu}, \quad \textit{with} \quad (\boldsymbol{\nu}\cdot\boldsymbol{C}\cdot\boldsymbol{\nu})_{jk} = \sum_{i,l=1}^{3} \nu_i\, c_{ijkl}\, \nu_l\,. \tag{3.41}$$

Proposition 1 (Identity)**.** *The Kelvin–Christoffel matrix $\boldsymbol{\Gamma}$ can be written as*

$$\boldsymbol{\Gamma}(\boldsymbol{\nu}) = \mathbb{A}(\boldsymbol{\nu})\,{}^{\dagger}\overline{\overline{\boldsymbol{C}}}^{\dagger}\,\mathbb{A}^{t}(\boldsymbol{\nu})\,. \tag{3.42}$$

Proof. This is seen as follows. Using identity (3.17), we have

$$\mathbb{A}^{t}(\boldsymbol{\nu})\mathbf{w} = \overrightarrow{\boldsymbol{\nu}\odot\mathbf{w}} \quad \Rightarrow \quad \overline{\overline{\boldsymbol{C}}}^{\dagger}\mathbb{A}^{t}(\boldsymbol{\nu})\mathbf{w} = \overrightarrow{\boldsymbol{C}\,(\boldsymbol{\nu}\odot\mathbf{w})}\,. \tag{3.43}$$

Next with identity (3.18), $\mathbb{A}^{\dagger}(\mathbf{w})\overrightarrow{\boldsymbol{\chi}} = \boldsymbol{\chi}\mathbf{w}$, with $\boldsymbol{\chi} = \boldsymbol{C}\,(\boldsymbol{\nu}\odot\mathbf{w})$, we obtain

$$\mathbb{A}^{\dagger}(\boldsymbol{\nu})\,\overline{\overline{\boldsymbol{C}}}^{\dagger}\mathbb{A}^{t}(\boldsymbol{\nu})\,\mathbf{w} = (\boldsymbol{C}\,(\boldsymbol{\nu}\odot\mathbf{w}))\,\boldsymbol{\nu} = (\boldsymbol{\nu}\cdot\boldsymbol{C}\cdot\boldsymbol{\nu})\cdot\mathbf{w}\,. \tag{3.44}$$

□

Proposition 2 (Symmetry)**.** *By the symmetry of $\boldsymbol{C}$, we have,*

$$(\boldsymbol{\nu}\cdot\boldsymbol{C}\cdot\boldsymbol{\nu})_{il} = \sum_{j,k} \nu_j\, c_{ijkl}\, \nu_k = \sum_{j,k} \nu_j\, c_{lkji}\, \nu_k = (\boldsymbol{\nu}\cdot\boldsymbol{C}\cdot\boldsymbol{\nu})_{li}\,. \tag{3.45}$$

From the above identity, it follows that $\boldsymbol{\Gamma}(\boldsymbol{\nu})$ is a symmetric matrix.

[8] In particular, for $\mathfrak{J} = II$ with $I = x, y, z$ then $\hat{\mathsf{E}}_{II} = \mathbf{e}_I \odot \mathbf{e}_I$, while $\mathfrak{J} \in \mathcal{I}_{\rm sm}$ and $\mathfrak{J} = IJ$ then $\hat{\mathsf{E}}_{\mathfrak{J}} = 2\mathbf{e}_I \odot \mathbf{e}_J$.

The derivation (3.44) also gives us

$$\mathbf{w}\cdot\left(\mathbb{A}^{\dagger}(\boldsymbol{\nu})\,\overline{\overline{\boldsymbol{C}}}^{\dagger}\mathbb{A}^{t}(\boldsymbol{\nu})\right)\cdot\mathbf{w}=\mathbf{w}\cdot\left(\boldsymbol{C}\left(\boldsymbol{\nu}\odot\mathbf{w}\right)\right)\boldsymbol{\nu}=(\boldsymbol{\nu}\odot\mathbf{w}):\boldsymbol{C}:(\boldsymbol{\nu}\odot\mathbf{w})>0\,. \tag{3.46}$$

This follows from the assumption of a positive definite stiffness tensor $\boldsymbol{C}$, and we have,

$$\mathbb{A}^{\dagger}(\boldsymbol{\nu})\,\overline{\overline{\boldsymbol{C}}}^{\dagger}\mathbb{A}^{t}(\boldsymbol{\nu})=\boldsymbol{\nu}\cdot\boldsymbol{C}\cdot\boldsymbol{\nu}=\boldsymbol{\Gamma}(\boldsymbol{\nu})\qquad\text{is positive-definite and symmetric.} \tag{3.47}$$

It is thus diagonalizable with 3 positive eigenvalues, listed in descending order,

$$\rho\mathrm{c}_{qP}^{2}\,,\qquad\rho\mathrm{c}_{qS1}^{2}\,,\qquad\rho\mathrm{c}_{qS2}^{2}\,. \tag{3.48}$$

Proposition 3. *The components of matrix* $\boldsymbol{\Gamma}$ *can be computed as a matrix as*

$$[\boldsymbol{\Gamma}(\boldsymbol{\nu})]_{IJ}=(\mathbb{A}(\boldsymbol{\nu})\,\mathbf{e}_I)\cdot{}^{\dagger}\overline{\overline{\boldsymbol{C}}}^{\dagger}\cdot(\mathbb{A}(\boldsymbol{\nu})\,\mathbf{e}_J) \tag{3.49a}$$

$$=(\mathbf{e}_I\odot\boldsymbol{\nu}):\boldsymbol{C}:(\mathbf{e}_J\odot\boldsymbol{\nu})=\mathbf{e}_I\cdot(\boldsymbol{C}(\mathbf{e}_J\odot\boldsymbol{\nu}))\cdot\boldsymbol{\nu}\,. \tag{3.49b}$$

In Voigt's notation, it can be written as a vector given by matrix-vector multiplication,

$$\overrightarrow{\boldsymbol{\Gamma}(\boldsymbol{\nu})}=\begin{pmatrix}c_{11}&c_{66}&c_{55}&c_{56}&c_{15}&c_{16}\\c_{66}&c_{22}&c_{44}&c_{24}&c_{46}&c_{26}\\c_{55}&c_{44}&c_{33}&c_{34}&c_{35}&c_{45}\\c_{16}&c_{26}&c_{45}&\frac{c_{46}+c_{25}}{2}&\frac{c_{14}+c_{56}}{2}&\frac{c_{12}+c_{66}}{2}\\c_{15}&c_{46}&c_{35}&\frac{c_{45}+c_{36}}{2}&\frac{c_{13}+c_{55}}{2}&\frac{c_{14}+c_{56}}{2}\\c_{56}&c_{24}&c_{34}&\frac{c_{44}+c_{23}}{2}&\frac{c_{36}+c_{45}}{2}&\frac{c_{25}+c_{46}}{2}\end{pmatrix}\overrightarrow{\boldsymbol{\nu}\odot\boldsymbol{\nu}}^{\,\dagger}\,. \tag{3.50}$$

Proof. The first equality in (3.49) is obtained by using identity (3.42). The second and third identities can be derived as follows,

$$\begin{aligned}[\boldsymbol{\Gamma}(\boldsymbol{\nu})]_{IJ}&=\mathbf{e}_I\cdot\boldsymbol{\Gamma}(\boldsymbol{\nu})\cdot\mathbf{e}_J=\mathbf{e}_I\cdot(\boldsymbol{\nu}\cdot\boldsymbol{C}\boldsymbol{\nu})\cdot\mathbf{e}_J\\&=(\mathbf{e}_I\odot\boldsymbol{\nu}):\boldsymbol{C}:(\mathbf{e}_J\odot\boldsymbol{\nu})=\mathbf{e}_I\cdot(\boldsymbol{C}(\mathbf{e}_J\odot\boldsymbol{\nu}))\cdot\boldsymbol{\nu}\,.\end{aligned} \tag{3.51}$$

The Voigt expression (3.50) is obtained by direct computation, see also [11, Equation 1.73].

□

3.4.3 Voigt representation of stiffness and compliance tensor

Relation between the Voigt representation of stiffness and compliance tensor The stress-strain relation and the strain-stress relation[9] can be written in the form of the action of a dimension 4 tensor to a matrix such that, (3.21a),

$$\boldsymbol{\sigma}=\boldsymbol{C}\boldsymbol{\varepsilon}\,,\qquad\boldsymbol{\varepsilon}=\boldsymbol{S}\boldsymbol{\sigma}\,, \tag{3.52}$$

and are in Voigt representation,

$$\begin{aligned}\overrightarrow{\boldsymbol{\sigma}}=\overline{\overline{\boldsymbol{C}}}\,D^{\dagger}\,\overrightarrow{\boldsymbol{\varepsilon}}\,,\qquad\overrightarrow{\boldsymbol{\epsilon}}=\overline{\overline{\boldsymbol{S}}}\,D^{\dagger}\,\overrightarrow{\boldsymbol{\sigma}}\,,\\\Rightarrow\overrightarrow{\boldsymbol{\varepsilon}}=\left[(D^{\dagger})^{-1}\,\overline{\overline{\boldsymbol{C}}}^{\,-1}(D^{\dagger})^{-1}\right]D^{\dagger}\,\overline{\overline{\boldsymbol{C}}}\,\overrightarrow{\boldsymbol{\sigma}}\,.\end{aligned} \tag{3.53}$$

This gives us the definition of the compliance tensor $\boldsymbol{S}$ in Voigt notation:

$$\overline{\overline{\boldsymbol{S}}}\;=\;(D^{\dagger})^{-1}\,(\overline{\overline{\boldsymbol{C}}})^{-1}(D^{\dagger})^{-1}\;=\;(D^{\dagger}\,\overline{\overline{\boldsymbol{C}}}\,D^{\dagger})^{-1}\;=\;({}^{\dagger}\overline{\overline{\boldsymbol{C}}}^{\dagger})^{-1}\,. \tag{3.54}$$

We thus obtain a relation between the Voigt representation of $\boldsymbol{C}$ and $\boldsymbol{S}$,

$$\overline{\overline{\boldsymbol{S}}}\;=\;({}^{\dagger}\overline{\overline{\boldsymbol{C}}}^{\dagger})^{-1}\,,\qquad{}^{\dagger}\overline{\overline{\boldsymbol{S}}}^{\dagger}\;=\;\left(\overline{\overline{\boldsymbol{C}}}\right)^{-1}\,. \tag{3.55}$$

[9] Precisely, these are $\sigma_{ij}=\sum_{k,l=1,2,3}c_{ijkl}\varepsilon_{kl}$ and $\varepsilon_{ij}=\sum_{k,l=1,2,3}s_{ijkl}\sigma_{kl}$.

3.4.4 Integration by parts identity

With test functions $\boldsymbol{\chi} \in V_h$ and $\mathbf{w} \in U_h$ from (2.24), the identity for the integration by part,

$$\int_K \nabla^{\mathfrak{s}} \mathbf{v} : \boldsymbol{\chi} = -\int_K \mathbf{v} \cdot \nabla \cdot \boldsymbol{\chi} + \int_{\partial K} \mathbf{v} \odot \boldsymbol{\nu} : \boldsymbol{\chi}\,, \tag{3.56a}$$

$$\int_K (\nabla \cdot \boldsymbol{C}\boldsymbol{\epsilon}) \cdot \mathbf{w} = -\int_K \boldsymbol{\epsilon} : \boldsymbol{C}\nabla^{\mathfrak{s}} \mathbf{w} + \int_{\partial K} \boldsymbol{\nu} \cdot (\boldsymbol{C}\boldsymbol{\epsilon}) \cdot \mathbf{w}\,, \tag{3.56b}$$

writes as, using Voigt and Kelvin notations,

$$\int_K \mathbb{A}^t(\partial_{\mathbf{x}})\mathbf{v} \cdot \overrightarrow{\boldsymbol{\chi}} = -\int_K \mathbf{v} \cdot \mathbb{A}(\partial_{\mathbf{x}})\overrightarrow{\boldsymbol{\chi}}^{\dagger} + \int_{\partial K} \mathbb{A}^t(\boldsymbol{\nu})\mathbf{v} \cdot \overrightarrow{\boldsymbol{\chi}}^{\dagger}\,, \tag{3.57a}$$

$$\int_K \left(\mathbb{A}(\partial_{\mathbf{x}})\,{}^{\dagger}\overline{\overline{\boldsymbol{C}}}^{\dagger}\,\overrightarrow{\boldsymbol{\epsilon}}\right) \cdot \mathbf{w} = -\int_K \overrightarrow{\boldsymbol{\epsilon}} \cdot {}^{\dagger}\overline{\overline{\boldsymbol{C}}}^{\dagger}\,\mathbb{A}(\partial_{\mathbf{x}})^t\,\mathbf{w} + \int_{\partial K} \left(\mathbb{A}(\boldsymbol{\nu})\,{}^{\dagger}\overline{\overline{\boldsymbol{C}}}^{\dagger}\,\overrightarrow{\boldsymbol{\epsilon}}\right) \cdot \mathbf{w}\,. \tag{3.57b}$$

We reunite these two identities in matrix form,

$$\begin{aligned}\int_K \left[\begin{pmatrix} 0 & \mathbb{A}^t(\partial_{\mathbf{x}})\rho^{-1} \\ \mathbb{A}(\partial_{\mathbf{x}})\,{}^{\dagger}\overline{\overline{\boldsymbol{C}}}^{\dagger} & 0 \end{pmatrix} \begin{pmatrix} \overrightarrow{\boldsymbol{\epsilon}} \\ \rho\mathbf{v} \end{pmatrix}\right] \cdot \begin{pmatrix} \overrightarrow{\boldsymbol{\chi}}^{\dagger} \\ \mathbf{w} \end{pmatrix} &= -\int_K \begin{pmatrix} \overrightarrow{\boldsymbol{\epsilon}} \\ \rho\mathbf{v} \end{pmatrix} \cdot \begin{pmatrix} 0 & {}^{\dagger}\overline{\overline{\boldsymbol{C}}}^{\dagger}\,\mathbb{A}(\partial_{\mathbf{x}})^t \\ \rho^{-1}\,\mathbb{A}(\partial_{\mathbf{x}}) & 0 \end{pmatrix} \begin{pmatrix} \overrightarrow{\boldsymbol{\chi}}^{\dagger} \\ \mathbf{w} \end{pmatrix} \\ &\quad + \int_{\partial K} \left[\begin{pmatrix} 0 & \mathbb{A}^t(\boldsymbol{\nu})\rho^{-1} \\ \mathbb{A}(\boldsymbol{\nu})\,{}^{\dagger}\overline{\overline{\boldsymbol{C}}}^{\dagger} & 0 \end{pmatrix} \begin{pmatrix} \overrightarrow{\boldsymbol{\epsilon}} \\ \rho\mathbf{v} \end{pmatrix}\right] \cdot \begin{pmatrix} \overrightarrow{\boldsymbol{\chi}}^{\dagger} \\ \mathbf{w} \end{pmatrix}.\end{aligned} \tag{3.58}$$

3.4.5 Relation of quantities under rotation

Notations The basis vector of Cartesian coordinates is denoted by $(\mathbf{e}_x, \mathbf{e}_y, \mathbf{e}_z)$. In a second coordinate system, the orthonormal basis is given by the ordered set $(\tilde{\mathbf{e}}_x, \tilde{\mathbf{e}}_y, \tilde{\mathbf{e}}_z)$. We introduce the matrix $\mathcal{R}$ whose columns are the components of these vectors in original basis,

$$\mathcal{R} = (\mathfrak{r}_{ij}) := \begin{pmatrix} \tilde{e}_{xx} & \tilde{e}_{yx} & \tilde{e}_{zx} \\ \tilde{e}_{xy} & \tilde{e}_{yy} & \tilde{e}_{zy} \\ \tilde{e}_{xz} & \tilde{e}_{yz} & \tilde{e}_{zz} \end{pmatrix}, \quad \text{and} \quad \tilde{\mathbf{e}}_i = \sum_j \mathfrak{r}_{ji}\,\mathbf{e}_j \quad . \tag{3.59}$$

We also have that $\mathcal{R}$ is orthonormal,

$$\mathcal{R}^t = \mathcal{R}^{-1}\,. \tag{3.60}$$

In the following discussion, we use over-script '$\sim$' to distinguish the coordinates of vector $\mathbf{u}$ and of symmetric tensor $\boldsymbol{\sigma}$ in these bases; specifically,

$$\mathbf{u} = \sum_{j=1}^{3} u_j\,\mathbf{e}_j = \sum_{j=1}^{3} \tilde{u}_j \tilde{\mathbf{e}}_j\,, \tag{3.61}$$

and

$$\begin{aligned}\boldsymbol{\sigma} &= \sum_{j=1}^{3} \sigma_{jj}\,\mathbf{e}_i \odot \mathbf{e}_j \;+\; 2\sigma_{23}\,\mathbf{e}_2 \odot \mathbf{e}_3 + 2\sigma_{13}\,\mathbf{e}_1 \odot \mathbf{e}_3 + 2\sigma_{12}\,\mathbf{e}_1 \odot \mathbf{e}_2 \\ &= \sum_{j=1}^{3} \tilde{\sigma}_{jj}\,\tilde{\mathbf{e}}_i \odot \tilde{\mathbf{e}}_j \;+\; 2\tilde{\sigma}_{23}\,\tilde{\mathbf{e}}_2 \odot \tilde{\mathbf{e}}_3 + 2\tilde{\sigma}_{13}\,\tilde{\mathbf{e}}_1 \odot \tilde{\mathbf{e}}_3 + 2\tilde{\sigma}_{12}\,\tilde{\mathbf{e}}_1 \odot \tilde{\mathbf{e}}_2\,.\end{aligned} \tag{3.62}$$

We gather the coordinates in vectors and matrices form, for $i, j = 1, 2, 3$,

$$\begin{aligned}&\text{In Cartesian basis,} \quad \mathbf{u} = (u_j)\,, \quad \boldsymbol{\sigma} = (\sigma_{ij})\,, \quad \boldsymbol{\epsilon} = (\epsilon_{ij})\,, \quad \mathbf{q} = \begin{pmatrix} \boldsymbol{\epsilon} \\ \rho\mathbf{u} \end{pmatrix}, \quad \boldsymbol{C} = (\mathrm{c}_{ijkl})\,, \\ &\text{In rotated basis,} \quad \tilde{\mathbf{u}} = (\tilde{u}_j)\,, \quad \tilde{\boldsymbol{\sigma}} = (\tilde{\sigma}_{ij})\,, \quad \tilde{\boldsymbol{\epsilon}} = (\tilde{\epsilon}_{ij})\,, \quad \tilde{\mathbf{q}} = \begin{pmatrix} \tilde{\boldsymbol{\epsilon}} \\ \rho\tilde{\mathbf{u}} \end{pmatrix}, \quad \tilde{\boldsymbol{C}} = (\tilde{\mathrm{c}}_{ijkl})\,.\end{aligned} \tag{3.63}$$

Bond matrix Given 3 vectors $\mathfrak{v}_i, i=1,2,3$ we define the following operators $\mathcal{M}^\dagger$ and $\mathcal{M}$ which create a 6×6 matrix whose row columns are given by $\overrightarrow{\mathfrak{v}_i\odot\mathfrak{v}_j}^\dagger$, respectively $\overrightarrow{\mathfrak{v}_i\odot\mathfrak{v}_j}$ (cf. notation in (3.16)),

$$\mathcal{M}^\dagger(\mathfrak{v}_1,\mathfrak{v}_2,\mathfrak{v}_3) := \begin{pmatrix} \left(\overrightarrow{\mathfrak{v}_1\odot\mathfrak{v}_1}^\dagger\right)^t \\ \left(\overrightarrow{\mathfrak{v}_2\odot\mathfrak{v}_2}^\dagger\right)^t \\ \left(\overrightarrow{\mathfrak{v}_3\odot\mathfrak{v}_3}^\dagger\right)^t \\ \left(\overrightarrow{\mathfrak{v}_2\odot\mathfrak{v}_3}^\dagger\right)^t \\ \left(\overrightarrow{\mathfrak{v}_1\odot\mathfrak{v}_3}^\dagger\right)^t \\ \left(\overrightarrow{\mathfrak{v}_1\odot\mathfrak{v}_2}^\dagger\right)^t \end{pmatrix}, \quad \mathcal{M}(\mathfrak{v}_1,\mathfrak{v}_2,\mathfrak{v}_3) := \begin{pmatrix} \left(\overrightarrow{\mathfrak{v}_1\odot\mathfrak{v}_1}\right)^t \\ \vdots \\ \left(\overrightarrow{\mathfrak{v}_1\odot\mathfrak{v}_2}\right)^t \end{pmatrix}. \tag{3.64}$$

We then define operators $\mathcal{M}^\dagger$ and $\mathcal{M}$ for a 3×3 matrix $R=(r_{ij})_{i,j=1,2,3}$, that will act on its column vectors,

$$\begin{gathered} \mathcal{M}^\dagger[R] := \mathcal{M}^\dagger(\mathfrak{c}_1,\mathfrak{c}_2,\mathfrak{c}_3)\,, \qquad \mathcal{M}[R] := \mathcal{M}(\mathfrak{c}_1,\mathfrak{c}_2,\mathfrak{c}_3)\,, \\ \text{where } \mathfrak{c}_j \text{ are column vectors of } R\,,\ \text{i.e.,} \mathfrak{c}_j = \begin{pmatrix} r_{1j} \\ r_{2j} \\ r_{3j}\end{pmatrix}. \end{gathered} \tag{3.65}$$

They are related to each other by

$$\mathcal{M}[R] = \mathcal{M}^\dagger[R]\,(D^\dagger)^{-1}\,. \tag{3.66}$$

We then define the Bond matrices $\mathbf{M}$ and $\mathbf{N}$ associated to the orthonormal matrix $\mathcal{R}$ (3.59) as

$$\mathbf{M} := \mathcal{M}^\dagger[\mathcal{R}]\,, \qquad \mathbf{N} := D^\dagger\mathbf{M}(D^\dagger)^{-1}\,. \tag{3.67}$$

Remark 3. *By its definition,* $\mathbf{N}$ *is obtained from* $\mathbf{M}$ *by the multiplication of the last 3 columns by* $\frac{1}{2}$ *and the last 3 rows by* 2*. Their components are also explicitly given in [11, Equations (1.54) and (1.56)]. Note the difference in notation with [11] that the matrix* $\mathbf{a}$ *given in [11, Equations (1.52)] corresponds to* $\mathcal{R}^t$*. On the other hand,* $\mathbf{M}$ *is built with the row columns of matrix* $\mathbf{a}$ *in the notation of [11]. In fact by direct inspection of the components of* $\mathbf{N}$*, cf. [11, Equations (1.55) and (1.56)] keeping in mind the difference in notation, we obtain another description of* $\mathbf{N}$*,*

$$\mathbf{N}^t = \mathcal{M}[\mathcal{R}^t]\,. \tag{3.68}$$

As a result of Remark 3, $\mathbf{N}$ written here by its transpose has two defining expressions. Thus the Bond matrices $\mathbf{M}$ and $\mathbf{N}^t$ can be written as.

$$\mathbf{M} = \mathcal{M}^\dagger[\mathcal{R}]\,, \qquad \mathbf{N}^t = \mathcal{M}[\mathcal{R}^t] = (D^\dagger)^{-1}\mathbf{M}^t D^\dagger\,. \tag{3.69}$$

They are further related by the fact that the inverse of one is the transpose of the other. This fact is stated in the following proposition.

Proposition 4. *For a* 3×3 *orthonormal matrix* $\mathcal{R}$*, and the operator* $\mathcal{M}^\dagger$ *defined in* (3.65)*, we have the following identity*

$$\left(\mathcal{M}^\dagger[\mathcal{R}]\right)^{-1} \;=\; \mathcal{M}^\dagger(\mathcal{R}^t)\,. \tag{3.70}$$

This above result takes the following equivalent form,

$$\mathbf{M}^{-1} \;=\; \mathbf{N}^t \;=\; \mathcal{M}^\dagger[\mathcal{R}^t] \;=\; (D^\dagger)^{-1}\mathbf{M}^t D^\dagger\,, \tag{3.71a}$$

$$\mathbf{N}^{-1} \;=\; \mathbf{M}^t \;=\; \left(\mathcal{M}^\dagger[\mathcal{R}]\right)^t\,. \tag{3.71b}$$

Proof. It suffices to prove (3.70) since (3.71) is just an equivalent rewrite of (3.70) in terms of the Bond matrices $\mathbf{M}$ and $\mathbf{N}$ using (3.69). To establish (3.70), we will use the notation of the Bond matrices:

$$\mathbf{M} = \mathcal{M}^\dagger[\mathcal{R}]\,, \quad \mathbf{N}^t = \mathcal{M}^\dagger[\mathcal{R}^t]\,.$$

We thus need to show that

$$\mathbf{M}\,\mathbf{N}^t \;=\; \mathbf{N}^t\mathbf{M} \;=\; \mathbb{Id}_6\,.$$

The key ingredients are the orthonormality of the column vectors and the row vectors of $\mathcal{R}=(\mathfrak{r}_{ij})_{i,j=1}^3$ which are respectively denoted as $\mathfrak{c}_i$ and $\mathfrak{r}_j$, i.e.,

$$\text{for } k=1,2,3, \quad \mathfrak{c}_k = (\mathfrak{r}_{ij})_{i=1}^3\,, \quad \mathfrak{r}_k = (\mathfrak{r}_{kj})_{j=1}^3\,. \tag{3.72}$$

Left inverse We evaluate the expression $\mathbf{M}\mathbf{N}^t$ which is first rewritten as

$$\mathbf{M}\mathbf{N}^t = \mathbf{M}(D^\dagger)^{-1}\mathbf{M}^t D^\dagger = \left(\mathbf{M}(D^\dagger)^{-1}\mathbf{M}^t\right) D^\dagger . \tag{3.73}$$

It is thus equivalent to compute the value of

$$\mathcal{I} := \mathbf{M}\,(D^\dagger)^{-1}\mathbf{M}^t \;=\; \mathbf{M}\,\tilde{\mathbf{M}}^t , \tag{3.74}$$

where,

$$\tilde{\mathbf{M}} := \mathbf{M}(D^\dagger)^{-1} \underset{(3.66)}{\Rightarrow} \tilde{\mathbf{M}} = \mathcal{M}(\mathcal{R}) . \tag{3.75}$$

Its transpose is described by column vectors $\overrightarrow{\mathfrak{v}_i \odot \mathfrak{v}_j}$,

$$\tilde{\mathbf{M}}^t = (D^\dagger)^{-1}\mathbf{M}^t = \left(\overrightarrow{\mathfrak{v}_1 \odot \mathfrak{v}_1} \,,\; \overrightarrow{\mathfrak{v}_2 \odot \mathfrak{v}_2} \,,\; \overrightarrow{\mathfrak{v}_3 \odot \mathfrak{v}_3} \,,\; \overrightarrow{\mathfrak{v}_2 \odot \mathfrak{v}_3} \,,\; \overrightarrow{\mathfrak{v}_1 \odot \mathfrak{v}_3},\; \overrightarrow{\mathfrak{v}_1 \odot \mathfrak{v}_2}\right) . \tag{3.76}$$

We also denote the components of $\mathbf{M}$ and $\tilde{\mathbf{M}}$ by m and $\tilde{\mathsf{m}}$, i.e.,

$$\mathbf{M} = (\mathsf{m}_{IJ})_{I,J=1,\dots,6} \,, \qquad \tilde{\mathbf{M}} = (\tilde{\mathsf{m}}_{IJ})_{I,J=1,\dots,6} \,. \tag{3.77}$$

The components of $\mathcal{I}$ are the vector products between a row vector of $\mathbf{M}$ and column vector of $\tilde{\mathbf{M}}$,

$$\mathcal{I}_{IJ} = (\mathsf{m}_{I\tilde{I}})_{\tilde{I}=1,\dots,6} \cdot (\tilde{\mathsf{m}}_{\tilde{J}J})_{\tilde{J}=1,\dots,6} \;=\; \overrightarrow{\mathfrak{c}_i \odot \mathfrak{c}_j}^{\dagger} \,\cdot\, \overrightarrow{\mathfrak{c}_k \odot \mathfrak{c}_l} . \tag{3.78}$$

In the above expression, we have used Voigt identification (3.3) to relate $I \leftrightarrow \{i,j\}$ and $J \leftrightarrow \{k,l\}$. Due to the symmetry in the last expression, we can assume that

$$i \le j \;,\;\; k \le l \,. \tag{3.79}$$

Next recalling identity (3.20) for contraction between two symmetric matrices, we have

$$\mathcal{I}_{IJ} = \mathfrak{c}_i \odot \mathfrak{c}_j \;:\; \mathfrak{c}_k \odot \mathfrak{c}_l \;=\; \underset{\text{with assumption (3.79)}}{\mathfrak{c}_k \cdot (\mathfrak{c}_i \odot \mathfrak{c}_j) \cdot \mathfrak{c}_l} \quad . \tag{3.80}$$

Since $\mathfrak{c}_i$ are mutually orthonormal, we have $\mathfrak{c}_i \cdot \mathfrak{c}_j = \delta_{ij}$,

$$\mathcal{I}_{IJ} = \frac{\delta_{ki}\delta_{jl} \,+\, \delta_{kj}\delta_{il}}{2} , \quad \text{together with (3.79).} \tag{3.81}$$

We next investigate the values of $\mathcal{I}_{IJ}$ off and along the diagonal.

Case 1: $I \neq J$. In this case, we have

$$i \neq k \quad \text{or} \quad k \neq l \,. \tag{3.82}$$

This is equivalent to

$$\delta_{ik} = 0 \quad \text{or} \quad \delta_{jl} = 0 \,. \tag{3.83}$$

Each of the above statement leads to the following implications,

$$\delta_{ik} = 0 \;\;\Longrightarrow\;\; \left[\begin{array}{ll} & \delta_{li} = 0 \,, \text{ or} \\ \delta_{li} = 1 \;\Rightarrow\; k < i \le j \;\Rightarrow & \delta_{kj} = 0 \,. \end{array}\right. \tag{3.84}$$

Similarly,

$$\delta_{jl} = 0 \;\;\Longrightarrow\;\; \left[\begin{array}{ll} & \delta_{kj} = 0 \text{ or} \\ \delta_{jk} = 1 \Rightarrow i \le j < l \Rightarrow & \delta_{il} = 0 \,. \end{array}\right. \tag{3.85}$$

Substitute this into (3.81), we thus arrive at,

$$\mathcal{I}_{IJ} = 0 \quad \text{when} \quad I \neq J \,. \tag{3.86}$$

Case 2: $I = J$. In this case, we have

$$i = k \quad \text{and} \quad k = l\,. \tag{3.87}$$

We distinguish further two cases: $\delta_{il} = 1$ or $\delta_{il} = 0$, each of which has the following implication,

$$\begin{cases} \delta_{il} = 1 \;\Rightarrow\; i = j = k = l & \Rightarrow I = J \in \{1,2,3\} \;\text{ and }\; \mathcal{I}_{IJ} = 1\,, \\ \delta_{il} = 0 & \Rightarrow I = J \in \{3,5,6\} \;\text{ and }\; \mathcal{I}_{IJ} = \frac{1}{2} \end{cases}. \tag{3.88}$$

The identities (3.86) and (3.88) give that $\mathcal{I}$ is a diagonal matrix with

$$\mathcal{I} \;=\; \mathrm{diag}\left(1,1,1,\tfrac{1}{2},\tfrac{1}{2},\tfrac{1}{2}\right)\,. \tag{3.89}$$

Since multiplication to the right with $D^\dagger$ has the effect of multiplying the last 3 columns by 2, we thus obtain the identity

$$\mathcal{I} D^\dagger = \mathbb{Id}_6\,. \tag{3.90}$$

Right inverse We next show $\mathbf{N}^t\mathbf{M} = \mathbb{Id}_6$. This follows in the same manner as that for the left inverse, however exploiting this time the orthonormality of the row vectors $\mathfrak{r}_i$ of $\mathcal{R}$. We thus first rewrite expression $\mathbf{N}^t\mathbf{M}$ in a form similar to (3.74) by introducing $\mathbf{H}$,

$$\mathbf{H} := \mathbf{N}^t\,. \tag{3.91}$$

Additionally, from expression (3.69) we have

$$\begin{aligned} &\mathbf{H} = \mathcal{M}^\dagger[\mathcal{R}^t] = \mathcal{M}^\dagger(\mathfrak{r}_1,\mathfrak{r}_2,\mathfrak{r}_3)\,, \\ \text{and}\;\; &\mathbf{H} = (D^\dagger)^{-1}\mathbf{M}^t D^\dagger \;\;\Rightarrow\;\; \mathbf{H}^t = (D^\dagger)\mathbf{M}(D^\dagger)^{-1} \;\;\Rightarrow\;\; \mathbf{M}^t = (D^\dagger)^{-1}\mathbf{H}^t D^\dagger\,. \end{aligned} \tag{3.92}$$

The expression $\mathbf{N}^t\mathbf{M}$ is rewritten as,

$$\mathbf{N}^t\mathbf{M} = \mathbf{H}(D^\dagger)^{-1}\mathbf{H}^t D^\dagger = \left(\mathbf{H}(D^\dagger)^{-1}\mathbf{H}^t\right) D^\dagger\,. \tag{3.93}$$

Similarly as before, we first evaluate the expression in the last parenthesis,

$$\mathcal{J} := \mathbf{H}(D^\dagger)^{-1}\mathbf{H}^t = \mathbf{H}\,\tilde{\mathbf{H}}^t\,, \quad \text{where } \tilde{\mathbf{H}} := \mathbf{H}D^\dagger = \mathcal{M}^\dagger(\mathcal{R}^t)\,. \tag{3.94}$$

The components of matrices $\mathbf{H}$ and $\tilde{\mathbf{H}}$ are denoted as

$$\mathbf{H} = (\mathsf{h}_{IJ})_{I,J=1,\dots,6}\,, \qquad \tilde{\mathbf{H}} = \left(\tilde{\mathsf{h}}_{IJ}\right)_{I,J=1,\dots,6}\,. \tag{3.95}$$

The definition of their components are defined in a similar way to those of $\mathbf{M}$ however in terms of the row vectors of $\mathcal{R}$. Similar to (3.81), we have

$$\mathcal{J}_{IJ} = (\mathsf{h}_{I\tilde{I}})_{\tilde{I}=1,\dots,6} \cdot \left(\tilde{\mathsf{h}}_{\tilde{J}J}\right)_{\tilde{J}=1,\dots,6} \;=\; \overrightarrow{\mathfrak{r}_i \odot \mathfrak{r}_j}^\dagger \cdot \overrightarrow{\mathfrak{r}_k \odot \mathfrak{r}_l}\,, \tag{3.96}$$

where the indices are related by Voigt identification (3.3), $I \leftrightarrow \{i,j\}$ and $J \leftrightarrow \{k,l\}$, $I \leftrightarrow \{i,j\}$ and $J \leftrightarrow \{k,l\}$. From this point on, the same argument goes through to obtain

$$\mathcal{J} = \mathrm{diag}(1,1,1,\tfrac{1}{2},\tfrac{1}{2},\tfrac{1}{2}) \quad\Rightarrow\quad \mathbf{N}^t\mathbf{M} = \mathcal{J}D^\dagger = \mathbb{Id}_6\,. \tag{3.97}$$

□

Proposition 5. *For matrix $\mathcal{R}$ whose column vectors form an orthonormal basis $\boldsymbol{\nu}, \mathbf{t}, \tilde{\mathbf{t}}$, i.e. $\mathcal{R} = \left(\boldsymbol{\nu}, \mathbf{t}, \tilde{\mathbf{t}}\right)$, its associated Bond matrix $\mathbf{M} = \mathcal{M}^\dagger[\mathcal{R}]$ satisfies the following identity*

$$\mathcal{R}^t\;\mathbb{A}(\boldsymbol{\nu})\,\mathbf{M}^t = \mathbb{A}_1\,, \quad \textit{where} \quad \mathbb{A}_1 := \begin{pmatrix} 1 & 0 & 0 & 0 & 0 & 0 \\ 0 & 0 & 0 & 0 & 0 & \frac{1}{2} \\ 0 & 0 & 0 & 0 & \frac{1}{2} & 0 \end{pmatrix} \;\textit{and}\; \mathbb{A}(\boldsymbol{\nu}) \;\textit{defined in (3.13).} \tag{3.98}$$

Proof. We will show identity (3.98) column by column. We thus compute the J-th of the right-hand side of (3.98) and show that it takes the value of the corresponding column vector of $\mathbb{A}_1$. If we denote by $\mathbf{v}_J$ the row vector of $\mathbf{M}$ which is the column of $\mathbf{M}^t$, then

$$\mathbf{v}_J = \overrightarrow{\mathfrak{c}_i \odot \mathfrak{c}_j}^\dagger, \quad \text{with } i \le j\,. \tag{3.99}$$

The J-th column vector of (3.98) denoted by $\mathbf{w}_J$, is given by

$$\mathbf{w}_J = \mathcal{R}^t \mathbb{A}(\boldsymbol{\nu}) \mathbf{v}_J\,. \tag{3.100}$$

By identity (3.18) we have,

$$\mathbb{A}(\boldsymbol{\nu})\mathbf{v}_J = \mathbb{A}(\boldsymbol{\nu})\overrightarrow{\mathfrak{c}_i \odot \mathfrak{c}_j}^\dagger = \mathbb{A}^\dagger(\boldsymbol{\nu})\overrightarrow{\mathfrak{c}_i \odot \mathfrak{c}_j}^\dagger = (\mathfrak{c}_i \odot \mathfrak{c}_j)\cdot\boldsymbol{\nu} = \frac{1}{2}\left(\mathfrak{c}_i\delta_{j1} + \mathfrak{c}_j\delta_{i1}\right)\,. \tag{3.101}$$

Substitute the above expression into (3.100), we obtain,

$$\mathbf{w}_J = \mathcal{R}^t\mathbb{A}(\boldsymbol{\nu})\mathbf{v}_J = \frac{1}{2}\left(\delta_{j1}\begin{pmatrix}\delta_{1i}\\ \delta_{2i}\\ \delta_{3i}\end{pmatrix} + \delta_{i1}\begin{pmatrix}\delta_{1j}\\ \delta_{2j}\\ \delta_{3j}\end{pmatrix}\right)\,. \tag{3.102}$$

The right-hand-side of (3.102) is nonzero only when $j = 1$ or $i = 1$. In these cases and under the assumption $i \le j$, it can take the following values,

$$\begin{aligned} i = j = 1 \;&\Rightarrow\; J = 1 \quad &&: \mathbf{w}_J^t = (1,0,0)^t\,,\\ i = 1,\, j = 3 \;&\Rightarrow\; J = 5 \quad &&: \mathbf{w}_J^t = (0,0,\tfrac{1}{2})^t\,,\\ i = 1,\, j = 2 \;&\Rightarrow\; J = 7 \quad &&: \mathbf{w}_J^t = (0,\tfrac{1}{2},0)^t\,. \end{aligned} \tag{3.103}$$

□

Relation between the components in two coordinates The Bond matrices are used to describe the relation between the components (3.63) in two coordinate system[10],

$$\tilde{\mathbf{u}} = \mathcal{R}^t\mathbf{u}\,, \qquad \overrightarrow{\tilde{\boldsymbol{\sigma}}} = \mathbf{M}\overrightarrow{\boldsymbol{\sigma}}\,, \qquad \overrightarrow{\tilde{\boldsymbol{\epsilon}}} = \mathbf{M}\overrightarrow{\boldsymbol{\epsilon}} = \mathbf{M}\overrightarrow{\boldsymbol{\epsilon}}\,. \tag{3.106}$$

From this, we obtain the relation,

$$\tilde{\mathbf{q}} = \begin{pmatrix}\overrightarrow{\tilde{\boldsymbol{\epsilon}}}\\ \rho\tilde{\mathbf{u}}\end{pmatrix} = \begin{pmatrix}\overrightarrow{\tilde{\boldsymbol{\epsilon}}}\\ \rho\tilde{\mathbf{u}}\end{pmatrix} = \begin{pmatrix}\mathbf{M}\overrightarrow{\boldsymbol{\epsilon}}\\ \mathcal{R}^t\mathbf{u}\end{pmatrix} = \begin{pmatrix}\mathbf{M} & \mathbf{0}\\ \mathbf{0} & \mathcal{R}^t\end{pmatrix}\mathbf{q}\,, \tag{3.107}$$

and the stiffness tensor in Voigt notation is, cf. (3.7) and (3.10),

$$\overline{\overline{\tilde{C}}} = \mathbf{M}\,\overline{\overline{C}}\,\mathbf{M}^t\,, \qquad {}^\dagger\overline{\overline{\tilde{C}}}^\dagger = \mathbf{N}\,{}^\dagger\overline{\overline{C}}^\dagger\,\mathbf{N}^t = \mathbf{M}^{-t}\,{}^\dagger\overline{\overline{C}}^\dagger\,\mathbf{M}^{-1}. \tag{3.108}$$

[10] This can be seen as follows.

$$\tilde{u}_i := \mathbf{u}\cdot\tilde{\mathbf{e}}_i = \mathbf{u}\cdot\sum_j r_{ji}\mathbf{e}_j = \sum_j r_{ji}\,u_j \quad\Rightarrow\quad \tilde{\boldsymbol{u}} = \mathcal{R}^t\mathbf{u}\,. \tag{3.104}$$

The relation for components of $\boldsymbol{\sigma}$ is as follows,

$$\begin{aligned}\tilde{\sigma}_{\alpha\beta} := \tilde{\mathbf{e}}_\beta\cdot\boldsymbol{\sigma}\cdot\tilde{\mathbf{e}}_\alpha = \left(\sum_i \mathfrak{r}_{i\beta}\mathbf{e}_i\right)\cdot\boldsymbol{\sigma}\cdot\left(\sum_j \mathfrak{r}_{j\alpha}\mathbf{e}_j\right) = \sum_{i,j}\mathfrak{r}_{i\beta}\,\mathfrak{r}_{j\alpha}\mathbf{e}_i\cdot\boldsymbol{\sigma}\cdot\mathbf{e}_j = \sum_{i,j}\mathfrak{r}_{i\beta}\,\mathfrak{r}_{j\alpha}\,\sigma_{ij}\\ \overset{\text{def of}}{=}{}_{\text{contraction}}\;\mathfrak{r}_\beta\otimes\mathfrak{r}_\alpha\;:\;\boldsymbol{\sigma}\;\overset{\text{contract with}}{=}{}_{\text{symmetrix matrix}}\;\mathfrak{r}_\beta\odot\mathfrak{r}_\alpha\;:\;\boldsymbol{\sigma}\;\overset{(3.20)}{=}\;\overrightarrow{\mathfrak{r}_\beta\odot\mathfrak{r}_\alpha}^\dagger\cdot\overrightarrow{\boldsymbol{\sigma}}\,.\end{aligned} \tag{3.105}$$

Finally, recall that matrix A and vectors $\mathbf{u}$, $\mathbf{v}$, with $A\mathbf{u} = \mathbf{v}$ we have $v_i = [RA]_i\cdot A\mathbf{u}$ where $[RA]_i$ is the i-th row vector of matrix A. Since $\overrightarrow{\mathfrak{r}_\beta\odot\mathfrak{r}_\alpha}^\dagger$ is exactly the row vectors of $\mathbf{M}$, the above computation gives $\overrightarrow{\tilde{\boldsymbol{\sigma}}} = \mathbf{M}\overrightarrow{\boldsymbol{\sigma}}$. Bond matrix is also given in [11, p. 11], and [11, Eqn 1.53-1.54] gives the relation between components of $\boldsymbol{\sigma}$ and $\boldsymbol{\epsilon}$ in original and rotated coordinates.

The first expression also gives

$$\overline{\overline{\boldsymbol{C}}} \;=\; \mathbf{M}^{-1}\;\overline{\overline{\tilde{\boldsymbol{C}}}}\,\mathbf{M}^{-t}\,. \tag{3.109}$$

In employing Proposition 4, we also have the following identity:

$$\overline{\overline{\boldsymbol{C}}} \;=\; \mathcal{M}^{\dagger}[\mathcal{R}^t]\;\overline{\overline{\tilde{\boldsymbol{C}}}}\;\left(\mathcal{M}^{\dagger}[\mathcal{R}^t]\right)^t = \mathbf{N}^t\;\overline{\overline{\tilde{\boldsymbol{C}}}}\;\mathbf{N}\,. \tag{3.110}$$

3.5 Elastic isotropy and transverse isotropy

Using the Voigt notation, the elasticity tensor $\boldsymbol{C}$ can be represented as a six-by-six matrix $\overline{\overline{\boldsymbol{C}}}$. With the elasticity tensor symmetric, it leads to 21 independent coefficients, [11]. Nonetheless, its structure can be simplified depending on the assumption on the medium, and we consider here elastic isotropy, vertical transverse isotropy (VTI), and tilted transverse isotropy (TTI).

3.5.1 Isotropic elasticity

• The stiffness tensor for an isotropic elastic material has the following form,

$$\boldsymbol{C}_{\rm iso} = (c_{ijkl})\,, \quad \text{with } c_{ijkl} \;=\; \mu\,(\delta_{ik}\,\delta_{jl} \;+\; \delta_{il}\,\delta_{jk}) \;+\; \lambda\,\delta_{ij}\,\delta_{kl}\,; \tag{3.111a}$$

$$\boldsymbol{S}_{\rm iso} = (s_{ijkl})\,, \quad \text{with } s_{ijkl} \;=\; \frac{1}{4\mu}\;(\delta_{ik}\,\delta_{jl} \;+\; \delta_{il}\,\delta_{jk}) - \frac{\lambda}{2\mu(3\lambda+2\mu)}\delta_{ij}\,\delta_{kl}\,. \tag{3.111b}$$

Here the two degrees of freedom are given by Lamé parameters λ and μ. They can also be defined in terms of the equivalent set of parameters: the Young modulus E and Poisson coefficient (ratio) defined as,

$$E := \frac{(3\lambda+2\mu)\mu}{\lambda+\mu}\,, \qquad \nu := \frac{\lambda}{2(\lambda+\mu)} \quad \Rightarrow \quad \frac{\nu}{E} = \frac{\lambda}{2\mu(3\lambda+2\mu)}\,. \tag{3.112}$$

Introduce the P- and S-wave speed, which we see below related to the eigenvalues of the KC matrix,

$$\mathrm{c_P} \;=\; \sqrt{\frac{\lambda+2\mu}{\rho}}\,, \qquad \mathrm{c_S} \;=\; \sqrt{\frac{\mu}{\rho}}\,. \tag{3.113}$$

• The constitutive law (2.8b) simplifies under linear isotropy as,

$$\boldsymbol{\sigma}(\mathbf{x},\omega) \;=\; \lambda(\mathbf{x})\,\mathrm{Tr}\left(\boldsymbol{\epsilon}(\mathbf{x},\omega)\right)\mathbb{Id} \;+\; 2\,\mu(\mathbf{x})\,\boldsymbol{\epsilon}(\mathbf{x},\omega), \quad \text{elastic isotropy}\,, \tag{3.114}$$

where Tr denotes the trace and $\mathbb{Id}$ the identity matrix.

• By identification, (3.7), their Voigt representations are,

$$\overline{\overline{\boldsymbol{C}}}_{\rm iso} = \begin{pmatrix} \lambda{+}2\mu & \lambda & \lambda & 0 & 0 & 0 \\ \lambda & \lambda{+}2\mu & \lambda & 0 & 0 & 0 \\ \lambda & \lambda & \lambda{+}2\mu & 0 & 0 & 0 \\ 0 & 0 & 0 & \mu & 0 & 0 \\ 0 & 0 & 0 & 0 & \mu & 0 \\ 0 & 0 & 0 & 0 & 0 & \mu \end{pmatrix}, \qquad \overline{\overline{\boldsymbol{S}}}_{\rm iso} = \begin{pmatrix} \frac{1}{E} & -\frac{\nu}{E} & -\frac{\nu}{E} & 0 & 0 & 0 \\ -\frac{\nu}{E} & \frac{1}{E} & -\frac{\nu}{E} & 0 & 0 & 0 \\ -\frac{\nu}{E} & -\frac{\nu}{E} & \frac{1}{E} & 0 & 0 & 0 \\ 0 & 0 & 0 & \frac{1}{4\mu} & 0 & 0 \\ 0 & 0 & 0 & 0 & \frac{1}{4\mu} & 0 \\ 0 & 0 & 0 & 0 & 0 & \frac{1}{4\mu} \end{pmatrix}, \tag{3.115}$$

By direct calculation, we note that $\overline{\overline{\boldsymbol{C}}}_{\rm iso}$ and $\overline{\overline{\boldsymbol{S}}}_{\rm iso}$ satisfy relation (3.55), with the upper left 3×3 block of $\overline{\overline{\boldsymbol{S}}}_{\rm iso}$ being the inverse of that of $\overline{\overline{\boldsymbol{C}}}_{\rm iso}$.

Proposition 6 (Kelvin–Christoffel matrix for linear isotropy)**.** *Under linear isotropy, the Kelvin–Christoffel matrix* $\boldsymbol{\Gamma}_{\rm iso}(\boldsymbol{\nu})$ *is,*

$$\boldsymbol{\Gamma}_{\rm iso}(\boldsymbol{\nu}) = \mu\mathbb{Id} + (\lambda+\mu)\boldsymbol{\nu}\otimes\boldsymbol{\nu} = \rho\left(\mathrm{c_S^2}\mathbb{Id} + (\mathrm{c_P^2}-\mathrm{c_S^2})\boldsymbol{\nu}\otimes\boldsymbol{\nu}\right)\,. \tag{3.116}$$

Its eigenvalues are $\mu = \rho\mathrm{c_S^2}$ *of multiplicity 2, and* $\lambda+\mu = \rho\mathrm{c_P^2}$ *of multiplicity 1. Additionally, their values are independent of direction* $\boldsymbol{\nu}$*.*

Proof (version 1). We start from the action of isotropic stiffness tensor,

$$\boldsymbol{C}_{\rm iso}\boldsymbol{\gamma} = 2\mu\boldsymbol{\gamma} + \lambda(\mathrm{tr}\,\boldsymbol{\gamma})\mathbb{1}_{\mathbb{d}}\,. \tag{3.117}$$

For symmetric $\boldsymbol{\gamma} = \mathbf{v}\odot\mathbf{w}$, we have

$$\boldsymbol{C}_{\rm iso}\mathbf{v}\odot\mathbf{w} \;=\; 2\mu\,\mathbf{v}\odot\mathbf{w} \;+\; \lambda(\mathbf{v}\cdot\mathbf{w})\mathbb{1}_{\mathbb{d}}\,, \tag{3.118}$$

We have

$$\boldsymbol{C}_{\rm iso}\,\mathbf{e}_J\odot\boldsymbol{\nu} \;=\; 2\mu\,\mathbf{e}_J\odot\boldsymbol{\nu} + \lambda\nu_J\mathbb{1}_{\mathbb{d}} \quad\Rightarrow\quad (\boldsymbol{C}_{\rm iso}\,\mathbf{e}_I\odot\boldsymbol{\nu})\cdot\boldsymbol{\nu} = \mu(\boldsymbol{\nu}\nu_J + \mathbf{e}_J) + \lambda\nu_J\boldsymbol{\nu}. \tag{3.119}$$

Using (3.49b), this gives,

$$\begin{aligned}[\boldsymbol{\Gamma}(\boldsymbol{\nu})]_{IJ} \;&=\; \mathbf{e}_I\cdot(\boldsymbol{C}_{\rm iso}(\mathbf{e}_J\odot\boldsymbol{\nu}))\cdot\boldsymbol{\nu}\\ &=\; \mu(\nu_I\nu_J+\delta_{IJ}) + \lambda\nu_I\nu_J = \mu\delta_{IJ} + (\mu+\lambda)\nu_I\nu_J\,.\end{aligned} \tag{3.120}$$

□

Proof (version 2). We can also work with identity (3.42) to obtain the expression for the KC matrix. The whole matrix is then defined in terms of matrix-matrix product and matrix-vector product, by using the expression in Voigt notation of the stiffness tensor, cf. (3.115) and recall definition of $\mathbb{A}(\boldsymbol{\nu})$ in (3.13), and its explicit expression is

$$\frac{\boldsymbol{\Gamma}(\boldsymbol{\nu})}{\rho} = \frac{1}{\rho}\begin{pmatrix} (\lambda{+}2\mu)\nu_x & \lambda\nu_x & \lambda\nu_x & 0 & 2\mu\nu_z & 2\mu\nu_y\\ \lambda\nu_y & (\lambda{+}2\mu)\nu_y & \lambda\nu_y & 2\mu\nu_z & 0 & 2\mu\nu_x\\ \lambda\nu_z & \lambda\nu_z & (\lambda{+}2\mu)\nu_z & 2\mu\nu_y & 2\mu\nu_x & 0\end{pmatrix}\begin{pmatrix}\nu_x & 0 & 0\\ 0 & \nu_y & 0\\ 0 & 0 & \nu_z\\ 0 & \frac{\nu_z}{2} & \frac{\nu_y}{2}\\ \frac{\nu_z}{2} & 0 & \frac{\nu_x}{2}\\ \frac{\nu_y}{2} & \frac{\nu_x}{2} & 0\end{pmatrix}. \tag{3.121}$$

Note that $\lambda+\mu = \lambda+2\mu-\mu = \rho(\mathrm{c}_{\rm P}^2-\mathrm{c}_{\rm S}^2)$ using (3.113), hence,

$$\frac{\boldsymbol{\Gamma}(\boldsymbol{\nu})}{\rho} = \begin{pmatrix} \mathrm{c}_{\rm P}^2\nu_x^2 + \mathrm{c}_{\rm S}^2\left(\nu_y^2+\nu_z^2\right) & \left(\mathrm{c}_{\rm P}^2-\mathrm{c}_{\rm S}^2\right)\nu_x\nu_y & \left(\mathrm{c}_{\rm P}^2-\mathrm{c}_{\rm S}^2\right)\nu_x\nu_z\\ \left(\mathrm{c}_{\rm P}^2-\mathrm{c}_{\rm S}^2\right)\nu_x\nu_y & \mathrm{c}_{\rm P}^2\nu_y^2 + \mathrm{c}_{\rm S}^2\left(\nu_x^2+\nu_z^2\right) & \left(\mathrm{c}_{\rm P}^2-\mathrm{c}_{\rm S}^2\right)\nu_y\nu_z\\ \left(\mathrm{c}_{\rm P}^2-\mathrm{c}_{\rm S}^2\right)\nu_x\nu_z & \left(\mathrm{c}_{\rm P}^2-\mathrm{c}_{\rm S}^2\right)\nu_y\nu_z & \mathrm{c}_{\rm P}^2\nu_z^2 + \mathrm{c}_{\rm S}^2\left(\nu_y^2+\nu_x^2\right)\end{pmatrix}. \tag{3.122}$$

By writing the diagonal as, e.g., $\mathrm{c}_{\rm P}^2\nu_x^2 + \mathrm{c}_{\rm S}^2\left(\nu_y^2+\nu_z^2\right) = (\mathrm{c}_{\rm P}^2-\mathrm{c}_{\rm S}^2)\nu_x^2 + \mathrm{c}_{\rm S}^2|\boldsymbol{\nu}|^2$, we have

$$\frac{\boldsymbol{\Gamma}(\boldsymbol{\nu})}{\rho} = \mathrm{c}_{\rm S}^2|\boldsymbol{\nu}|^2\,\mathbb{1}_{\mathbb{d}} \;+\; (\mathrm{c}_{\rm P}^2-\mathrm{c}_{\rm S}^2)\begin{pmatrix}\nu_x^2 & \nu_x\nu_y & \nu_x\nu_z\\ \nu_x\nu_y & \nu_y^2 & \nu_y\nu_z\\ \nu_x\nu_z & \nu_y\nu_z & \nu_z^2\end{pmatrix} = \mathrm{c}_{\rm S}^2|\boldsymbol{\nu}|^2\,\mathbb{1}_{\mathbb{d}} \;+\; (\mathrm{c}_{\rm P}^2-\mathrm{c}_{\rm S}^2)\,\boldsymbol{\nu}\otimes\boldsymbol{\nu}\,.$$

□

3.5.2 Vertical transverse isotropy (VTI)

Vertical transverse isotropy (VTI) refers to the family of linear elastic materials that are rotational symmetric around $\mathbf{e}_z$. Their stiffness tensor in Voigt representation is given with five independent coefficients, cf. [11, Equation (1.39) in Subsection 1.2.1],

$$\overline{\overline{\boldsymbol{C}}}_{\rm VTI} \;=\; \begin{pmatrix} c_{11} & c_{11}-2c_{66} & c_{13} & 0 & 0 & 0\\ c_{11}-2c_{66} & c_{11} & c_{13} & 0 & 0 & 0\\ c_{13} & c_{13} & c_{33} & 0 & 0 & 0\\ 0 & 0 & 0 & c_{44} & 0 & 0\\ 0 & 0 & 0 & 0 & c_{44} & 0\\ 0 & 0 & 0 & 0 & 0 & c_{66}\end{pmatrix}. \tag{3.123}$$

Positive definiteness of $\mathbf{C}$ requires that

$$c_{11} > |c_{12}|\,, \quad (c_{11}+c_{12})\,c_{33} \;>\; 2\,c_{13}^2\,, \quad c_{55} > 0\,. \tag{3.124}$$

A description of planewaves sustained in VTI materials is further given in Appendix A.

Thomsen's parametrization of VTI As an alternative to prescribing directly the values of c_{ij}, VTI material can also be described in terms of the (unitless) Thomsen's parameters [54], which quantify more clearly the level of anisotropy in a VTI material. Their definitions in terms of components of stiffness tensor are:

$$\alpha_0 = \sqrt{c_{33}/\rho}\,, \qquad \text{vertical P-wave speed}\,, \tag{3.125a}$$

$$\beta_0 = \sqrt{c_{55}/\rho}\,, \qquad \text{vertical (or horizontal) S-wave speed}\,, \tag{3.125b}$$

$$\epsilon = \frac{c_{11}-c_{33}}{2c_{33}}\,, \tag{3.125c}$$

$$\delta = \frac{\big(c_{13}+c_{44}\big)^2 - \big(c_{33}-c_{44}\big)^2}{2c_{33}\big(c_{33}-c_{44}\big)}\,, \tag{3.125d}$$

$$\gamma = \frac{c_{66}-c_{44}}{2c_{44}}\,. \tag{3.125e}$$

The planewave analysis and Remark 13 in Appendix A explain the meaning of parameters α_0 and β_0, which are speeds of true P- and S-planewaves propagating along vertical axis $\mathbf{e}_z$. To encode this significance, we can represent α_0 and β_0 with λ^{TI} and μ^{TI}, called here TI-Lamé parameters,

$$c_{33} = \lambda^{\mathrm{TI}} + 2\mu^{\mathrm{TI}}\,, \quad c_{55} = \mu^{\mathrm{TI}}\,, \quad \text{equivalently} \quad \alpha_0 = \sqrt{\frac{\mu^{\mathrm{TI}}}{\rho}}\,, \quad \beta_0 = \sqrt{\frac{\lambda^{\mathrm{TI}}+2\mu^{\mathrm{TI}}}{\rho}}\,. \tag{3.126}$$

In short, the Thomsen's parametrization can be given in terms of

$$(\rho\,;\,\alpha_0\,,\,\beta_0\,,\,\epsilon\,,\,\delta\,,\,\gamma)\,, \qquad \text{or equivalently} \quad (\rho\,;\,\lambda^{\mathrm{TI}}\,,\,\mu^{\mathrm{TI}}\,,\,\epsilon\,,\,\delta\,,\,\gamma)\,. \tag{3.127}$$

Conversely, given a set of TI-Lamé and Thomsen's parameters $(\rho;\lambda^{\mathrm{TI}},\mu^{\mathrm{TI}},\epsilon,\delta,\gamma)$, the components of stiffness tensor can be retrieved as follows,

$$c_{11} = (\lambda^{\mathrm{TI}}+2\mu^{\mathrm{TI}})\,(1+2\epsilon)\,, \tag{3.128a}$$

$$c_{33} = \lambda^{\mathrm{TI}}+2\mu^{\mathrm{TI}}\,, \tag{3.128b}$$

$$c_{44} = c_{55} = \mu^{\mathrm{TI}}\,, \tag{3.128c}$$

$$c_{66} = \mu^{\mathrm{TI}}\,(1+2\gamma^{\mathrm{TI}})\,, \tag{3.128d}$$

$$c_{13} = -\mu^{\mathrm{TI}} + \sqrt{(\lambda^{\mathrm{TI}}+\mu^{\mathrm{TI}})^2 + 2\delta(\lambda^{\mathrm{TI}}+2\mu^{\mathrm{TI}})(\lambda^{\mathrm{TI}}+\mu^{\mathrm{TI}})}\,, \tag{3.128e}$$

See Remark 5 below regarding the choice of sign for c_{13}.

Remark 4. *In isotropy, we have $c_{11} = c_{33}$, $c_{66} = c_{44}$ and $c_{13}+c_{44} = c_{33}-c_{44}$. This means that $\epsilon = \delta = \gamma = 0$, and VTI reduces to isotropy. In another word, the deviation of ϵ, δ and γ from zero indicates the deviation from isotropy, that is, the level of anisotropy. We further note the following case of anisotropy:*

$$\begin{aligned} \textit{Weak anisotropy}: &\quad |\epsilon|, |\delta|, |\gamma| < 0.2\,, \\ \textit{Elliptical anisotropy}: &\quad \epsilon = \delta\,. \end{aligned} \tag{3.129}$$

Remark 5. *Expression (3.128) for c_{13} is obtained by solving the quadratic relation (3.125) with a choice of sign so that when $\delta = 0$, one can retrieve isotropy, specifically, $c_{13} = \lambda^{\mathrm{TI}}$ when $\delta = 0$.*

The Kelvin–Christoffel matrix for VTI material is obtained from Proposition 3 by replacing the expression of the stiffness tensor with its VTI form (3.123).

Proposition 7. *For a VTI medium, the Kelvin–Christoffel matrix $\mathbf{\Gamma}_{\mathrm{VTI}}(\boldsymbol{\nu})$ is given in symmetric matrix form as*

$$\mathbf{\Gamma}_{\mathrm{VTI}}(\boldsymbol{\nu}) = \begin{pmatrix} c_{11}\,\nu_x^2 + c_{66}\,\nu_y^2 + c_{55}\,\nu_z^2 & (c_{13}+c_{55})\nu_y\nu_z & (c_{13}+c_{55})\,\nu_x\nu_z \\ & c_{66}\nu_x^2 + c_{11}\,\nu_y^2 + c_{55}\,\nu_z^2 & (c_{11}-c_{66})\,\nu_x\,\nu_y \\ & & c_{55}(\nu_x^2+\nu_y^2) + c_{33}\,\nu_z^2 \end{pmatrix}, \tag{3.130}$$

and in form of a matrix-vector product as,

$$\overrightarrow{\boldsymbol{\Gamma}_{\mathrm{VTI}}(\boldsymbol{\nu})} = \begin{pmatrix} c_{11} & c_{66} & c_{55} & 0 & 0 & 0 \\ c_{66} & c_{11} & c_{55} & 0 & 0 & 0 \\ c_{55} & c_{55} & c_{33} & 0 & 0 & 0 \\ 0 & 0 & 0 & 0 & 0 & \frac{c_{11}-c_{66}}{2} \\ 0 & 0 & 0 & 0 & \frac{c_{13}+c_{55}}{2} & 0 \\ 0 & 0 & 0 & \frac{c_{55}+c_{13}}{2} & 0 & 0 \end{pmatrix} \overrightarrow{\boldsymbol{\nu} \odot \boldsymbol{\nu}}^{\dagger} . \tag{3.131}$$

3.5.3 Tilted transverse isotropy (TTI)

Tilted transverse isotropy is the name for linear elastic material having rotational symmetry around an axis, denoted by unit vert $\mathbf{e}_{\mathrm{TIsym}}$, which is not parallel to $\mathbf{e}_z$. TTI is related to VTI by rotation. This means that by a rotation so that $\mathbf{e}_z$ points in the same direction as $\mathbf{e}_{\mathrm{TIsym}}$, the stiffness tensor in the rotated coordinates takes the structure of a VTI tensor in the rotated coordinates. Denote by $\mathbf{C}_{\mathrm{TTI}}$ the stiffness tensor of a TTI medium.

– Representation in Cartesian coordinates: by abuse of notation, we also denote by $\mathbf{C}_{\mathrm{TTI}}$ the tensor whose components are the coefficients of $\mathbf{C}_{\mathrm{TTI}}$ in Cartesian coordinates. Use this to denote its Voigt representation and tensor form,

$$\mathbf{C}_{\mathrm{TTI}} = \left(\mathsf{c}^{\mathrm{TTI}}_{ijkl}\right)_{i,j,k,l=1}^{3} , \qquad \overline{\overline{\mathbf{C}}}_{\mathrm{TTI}} \tag{3.132}$$

– Representation in rotated coordinates: we denote by $(\mathbf{e}_{\tilde{x}}, \mathbf{e}_{\tilde{y}}, \mathbf{e}_{\tilde{z}})$ the coordinates after rotation. The components in rotated coordinates are denoted by, cf. (3.137)

$$\overline{\overline{\tilde{\mathbf{C}}}} = \left(\tilde{\mathsf{c}}_{ijkl}\right)_{i,j,k,l=1}^{3} , \qquad \overline{\overline{\tilde{\mathbf{C}}}} . \tag{3.133}$$

Their relation is given by identity (3.110), which will be exploited to compute the quantity in (3.132) from their VTI structure cf. (3.137) in rotated coordinates.

θ-TI Suppose the rotational symmetry axis in $(\mathbf{e}_x, \mathbf{e}_z)$ is

$$\mathbf{e}_{\mathrm{TIsym}} = \begin{pmatrix} \sin\theta \\ 0 \\ \cos\theta \end{pmatrix} , \quad -\pi \le \theta \le \pi . \tag{3.134}$$

The Cartesian basis is rotated to,

$$\mathbf{e}_{\tilde{x}} = \begin{pmatrix} \cos\theta \\ 0 \\ -\sin\theta \end{pmatrix} , \quad \mathbf{e}_{\tilde{y}} = \mathbf{e}_y = \begin{pmatrix} 0 \\ 1 \\ 0 \end{pmatrix} , \quad \mathbf{e}_{\tilde{z}} = \mathbf{e}_{\mathrm{TIsym}} = \begin{pmatrix} \sin\theta \\ 0 \\ \cos\theta \end{pmatrix} . \tag{3.135}$$

Note the above vectors are described in Cartesian coordinates. Define

$$\begin{aligned} \mathcal{R}_\theta &:= \left(\mathbf{e}_{\tilde{x}}, \mathbf{e}_{\tilde{y}}, \mathbf{e}_{\tilde{z}}\right) = \begin{pmatrix} \cos\beta & 0 & \sin\theta \\ 0 & 1 & 0 \\ -\sin\beta & 0 & \cos\theta \end{pmatrix} , \\ \mathcal{R}_\theta^t &:= \mathcal{R}_\theta^{-1} = \mathcal{R}_{-\theta} = \begin{pmatrix} \cos\theta & 0 & -\sin\theta \\ 0 & 1 & 0 \\ \sin\theta & 0 & \cos\theta \end{pmatrix} . \end{aligned} \tag{3.136}$$

In coordinates with axes $(\mathbf{e}_{\tilde{x}}, \mathbf{e}_{\tilde{y}}, \mathbf{e}_{\tilde{z}})$, the Voigt representation of the stiffness tensor of θ-TI takes the form of a VTI tensor,

$$\overline{\overline{\tilde{\mathbf{C}}}} = \begin{pmatrix} \tilde{\mathsf{c}}_{11} & \tilde{\mathsf{c}}_{11} - 2\tilde{\mathsf{c}}_{66} & \tilde{\mathsf{c}}_{13} & 0 & 0 & 0 \\ \tilde{\mathsf{c}}_{21} & \tilde{\mathsf{c}}_{11} & \tilde{\mathsf{c}}_{13} & 0 & 0 & 0 \\ \tilde{\mathsf{c}}_{13} & \tilde{\mathsf{c}}_{13} & \tilde{\mathsf{c}}_{33} & 0 & 0 & 0 \\ 0 & 0 & 0 & \tilde{\mathsf{c}}_{44} & 0 & 0 \\ 0 & 0 & 0 & 0 & \tilde{\mathsf{c}}_{44} & 0 \\ 0 & 0 & 0 & 0 & 0 & \tilde{\mathsf{c}}_{66} \end{pmatrix} . \tag{3.137}$$

In using identity (3.110), the θ-TI stiffness tensor in Voigt representation in Cartesian coordinates is given by,

$$\overline{\overline{\mathbf{C}}}_{\theta\mathrm{TI}} := \mathbf{M}_\theta \, \overline{\overline{\tilde{\mathbf{C}}}} \, \mathbf{M}_\theta^t , \quad \text{with } \mathbf{M}_\theta := \mathcal{M}^\dagger[\mathcal{R}_\theta^t] \quad \text{and} \quad \overline{\overline{\tilde{\mathbf{C}}}} \text{ given in (3.137)} . \tag{3.138}$$

Recall from its definition $\mathcal{M}^\dagger$ in (3.65), $\mathbf{M}_y(\theta)$ is defined with the columns of $\mathcal{R}_\theta^t$ (equivalently the rows of $\mathcal{R}(\beta)$),

$$\mathbf{M}_\beta := \mathcal{M}^\dagger[\mathcal{R}_\beta^t] = \begin{pmatrix} \left(\overrightarrow{\mathfrak{r}_1 \odot \mathfrak{r}_1}^\dagger\right)^t \\ \left(\overrightarrow{\mathfrak{r}_2 \odot \mathfrak{r}_2}^\dagger\right)^t \\ \left(\overrightarrow{\mathfrak{r}_3 \odot \mathfrak{r}_3}^\dagger\right)^t \\ \left(\overrightarrow{\mathfrak{r}_2 \odot \mathfrak{r}_3}^\dagger\right)^t \\ \left(\overrightarrow{\mathfrak{r}_1 \odot \mathfrak{r}_3}^\dagger\right)^t \\ \left(\overrightarrow{\mathfrak{r}_1 \odot \mathfrak{r}_2}^\dagger\right)^t \end{pmatrix} , \quad \text{with} \quad \mathfrak{r}_1 = \begin{pmatrix} \cos\theta \\ 0 \\ \sin\theta \end{pmatrix} , \ \mathfrak{r}_2 = \begin{pmatrix} 0 \\ 1 \\ 0 \end{pmatrix} , \ \mathfrak{r}_3 = \begin{pmatrix} -\sin\theta \\ 0 \\ \cos\theta \end{pmatrix} . \tag{3.139}$$

In expanding out components of the row vectors, we retrieve the same matrix as in [11, Equation (1.195)],

$$\mathbf{M}_\beta = \begin{pmatrix} \cos^2\theta & 0 & \sin^2\theta & 0 & \sin(2\theta) & 0 \\ 0 & 1 & 0 & 0 & 0 & 0 \\ \sin^2\theta & 0 & \cos^2\theta & 0 & -\sin(2\theta) & 0 \\ 0 & 0 & 0 & \cos\theta & 0 & -\sin\theta \\ -\frac{1}{2}\sin(2\theta) & 0 & \frac{1}{2}\sin(2\theta) & 0 & \cos(2\theta) & 0 \\ 0 & 0 & 0 & 0 & 0 & \cos\theta \end{pmatrix} . \tag{3.140}$$

Remark 6. *Equations (3.138) and (3.140) also agree with [11] in using equations (1.58) and (1.195). When $\beta = \frac{\pi}{2}$, we obtain the Horizontal Transverse Isotropy (HTI) tensor, [11].*

General Transverse Isotropy Suppose the rotational symmetry axis is in Cartesian coordinates

$$\mathbf{e}_{\mathrm{TIsym}} = \begin{pmatrix} \sin\theta\cos\phi \\ \sin\theta\sin\phi \\ \cos\theta \end{pmatrix} \tag{3.141}$$

The Cartesian basis is rotated to

$$\mathbf{e}_{\tilde{x}} = \begin{pmatrix} \cos\theta\cos\phi \\ \cos\theta\sin\phi \\ -\sin\theta \end{pmatrix} , \quad \mathbf{e}_{\tilde{y}} = \begin{pmatrix} -\sin\phi \\ \cos\phi \\ 0 \end{pmatrix} , \quad \mathbf{e}_{\tilde{z}} = \mathbf{e}_{\mathrm{TIsym}} = \begin{pmatrix} \sin\theta\cos\phi \\ \sin\theta\sin\phi \\ \cos\theta \end{pmatrix} . \tag{3.142}$$

Define

$$\begin{aligned} \mathcal{R}_{\theta,\phi} &:= \left(\mathbf{e}_{\tilde{x}}, \mathbf{e}_{\tilde{y}}, \mathbf{e}_{\tilde{z}}\right) = \begin{pmatrix} \cos\theta\cos\phi & -\sin\phi & \sin\theta\cos\phi \\ \cos\theta\sin\phi & \cos\phi & \sin\theta\sin\phi \\ -\sin\theta & 0 & \cos\theta \end{pmatrix} , \\ \mathcal{R}_{\theta,\phi}^t &:= \mathcal{R}_{-\theta,-\phi} = \mathcal{R}_{\theta,\phi}^t = \begin{pmatrix} \cos\theta\cos\phi & \cos\theta\sin\phi & -\sin\theta \\ -\sin\phi & \cos\phi & 0 \\ \sin\theta\cos\phi & \sin\theta\sin\phi & \cos\theta \end{pmatrix} . \end{aligned} \tag{3.143}$$

In Cartesian coordinates, the Voigt representation of a TTI stiffness tensor is given using identity (3.110), now with $\mathbf{M}_{\theta,\phi}$ defined in (3.65) with the columns of $\mathcal{R}^t_{\theta,\phi}$ (i.e., rows of $\mathcal{R}_{\theta,\phi}$),

$$\mathbf{M}_{\theta,\phi} := \mathcal{M}^\dagger[\mathcal{R}^t_{\theta,\phi}] = \begin{pmatrix} \left(\overrightarrow{\mathfrak{r}_1 \odot \mathfrak{r}_1}^\dagger\right)^t \\ \left(\overrightarrow{\mathfrak{r}_2 \odot \mathfrak{r}_2}^\dagger\right)^t \\ \left(\overrightarrow{\mathfrak{r}_3 \odot \mathfrak{r}_3}^\dagger\right)^t \\ \left(\overrightarrow{\mathfrak{r}_2 \odot \mathfrak{r}_3}^\dagger\right)^t \\ \left(\overrightarrow{\mathfrak{r}_1 \odot \mathfrak{r}_3}^\dagger\right)^t \\ \left(\overrightarrow{\mathfrak{r}_1 \odot \mathfrak{r}_2}^\dagger\right)^t \end{pmatrix}, \text{ with } \quad \mathfrak{r}_1 = \begin{pmatrix} \cos\theta\cos\phi \\ -\sin\phi \\ \sin\theta\cos\phi \end{pmatrix}, \ \mathfrak{r}_2 = \begin{pmatrix} \cos\theta\sin\phi \\ \cos\phi \\ \sin\theta\sin\phi \end{pmatrix}, \ \mathfrak{r}_3 = \begin{pmatrix} -\sin\theta \\ 0 \\ \cos\theta \end{pmatrix}. \tag{3.144}$$

We summarize the results in the following proposition.

Proposition 8. *The components in Cartesian coordinates of a TTI stiffness tensor* $\mathbf{C}_{\text{TTI}}$ *with rotational axis symmetry* $\mathbf{e}_{\text{TIsym}} = (\sin\theta\cos\phi\,,\, \sin\theta\sin\phi\,,\, \cos\theta)^t$*, are given as follows.*

– *With* $\mathbf{M}_{\theta,\phi}$ *defined in* (3.144) *and* $\tilde{\overline{\overline{\mathbf{C}}}}$ *in* (3.137)*, its Voigt representation is,*

$$\overline{\overline{\mathbf{C}}}_{\text{TTI}} = \mathbf{M}_{\theta,\phi}\, \tilde{\overline{\overline{\mathbf{C}}}}\, \mathbf{M}^t_{\theta,\phi}\,. \tag{3.145}$$

– *Equivalently, with* r_{ij} *denoting the components of rotation matrix* $\mathcal{R}^t_{\theta,\phi} = (\mathsf{r}_{ij})_{i,j=1,2,3}$*, components of its form as a fourth-order tensor is*

$$\mathsf{c}^{\text{TTI}}_{ijkl} = \sum_{p,q,r,s=1}^{3} \mathsf{r}_{ip}\,\mathsf{r}_{jq}\,\mathsf{r}_{kr}\,\mathsf{r}_{lr}\,\tilde{\mathsf{c}}^{\text{VTI}}_{pqrs}\,. \tag{3.146}$$

Proof. It remains to prove identity (3.146). Under Voigt representation (3.7),

$$[\overline{\overline{\mathbf{C}}}_{\text{TTI}}]_{IJ} = \mathsf{c}^{\text{TTI}}_{ijkl}\,, \tag{3.147}$$

with identification $(i,j) \leftrightarrow I$ and $(k,l) \leftrightarrow J$ under (3.3). By the definition $\mathbf{M}_{\theta,\phi}$, if we denote by $\mathbf{v}_I$ the I-th row vector of $\mathbf{M}_{\theta,\phi}$, and by $\tilde{\mathbf{v}}_J$ J-th column of its transpose, i.e. equivalently, J-th row vector of $\mathbf{M}_{\theta,\phi}$, then

$$\mathbf{v}_I = \overrightarrow{\mathfrak{r}_i \odot \mathfrak{r}_j}^\dagger\,, \quad \mathbf{v}_J = \overrightarrow{\mathfrak{r}_k \odot \mathfrak{r}_l}^\dagger\,. \tag{3.148}$$

We start with the expression given by the left-hand-side of (3.145),

$$\begin{aligned} [\overline{\overline{\mathbf{C}}}_{\text{TTI}}]_{IJ} &\overset{(3.145)}{=} \mathbf{v}_I \cdot \tilde{\overline{\overline{\mathbf{C}}}} \cdot \tilde{\mathbf{v}}_J \;=\; \overrightarrow{\mathfrak{r}_i \odot \mathfrak{r}_j}^\dagger \cdot \tilde{\overline{\overline{\mathbf{C}}}} \cdot \overrightarrow{\mathfrak{r}_k \odot \mathfrak{r}_l}^\dagger \\ &\overset{(3.22)}{=} \mathfrak{r}_i \odot \mathfrak{r}_j \,:\, \tilde{\mathbf{C}} \,:\, \mathfrak{r}_j \odot \mathfrak{r}_l \;=\; \text{lhs of (3.146)}\,. \end{aligned} \tag{3.149}$$

This combined with (3.147) gives identity (3.146).

□

4 Discretization of HDG problem

In this section, we give a complete description of the HDG discretization for the elastic problem (2.36) and (2.39) for the formulation $(\mathbf{u},\boldsymbol{\sigma})_{\boldsymbol{S}}$ with unknowns $(\mathbf{u}^h, \boldsymbol{\sigma}^h, \boldsymbol{\lambda}_{\mathbf{u}h})$, the formulation $(\mathbf{v},\boldsymbol{\sigma})_{\boldsymbol{S}}$ follows the same step, see Remark 8. In the HDG method, the numerical flux plays the role of the global unknown. Here, we obtain linear systems which are satisfied by the coefficients of these unknowns with respect to the chosen basis for the local function spaces U_h, V_h and M_h introduced in (2.24). The matrix form of the local and global systems will employ Voigt formalism developed in Section 3. This helps exploit the block structure of the system, and enables matrixification and optimization of the direct solver.

4.1 Notations

Local and global indexes of an edge We recall from the initial discussion in Subsection 2.3, $|\Sigma_h|$ is the number of faces in the mesh and $|\mathcal{T}_h|$ is the number of elements in the mesh. An edge $\mathsf{F} \in \Sigma_h$ can be referred to in two ways,

1. as F^k, with $1 \leq k \leq |\Sigma_h|$, here k is the index of the face in the ordered set Σ_h,
2. as $\mathsf{F}^{(e,\ell)}$ with $1 \leq e \leq |\mathcal{T}_h|$, $1 \leq \ell \leq \mathsf{n}^e_{\text{face}}$, when it is considered as part of the boundary of an element K^e, and ℓ is its index among the set of faces of K^e. Note that $\mathsf{n}^e_{\text{face}}$ is the number of edges in element K^e, for instance four with a tetrahedron.

We denote by $\mathfrak{f}$ the mapping which relates these local and global labels of an edge:

$$\mathfrak{f} \quad : \quad (e,\ell) \qquad \mapsto \quad k = \mathfrak{f}(e,\ell)\,, \quad \text{where} \quad \mathsf{F}^{(e,\ell)} = \mathsf{F}^k\,. \tag{4.1}$$

Local Basis functions We have three groups of basis functions for the local finite element spaces introduced in (2.24),

$$\begin{aligned} &\text{basis functions for } U_h(K^e),\ 1 \leq e \leq |\mathcal{T}_h| \quad : \quad \phi^e_j\,, \quad 1 \leq j \leq \mathsf{n}_e\,,; \\ &\text{basis functions for } V_h(K^e),\ 1 \leq e \leq |\mathcal{T}_h| \quad : \quad \psi^e_j\,, \quad 1 \leq j \leq \mathsf{m}_e\,, \\ &\text{basis functions for } M_h(\mathsf{F}^k),\ 1 \leq k \leq |\Sigma_h| \quad : \quad \xi^k_j\,, \quad 1 \leq j \leq \hat{\mathsf{n}}_k\,. \end{aligned} \tag{4.2}$$

We have denoted by

$$\mathsf{n}_e : \text{dimension of basis of } U_h(K^e)\,; \tag{4.3}$$

$$\mathsf{m}_e : \text{dimension of basis of } V_h(K^e)\,; \tag{4.4}$$

$$\hat{\mathsf{n}}_k \ = \ \hat{\mathsf{n}}_{(e,\ell)} : \text{dimension of basis of } M_h(\mathsf{F}^k) = M_h(\mathsf{F}^{(e,\ell)})\,. \tag{4.5}$$

Also denote the total number of face degrees of freedom in each direction I by,

$$\hat{\mathrm{n}}_I = \hat{\mathrm{n}} = \sum_{k=1}^{|\Sigma_h|} \hat{\mathsf{n}}_k\,. \tag{4.6}$$

Volume discrete unknowns With formulation $(\mathbf{u},\boldsymbol{\sigma})_{\boldsymbol{S}}$, the volume unknowns are the approximations of the displacement vector field $\mathbf{u}$ and of strain tensor $\boldsymbol{\sigma}$ on each cell K^e, $1 \leq e \leq |\mathcal{T}_h|$. For the displacement we have,

$$\mathbf{u}^h = \sum_{\alpha=x,y,z} u^h_I\ \hat{\mathbf{e}}_I\,, \quad \text{with} \quad u^h_I\big|_{K^e} = \sum_{j=1}^{\mathsf{n}_e} \mathsf{u}^e_{Ij}\ \phi^e_j\,, \quad \text{for } I = x,y,z\,. \tag{4.7}$$

For the strain tensor, we work directly with its Voigt representation as a vector of length 6, cf. (3.39),

$$\begin{aligned} \boldsymbol{\sigma}_h = \sum_{\mathfrak{J}\in\mathcal{I}_{\text{sm}}} \sigma^h_{\mathfrak{J}}\ \hat{\mathbb{e}}_{\mathfrak{J}} \qquad &\longleftrightarrow \qquad \overrightarrow{\boldsymbol{\sigma}}_h = \sum_{\mathfrak{J}\in\mathcal{I}_{\text{sm}}} \sigma^h_{\mathfrak{J}}\ \hat{\mathsf{e}}_{\mathfrak{J}}\,, \\ \text{with} \qquad \sigma^h_{\mathfrak{J}}\big|_{K^e} &= \sum_{j=1}^{\mathsf{m}_e} \mathsf{v}^e_{\mathfrak{J}j}\ \psi^e_j\,, \quad \text{for } \mathfrak{J} \in \mathcal{I}_{\text{sm}}\,. \end{aligned} \tag{4.8}$$

Above we use $\hat{\mathbf{e}}_I$ for $I = x,y,z$ the unit Cartesian vector in $\mathbb{R}^3$, and $\hat{\mathsf{E}}_{\mathfrak{J}}$ for $\mathfrak{J} \in \mathcal{I}_{\text{sm}}$ for unit Cartesian vectors in $\mathbb{R}^6$ with $\mathcal{I}_{\text{sm}}$ the ordered set (3.3). We gather all volume unknowns into vector $\mathbf{W}$ such that,

$$\begin{aligned} \mathbf{W} = (\mathbf{W}^e)_{1\leq e\leq|\mathcal{T}_h|}\,, \quad \text{with} \quad \mathbf{W}^e := \begin{pmatrix} \mathbf{U}^e \\ \mathbf{V}^e \end{pmatrix} \\ \text{and} \quad \mathbf{U}^e = (\mathsf{U}^e_I)_{I=x,y,z}\,,\ \mathbf{V}^e = \left(\mathsf{V}^e_{\mathfrak{J}}\right)_{\mathfrak{J}\in\mathcal{I}_{\text{sm}}}\,, \end{aligned} \tag{4.9}$$

Their corresponding sub-blocks are given by

$$\mathsf{U}^e_I = \left(\mathsf{u}^e_{Ij}\right)_{j=1,\ldots,\mathsf{n}_e}\,, \quad \mathsf{V}^e_{\mathfrak{J}} = \left(\mathsf{v}^e_{\mathfrak{J}j}\right)_{j=1,\ldots,\mathsf{m}_e}\,. \tag{4.10}$$

Edge discrete unknowns Unknowns defined on the edges Σ_h are numerical approximations of the trace of the displacement $\mathbf{u}$ on the edges Σ_h. Specifically, on each edge F^k, $k = 1, \dots, \hat{\mathsf{n}}_k$,

$$\boldsymbol{\lambda}_h = \sum_{I\in\{x,y,z\}} \lambda_I^h \, \hat{\mathbf{e}}_I \,, \quad \text{with} \quad \lambda_I^h\big|_{\mathsf{F}^k} = \sum_{j=1}^{\hat{\mathsf{n}}_k} \lambda_{Ij}^k \, \xi_j^k \,. \tag{4.11}$$

Gather these coefficients into global vector $\boldsymbol{\Lambda}$ which has the following substructure,

$$\boldsymbol{\Lambda} = \left(\boldsymbol{\Lambda}^k\right)_{k=1,\dots,|\Sigma_h|} \,, \quad \text{with} \quad \boldsymbol{\Lambda}^k = \left(\Lambda_I^k\right)_{I=x,y,z} \quad \text{and} \quad \Lambda_I^k = \left(\lambda_{Ij}^k\right)_{1\le j\le \hat{\mathsf{n}}_k} \,. \tag{4.12}$$

Remark 7. *The above expressions are written in global edge indices. Using (4.1), it can also be written in terms of the local edge indices, specifically for $k = \mathfrak{f}(e,\ell)$, that is, (e,ℓ) is identified with k, then*

$$\mathsf{F}^k = \mathsf{F}^{(e,\ell)} \,, \quad \lambda_{Ij}^{(e,\ell)} = \lambda_{Ij}^k \,, \quad \xi_j^{(e,\ell)} = \xi_j^k \,, \quad \textit{where } k = \mathfrak{f}(e,\ell) \,. \tag{4.13}$$

4.2 Discretization for elastic wave formulation $(\mathbf{u}, \boldsymbol{\sigma})_S$

4.2.1 Discretized local problem

From (2.36), we write the local (on each mesh cell) variational formulations for the equation of motion and of constitutive law, with test-functions $\boldsymbol{\phi}$ and $\boldsymbol{\psi}$:

$$\begin{cases} -\omega^2 \displaystyle\int_{K^e} \mathbf{u}_h \cdot \overline{\boldsymbol{\phi}} \,\mathrm{d}\mathbf{x} - \int_{K^e} (\nabla\cdot\boldsymbol{\sigma}_h)\cdot\overline{\boldsymbol{\phi}}\,\mathrm{d}\mathbf{x} + \int_{\partial K^e} \overline{\boldsymbol{\phi}}\cdot\boldsymbol{\tau}_{\mathbf{u}}(\mathbf{u}_h - \boldsymbol{\lambda}_h)\,\mathrm{d}s_{\mathbf{x}} = \int_{K^e} \mathbf{f}\cdot\overline{\boldsymbol{\phi}}\,\mathrm{d}\mathbf{x} \,, & \text{(4.14a)} \\ \displaystyle\int_{K^e} \boldsymbol{\sigma}_h : \mathbf{S} : \overline{\Psi}\,\mathrm{d}\mathbf{x} = -\int_{K^e} \mathbf{u}_h \cdot \nabla\cdot\overline{\Psi}\mathrm{d}\mathbf{x} + \int_{\partial K^e} \boldsymbol{\nu}\cdot\overline{\Psi}\cdot\boldsymbol{\lambda}_h\,\mathrm{d}s_{\mathbf{x}} \,. & \text{(4.14b)} \end{cases}$$

Equation of motion We integrate the equation of motion (4.14a) against test functions

$$\boldsymbol{\phi} = \phi_i^e \, \hat{\mathbf{e}}_I, \qquad I = x,y,z \;\; 1 \le i \le \mathsf{n}_e \,. \tag{4.15}$$

The two volume integrals are discretized as,

$$\int_{K^e} \rho\,\omega^2\,\mathbf{u}_h\cdot\overline{\phi_i^e}\,\hat{\mathbf{e}}_I\,\mathrm{d}\mathbf{x} \;=\; \omega^2 \sum_{j=1}^{\mathsf{n}_e} \mathsf{u}_{I,j}^e \int_{K^e} \rho\,\overline{\phi_i^e}\,\phi_j^e\,\mathrm{d}\mathbf{x} \,; \tag{4.16a}$$

$$\int_{K^e} (\nabla\cdot\boldsymbol{\sigma}_h)\cdot\overline{\phi_i^e}\,\hat{\mathbf{e}}_I\,\mathrm{d}\mathbf{x} \overset{(3.40)}{=} \sum_{\mathfrak{J}\in\mathcal{I}_{\mathrm{sm}}} \sum_{j=1}^{\mathsf{m}_e} \sigma_{\mathfrak{J},j}^e \,\hat{\mathbf{e}}_I \cdot \left(\int_{K^e} \overline{\phi_i^e}\,\mathbb{A}^\dagger(\nabla\psi_j^e)\,\mathrm{d}\mathbf{x}\right)\cdot\hat{\mathbf{e}}_{\mathfrak{J}} \,. \tag{4.16b}$$

while the boundary integrals are written as

$$\int_{\partial K^e} \overline{\phi}\,\hat{\mathbf{e}}_I\cdot\boldsymbol{\tau}_{\mathbf{u}}\mathrm{d}s_{\mathbf{x}} \;=\; \sum_{\ell=1}^{\mathsf{n}_{\mathrm{face}}^e} \sum_{J=x,y,z} \sum_{j=1}^{\mathsf{n}_e} \mathsf{u}_{J,j}^e \int_{\mathsf{F}^{(e,\ell)}} \tau_{IJ}\,\overline{\phi_i^e}\,\phi_j^e\,\mathrm{d}s_{\mathbf{x}} \,; \tag{4.17a}$$

$$\int_{\partial K^e} \overline{\phi}\hat{\mathbf{e}}_I\cdot\boldsymbol{\tau}_{\mathbf{u}}\boldsymbol{\lambda}\,\mathrm{d}s_{\mathbf{x}} = \sum_{\ell=1}^{\mathsf{n}_{\mathrm{face}}^e} \sum_{J=x,y,z} \sum_{j=1}^{\hat{\mathsf{n}}_k} \lambda_{J,j}^{(e,\ell)} \int_{\mathsf{F}^{(e,\ell)}} \tau_{IJ}\,\overline{\phi_i^e}\,\xi_j^{(e,\ell)}\,\mathrm{d}s_{\mathbf{x}} \,. \tag{4.17b}$$

Constitutive law We integrate the constitutive equation (4.14b) against test functions, cf. (3.37) and (3.36) for notation,

$$\Psi = \psi_i^e \,\overline{\overline{\mathfrak{e}}}_{\mathfrak{J}} \quad \underset{\text{Voigt identification}}{\leftrightarrow} \quad \overrightarrow{\Psi} = \psi_i^e\,\hat{\mathfrak{e}}_{\mathfrak{J}}, \qquad \text{for } \mathfrak{J}\in\mathcal{I}_{\mathrm{sm}} \,,\; 1\le i\le \mathsf{m}_e, \tag{4.18}$$

the two volume integrals are discretized as

$$\int_{K^e} \boldsymbol{\sigma}_h \cdot \mathbf{S} \cdot \boldsymbol{\Psi} \, \mathrm{d}\mathbf{x} \overset{(3.22)}{=} \sum_{\mathfrak{J}' \in \mathcal{I}_{\mathrm{sm}}} \sum_{j=1}^{\mathsf{m}_e} \sigma^e_{\mathfrak{J}',j} \, \hat{\mathbf{e}}_{\mathfrak{J}} \cdot \left(\int_{K^e} \overline{\psi^e_i} \, \psi^e_j \, \overline{\overline{\mathbf{S}}^{\dagger}} \, \mathrm{d}\mathbf{x} \right) \cdot \hat{\mathbf{e}}_{\mathfrak{J}'} \, ; \tag{4.19a}$$

$$\int_{K^e} \mathbf{u}_h \cdot \nabla \cdot \left(\overline{\psi^e_i} \, \hat{\mathsf{E}}_{\mathfrak{J}} \right) \mathrm{d}\mathbf{x} \overset{(3.40)}{=} \sum_{J=x,y,z} \sum_{j=1}^{\mathsf{n}_e} \mathsf{u}^e_{J,j} \, \hat{\mathbf{e}}_J \cdot \left(\int_{K^e} \phi^e_i \, \overline{\mathbb{A}^{\dagger}(\nabla \psi^e_i)} \, \mathrm{d}\mathbf{x} \right) \cdot \hat{\mathbf{e}}_{\mathfrak{J}} \, . \tag{4.19b}$$

The boundary integral is discretized as,

$$\int_{\partial K^e} \boldsymbol{\nu} \cdot \overline{\boldsymbol{\Psi}} \cdot \boldsymbol{\lambda}_h \mathrm{d}s_{\mathbf{x}} = \sum_{\ell=1}^{\mathsf{n}^e_{\mathrm{face}}} \sum_{J=x,y,z} \sum_{j=1}^{\hat{\mathsf{n}}_k} \lambda^{(e,\ell)}_{J,j} \left(\int_{\mathsf{F}^{(e,\ell)}} \overline{\psi^e_i} \, \xi^{(e,\ell)}_j \, \overline{\overline{\mathbf{e}}_{\mathfrak{J}}} \, \boldsymbol{\nu}^{(e,\ell)} \, \mathrm{d}s_{\mathbf{x}} \right) \cdot \hat{\mathbf{e}}_J \, . \tag{4.20}$$

Discretized local problem in matrix form Using the above expressions, we arrive at the discretized problem defined on each element K^e,

$$\mathbb{A}^e \, \mathbf{W}^e \, + \, \mathbb{D}^e \, \boldsymbol{\Lambda}^e \, = \, \mathsf{S}^e \, , \qquad \text{for } 1 \leq e \leq |\mathcal{T}_h| \, . \tag{4.21}$$

The upper row blocks of $\mathbb{A}^e$ and $\mathbb{D}^e$ correspond to the discretization of the equation of motion (4.14a), while the blocks of the second row are related to the constitutive law (4.14b),

$$\mathbb{A}^e = \begin{pmatrix} -\omega^2 \, \mathbb{M}^e_{\mathbf{u}} + \mathbb{M}^e_{\partial} & -\mathbb{K}^e_{\boldsymbol{\sigma}} \\ -\mathbb{K}^e_{\mathbf{u}} & -\mathbb{M}^e_{\boldsymbol{\sigma}} \end{pmatrix} , \quad \mathbb{D}^e = \begin{pmatrix} -\mathbb{D}^{(e,1)}_{\mathrm{m}} & \dots & -\mathbb{D}^{(e,\mathsf{n}^e_{\mathrm{face}})}_{\mathrm{m}} \\ \mathbb{D}^{(e,1)}_{\mathrm{c}} & \dots & \mathbb{D}^{(e,\mathsf{n}^e_{\mathrm{face}})}_{\mathrm{c}} \end{pmatrix} . \tag{4.22}$$

The components of the sub-blocks matrices are given below. The source of (4.21) comes from the volume source $\mathbf{f}$ of equation of motion (4.14a),

$$\mathsf{S}^e = \begin{pmatrix} \mathsf{S}^e_{\mathrm{m}} \\ \mathbf{0}_{(6\mathsf{m}_e)\times 1} \end{pmatrix} , \quad \mathsf{S}^e_{\mathrm{m}} = ({}_{\mathrm{m}}\mathsf{S}^e_I)_{I=x,y,z} \, , \quad [{}_{\mathrm{m}}\mathsf{S}^e_I]_i = \langle \mathbf{f}, \phi^e_i \, \hat{\mathbf{e}}_I \rangle \, , \; 1 \leq i \leq \mathsf{n}_e \, . \tag{4.23}$$

• The upper left block of $\mathbb{A}^e$ in (4.21) is given by matrix $\mathbb{M}^e_{\mathbf{u}}$ which has a 3×3 block structure and is block-diagonal[11], the definition of its components comes from (4.16a),

$$\mathbb{M}^e_{\mathbf{u}} = (\mathbb{M}^{\mathbf{u}e}_{IJ})_{I,J=x,y,z} \, , \qquad \mathbb{M}^{\mathbf{u}e}_{IJ} = \begin{cases} \mathbf{0}_{\mathsf{n}_e \times \mathsf{n}_e} \, , & \text{for } I \neq J \, ; \\ [\mathbb{M}^{\mathbf{u}e}_{II}]_{ij} = \displaystyle\int_{K^e} \rho \, \overline{\phi^e_i} \, \phi^e_j \, \mathrm{d}\mathbf{x} \, , & \text{for } I = J, \; I = x,y,z \, . \end{cases} \tag{4.25}$$

On the other hand, matrix $\mathbb{M}^e_{\partial}$ has a 3×3 block structure, where each block is a matrix of size $\mathsf{n}_e \times \mathsf{n}_e$, the definition of its components comes from (4.17a),

$$\mathbb{M}^e_{\partial} = \left(\mathbb{M}^{\partial e}_{IJ} \right)_{I,J=x,y,z} \, , \quad \text{with } \left[\mathbb{M}^{\partial e}_{IJ} \right]_{ij} = \sum_{\ell=1}^{\mathsf{n}^e_{\mathrm{face}}} \int_{\mathsf{F}^{(e,\ell)}} \tau_{IJ} \, \overline{\phi^e_i} \, \phi^e_j \, \mathrm{d}s_{\mathbf{x}} \, . \tag{4.26}$$

Finally, matrix $\mathbb{K}^e_{\boldsymbol{\sigma}}$ has a 6×3 block structure[12], the definition of its components comes from (4.16b),

$$\begin{aligned} \mathbb{K}^e_{\boldsymbol{\sigma}} = \left(\mathbb{K}^{\boldsymbol{\sigma}e}_{I\mathfrak{J}} \right)_{\substack{I=x,y,z, \\ \mathfrak{J} \in \mathcal{I}_{\mathrm{sm}}}} \text{with} \quad \left[\mathbb{K}^{\boldsymbol{\sigma}e}_{I\mathfrak{J}} \right]_{ij} &= \hat{\mathbf{e}}_I \cdot \left(\int_{K^e} \overline{\phi^e_i} \, \mathbb{A}^{\dagger}(\nabla \psi^e_j) \, \mathrm{d}\mathbf{x} \right) \cdot \hat{\mathbf{e}}_{\mathfrak{J}} \\ &= \sum_{\alpha=x,y,z} \left(\mathbb{A}^{\dagger}_{\alpha} \right)_{I\mathfrak{J}} \int_{K^e} \overline{\phi^e_i} \, \partial_{\alpha} \psi^e_j \, \mathrm{d}\mathbf{x} \, . \end{aligned} \tag{4.27}$$

[11] We write out explicitly the block structure for $\mathbb{M}^e_{\partial}$ and $\mathbb{M}^e_{\mathbf{u}}$; compared to $\mathbb{M}^e_{\mathbf{u}}$, one has a similar diagonal structure for $\mathbb{M}^e_{\boldsymbol{\sigma}}$ with 6 diagonal blocks $\mathbb{M}^{\boldsymbol{\sigma}e}_{\mathfrak{J}\mathfrak{J}}$ with $\mathfrak{J} \in \mathcal{I}_{\mathrm{sm}}$,

$$\mathbb{M}^e_{\mathbf{u}} = \begin{pmatrix} \mathbb{M}^{\mathbf{u}e}_{xx} & \mathbf{0} & \mathbf{0} \\ \mathbf{0} & \mathbb{M}^{\mathbf{u}e}_{yy} & \mathbf{0} \\ \mathbf{0} & \mathbf{0} & \mathbb{M}^{\mathbf{u}e}_{zz} \end{pmatrix} , \quad \mathbb{M}^e_{\partial} = \begin{pmatrix} \mathbb{M}^{\partial e}_{xx} & \mathbb{M}^{\partial e}_{xy} & \mathbb{M}^{\partial e}_{xz} \\ \mathbb{M}^{\partial e}_{yx} & \mathbb{M}^{\partial e}_{yy} & \mathbb{M}^{\partial e}_{yz} \\ \mathbb{M}^{\partial e}_{zx} & \mathbb{M}^{\partial e}_{zy} & \mathbb{M}^{\partial e}_{zz} \end{pmatrix} . \tag{4.24}$$

[12] This is the transpose of the row block of $\mathbb{K}_{\mathbf{u}e}$ in Footnote 13

In the blocks of the lower row of $\mathbb{A}^e$, matrix $\mathbb{M}^e_{\boldsymbol{\sigma}}$ consists of 6×6 blocks with each block a matrix of size $\mathsf{m}_e\times\mathsf{m}_e$, the definition of its components comes from (4.19a),

$$\begin{aligned}\mathbb{M}^e_{\boldsymbol{\sigma}} = \big(\mathbb{M}^{\boldsymbol{\sigma}e}_{\mathfrak{I}\mathfrak{J}'}\big)_{\mathfrak{I},\mathfrak{J}'\in\mathcal{I}_{\rm sm}}\,, \quad \text{with} \quad \big[\mathbb{M}^{\boldsymbol{\sigma}e}_{\mathfrak{I}\mathfrak{J}'}\big]_{ij} &= \hat{\mathbf{e}}_{\mathfrak{I}}\cdot\left(\int_{K^e}\overline{\psi^e_i}\,\psi^e_j\,\overline{\overline{{}^{\dagger}\mathbf{S}^{\dagger}}}\,\mathrm{d}\mathbf{x}\right)\cdot\hat{\mathbf{e}}_{\mathfrak{J}'}\,,\\ &= \int_{K^e}\overline{\psi^e_i}\,\psi^e_j\left[\overline{\overline{{}^{\dagger}\mathbf{S}^{\dagger}}}\right]_{\mathfrak{I}\mathfrak{J}'}\mathrm{d}\mathbf{x}\,.\end{aligned} \tag{4.28}$$

If the compliance matrix is constant on each mesh cell, then

$$\big[\mathbb{M}^{\boldsymbol{\sigma}e}_{\mathfrak{I}\mathfrak{J}'}\big]_{ij} = \left[\overline{\overline{{}^{\dagger}\mathbf{S}^{\dagger}}}\right]_{\mathfrak{I}\mathfrak{J}'}\int_{K^e}\overline{\psi^e_i}\,\psi^e_j\,\mathrm{d}\mathbf{x}\,. \tag{4.29}$$

On the other hand, matrix $\mathbb{K}^e_{\mathbf{u}}$ consists of 3×6 block[13], the definition of its components comes from (4.19b),

$$\begin{aligned}\mathbb{K}^e_{\mathbf{u}} = (\mathbb{K}^{\mathbf{u}e}_{\mathfrak{I}J})_{\substack{\mathfrak{I}\in\mathcal{I}_{\rm sm},\\ J=x,y,z}} \quad \text{with} \quad [\mathbb{K}^{\mathbf{u}e}_{\mathfrak{I}J}]_{ij} &= \hat{\mathbf{e}}_J\cdot\left(\int_{K^e}\phi^e_j\,\overline{\mathbb{A}^{\dagger}(\nabla\psi^e_i)}\,\mathrm{d}\mathbf{x}\right)\cdot\hat{\mathbf{e}}_{\mathfrak{I}}\\ &= \sum_{\alpha=x,y,z}(\mathbb{A}^{\dagger}_{\alpha})_{I\mathfrak{I}}\int_{K^e}\phi^e_j\,\overline{\partial_\alpha\psi^e_i}\;\mathrm{d}\mathbf{x}\,.\end{aligned} \tag{4.31}$$

• For matrix $\mathbb{D}^e$, the upper row blocks are made up of sub-blocks $\mathbb{D}^{(e,\ell)}_{\rm m}$ which consists of 3×3 block structure (similarly to $\mathbb{M}^e_{\partial}$) with components given by (4.17b),

$$\mathbb{D}^{(e,\ell)}_{\rm m} = \Big({}_{\rm m}\mathbb{D}^{(e,\ell)}_{IJ}\Big)_{I,J=x,y,z}\,, \quad \text{with} \quad \Big[{}_{\rm m}\mathbb{D}^{(e,\ell)}_{IJ}\Big]_{ij} = \int_{\mathsf{F}^{(e,\ell)}}\tau_{IJ}\;\overline{\phi^e_i}\,\xi^{(e,\ell)}_j\,\mathrm{d}s_{\mathbf{x}}\,. \tag{4.32}$$

• In the lower row matrix $\mathbb{D}^e$, $\mathbb{D}^{(e,\ell)}_{\rm c}$ has a 6×3 structure such that,

$$\mathbb{D}^{(e,\ell)}_{\rm c} = \Big({}_{\rm c}\mathbb{D}^{(e,\ell)}_{\mathfrak{I}J}\Big)_{\substack{\mathfrak{I}\in\mathcal{I}_{\rm sm},\\ J=x,y,z}}\,. \tag{4.33}$$

The definition of its components comes from (4.20),

$$\begin{aligned}\Big[{}_{\rm c}\mathbb{D}^{(e,\ell)}_{\mathfrak{I}J}\Big]_{ij} &= \int_{\mathsf{F}^{(e,\ell)}}\overline{\psi^e_i}\,\xi^{(e,\ell)}_j\;\hat{\mathbf{e}}_J\cdot\overline{\overline{\mathbf{e}}}_{\mathfrak{I}}\cdot\boldsymbol{\nu}^{(e,\ell)}\,\mathrm{d}s_{\mathbf{x}}\,,\\ &\text{where}\quad \hat{\mathbf{e}}_J\cdot\overline{\overline{\mathbf{e}}}_{\mathfrak{I}}\cdot\boldsymbol{\nu}^{(e,\ell)} = \mathbb{A}^{\dagger}(\boldsymbol{\nu}^{(e,\ell)})_{J\mathfrak{I}} = \sum_{\alpha=x,y,z}\nu^{(e,\ell)}_{\alpha}\;[\mathbb{A}^{\dagger}_{\alpha}]_{J\mathfrak{I}}\,.\end{aligned} \tag{4.34}$$

4.2.2 Discretized problem for the edges

We recall from (2.37) the approximate condition imposed on Neumann boundary and interior interfaces:

$$\sum_{e=1}^{|\mathcal{T}_h|}\int_{\partial K^e\cap(\Sigma_{\rm int}\cup\Sigma_{\rm N})}\big(\boldsymbol{\nu}\cdot\boldsymbol{\sigma}_h\cdot\overline{\boldsymbol{\xi}}-\overline{\boldsymbol{\xi}}\cdot\boldsymbol{\tau}_{\mathbf{u}}\cdot(\boldsymbol{u}_h-\boldsymbol{\lambda}_h)\big)\,\mathrm{d}s_{\mathbf{x}} = 0\,,\quad\forall\boldsymbol{\xi}\in\mathbf{M}_h(\Sigma_{\rm int}\cup\Sigma_{\rm N})\,. \tag{4.35}$$

Using as test functions $\boldsymbol{\xi} = \xi^{(e,\ell)}_i\,\hat{\mathbf{e}}_I$, the integrals in equation (4.35) take the following form,

$$\int_{\mathsf{F}^{(e,\ell)}}\overline{\boldsymbol{\xi}}\cdot\boldsymbol{\sigma}^K_h\cdot\boldsymbol{\nu}^{(e,\ell)}\,\mathrm{d}s_{\mathbf{x}}\overset{(3.23)}{=}\sum_{\mathfrak{I}\in\mathcal{I}_{\rm sm}}\sum_{j=1}^{\mathsf{m}_e}\sigma^e_{\mathfrak{I},j}\,\hat{\mathbf{e}}_I\cdot\left(\int_{\mathsf{F}^{(e,\ell)}}\overline{\xi^{(e,\ell)}_i}\;\psi^e_j\,\mathbb{A}^{\dagger}(\boldsymbol{\nu}^{(e,\ell)})\,\mathrm{d}s_{\mathbf{x}}\right)\cdot\hat{\mathbf{e}}_{\mathfrak{I}}\,. \tag{4.36}$$

[13] We write out explicitly the structure of $\mathbb{K}^e_{\mathbf{u}}$, the structure of $\mathbb{K}^e_{\boldsymbol{\sigma}}$ is the transpose of this block structure containing 6×3 blocks,

$$\mathbb{K}^e_{\mathbf{u}} = \begin{pmatrix}\mathbb{K}^{\mathbf{u}e}_{x,xx} & \mathbb{K}^{\mathbf{u}e}_{x,yy} & \mathbb{K}^{\mathbf{u}e}_{x,zz} & \mathbb{K}^{\mathbf{u}e}_{x,yz} & \mathbb{K}^{\mathbf{u}e}_{x,xz} & \mathbb{K}^{\mathbf{u}e}_{x,xy}\\ \mathbb{K}^{\mathbf{u}e}_{y,xx} & \mathbb{K}^{\mathbf{u}e}_{y,yy} & \mathbb{K}^{\mathbf{u}e}_{y,zz} & \mathbb{K}^{\mathbf{u}e}_{y,yz} & \mathbb{K}^{\mathbf{u}e}_{y,xz} & \mathbb{K}^{\mathbf{u}e}_{y,xy}\\ \mathbb{K}^{\mathbf{u}e}_{z,xx} & \mathbb{K}^{\mathbf{u}e}_{z,yy} & \mathbb{K}^{\mathbf{u}e}_{z,zz} & \mathbb{K}^{\mathbf{u}e}_{z,yz} & \mathbb{K}^{\mathbf{u}e}_{z,xz} & \mathbb{K}^{\mathbf{u}e}_{z,xy}\end{pmatrix}. \tag{4.30}$$

The boundary integral is discretized in the exact same way as (4.17), and similarly for the condition along Σ_∞.

The discretized problem on the interface Σ is

$$\sum_{e=1}^{|\mathcal{T}|} \mathcal{R}_e^t \left(\mathbb{B}^e \, \mathbf{W}^e + \mathbb{L}^e \, \mathcal{R}_e \mathbf{\Lambda} \right) = \sum_{e=1}^{|\mathcal{T}|} \mathcal{R}_e^t \, \mathfrak{s}^e \, . \tag{4.37}$$

Both matrices $\mathbb{B}^e$ and $\mathbb{L}^e$ have $\mathsf{n}^e_{\text{face}}$ row-blocks, corresponding to face (e,ℓ). Within each (e,ℓ) block-row, j-th row is obtained by integrating test function

$$\boldsymbol{\xi}\big|_{F^{(e,\ell)}} = \xi_j^{(e,\ell)} \, \hat{\mathbf{e}}_I \, , \quad \text{with } I = x,y,z \, . \tag{4.38}$$

The columns of $\mathbb{B}^e$ are grouped into $\mathbb{B}^{(e,\ell)}_{\mathbf{u}}$ and $\mathbb{B}^{(e,\ell)}_{\boldsymbol{\sigma}}$, while $\mathbb{L}^e$ has diagonal block structure

$$\mathbb{B}^e = \begin{pmatrix} -\mathbb{B}^{(e,1)}_{\mathbf{u}} & \mathbb{B}^{(e,1)}_{\boldsymbol{\sigma}} \\ \vdots & \vdots \\ -\mathbb{B}^{(e,\mathsf{n}^e_{\text{face}})}_{\mathbf{u}} & \mathbb{B}^{(e,\mathsf{n}^e_{\text{face}})}_{\boldsymbol{\sigma}} \end{pmatrix} , \quad \mathbb{L}^e = \begin{pmatrix} \mathbb{L}^{(e,1)} & \mathbf{0} & \mathbf{0} & \mathbf{0} \\ \mathbf{0} & \mathbb{L}^{(e,2)} & \mathbf{0} & \mathbf{0} \\ & & \ddots & \\ \mathbf{0} & \mathbf{0} & \mathbf{0} & \mathbf{0} \\ \mathbf{0} & \mathbf{0} & \mathbf{0} & \mathbb{L}^{(e,\mathsf{n}^e_{\text{face}})} \end{pmatrix} . \tag{4.39}$$

• For each (e,ℓ), matrix $\mathbb{B}^{(e,\ell)}_{\mathbf{u}}$ consists of 3×3 blocks[14],

$$\mathbb{B}^{(e,\ell)}_{\mathbf{u}} = \left({}_{\mathbf{u}}\mathbb{B}^{(e,\ell)}_{IJ} \right)_{I,J=x,y,z} , \tag{4.40}$$

with sub-block ${}_{\mathbf{u}}\mathbb{B}^{(e,\ell)}_{IJ}$ of size $\hat{\mathsf{n}}_k \times \mathsf{n}_e$; its components come from (4.17), for $1 \le i \le \hat{\mathsf{n}}_k$, $1 \le j \le \mathsf{n}_e$,

$$\left[{}_{\mathbf{u}}\mathbb{B}^{(e,\ell)}_{IJ} \right]_{ij} = \begin{cases} \displaystyle\int_{\mathsf{F}^{(e,\ell)}} \tau_{IJ} \, \overline{\xi_i^{(e,\ell)}} \, \phi_j^e \, \mathrm{d}s_{\mathbf{x}} & , \quad \mathsf{F}^{(e,\ell)} \in \Sigma_{\text{int}} \cup \Sigma_{\text{N}} \cup \Sigma_\infty \, , \\ 0 & , \quad \mathsf{F}^{(e,\ell)} \in \Sigma_{\text{D}} \, . \end{cases} \tag{4.41}$$

• For matrix $\mathbb{L}^e$, the zero off-diagonal block is of size $3\hat{\mathsf{n}}_k \times \hat{\mathsf{n}}_k$. Each diagonal block of $\mathbb{L}^{(e,\ell)}$ consists of 3×3 sub-blocks

$$\mathbb{L}^{(e,\ell)} = \left(\mathbb{L}^{(e,\ell)}_{IJ} \right)_{I,J=x,y,z} , \tag{4.42}$$

with sub-block $\mathbb{L}^{(e,\ell)}_{IJ}$ of size $\hat{\mathsf{n}}_k \times \mathsf{m}_e$ and components: for $1 \le i,j \le \hat{\mathsf{n}}_k$,

$$\left[\mathbb{L}^{(e,\ell)}_{IJ} \right]_{ij} = \begin{cases} \displaystyle\int_{\mathsf{F}^{(e,\ell)}} \tau_{IJ} \, \overline{\xi_i^{(e,\ell)}} \, \xi_j^{(e,\ell)} \, \mathrm{d}s_{\mathbf{x}} \, , & \mathsf{F}^{(e,\ell)} \in \Sigma_{\text{int}} \cup \Sigma_{\text{N}} \\ \displaystyle\int_{\mathsf{F}^{(e,\ell)}} \overline{\xi_i^{(e,\ell)}} \, \xi_j^{(e,\ell)} \, \left(\tau_{IJ} + \mathcal{Z}^{\text{abc}}_{IJ} \right) \mathrm{d}s_{\mathbf{x}} \, , & \mathsf{F}^{(e,\ell)} \in \Sigma_\infty \\ \mathbb{I}_{3\hat{\mathsf{n}}_k \times 3\hat{\mathsf{n}}_k} \, , & \mathsf{F}^{(e,\ell)} \in \Sigma_{\text{D}} \, . \end{cases} \tag{4.43}$$

• On the other hand, the matrix $\mathbb{B}^{(e,\ell)}_{\boldsymbol{\sigma}}$ consists of 3×6 block structure[15] such that,

$$\mathbb{B}^{(e,\ell)}_{\boldsymbol{\sigma}} = \left({}_{\boldsymbol{\sigma}}\mathbb{B}^{(e,\ell)}_{I\mathfrak{J}} \right)_{I=x,y,z \, , \, \mathfrak{J} \in \mathcal{I}_{\text{sm}}} , \tag{4.44}$$

with its sub-block ${}_{\boldsymbol{\sigma}}\mathbb{B}^{(e,\ell)}_{IJ}$ of size $\hat{\mathsf{n}}_k \times \hat{\mathsf{n}}_k$ having components given by (4.36), for $1 \le i \le \hat{\mathsf{n}}_k$, $1 \le j \le \mathsf{m}_e$,

$$ {}_{\boldsymbol{\sigma}}\mathbb{B}^{(e,\ell)}_{I\mathfrak{J}} = \mathbf{0} \, , \quad \text{for} \quad \mathsf{F}^{(e,\ell)} \in \Sigma_{\text{D}} \, , \tag{4.45}$$

[14] Similarly to $\mathbb{M}^e_{\mathbf{u}}$ and $\mathbb{M}^e_{\partial}$, cf. Footnote 11

[15] Similar to $\mathbb{K}^e_{\mathbf{u}}$ cf.Footnote 13.

while for $\mathsf{F}^{(e,\ell)} \in \Sigma_{\text{int}} \cup \Sigma_{\text{N}} \cup \Sigma_{\infty}$,

$$\begin{aligned} \left[\boldsymbol{\sigma}\mathbb{B}_{I\mathfrak{J}}^{(e,\ell)}\right]_{ij} &= \int_{\mathsf{F}^{(e,\ell)}} \overline{\xi_i^{(e,\ell)}}\, \psi_j^e\, \mathbb{A}^\dagger(\boldsymbol{\nu}^{(e,\ell)})_{I\mathfrak{J}}\, \mathrm{d}s_{\mathbf{x}}\,, \\ \text{with} \quad \mathbb{A}^\dagger(\boldsymbol{\nu}^{(e,\ell)})_{I\mathfrak{J}} &= \sum_{\alpha=x,y,z} \nu_\alpha^{(e,\ell)}\, (\mathbb{A}_\alpha^\dagger)_{I\mathfrak{J}}\,. \end{aligned} \tag{4.46}$$

Remark 8 (HDG with formulation $(\mathbf{v},\boldsymbol{\sigma})_{\boldsymbol{S}}$)**.** *The discretization of the formulation in terms of the velocity instead of displacement, (2.27) and (2.30), follows the same step as above, with mild modification in the coefficients of the matrices. Namely, we arrive at the discrete problem,*

$$\begin{cases} \mathcal{A}^e\, \mathbf{W}^e \,+\, \mathbb{D}^e\, \boldsymbol{\Lambda}^e \,=\, \mathsf{S}^e\,, & \text{for } 1 \le e \le |\mathcal{T}_h| \\ \displaystyle\sum_{e=1}^{|\mathcal{T}|} \mathcal{R}_e^t\, (\mathbb{B}^e\, \mathbf{W}^e + \mathbb{L}^e\, \mathcal{R}_e \boldsymbol{\Lambda}) \,=\, \sum_{e=1}^{|\mathcal{T}|} \mathcal{R}_e^t\, \mathfrak{s}^e\,. \end{cases} \tag{4.47}$$

with matrices

$$\mathcal{A}^e = \begin{pmatrix} \mathrm{i}\omega\, \mathbb{M}_{\mathbf{u}}^e + \mathbb{M}_{\partial}^e & -\mathbb{K}_{\boldsymbol{\sigma}}^e \\ -\mathbb{K}_{\mathbf{u}}^e & -\mathrm{i}\omega\, \mathbb{M}_{\boldsymbol{\sigma}}^e \end{pmatrix}, \quad \mathbb{D}^e = \begin{pmatrix} -\mathbb{D}_{\mathrm{m}}^{(e,1)} & \dots & -\mathbb{D}_{\mathrm{m}}^{(e,\mathsf{n}_{\mathrm{face}}^e)} \\ \mathbb{D}_{\mathrm{c}}^{(e,1)} & \dots & \mathbb{D}_{\mathrm{c}}^{(e,\mathsf{n}_{\mathrm{face}}^e)} \end{pmatrix}, \tag{4.48}$$

and

$$\mathbb{B}^e = \begin{pmatrix} -\mathbb{B}_{\mathbf{u}}^{(e,1)} & \mathrm{i}\omega\, \mathbb{B}_{\boldsymbol{\sigma}}^{(e,1)} \\ \vdots & \vdots \\ -\mathbb{B}_{\mathbf{u}}^{(e,\mathsf{n}_{\mathrm{face}}^e)} & \mathrm{i}\omega\, \mathbb{B}_{\boldsymbol{\sigma}}^{(e,\mathsf{n}_{\mathrm{face}}^e)} \end{pmatrix}, \quad \mathbb{L}^e = \begin{pmatrix} \mathbb{L}^{(e,1)} & \mathbf{0} & \mathbf{0} & \mathbf{0} \\ \mathbf{0} & \mathbb{L}^{(e,2)} & \mathbf{0} & \mathbf{0} \\ & & \ddots & \\ \mathbf{0} & \mathbf{0} & & \mathbf{0} \\ \mathbf{0} & \mathbf{0} & \mathbf{0} & \mathbb{L}^{(e,\mathsf{n}_{\mathrm{face}}^e)} \end{pmatrix}. \tag{4.49}$$

The components of the above matrices are as given in Subsection 4.2, with the exception of

$$\underset{(4.26)}{\mathbb{M}_{\partial}^e}\,, \quad \underset{(4.32)}{\mathbb{D}_{\mathrm{m}}^{(e,\ell)}}\,, \quad \underset{(4.41)}{\mathbb{B}_{\mathbf{u}}^{(e,\ell)}}\,, \quad \underset{(4.43)}{\mathbb{L}^e}\,, \tag{4.50}$$

for which a slight modification is made by replacing the notation of the stabilization, $\boldsymbol{\tau}_{\mathbf{u}}$ by $\boldsymbol{\tau}_{\mathbf{v}}$.

4.3 Summary of the HDG formulations

We put together the discussion in Subsection 4.2. The HDG discretization (2.36)–(2.39) takes the following form with unknowns $(\mathbf{W}, \boldsymbol{\Lambda})$, cf. (4.9) and (4.12),

$$\mathbb{A}^e\, \mathbf{W}^e \,+\, \mathbb{D}^e\, \mathcal{R}_e\, \boldsymbol{\Lambda} = \mathbf{S}^e\,, \qquad \forall\, e = 1 \ldots, |\mathcal{T}_h|\,, \tag{4.51a}$$

$$\sum_{e=1}^{|\mathcal{T}|} \mathcal{R}_e^t \left(\mathbb{B}^e\, \mathbf{W}^e \,+\, \mathbb{L}^e\, \mathcal{R}_e\, \boldsymbol{\Lambda} \right) = \sum_{e=1}^{|\mathcal{T}|} \mathcal{R}_e^t\, \mathfrak{s}^e\,, \tag{4.51b}$$

with (4.51a) the local problem on K^e. Problem (4.51b) can be reduced to one in terms of $\boldsymbol{\Lambda}$, called the *global problem*, that we write as,

$$\mathbb{K}\, \boldsymbol{\Lambda} \,=\, \mathcal{S}\,, \tag{4.52}$$

with global coefficient matrix and right-hand side given by

$$\mathbb{K} := \sum_{e=1}^{|\mathcal{T}_h|} \mathcal{R}_e^t\, \mathbb{K}^e\, \mathcal{R}_e\,, \quad \text{with} \quad \mathbb{K}^e := -\,\mathbb{B}_e\, (\mathbb{A}^e)^{-1}\, \mathbb{D}^e \,+\, \mathbb{L}_e\,; \tag{4.53a}$$

$$\mathcal{S} := -\sum_{e=1}^{|\mathcal{T}|} \mathcal{R}_e^t\, \mathbb{B}_e\, \mathbb{A}_e^{-1}\, \mathbf{S}^e\,. \tag{4.53b}$$

In a summary, problem (4.54) is equivalent to,

$$(4.51) \quad \Leftrightarrow \quad \begin{cases} \mathbf{W}^e = -\left(\mathbb{A}^e\right)^{-1}\left(\mathbb{D}^e\,\mathcal{R}_e\,\mathbf{\Lambda} + \mathbf{S}^e\right), \quad \forall e = 1,\dots,|\mathcal{T}_h|; & (4.54a) \\ \mathbb{K}\,\mathbf{\Lambda} = \mathcal{S}\,. & (4.54b) \end{cases}$$

This means that the HDG method divides the problem into two stages. Firstly, one solves the global problem (4.54b) in terms of the trace $\mathbf{\Lambda}$; secondly, the value of the volume unknowns $\mathbf{W}^e$ is retrieved element-by-element with the right-hand side of (4.54a).

Remark 9 (Implementation with simplexes)**.** *In the case where the normal direction $\boldsymbol{\nu}$ is constant on a face $\mathsf{F}^{(e,\ell)}$, that is, with straight edges in 2D and plane faces in 3D, $\boldsymbol{\nu}$ can be put outside of the integrands. This concerns the matrices*

$$\mathbb{M}^e_\partial\,,\ \mathbb{D}^{(e,\ell)}_{\mathrm{m}}\,,\ \mathbb{B}^{(e,\ell)}_{\mathbf{u}}\,,\ \mathbb{L}^{(e,\ell)}. \tag{4.55}$$

For instance, from (4.34) and (4.46), we have,

$$\begin{aligned} \left[{}_{\mathrm{c}}\mathbb{D}^{(e,\ell)}_{\mathfrak{I}J}\right]_{ij} &= \mathbb{A}^\dagger(\boldsymbol{\nu}^{(e,\ell)})_{J\mathfrak{J}} \int_{\mathsf{F}^{(e,\ell)}} \overline{\psi^e_i}\,\xi^{(e,\ell)}_j \,\mathrm{d}s_{\mathbf{x}}\,, \\ \left[\boldsymbol{\sigma}\mathbb{B}^{(e,\ell)}_{I\mathfrak{J}}\right]_{ij} &= \mathbb{A}^\dagger(\boldsymbol{\nu}^{(e,\ell)})_{I\mathfrak{J}} \int_{\mathsf{F}^{(e,\ell)}} \overline{\xi^{(e,\ell)}_i}\,\psi^e_j \,\mathrm{d}s_{\mathbf{x}}\,. \end{aligned} \tag{4.56}$$

with

$$\mathbb{A}^\dagger(\boldsymbol{\nu}^{(e,\ell)})_{I\mathfrak{J}} = \sum_{\alpha=x,y,z} \nu^{(e,\ell)}_\alpha\ [\mathbb{A}^\dagger_\alpha]_{I\mathfrak{J}}\,, \quad \textit{with} \quad I = x,y,z,\ \mathfrak{J} \in \mathcal{I}_{\mathrm{sm}}\,. \tag{4.57}$$

Remark 10 (Optimal convergence rate)**.** *Theoretical investigation for the convergence of the HDG method for elasticity is well-established, e.g., for static elasticity [52, 24, 33, 47], and for time-harmonic elasticity [42]. In their numerical investigations, the authors report optimal convergence rate, that is, order $k+1$ for approximation polynomials of order k, for both the primal (displacement) and mixed unknowns (strain or stress). Optimal convergence rate $k+1$ using approximation spaces of equal order for all unknowns are observed and confirmed in [49, Section 5.1], in particular their Figure 3 in 2D, and Figure 6 for 3D, even in the incompressible limit, i.e., for so-called locking-free feature. Here, one does not need the strategy of HDG+ for optimal convergence, cf. [42], which employs different degrees of polynomials for the primal, mixed and hybrid variables, and which also needs a projection operator. This observation is also stated in [28] following [43, Tables 6 and 7] for static elasticity. In these investigations, convergence rate is also compared with CG method, showing the higher rate for HDG method. This optimal convergence of the mixed variable is then exploited to obtain the superconvergence for the displacement unknown.*

4.4 Stabilization of the HDG formulations

The HDG discretizations, (4.14) and (4.35), are written in terms of the stabilization $\boldsymbol{\tau}_{\mathbf{u}}$ and $\boldsymbol{\tau}_{\mathbf{v}}$, respectively associated with the formulations $(\mathbf{u},\boldsymbol{\sigma})_{\boldsymbol{S}}$ and $(\mathbf{v},\boldsymbol{\sigma})_{\boldsymbol{S}}$. These stabilization operators, $\boldsymbol{\tau}_{\mathbf{v}}$ and $\boldsymbol{\tau}_{\mathbf{u}}$, are key ingredients in the definition of the numerical trace of traction, we remind from (2.26) and (2.35),

$$\widehat{\boldsymbol{\sigma}\boldsymbol{\nu}} = \boldsymbol{\sigma}_h\,\boldsymbol{\nu} - \boldsymbol{\tau}_{\mathbf{v}}\,(\mathbf{v}_h - \boldsymbol{\lambda}_{\mathbf{v}h})\,, \qquad \text{variant } (\mathbf{v},\boldsymbol{\sigma})_{\boldsymbol{S}}\,, \tag{4.58a}$$

$$\widehat{\boldsymbol{\sigma}\boldsymbol{\nu}} = \boldsymbol{\sigma}_h\,\boldsymbol{\nu} - \boldsymbol{\tau}_{\mathbf{u}}(\mathbf{u}_h - \boldsymbol{\lambda}_{\mathbf{u}h})\,, \qquad \text{variant } (\mathbf{u},\boldsymbol{\sigma})_{\boldsymbol{S}}\,. \tag{4.58b}$$

The stabilizations can be categorized into two groups,

– Group 1: one chooses or constructs a form for $\boldsymbol{\tau}_{\mathbf{v}}$ associated with variant $(\mathbf{v},\boldsymbol{\sigma})_{\boldsymbol{S}}$. Next, using relation $\mathbf{v} = -\mathrm{i}\omega\mathbf{u}$, the stabilization $\boldsymbol{\tau}_{\mathbf{u}}$ is determined by,

$$\boldsymbol{\tau}_{\mathbf{u}} = -\mathrm{i}\omega\,\boldsymbol{\tau}_{\mathbf{v}}\,. \tag{4.59}$$

– In group 2, the stabilization $\boldsymbol{\tau}_{\mathbf{u}}$ employs those derived for elastostatics, e.g., [52, 41]. The stabilization $\boldsymbol{\tau}_{\mathbf{v}}$ can then be obtained by the relation (4.59).

In Table 1, we give a list of variants considered in our work and analyzed in our numerical experiments Sections 6 and 7.

Identity-based In most general form, stabilization operators $\boldsymbol{\tau}_{\mathbf{u}}$ and $\boldsymbol{\tau}_{\mathbf{v}}$ are symmetric definite positive matrices. The simplest choice is given by a multiple of the identity matrix,

$$\boldsymbol{\tau}_{\mathbf{v}} \;=\; \tau\, \mathbb{Id} \qquad \text{Identity stabilization,} \tag{4.60}$$

with τ a scalar number.

Kelvin–Christoffel matrix More complicated forms of stabilization involve the 3×3 Kelvin–Christoffel matrix $\boldsymbol{\Gamma}$ of Subsection 3.4.2. We remind its definition associated with a vector $\boldsymbol{\nu}$:

$$\boldsymbol{\Gamma}(\boldsymbol{\nu}) := \boldsymbol{\nu}\cdot\boldsymbol{C}\cdot\boldsymbol{\nu}, \qquad \text{with} \qquad (\boldsymbol{\nu}\cdot\boldsymbol{C}\cdot\boldsymbol{\nu})_{jk} = \sum_{i,l} \nu_i\, c_{ijkl}\, \nu_l\,, \tag{4.61}$$

with definitions of its coefficients given in Subsection 3.5. From the assumption on the stiffness tensor $\boldsymbol{C}$, $\boldsymbol{\Gamma}(\boldsymbol{\nu})$ is symmetric and definite positive. It is thus diagonalizable with eigenvalues associated with wavespeeds in elasticity (up to three), cf. discussion in Subsection 3.4.2. For isotropic elasticity, the well-known speeds are the P- and S- wave speed, $\mathrm{c_P}$ and $\mathrm{c_S}$, (3.113), and $\boldsymbol{\Gamma}(\boldsymbol{\nu})$ has two distinct eigenvalues: $\rho\,\mathrm{c_P^2}$ and $\rho\,\mathrm{c_S^2}$. For anisotropy, we label three positive eigenvalues, listed in descending order: $\rho\mathrm{c_{qP}^2}$, $\rho\mathrm{c_{qS1}^2}$, and $\rho\mathrm{c_{qS2}^2}$. In our work, for anisotropic elasticity, we restrict to the case of three distinct wavespeeds such that

$$\rho\mathrm{c_{qP}^2} \;>\; \rho\mathrm{c_{qS1}^2} \;>\; \rho\mathrm{c_{qS2}^2}\,. \tag{4.62}$$

Hybridized Godunov stabilization From the construction and hybridization of the Godunov flux (detailed in Section 5), the Godunov matrix M_{Godunov} is defined such that

$$M_{\mathrm{Godunov}}(\boldsymbol{\nu}) = \begin{cases} M_{\mathrm{Giso}}(\boldsymbol{\nu})\,, & \text{for } \boldsymbol{C} \text{ isotropic} \\ M_{\mathrm{Gani}}(\boldsymbol{\nu})\,, & \text{for } \boldsymbol{C} \text{ anisotropic with 3 distinct speeds, (4.62).} \end{cases} \tag{4.63}$$

The Godunov flux for isotropic elasticity is defined as (with normalized normal direction $|\boldsymbol{\nu}| = 1$),

$$\begin{aligned} M_{\mathrm{Giso}}(\boldsymbol{\nu}) &= \frac{\rho}{\mathrm{c_P}+\mathrm{c_S}}\left(\mathrm{c_P c_S}\,\mathbb{Id} + \frac{\boldsymbol{\Gamma}(\boldsymbol{\nu})}{\rho}\right) = \rho\left(\mathrm{c_S}\,\mathbb{Id} + (\mathrm{c_P}-\mathrm{c_S})\boldsymbol{\nu}\otimes\boldsymbol{\nu}\right) \\ &= \rho\left(\mathrm{c_P}\,\mathbb{Id} + (\mathrm{c_P}-\mathrm{c_S})\left(\boldsymbol{\nu}\otimes\boldsymbol{\nu} - \mathbb{Id}\right)\right)\,, \end{aligned} \tag{4.64}$$

where $\otimes$ is the tensor product (2.3). The derivation of the equivalent expressions is given in Subsection 5.3 which follows the method in [53]. For anisotropy with 3 distinct wave speeds (i.e., assumption (4.62)),

$$M_{\mathrm{Gani}}(\boldsymbol{\nu}) := \rho\left(\mathrm{c_{qS1}} + \mathrm{c_{qS2}} + \mathrm{c_{qP}}\right)\left(1 + \gamma\left(\frac{\boldsymbol{\Gamma}(\boldsymbol{\nu})}{\rho} + \mathfrak{p}_2\right)^{-1}\right)\,, \tag{4.65}$$

with auxiliary quantities $\mathfrak{p}_2$ and γ defined from the 3 wave speeds,

$$\begin{aligned} \mathfrak{p}_2 &:= \mathrm{c_{qS1}\,c_{qS2}} \;+\; \mathrm{c_{qS1}\,c_{qP}} \;+\; \mathrm{c_{qS2}\,c_{qP}}\,, \\ \text{and} \qquad \gamma &:= \frac{\mathrm{c}_{qS1}\,\mathrm{c}_{qS2}\,\mathrm{c_{qP}}}{\mathrm{c}_{qS1}+\mathrm{c}_{qS2}+\mathrm{c}_{qP}} - \mathfrak{p}_2\,. \end{aligned} \tag{4.66}$$

Table 1: List of the stabilizations considered. Penalization $\boldsymbol{\tau}_{\mathbf{v}}$ has unit $[\mathrm{kg\,m^{-2}\,s^{-1}}]$, $\boldsymbol{\tau}_{\mathbf{u}}$ has unit $[\mathrm{kg\,m^{-2}\,s^{-2}}]$. The scalar coefficient τ and the Godunov matrix M_{Godunov} have unit $[\mathrm{kg\,m^{-2}\,s^{-1}}]$, the Kelvin–Christoffel matrix $\boldsymbol{\Gamma}$ has unit $[\mathrm{kg\,m^{-1}\,s^{-2}}]$ and the scalar coefficient β has unit $[\mathrm{s\,m^{-1}}]$.

Formulation	Numerical traces	Stabilization operator	
$(\mathbf{v},\boldsymbol{\sigma})_{\boldsymbol{S}}$	$\widehat{\mathbf{v}} = \boldsymbol{\lambda}_{\mathbf{v}}$, $\widehat{\boldsymbol{\sigma\nu}} = \boldsymbol{\sigma}_h - \boldsymbol{\tau}_{\mathbf{v}}(\mathbf{v}_h - \boldsymbol{\lambda}_{\mathbf{v}h})$	$\boldsymbol{\tau}_{\mathbf{v}} =$	$\tau\,\mathbb{I}_{\mathbb{d}}$
			$\boldsymbol{\Gamma}\,\beta$
			M_{Godunov}
$(\mathbf{u},\boldsymbol{\sigma})_{\boldsymbol{S}}$	$\widehat{\mathbf{u}} = \boldsymbol{\lambda}_{\mathbf{u}}$, $\widehat{\boldsymbol{\sigma\nu}} = \boldsymbol{\sigma}_h - \boldsymbol{\tau}_{\mathbf{u}}(\mathbf{u}_h - \boldsymbol{\lambda}_{\mathbf{u}h})$	$\boldsymbol{\tau}_{\mathbf{u}} =$	$-\mathrm{i}\omega\tau\ \mathbb{I}_{\mathbb{d}}$
			$-\mathrm{i}\omega\,\boldsymbol{\Gamma}\,\beta$
			$-\mathrm{i}\omega\,M_{\mathrm{Godunov}}$

5 Construction of hybridized Godunov stabilization operators

In this section, we provide details for the construction of the hybridized Godunov stabilization operator $M_{\mathrm{Godunov}}(\boldsymbol{\nu})$ (4.63) introduced in Subsection 4.4, in particular for anisotropic elasticity under the assumption of distinct speeds. Specifically, we need an expression for $\widehat{\boldsymbol{\sigma\nu}}$ along the interface F shared by two cells K^- and K^+. This is carried out by extending the method in [53] where isotropic elasticity is considered. For completeness, the construction of [53] for isotropy was reviewed in Subsection 5.3 and rewritten in the notation of Section 3, which helps out highlight the connection with Kelvin–Christoffel matrix.

As in [53], first-order formulation (5.1) with unknown $\mathbf{q} = (\boldsymbol{\epsilon}, \rho\mathbf{v})$ is employed. Integrating against test functions and by integrating by parts, cf. (5.5), we make appear the flux operator $\mathfrak{B}(\boldsymbol{\nu})$ (5.4) whose last 3 components give $\boldsymbol{\sigma\nu}$, cf. (5.13). This means that one first constructs the numerical trace $\widehat{\mathfrak{B}(\boldsymbol{\nu})}$ on an interface F, which consists of 3 mains ideas.

- The numerical flux on F is given by the Godunov flux $\mathfrak{B}(\boldsymbol{\nu})\mathbf{q}^\star$, with the value of flux at intermediate states $\mathbf{q}^\star$. These states are exact solution to a Riemann problem in a neighborhood of F, denoted by $\mathrm{RP}(\mathbf{q}^-,\mathbf{q}^+)$ having as initial data the trace of $\mathbf{q}$ from the left and right of F, written[16] respectively $\mathbf{q}^\pm$.

- The relation between the flux of the intermediate states and the left and right data is obtained from a system of Rankine–Hugoniot (RH) jump conditions, cf. (5.46) in Subsection 5.2. In this step, starting from the RH jump written in Cartesian coordinates, (5.54) for isotropic elasticity and (5.69) for anisotropy, we retrieve the usual transmission condition for elasticity, and an expression of the Godunov flux only in terms of one-sided data (i.e., either $\mathbf{q}^+$ or $\mathbf{q}^-$).

- In a third step, called 'hybridization', the transmission conditions ((5.56) for isotropy and (5.70) for anisotropy) and the aforementioned expression of the Godunov flux in terms of one-sided data ((5.60) and (5.62) for isotropy, and (5.89) and (5.92) for anisotropy) are exploited to obtain HDG numerical flux (5.95) and (5.95).

The first two ingredients are employed in the construction of upwind fluxes for DG implemention in time domain, cf. [61, 56, 55, 63], and for HDG scheme [53]. For applications with DG, the constructed numerical flux depends on information from both left and right of the interface. For implementation with HDG, also starting from these ingredients, [53] however proceeds differently to arrive at an expression of the flux which contains only one-sided data. Hybridization of Godunov flux is also discussed in a series of work with different formalisms [8, 9, 10] and in which Rankine–Hugoniot jump condition is recognized in sequel works ([9, 10]) to be a more natural and direct way to devise HDG flux.

[16] Recall that $\mathbf{q} = \cup_{K\in\mathcal{T}_h}\mathbf{q}^K$ along interface $\mathsf{F} = \mathsf{F}^+ = \mathsf{F}^-$ $\mathsf{F} = \partial K^-\cap\partial K^+$ and $\mathsf{F}^\pm = \partial K^\pm\cap\mathsf{F}$ then with $\mathbf{q}^\pm = \mathbf{q}^{K^\pm}|_{\mathsf{F}^\pm}$.

5.1 First order system and flux operator

First order system Consider the time-domain first order system with unknowns $(\boldsymbol{\epsilon}, \rho\mathbf{v})$,

$$\begin{cases} \partial_t \boldsymbol{\epsilon} - \nabla^{\mathfrak{s}} \mathbf{v} \;=\; 0\,, \\ \partial_t \rho\mathbf{v} - \nabla\cdot \boldsymbol{C}\boldsymbol{\epsilon} \;=\; \mathbf{f} \end{cases} \quad \Leftrightarrow \quad \partial_t \begin{pmatrix} \boldsymbol{\epsilon} \\ \rho\mathbf{v} \end{pmatrix} = \begin{pmatrix} 0 & \nabla^{\mathfrak{s}} \rho^{-1} \\ \nabla\cdot \boldsymbol{C} & 0 \end{pmatrix} \begin{pmatrix} \boldsymbol{\epsilon} \\ \rho\mathbf{v} \end{pmatrix}. \tag{5.1}$$

Introduce

$$\mathfrak{B}(\partial_{\mathbf{x}}) := -\begin{pmatrix} 0 & \mathbb{A}^t(\partial_{\mathbf{x}})\,\rho^{-1} \\ \mathbb{A}(\partial_{\mathbf{x}})\,{}^{\dagger}\overline{\overline{\boldsymbol{C}}}^{\dagger} & 0 \end{pmatrix}, \tag{5.2}$$

in Voigt notation as

$$\partial_t \mathbf{q} + \mathfrak{B}(\partial\mathbf{x})\,\mathbf{q} = \begin{pmatrix} 0 \\ \mathbf{f} \end{pmatrix}, \quad \text{with } \mathbf{q} = \begin{pmatrix} \overrightarrow{\boldsymbol{\epsilon}} \\ \rho\mathbf{v} \end{pmatrix}. \tag{5.3}$$

This is due to identity (3.31), $\overrightarrow{\nabla^{\mathfrak{s}}\mathbf{v}} = \mathbb{A}(\partial_{\mathbf{x}})^t\mathbf{v}$, and by combining (3.21b) and (3.32), $\nabla\cdot(\boldsymbol{C}\boldsymbol{\epsilon}) = \mathbb{A}(\partial_{\mathbf{x}})\,{}^{\dagger}\overline{\overline{\boldsymbol{C}}}^{\dagger}\overrightarrow{\boldsymbol{\epsilon}}$.

Flux term We have introduced the flux operator at ∂K and

$$\mathfrak{B}(\boldsymbol{\nu}) := -\begin{pmatrix} 0 & \mathbb{A}^t(\boldsymbol{\nu})\rho^{-1} \\ \mathbb{A}(\boldsymbol{\nu})\,{}^{\dagger}\overline{\overline{\boldsymbol{C}}}^{\dagger} & 0 \end{pmatrix}. \tag{5.4}$$

This arises from integrating both sides of (5.1) against test function $\begin{pmatrix} \boldsymbol{\chi} \\ \mathbf{w} \end{pmatrix}$ and after carrying out an integration-by-parts. Next, using identity (3.58), we arrive at,

$$\begin{aligned} &\int_K \partial_t \mathbf{q}\cdot\begin{pmatrix} \overrightarrow{\boldsymbol{\chi}}^{\dagger} \\ \mathbf{w} \end{pmatrix} \mathrm{d}\mathbf{x} \;+\; \int_K \mathfrak{B}(\partial_{\mathbf{x}})\begin{pmatrix} \overrightarrow{\boldsymbol{\epsilon}} \\ \rho\mathbf{v} \end{pmatrix}\cdot\begin{pmatrix} \overrightarrow{\boldsymbol{\chi}}^{\dagger} \\ \mathbf{w} \end{pmatrix} \mathrm{d}\mathbf{x} \\ &\quad = \int_K \partial_t \mathbf{q}\cdot\begin{pmatrix} \overrightarrow{\boldsymbol{\chi}}^{\dagger} \\ \mathbf{w} \end{pmatrix} \mathrm{d}\mathbf{x} + \int_K \begin{pmatrix} \overrightarrow{\boldsymbol{\epsilon}} \\ \rho\mathbf{v} \end{pmatrix}\cdot\mathfrak{B}^{\mathrm{ad}}(\partial_{\mathbf{x}})\begin{pmatrix} \overrightarrow{\boldsymbol{\chi}}^{\dagger} \\ \mathbf{w} \end{pmatrix} \mathrm{d}\mathbf{x} \;+\; \int_{\partial K} \mathfrak{B}(\boldsymbol{\nu})\begin{pmatrix} \overrightarrow{\boldsymbol{\epsilon}} \\ \rho\mathbf{v} \end{pmatrix}\cdot\begin{pmatrix} \overrightarrow{\boldsymbol{\chi}}^{\dagger} \\ \mathbf{w} \end{pmatrix} \mathrm{d}s_{\mathbf{x}}\,, \end{aligned} \tag{5.5}$$

with the 'adjoint' operator associated with $\mathfrak{B}$,

$$\mathfrak{B}^{\mathrm{ad}}(\partial_{\mathbf{x}}) := \begin{pmatrix} 0 & {}^{\dagger}\overline{\overline{\boldsymbol{C}}}^{\dagger}\,\mathbb{A}(\partial_{\mathbf{x}})^t \\ \rho^{-1}\,\mathbb{A}(\partial_{\mathbf{x}}) & 0 \end{pmatrix}. \tag{5.6}$$

Eigenvalues of $\mathfrak{B}(\boldsymbol{\nu})$ Consider the eigenvalues α of the flux operator $\mathfrak{B}(\boldsymbol{\nu})$,

$$\begin{pmatrix} 0 & \mathbb{A}^t(\boldsymbol{\nu})\rho^{-1} \\ \mathbb{A}(\boldsymbol{\nu})\,{}^{\dagger}\overline{\overline{\boldsymbol{C}}}^{\dagger} & 0 \end{pmatrix}\begin{pmatrix} \overrightarrow{\boldsymbol{\tau}} \\ \mathbf{w} \end{pmatrix} = \alpha\begin{pmatrix} \overrightarrow{\boldsymbol{\tau}} \\ \mathbf{w} \end{pmatrix} \quad \Leftrightarrow \quad \begin{cases} \mathbb{A}^t(\boldsymbol{\nu})\rho^{-1}\mathbf{w} \;=\; \alpha\,\overrightarrow{\boldsymbol{\tau}} \\ \mathbb{A}(\boldsymbol{\nu})\,{}^{\dagger}\overline{\overline{\boldsymbol{C}}}^{\dagger}\overrightarrow{\boldsymbol{\tau}} \;=\; \alpha\,\mathbf{w} \end{cases}. \tag{5.7}$$

Apply to both sides of the first equation $\mathbb{A}(\boldsymbol{\nu})\,{}^{\dagger}\overline{\overline{\boldsymbol{C}}}^{\dagger}$, we obtain the eigenproblem for the 3×3 matrix of Kelvin–Christoffel matrix $\boldsymbol{\Gamma}(\boldsymbol{\nu})$, which is also called the Christoffel equation,

$$\mathbb{A}(\boldsymbol{\nu})\,{}^{\dagger}\overline{\overline{\boldsymbol{C}}}^{\dagger}\mathbb{A}^t(\boldsymbol{\nu})\,\mathbf{w} \;=\; \rho\,\alpha^2\,\mathbf{w} \quad \Leftrightarrow \quad \boldsymbol{\Gamma}(\boldsymbol{\nu})\,\mathbf{w} \;=\; \rho\,\alpha^2\,\mathbf{w}\,. \tag{5.8}$$

We have denoted in (4.62) the three (assumed distinct) eigenvalues of $\boldsymbol{\Gamma}(\boldsymbol{\nu})$:

$$\rho\,\mathrm{c}_{\mathrm{qP}}^2 \;<\; \rho\,\mathrm{c}_{\mathrm{qS1}}^2 \;<\; \rho\,\mathrm{c}_{\mathrm{qS2}}^2\,. \tag{5.9}$$

That is, under assumption (4.62), the eigenvalues of $\mathfrak{B}(\boldsymbol{\nu})$ are

$$-\mathrm{c}_{\mathrm{qP}}\;,\; -\mathrm{c}_{\mathrm{qS1}}\,,\; -\mathrm{c}_{\mathrm{qS2}}\;,\; \underbrace{0}_{\text{multiplicity 3}}\;,\; \mathrm{c}_{\mathrm{qS2}}\;,\; \mathrm{c}_{\mathrm{qS1}}\;,\; \mathrm{c}_{\mathrm{qP}}\,. \tag{5.10}$$

For elastic isotropy, Subsection 3.5.1, the eigenvalues of $\mathfrak{B}(\boldsymbol{\nu})$ are

$$-\mathrm{c}_{\mathrm{P}}\;,\; \underbrace{-\mathrm{c}_{\mathrm{S}}}_{\text{multiplicity 2}}\;,\; \underbrace{0}_{\text{multiplicity 3}}\;,\; \underbrace{\mathrm{c}_{\mathrm{S}}}_{\text{multiplicity 2}}\;,\; \mathrm{c}_{\mathrm{P}}\,. \tag{5.11}$$

Action of $\mathfrak{B}(\boldsymbol{\nu})$ From its definition, for vectors $\mathbf{W}$ of length 6 and $\mathbf{w}$ of length 3,

$$\mathfrak{B}(\boldsymbol{\nu}) \begin{pmatrix} \mathbf{W} \\ \mathbf{w} \end{pmatrix} = - \begin{pmatrix} \mathbb{A}^t(\boldsymbol{\nu}) \rho^{-1} \mathbf{w} \\ \mathbb{A}(\boldsymbol{\nu})\, {}^{\dagger}\overline{\overline{\boldsymbol{C}}}^{\dagger} \mathbf{W} \end{pmatrix}. \tag{5.12}$$

By using this on to $\mathbf{q} = \begin{pmatrix} \overrightarrow{\boldsymbol{\epsilon}} \\ \rho \mathbf{v} \end{pmatrix}$, we have

$$\mathfrak{B}(\boldsymbol{\nu})\mathbf{q} = - \begin{pmatrix} \mathbb{A}^t(\boldsymbol{\nu})\mathbf{v} \\ \mathbb{A}(\boldsymbol{\nu})\, {}^{\dagger}\overline{\overline{\boldsymbol{C}}}^{\dagger} \overrightarrow{\boldsymbol{\epsilon}} \end{pmatrix} = - \begin{pmatrix} \mathbb{A}^t(\boldsymbol{\nu})\mathbf{v} \\ \boldsymbol{\sigma}\boldsymbol{\nu} \end{pmatrix} = - \begin{pmatrix} \overrightarrow{\mathbf{v} \odot \boldsymbol{\nu}} \\ \boldsymbol{\sigma}\boldsymbol{\nu} \end{pmatrix} ; \tag{5.13a}$$

$$\mathfrak{B}(\boldsymbol{\nu})^2\mathbf{q} = \begin{pmatrix} \mathbb{A}^t(\boldsymbol{\nu})\, \rho^{-1}\, \boldsymbol{\sigma}\boldsymbol{\nu} \\ \rho \mathbb{A}(\boldsymbol{\nu})\, {}^{\dagger}\overline{\overline{\boldsymbol{C}}}^{\dagger}\, \mathbb{A}^t(\boldsymbol{\nu})\mathbf{v} \end{pmatrix} = \frac{1}{\rho} \begin{pmatrix} \mathbb{A}^t(\boldsymbol{\nu})\boldsymbol{\sigma}\boldsymbol{\nu} \\ \rho\, \boldsymbol{\Gamma}(\boldsymbol{\nu})\mathbf{v} \end{pmatrix} = \frac{1}{\rho} \begin{pmatrix} \overrightarrow{\boldsymbol{\nu} \odot \boldsymbol{\sigma}\boldsymbol{\nu}} \\ \rho\, \boldsymbol{\Gamma}(\boldsymbol{\nu})\mathbf{v} \end{pmatrix} ; \tag{5.13b}$$

$$\mathfrak{B}(\boldsymbol{\nu})^3\mathbf{q} = - \begin{pmatrix} \mathbb{A}^t(\boldsymbol{\nu})\rho^{-1}\mathbb{A}(\boldsymbol{\nu})\, {}^{\dagger}\overline{\overline{\boldsymbol{C}}}^{\dagger}\, \mathbb{A}^t(\boldsymbol{\nu})\mathbf{v} \\ \mathbb{A}(\boldsymbol{\nu})\, {}^{\dagger}\overline{\overline{\boldsymbol{C}}}^{\dagger} \mathbb{A}^t(\boldsymbol{\nu})\rho^{-1}\boldsymbol{\sigma}\boldsymbol{\nu} \end{pmatrix} = -\frac{1}{\rho} \begin{pmatrix} \mathbb{A}^t(\boldsymbol{\nu})\, \boldsymbol{\Gamma}(\boldsymbol{\nu})\mathbf{v} \\ \boldsymbol{\Gamma}(\boldsymbol{\nu})\boldsymbol{\sigma}\boldsymbol{\nu} \end{pmatrix} = -\frac{1}{\rho} \begin{pmatrix} \overrightarrow{\boldsymbol{\nu} \odot \boldsymbol{\Gamma}(\boldsymbol{\nu})\mathbf{v}} \\ \boldsymbol{\Gamma}(\boldsymbol{\nu})\boldsymbol{\sigma}\boldsymbol{\nu} \end{pmatrix}. \tag{5.13c}$$

Flux operator in rotated coordinates Given a normal vector $\boldsymbol{\nu}$ at a straight edge face F, we consider a second coordinate system obtained by rotation so that $\mathbf{e}_x$ is parallel to the axis $\boldsymbol{\nu}$. The basis of the rotated coordinate is given by the ordered set $(\boldsymbol{\nu}, \mathbf{t}, \tilde{\mathbf{t}})$ with the latter vectors being tangential to the straight-edge face F. The components of these vectors in Cartesian coordinates are written as

$$\nu_x, \nu_y, \nu_z\,; \quad t_x, t_y, t_z\,; \quad \tilde{t}_x, \tilde{t}_y, \tilde{t}_z\,. \tag{5.14}$$

The relation between the two coordinates is given by formula derived in Subsection 3.4.5 with rotation matrix $\mathcal{R}$ and Bond matrix $\mathbf{M}$ associated specifically to these two coordinates,

$$\mathcal{R} = (\mathfrak{r}_{ij}) := \begin{pmatrix} \nu_x & t_x & \tilde{t}_x \\ \nu_y & t_y & \tilde{t}_y \\ \nu_z & t_z & \tilde{t}_z \end{pmatrix}, \quad \text{and} \quad \mathbf{M} := \mathcal{M}^{\dagger}[\mathcal{R}] \quad \text{following definition (3.64)}\ . \tag{5.15}$$

With the matrices defined in (5.15), we introduce the block-diagonal matrix $\mathbb{T}$ defined as

$$\mathbb{T} := \begin{pmatrix} \mathbf{M} & \mathbf{0} \\ \mathbf{0} & \mathcal{R}^t \end{pmatrix}, \qquad \mathbb{T}^{-1} = \begin{pmatrix} \mathbf{M}^{-1} & \mathbf{0} \\ \mathbf{0} & \mathcal{R} \end{pmatrix}. \tag{5.16}$$

Denote by $\widetilde{\mathfrak{B}(\boldsymbol{\nu})}$ the matrix representation of the flux operator in rotated coordinates, i.e.,

$$(\mathfrak{B}(\boldsymbol{\nu})\mathbf{q}) \cdot \mathbf{p} = \widetilde{\mathfrak{B}(\boldsymbol{\nu})}\, \mathbf{q} \cdot \tilde{\mathbf{p}} = \left(\widetilde{\mathfrak{B}(\boldsymbol{\nu})}\, \tilde{\mathbf{q}}\right) \cdot \tilde{\mathbf{p}}\,. \tag{5.17}$$

By abuse of notation, $\mathfrak{B}(\boldsymbol{\nu})$ also denotes the matrix representation of the flux operator in Cartesian coordinates. From the relation derived in (3.107) between $\mathbf{q}$ and $\tilde{\mathbf{q}}$ (now with rotation and Bond matrix given in (5.15)), we obtain a more explicit expression for $\widetilde{\mathfrak{B}(\boldsymbol{\nu})}$ which is taken as its definition,

$$\widetilde{\mathfrak{B}(\boldsymbol{\nu})} := \begin{pmatrix} \mathbf{M} & \mathbf{0} \\ \mathbf{0} & \mathcal{R}^t \end{pmatrix} \mathfrak{B}(\boldsymbol{\nu}) \begin{pmatrix} \mathbf{M}^{-1} & \mathbf{0} \\ \mathbf{0} & \mathcal{R} \end{pmatrix}. \tag{5.18}$$

In more compact notation, matrix $\widetilde{\mathfrak{B}(\boldsymbol{\nu})}$ and $\mathfrak{B}(\boldsymbol{\nu})$ are conjugation of each other by $\mathbb{T}$ (5.16),

$$\widetilde{\mathfrak{B}(\boldsymbol{\nu})} = \mathbb{T}\, \mathfrak{B}(\boldsymbol{\nu})\, \mathbb{T}^{-1}\,, \quad \mathfrak{B}(\boldsymbol{\nu}) = \mathbb{T}^{-1}\, \widetilde{\mathfrak{B}(\boldsymbol{\nu})}\, \mathbb{T}\,. \tag{5.19}$$

To state the following identity for the rotated flux, we recall $\overline{\overline{\tilde{\boldsymbol{C}}}}$ is the stiffness tensor in rotated coordinates written in Voigt representation, and its scaled version ${}^{\dagger}\overline{\overline{\tilde{\boldsymbol{C}}}}^{\dagger}$ is defined in (3.10). We also recall from identity (3.98) the matrix,

$$\mathbb{A}_1 := \begin{pmatrix} 1 & 0 & 0 & 0 & 0 & 0 \\ 0 & 0 & 0 & 0 & 0 & \frac{1}{2} \\ 0 & 0 & 0 & 0 & \frac{1}{2} & 0 \end{pmatrix}. \tag{5.20}$$

Proposition 9. *The matrix representation of the flux operator $\mathfrak{B}(\boldsymbol{\nu})$ in Cartesian coordinates, also denoted by $\mathfrak{B}(\boldsymbol{\nu})$, and rotated coordinates $(\boldsymbol{\nu}, \mathbf{t}, \tilde{\mathbf{t}})$ denoted by $\widetilde{\mathfrak{B}(\boldsymbol{\nu})}$ are conjugation of each other by $\mathbb{T}$, (5.19), which means they have the same spectral structure stated in (5.10) or (5.25). Additionally, the representation in rotated coordinates is explicitly given by*

$$\widetilde{\mathfrak{B}(\boldsymbol{\nu})} = \begin{pmatrix} 0 & \mathbb{A}_1^t \rho^{-1} \\ \mathbb{A}_1 \, {}^{\dagger}\tilde{\tilde{\boldsymbol{C}}}^{\dagger} & 0 \end{pmatrix} . \tag{5.21}$$

Proof. Inject the definition (5.4) of $\mathfrak{B}(\boldsymbol{\nu})$ in the defining expression (5.18) of its rotated version, we obtain

$$\begin{aligned} \widetilde{\mathfrak{B}(\boldsymbol{\nu})} &= -\begin{pmatrix} \mathbf{M} & \mathbf{0} \\ \mathbf{0} & \mathcal{R}^t \end{pmatrix} \begin{pmatrix} 0 & \mathbb{A}^t(\boldsymbol{\nu}) \rho^{-1} \\ \mathbb{A}(\boldsymbol{\nu}) \, {}^{\dagger}\tilde{\tilde{\boldsymbol{C}}}^{\dagger} & 0 \end{pmatrix} \begin{pmatrix} \mathbf{M}^{-1} & \mathbf{0} \\ \mathbf{0} & \mathcal{R} \end{pmatrix} \\ &= -\begin{pmatrix} \mathbf{M} & \mathbf{0} \\ \mathbf{0} & \mathcal{R}^t \end{pmatrix} \begin{pmatrix} 0 & \mathbb{A}^t(\boldsymbol{\nu}) \mathcal{R} \rho^{-1} \\ \mathbb{A}(\boldsymbol{\nu}) \, {}^{\dagger}\tilde{\tilde{\boldsymbol{C}}}^{\dagger} \mathbf{M}^{-1} & 0 \end{pmatrix} = -\begin{pmatrix} 0 & \mathbf{M} \mathbb{A}^t(\boldsymbol{\nu}) \mathcal{R} \rho^{-1} \\ \mathcal{R}^t \mathbb{A}(\boldsymbol{\nu}) \, {}^{\dagger}\tilde{\tilde{\boldsymbol{C}}}^{\dagger} \mathbf{M}^{-1} & 0 \end{pmatrix} . \end{aligned} \tag{5.22}$$

The final expression is obtained by rewriting

$$\mathcal{R}^t \mathbb{A}(\boldsymbol{\nu}) \, {}^{\dagger}\tilde{\tilde{\boldsymbol{C}}}^{\dagger} \mathbf{M}^{-1} = \left(\mathcal{R}^t \mathbb{A}(\boldsymbol{\nu}) \mathbf{M}^t \right) \left(\mathbf{M}^{-t} \, {}^{\dagger}\tilde{\tilde{\boldsymbol{C}}}^{\dagger} \mathbf{M}^{-1} \right) , \tag{5.23}$$

and by applying identities (3.98) and (3.108).

□

5.2 Riemann problem and Rankine–Hugoniot jump conditions

5.2.1 Toy Riemann problem and its solution

Toy Riemann problem We adapt the discussion of Riemann problem from [57, Section 2.3.3] to incorporate the spectral structure of the flux operator in (5.10). We work in (rotated) coordinates having as variable $\tilde{\mathbf{x}} = (n, s, \tilde{s})^t$. The toy Riemann problem is defined in variable (t, n) with 9×9 constant coefficient matrix $\mathbb{B}_n$. It has as unknown the length-9 vector $\mathbf{u} = \mathbf{u}(\tilde{\mathbf{x}}, t) = \mathbf{u}(n, t)$ and initial data the piecewise constant length-9 vector $\mathfrak{u} = \mathfrak{u}(n)$,

$$\partial_t \mathbf{u} \; + \; \partial_n \mathbb{B}_n \mathbf{u} = 0 , \qquad \text{with} \quad \mathbf{u}(\tilde{\mathbf{x}}, 0) = \mathbf{u}(n) = \begin{cases} \mathbf{u}^L , & n < 0 , \\ \mathbf{u}^R , & n > 0 \end{cases} . \tag{5.24}$$

The solution to (5.24) is constructed below and takes the final form in (5.37).

Assumption on matrix $\mathbb{B}_n$ We will assume that $\mathbb{B}_n$ has the same spectral structure of $\mathfrak{B}$ (5.10). This means $\mathbb{B}_n$ is diagonalizable with eigenvalue 0 having multiplicity 3 and remaining nonzero eigenvalues λ_i having multiplicity 1; specifically,

$$\lambda_1 \; < \; \lambda_2 \; < \; \lambda_3 \; < \; \lambda_4 = \lambda_5 = \lambda_6 = 0 \; < \; \lambda_7 \; < \; \lambda_8 \; < \; \lambda_9 . \tag{5.25}$$

Denote by $\mathbf{k}_i$ the corresponding eigenvectors

$$\mathbb{B}_n \, \mathbf{k}_i = \lambda_i \, \mathbf{k}_i , \quad i = 1, \ldots, 9 . \tag{5.26}$$

We also denote by K the 9×9 matrix whose columns are $\mathbf{k}_i$, and $\boldsymbol{\Lambda}$ the diagonal matrix whose entries are the eigenvalues,

$$K = [\mathbf{k}_1, \ldots, \mathbf{k}_9] , \qquad \boldsymbol{\Lambda} = \operatorname{diag}(\lambda_1, \ldots, \lambda_9) , \tag{5.27}$$

We thus have,

$$\mathbb{B}_n \; = \; K \, \boldsymbol{\Lambda} \, K^{-1} . \tag{5.28}$$

Solution to the Riemann problem We next construct the general solution to (5.24), following the discussion in [57, Section 2.3.3]. In diagonalizing basis, i.e. $\mathbf{w} = K^{-1}\mathbf{u}$, the Riemann problem (5.24) is transformed to,

$$\partial_t \mathbf{w} + \partial_n \mathbf{\Lambda} \mathbf{w} = 0\,, \qquad \text{with} \quad \mathbf{w}(n,0) = \mathfrak{w}(n) = K^{-1}\mathbf{u}\,, \tag{5.29}$$

With $\mathbf{\Lambda}$ a diagonal matrix, (5.24) is decoupled to 9 advection equations, satisfied by each component w_i of $\mathbf{w}$,

$$\partial_t w_i \;+\; \lambda_i\, \partial_n w_i = 0\,, \qquad \text{with} \qquad w_i(n,0) = \mathfrak{w}_i(n)\,. \tag{5.30}$$

The solutions of (5.30) are given by advection of the initial condition $\mathfrak{w}_i$ along straight line at speed λ_i in the (n,t)-plane,

$$w_i(n,t) \;=\; \mathfrak{w}_i(n - \lambda_i t)\,. \tag{5.31}$$

This means that w_i is constant along the straight line with slope λ_i through the point $(n,0)$ and taking value $\mathfrak{w}_i(n_0)$ with $n_0 = n - \lambda_i t$. Using relation $\mathbf{u} = K\mathbf{w}$, we obtain the solution to the original Riemann problem (5.24),

$$\mathbf{u}(n,t) \;=\; \sum_{j=1}^{9} w_j(n,t)\,\mathbf{k}_j \;=\; \sum_{j=1}^{9} \mathfrak{w}_j(n - \lambda_j t)\,\mathbf{k}_j\,. \tag{5.32}$$

Next, we determine the value of $\mathfrak{w}_j$ in terms of the initial value $\mathfrak{u}$ in (5.24), which is rewritten in terms of the eigenfunctions $\mathbf{k}_i$ (5.26),

$$\mathbf{u}(n) = \begin{cases} \mathbf{u}^L = \displaystyle\sum_{i=1}^{9} \alpha_i\,\mathbf{k}_i\,, & n < 0 \\[2ex] \mathbf{u}^R = \displaystyle\sum_{i=1}^{9} \beta_i\,\mathbf{k}_i\,, & n > 0 \end{cases} \tag{5.33}$$

Setting $t = 0$ in (5.32), we obtain another expression of the initial value of $\mathbf{u}$,

$$\mathbf{u}(n) \;=\; \mathbf{u}(n,0) \;=\; \sum_{j=1}^{9} \mathfrak{w}_j(n)\,\mathbf{k}_j\,. \tag{5.34}$$

Comparing the two above expressions of initial values, (5.34) with (5.33), we obtain the value of $\mathfrak{w}_j$, which then yields,

$$\mathfrak{w}_j(n) = \begin{cases} \alpha_j\,, & \text{for } n < 0, \\ \beta_j\,, & \text{for } n > 0 \end{cases}\,. \tag{5.35}$$

This then gives the value of $\mathbf{w}_j$,

$$w_i(n,t) = \mathfrak{w}_j(n - \lambda_j t) = \begin{cases} \alpha_j\,, & \text{for } n - \lambda_j\, t < 0 \;\Leftrightarrow\; \frac{n}{t} < \lambda_j \\ \beta_j\,, & \text{for } n - \lambda_j\, t > 0 \;\Leftrightarrow\; \frac{n}{t} > \lambda_j \end{cases}\,. \tag{5.36}$$

Substitute the obtained expression of $\mathfrak{w}_j$ into (5.32), we arrive at, cf. [57, Equation (2.60)],

$$\mathbf{u}(n,t) = \sum_{j=1}^{I} \beta_j\,\mathbf{k}_j + \sum_{j=I+1}^{9} \alpha_j\,\mathbf{k}_j\,, \qquad \text{with } I \text{ defined by } \;\lambda_I < \frac{n}{t} < \lambda_{I+1}\,. \tag{5.37}$$

States From (5.37), we define the states associated to the distinct values of the eigenvalues, which give the value of solution $\mathbf{u}$ in the eight regions delimited by the ray along which the singularities of the initial conditions $\mathbf{u}$ are propagated, cf. Figure 2.

$$\underbrace{U_L\,,\;\; U^{a-}\,,\;\; U^{b-}\,,\;\; U^{\star-}}_{\text{value on } n<0}\,, \qquad \underbrace{U^{\star+}\,,\;\; U^{b+}\,,\;\; U^{a+}\,,\;\; U_R}_{\text{value on } n>0}\,. \tag{5.38}$$

Their explicit definitions in terms of the eigenfunctions $\mathbf{k}_i$ are,

– The states to the left of the interfaces (i.e., for $n < 0$) are,

$$\begin{aligned} U_L &= \sum_{i=1}^{9} \alpha_i \mathbf{k}_i \,, \qquad U^{a-} = \beta_1 \mathbf{k}_1 + \sum_{i=2}^{9} \alpha_i \mathbf{k}_i \,, \qquad U^{b-} = \sum_{j=1}^{2} \beta_j \mathbf{k}_j + \sum_{i=3}^{9} \alpha_i \mathbf{k}_i \,, \\ U^{\star -} &:= \sum_{i=1}^{3} \beta_i \mathbf{k}_i + \sum_{i=4}^{9} \alpha_i \mathbf{k}_i \;=\; U_L + \sum_{i=1}^{3} (\beta_i - \alpha_i) \mathbf{k}_i \,. \end{aligned} \tag{5.39}$$

– The states to the right of the interface (i.e., for $n > 0$) are

$$\begin{aligned} U_R &= \sum_{j=1}^{9} \beta_j \mathbf{k}_j \,, \qquad U^{a+} = \sum_{j=1}^{8} \beta_j \mathbf{k}_j + \alpha_9 \mathbf{k}_9 \,, \qquad U^{b+} = \sum_{j=1}^{7} \beta_j \mathbf{k}_j + \sum_{j=8}^{9} \alpha_j \mathbf{k}_j \,, \\ U^{\star +} &:= \sum_{i=1}^{6} \beta_i \mathbf{k}_i + \sum_{i=7}^{9} \alpha_i \mathbf{k}_i \;=\; U_R + \sum_{i=7}^{9} (\alpha_i - \beta_i) \mathbf{k}_i \,. \end{aligned} \tag{5.40}$$

Derivation of Rankine–Hugoniot (RH) jump conditions From the definition of the states on the left-hand side region (5.39), we have

$$U^{a-} - U_L = (\beta_1 - \alpha_1) \mathbf{k}_1 \,. \tag{5.41}$$

We apply $\mathbb{B}_n$ to both sides of the equation to obtain,

$$\mathbb{B}_n(U^{a-} - U_L) = (\beta_1 - \alpha_1) \mathbb{B}_n \mathbf{k}_1 \quad \Rightarrow \quad \mathbb{B}_n(U^{a-} - U_L) = \lambda_1 (\beta_1 - \alpha_1) \mathbf{k}_1 \,. \tag{5.42}$$

Next replace $\mathbf{k}_1$ using (5.41), we obtain the RH condition associated with speed λ_1,

$$\mathbb{B}_n(U^{a-} - U_L) = \lambda_1 (U^{a-} - U_L) \,. \tag{5.43}$$

The RH jump conditions with speed λ_2, λ_3, λ_8 and λ_9 are obtained in a similar manner, e.g., for λ_9 we have,

$$U^{a+-} - U_R = (\beta_9 - \alpha_9) \mathbf{k}_9 \quad \Rightarrow \quad \mathbb{B}_n(U^{a+-} - U_R) = \lambda_9 (U^{a+-} - U_R). \tag{5.44}$$

Lastly, the intermediate states 'separated' by the interface satisfy,

$$U^{\star -} - U^{\star +} = \sum_{i=3}^{6} (\alpha_i - \beta_i) \mathbf{k}_i \quad \Rightarrow \quad \mathbb{B}_n(U^{\star -} - U^{\star +}) = 0 \,. \tag{5.45}$$

We gather the jump conditions associated with the 7 distinct speeds (eigenvalues),

$$\begin{cases} \mathbb{B}_n(U^{a-} - U_L) &= \lambda_1 (U^{a-} - U_L) \,, \\ \mathbb{B}_n(U^{b-} - U^{a-}) &= \lambda_2 (U^{a-} - U^{a+}) \,, \\ \mathbb{B}_n(U^{\star -} - U^{b-}) &= \lambda_3 (U^{a-} - U^{a+}) \,, \\ \mathbb{B}_n(U^{\star -} - U^{\star +}) &= 0 \,, \\ \mathbb{B}_n(U^{\star +} - U^{b+}) &= \lambda_7 (U^{a-} - U^{a+}) \,, \\ \mathbb{B}_n(U^{b+-} - U^{a+}) &= \lambda_8 (U^{b+-} - U^{a+}) \,, \\ \mathbb{B}_n(U^{a+-} - U_R) &= \lambda_9 (U^{a+-} - U_R) \,. \end{cases} \tag{5.46}$$

5.2.2 Jump equations in original coordinates

We follow the notation and quantities introduced at the end of Subsection 5.1. Recall briefly that given a normal vector $\boldsymbol{\nu}$ at a straight edge face F, we consider a second coordinate system obtained by rotation so

that $\mathbf{e}_x$ is parallel to the axis $\boldsymbol{\nu}$. The orthonormal basis of the rotated coordinate is given by the ordered set $(\boldsymbol{\nu}, \mathbf{t}, \tilde{\mathbf{t}})$.

We return to the model problem considered in Subsection 5.2.1, now with $\mathbb{B}_n$ given by $\widetilde{\mathfrak{B}(\boldsymbol{\nu})}$ defined in (5.21), that is,

$$(\partial_t + \partial_n \mathbb{B}_n)\tilde{\mathbf{q}} = 0\,, \quad \text{with} \quad \mathbb{B}_n := \widetilde{\mathfrak{B}(\boldsymbol{\nu})}\,.$$

We recall from (5.19), that with $\mathbb{T}$ defined in (5.16),

$$\mathbb{B}_n = \mathbb{T}\,\mathfrak{B}(\boldsymbol{\nu})\,\mathbb{T}^{-1}\,, \quad \mathfrak{B}(\boldsymbol{\nu}) = \mathbb{T}^{-1}\,\mathbb{B}_n\,\mathbb{T}\,.$$

The jump condition with $\mathbb{B}_n$ was derived in (5.46) (now with the eigenvalues denoted by speed c_j)

$$\mathbb{B}_n(\tilde{\mathbf{q}}^\alpha - \tilde{\mathbf{q}}^\beta) = c_j(\tilde{\mathbf{q}}^\alpha - \tilde{\mathbf{q}}^\beta)\,. \tag{5.47}$$

Substitute in the relation between the operators and the solutions, $\tilde{\mathbf{q}}^\bullet = \mathbb{T}\mathbf{q}^\bullet$, we obtain

$$\mathbb{T}^{-1}\mathbb{B}_n\mathbb{T}(\mathbf{q}^\alpha - \mathbf{q}^\beta) = c_j(\mathbf{q}^\alpha - \mathbf{q}^\beta)\,, \tag{5.48}$$

which gives the jump condition in original coordinates,

$$\mathfrak{B}(\boldsymbol{\nu})(\mathbf{q}^\alpha - \mathbf{q}^\beta) \;=\; c_j(\mathbf{q}^\alpha - \mathbf{q}^\beta)\,. \tag{5.49}$$

Remark 11. *The above derivation can be extended for $\mathfrak{B}$ piecewise-constant to arrive at the same conditions, cf. e.g. [55, Equation (19))] for anisotropy, and [61, Equation (14)], [53, Equation (31)]. These states are explicitly given in terms of the eigenvalues and vectors of $\mathfrak{B}(\boldsymbol{\nu})$, which extend the discussion in [57, Section 2.3.3] with $\mathfrak{B}$ discontinuous across the interface. In addition, the differences $(\mathbf{q}^{\star\pm} - \mathbf{q}^{\pm})$ are linear combinations of corresponding eigenfunctions, cf. [63, Equation (20)], [55, Equation (20)],*

$$\mathbf{q}^{\star-} = \mathbf{q}^- + \sum_{i=1}^{3} \gamma_i^- \mathbf{k}_i^-\,, \qquad \mathbf{q}^{\star+} = \mathbf{q}^+ + \sum_{i=7}^{9} \gamma_i^+ \mathbf{k}_i^+\,. \tag{5.50}$$

5.3 Derivation for isotropic elasticity

Here we consider isotropic elasticity, Subsection 3.5.1, where the elasticity tensor is written from the two Lamé parameters λ and μ, that define the two wave speeds $\mathrm{c_P}$ and $\mathrm{c_S}$ (3.113). We denote by $\boldsymbol{\nu}$ the normal vector along the interface pointing from K^- to K^+, and $\boldsymbol{\nu}^\pm$ the outward pointing ones of $K^\pm$, we have

$$\boldsymbol{\nu} = \boldsymbol{\nu}^- = -\boldsymbol{\nu}^+\,. \tag{5.51}$$

To distinguish the medium on each side of an interface in particular allowing to be discontinuous across an interface, we write

$$\rho^\pm, \quad \boldsymbol{C}^\pm, \quad \mathfrak{B}(\boldsymbol{\nu})^\pm, \quad \text{and its eigenvalues } \mathrm{c}_\alpha^\pm\,. \tag{5.52}$$

Here, $\mathfrak{B}^-(\boldsymbol{\nu})$ is defined in (5.4) with physical parameters associated with mesh cell K^-, i.e., $(\rho^-, \lambda^-, \mu^-)$ and normal vector $\boldsymbol{\nu}^-$. Similarly for $\mathfrak{B}(\boldsymbol{\nu})^+$. Recall the spectral structure of $\mathfrak{B}(\boldsymbol{\nu})$ is as follows, cf. (5.11),

$$-\mathrm{c_P}\;,\quad \underbrace{-\mathrm{c_S}}_{\text{multiplicity 2}}\;,\quad \underbrace{0}_{\text{multiplicity 3}}\;,\quad \underbrace{\mathrm{c_S}}_{\text{multiplicity 2}}\;,\quad \mathrm{c_P}\,. \tag{5.53}$$

Rankine–Hugoniot jump conditions in Cartesian coordinates Apply the jump conditions obtained in (5.49) adapted to spectral structure (5.53), cf. Figure 1,

$$\begin{cases}
\mathfrak{B}(\boldsymbol{\nu})^- \left(\mathbf{q}^{a-} - \mathbf{q}^-\right) = -\mathrm{c_P^-} \left(\mathbf{q}^{a-} - \mathbf{q}^-\right)\,; & \text{(5.54a)}\\
\mathfrak{B}(\boldsymbol{\nu})^- \left(\mathbf{q}^{\star-} - \mathbf{q}^{a-}\right) = -\mathrm{c_S^-} \left(\mathbf{q}^{\star-} - \mathbf{q}^{a-}\right)\,; & \text{(5.54b)}\\
\mathfrak{B}(\boldsymbol{\nu})^- \mathbf{q}^{\star-} = \mathfrak{B}(\boldsymbol{\nu})^+ \mathbf{q}^{\star+}\,; & \text{(5.54c)}\\
\mathfrak{B}(\boldsymbol{\nu})^+ \left(\mathbf{q}^{\star+} - \mathbf{q}^{a+}\right) = \mathrm{c_S^+} \left(\mathbf{q}^{\star+} - \mathbf{q}^{a+}\right)\,; & \text{(5.54d)}\\
\mathfrak{B}(\boldsymbol{\nu})^+ \left(\mathbf{q}^{a+} - \mathbf{q}^+\right) = \mathrm{c_P^+} \left(\mathbf{q}^{a+} - \mathbf{q}^+\right)\,. & \text{(5.54e)}
\end{cases}$$

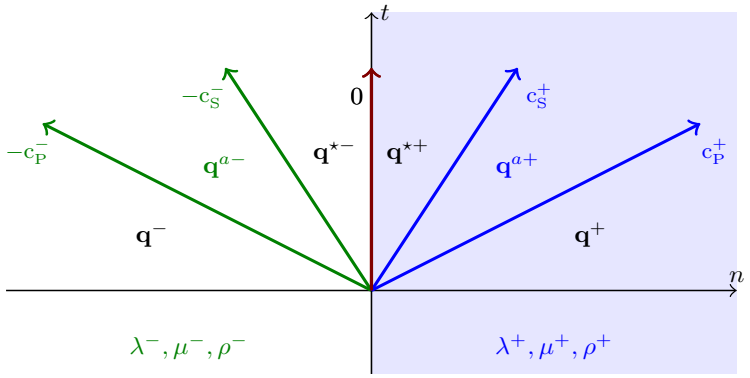

Figure 1: Spectral structure and the Godunov states appearing in the Rankine-Hugoniot jump condition for isotropic elasticity (5.54).

Transmission condition for interface states From the expressions in (5.13), we have

$$\mathbf{q} = \begin{pmatrix} \overrightarrow{\boldsymbol{\epsilon}} \\ \rho \mathbf{v} \end{pmatrix}, \quad \mathfrak{B}(\boldsymbol{\nu})\mathbf{q} = -\begin{pmatrix} \overrightarrow{\mathbf{v} \odot \boldsymbol{\nu}} \\ \boldsymbol{\sigma\nu} \end{pmatrix}, \qquad \boldsymbol{\sigma\nu} := \boldsymbol{C\epsilon} \cdot \boldsymbol{\nu}\,. \tag{5.55}$$

The first 3 components and last 3 components of the equality (5.54c) give

$$\begin{cases} \nu_I\, v_I^{\star-} = \nu_I v_I^{\star+}, \quad I = x, y, z \\ (\boldsymbol{\sigma\nu})^{\star-} = (\boldsymbol{\sigma\nu})^{\star+} \end{cases} \quad \Rightarrow \quad \begin{cases} \mathbf{v}^{\star-} = \mathbf{v}^{\star+}; \\ (\boldsymbol{\sigma\nu})^{\star-} = (\boldsymbol{\sigma\nu})^{\star+} \end{cases} . \tag{5.56}$$

Relating intermediate states to interface and boundary states Adding equation (5.54a) and (5.54b) and after some rearrangement, we obtain

$$\begin{cases} (\mathrm{c}_\mathrm{P}^- - \mathrm{c}_\mathrm{S}^-)\, \mathbf{q}^{a-} = -\mathfrak{B}(\boldsymbol{\nu})^-(\mathbf{q}^{\star-} - \mathbf{q}^-) + \mathrm{c}_\mathrm{P}^- \mathbf{q}^- - \mathrm{c}_\mathrm{S}^- \mathbf{q}^{\star-}; & \text{(5.57a)} \\ -\mathfrak{B}(\boldsymbol{\nu})^-\, \mathbf{q}^- = -\mathfrak{B}^-(\boldsymbol{\nu})\, \mathbf{q}^{a-} - \mathrm{c}_\mathrm{P}^- \mathbf{q}^{a-} + \mathrm{c}_\mathrm{P}^- \mathbf{q}^-\,. & \text{(5.57b)} \end{cases}$$

We next derive a relation between $(\boldsymbol{\sigma\nu})^-$ and $(\boldsymbol{\sigma\nu})^{\star-}$ as follows. Substitute the expression of $\mathbf{q}^a$ given by (5.57a) into (5.57b), we arrive at an expression for $-\mathfrak{B}^-\mathbf{q}^-$ in terms of only $\mathbf{q}^{\star-}$ and $\mathbf{q}^-$,

$$\begin{aligned} -\mathfrak{B}(\boldsymbol{\nu})^-\mathbf{q}^- = \frac{1}{\mathrm{c}_\mathrm{P}^- - \mathrm{c}_\mathrm{S}^-} \left[\mathfrak{B}(\boldsymbol{\nu})^-\mathfrak{B}(\boldsymbol{\nu})^-(\mathbf{q}^{\star-} - \mathbf{q}^-) - \mathrm{c}_\mathrm{P}^-\, \mathfrak{B}(\boldsymbol{\nu})^-\mathbf{q}^- + \mathrm{c}_\mathrm{S}^-\, \mathfrak{B}(\boldsymbol{\nu})^-\mathbf{q}^{\star-}\right] \\ + \frac{\mathrm{c}_\mathrm{P}^-}{\mathrm{c}_\mathrm{P}^- - \mathrm{c}_\mathrm{S}^-} \left[\mathfrak{B}(\boldsymbol{\nu})^-(\mathbf{q}^{\star-} - \mathbf{q}^-) - \mathrm{c}_\mathrm{P}^-\mathbf{q}^- + \mathrm{c}_\mathrm{S}^-\mathbf{q}^{\star-}\right] + \mathrm{c}_\mathrm{P}^-\mathbf{q}^-\,. \end{aligned} \tag{5.58}$$

The above expression is rearranged to obtain

$$\frac{\mathrm{c}_\mathrm{P}^- + \mathrm{c}_\mathrm{S}^-}{\mathrm{c}_\mathrm{P}^- - \mathrm{c}_\mathrm{S}^-}\mathfrak{B}(\boldsymbol{\nu})^-\mathbf{q}^- = \frac{\mathfrak{B}(\boldsymbol{\nu})^-\mathfrak{B}(\boldsymbol{\nu})^-(\mathbf{q}^{\star-} - \mathbf{q}^-)}{\mathrm{c}_\mathrm{P}^- - \mathrm{c}_\mathrm{S}^-} + \frac{\mathrm{c}_\mathrm{P}^- + \mathrm{c}_\mathrm{S}^-}{\mathrm{c}_\mathrm{P}^- - \mathrm{c}_\mathrm{S}^-}\mathfrak{B}(\boldsymbol{\nu})^-\mathbf{q}^{\star-} + \frac{\mathrm{c}_\mathrm{P}^-\mathrm{c}_\mathrm{S}^-}{\mathrm{c}_\mathrm{P}^- - \mathrm{c}_\mathrm{S}^-}\left(\mathbf{q}^{\star-} - \mathbf{q}^-\right). \tag{5.59}$$

By multiplying both sides by $(\mathrm{c}_\mathrm{P}^- - \mathrm{c}_\mathrm{S}^-)/(\mathrm{c}_\mathrm{P}^- + \mathrm{c}_\mathrm{S}^-)$, we obtain,

$$-\mathfrak{B}(\boldsymbol{\nu})^-\mathbf{q}^{\star-} = -\mathfrak{B}(\boldsymbol{\nu})^-\mathbf{q}^- + \frac{1}{\mathrm{c}_\mathrm{P}^- + \mathrm{c}_\mathrm{S}^-}\left[\mathrm{c}_\mathrm{P}^-\mathrm{c}_\mathrm{S}^- + \mathfrak{B}(\boldsymbol{\nu})^-\mathfrak{B}(\boldsymbol{\nu})^-\right](\mathbf{q}^{\star-} - \mathbf{q}^-)\,. \tag{5.60}$$

From the expressions in (5.13), we have

$$\mathbf{q} = \begin{pmatrix} \overrightarrow{\boldsymbol{\epsilon}} \\ \rho\mathbf{v} \end{pmatrix}, \quad \mathfrak{B}(\boldsymbol{\nu})\mathbf{q} = -\begin{pmatrix} \mathbb{A}^t(\boldsymbol{\nu})\mathbf{v} \\ \boldsymbol{\sigma\nu} \end{pmatrix}, \quad \mathfrak{B}(\boldsymbol{\nu})\,\mathfrak{B}(\boldsymbol{\nu})\,\mathbf{q} = \begin{pmatrix} \mathbb{A}^t(\boldsymbol{\nu})\rho^{-1}\boldsymbol{\sigma\nu} \\ \boldsymbol{\Gamma}(\boldsymbol{\nu})\mathbf{v} \end{pmatrix}. \tag{5.61}$$

The last 3 components of (5.59) thus give,

$$(\boldsymbol{\sigma\nu})^{\star-} = (\boldsymbol{\sigma\nu})^{-} + \frac{\rho^-}{\mathrm{c}_\mathrm{P}^- + \mathrm{c}_\mathrm{S}^-}\left(\mathrm{c}_\mathrm{P}^-\mathrm{c}_\mathrm{S}^- + \frac{\boldsymbol{\Gamma}^-(\boldsymbol{\nu})}{\rho^-}\right)\left(\mathbf{v}^{\star-} - \mathbf{v}^-\right). \tag{5.62}$$

We can carry out the same computation for the right-hand side of the interface to obtain,

$$(\boldsymbol{\sigma\nu})^{\star+} = (\boldsymbol{\sigma\nu})^{+} + \frac{\rho^+}{\mathrm{c}_\mathrm{P}^+ + \mathrm{c}_\mathrm{S}^+}\left(\mathrm{c}_\mathrm{P}^+\mathrm{c}_\mathrm{S}^+ + \frac{\boldsymbol{\Gamma}^+(\boldsymbol{\nu})}{\rho^+}\right)\left(\mathbf{v}^{\star+} - \mathbf{v}^+\right). \tag{5.63}$$

We thus retrieve the same result as in [53, Equation (36)].

Construction of HDG trace Following [53], the numerical traces for HDG are constructed using relations (5.56):

$$\widehat{\mathbf{v}}^{\pm} := \mathbf{v}^{\star\pm}, \qquad \widehat{\boldsymbol{\sigma\nu}} = (\boldsymbol{\sigma\nu})^{\star-}. \tag{5.64}$$

Using (5.62) obtained from the Rankine–Hugoniot jump condition at an interface with normal vector $\boldsymbol{\nu}$, we have,

$$\begin{cases} \widehat{\mathbf{v}} := \boldsymbol{\lambda}_\mathbf{v}; & (5.65a)\\ \widehat{\boldsymbol{\sigma\nu}} := (\boldsymbol{\sigma\nu})^{\star-} = (\boldsymbol{\sigma\nu})^{-} + \dfrac{\rho^-}{\mathrm{c}_\mathrm{P}^- + \mathrm{c}_\mathrm{S}^-}\left(\mathrm{c}_\mathrm{P}^-\mathrm{c}_\mathrm{S}^-\,\mathbb{I}_3 + \dfrac{\boldsymbol{\Gamma}(\boldsymbol{\nu})}{\rho^-}\right)\left(\boldsymbol{\lambda}_\mathbf{v} - \mathbf{v}^-\right). & (5.65b) \end{cases}$$

Using the explicit expression of $\boldsymbol{\Gamma}(\boldsymbol{\nu})$ in (3.116), the stabilization operator takes the following form[17] (using $|\boldsymbol{\nu}| = 1$),

$$\begin{aligned} M^{\mathrm{G-iso}} &:= \frac{\rho}{c_p + c_s}\left(c_p\, c_s \mathbb{I}\mathrm{d} + \frac{\boldsymbol{\Gamma}(\boldsymbol{\nu})}{\rho}\right) \\ &= \rho\left(c_s\,\mathbb{I}\mathrm{d} + (c_p - c_s)\boldsymbol{\nu}\otimes\boldsymbol{\nu}\right) = \rho\left(c_p\,\mathbb{I}\mathrm{d} + (c_p - c_s)\left(\boldsymbol{\nu}\otimes\boldsymbol{\nu} - \mathbb{I}\mathrm{d}\right)\right). \end{aligned} \tag{5.66}$$

5.4 Derivation for anistropic elasticity with distinct waves speeds

We follow the same notation given in (5.51) and (5.52). Under the assumption of spectral structure (5.10) of $\mathfrak{B}^{\pm}(\boldsymbol{\nu})$, we have 7 possible discontinuities propagating at the speed of corresponding eigenvalues,

$$-\mathrm{c}_\mathrm{qP}\ ,\ -\mathrm{c}_\mathrm{qS1}\ ,\ -\mathrm{c}_\mathrm{qS2}\ ,\ \underbrace{0}_{\text{multiplicity 3}}\ ,\ \mathrm{c}_\mathrm{qS2}\ ,\ \mathrm{c}_\mathrm{qS1}\ ,\ \mathrm{c}_\mathrm{qP}. \tag{5.67}$$

Denote the states in between the discontinuities, cf. Figure 2,

$$\mathbf{q}^-\ ,\ \mathbf{q}^{a-}\ ,\ \mathbf{q}^{b-}\ ,\ \mathbf{q}^{\star-}\ ,\ \mathbf{q}^{\star+}\ ,\ \mathbf{q}^{b+}\ ,\ \mathbf{q}^{a+}\ ,\ \mathbf{q}^+. \tag{5.68}$$

The jump condition associated with spectral structure (5.67) is, cf. [55, Equation (19)],

$$\begin{cases} \mathfrak{B}^-(\boldsymbol{\nu})\left(\mathbf{q}^{a-} - \mathbf{q}^-\right) = -\mathrm{c}_{q\mathrm{P}}^-\left(\mathbf{q}^{a-} - \mathbf{q}^-\right); & (5.69a)\\ \mathfrak{B}^-(\boldsymbol{\nu})\left(\mathbf{q}^{b-} - \mathbf{q}^{a-}\right) = -\mathrm{c}_{q\mathrm{S1}}^-\left(\mathbf{q}^{b-} - \mathbf{q}^{a-}\right); & (5.69b)\\ \mathfrak{B}^-(\boldsymbol{\nu})\left(\mathbf{q}^{\star-} - \mathbf{q}^{b-}\right) = -\mathrm{c}_{q\mathrm{S2}}^-\left(\mathbf{q}^{\star-} - \mathbf{q}^{b-}\right); & (5.69c)\\ \mathfrak{B}^-(\boldsymbol{\nu})\mathbf{q}^{\star-} = \mathfrak{B}^+(\boldsymbol{\nu})\mathbf{q}^{\star+}; & (5.69d)\\ \mathfrak{B}^+(\boldsymbol{\nu})\left(\mathbf{q}^{b+} - \mathbf{q}^{\star+}\right) = \mathrm{c}_{q\mathrm{S1}}^+\left(\mathbf{q}^{b+} - \mathbf{q}^{\star+}\right); & (5.69e)\\ \mathfrak{B}^+(\boldsymbol{\nu})\left(\mathbf{q}^{b+} - \mathbf{q}^{a+}\right) = \mathrm{c}_{q\mathrm{S1}}^+\left(\mathbf{q}^{b+} - \mathbf{q}^{a+}\right); & (5.69f)\\ \mathfrak{B}^+(\boldsymbol{\nu})\left(\mathbf{q}^{a+} - \mathbf{q}^+\right) = \mathrm{c}_{q\mathrm{S}}^+\left(\mathbf{q}^{a+} - \mathbf{q}^+\right). & (5.69g) \end{cases}$$

[17] This is due to $\dfrac{\boldsymbol{\Gamma}(\boldsymbol{\nu})}{\rho} = c_s^2\mathbb{I}\mathrm{d} + (c_p^2 - c_s^2)\boldsymbol{\nu}\otimes\boldsymbol{\nu}$ and $\dfrac{\boldsymbol{\Gamma}(\boldsymbol{\nu})}{\rho} + \mathrm{c}_\mathrm{P}\mathrm{c}_\mathrm{S}\mathbb{I}\mathrm{d} = \mathrm{c}_\mathrm{S}(\mathrm{c}_\mathrm{S} + \mathrm{c}_\mathrm{P})\mathbb{I}\mathrm{d} + (\mathrm{c}_\mathrm{P} - \mathrm{c}_\mathrm{P})(\mathrm{c}_\mathrm{P} + \mathrm{c}_\mathrm{S})\boldsymbol{\nu}\otimes\boldsymbol{\nu}$.

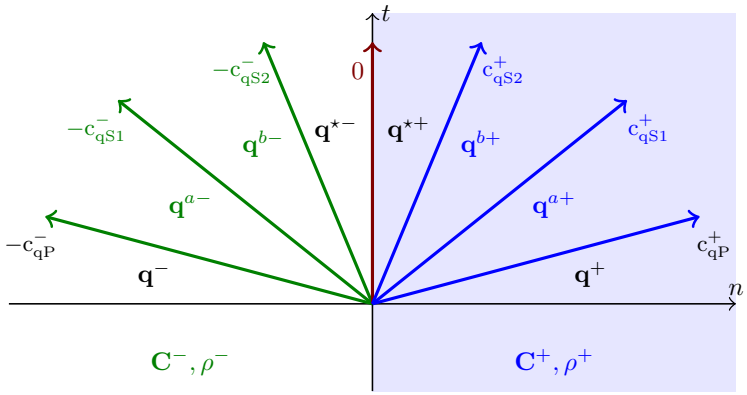

Figure 2: Spectral structure and the Godunov states appearing in the Rankine-Hugoniot jump condition (5.69) for anisotropic elasticity with 3 distinct speeds.

Transmission condition for interface states Similar to isotropy (cf. (5.56)), we obtain the transmission conditions from the first 3 and last 3 components of equation (5.69d) associated with the non-propagative state $\mathbf{q}^{\star\pm}$,

$$\begin{cases} \nu_I \, v_I^{\star-} \;=\; \nu_I \, v_I^{\star+}\,, \quad I = x,y,z \\ (\boldsymbol{\sigma\nu})^{\star-} \;=\; (\boldsymbol{\sigma\nu})^{\star+} \end{cases} \quad \Rightarrow \quad \begin{cases} \mathbf{v}^{\star-} \;=\; \mathbf{v}^{\star+}\,; \\ (\boldsymbol{\sigma\nu})^{\star-} \;=\; (\boldsymbol{\sigma\nu})^{\star+} \end{cases}. \tag{5.70}$$

Relating intermediate states to interface and boundary states Working on each side of the interface, we will express the state $\mathbf{q}^{a\pm}$ and $\mathbf{q}^{b\pm}$ in terms of the interface states $\mathbf{q}^{\star\pm}$ and boundary states $\mathbf{q}^{\pm}$.

Step 1a We start by working with the first three equations of (5.69), summing them, we obtain,

$$\mathfrak{B}(\boldsymbol{\nu})^- \left(\mathbf{q}^{\star-} - \mathbf{q}^-\right) = \left(-c^-_{qP} + c^-_{qS1}\right)\mathbf{q}^{a-} + \left(-c^-_{qS1} + c^-_{qS2}\right)\mathbf{q}^{b-} - c^-_{qS2}\mathbf{q}^{\star-} + c^-_{qP}\mathbf{q}^-\,. \tag{5.71}$$

After rearrangement, this leads to,

$$\left(c^-_{qP} - c^-_{qS1}\right)\mathbf{q}^{a-} + \left(c^-_{qS1} - c^-_{qS2}\right)\mathbf{q}^{b-} = -\mathfrak{B}(\boldsymbol{\nu})^- \left(\mathbf{q}^{\star-} - \mathbf{q}^-\right) - c^-_{qS2}\mathbf{q}^{\star-} + c^-_{qP}\mathbf{q}^-\,. \tag{5.72}$$

Next, take $c_{qP} \times$ (5.69a) $+ c_{qS1} \times$ (5.69b) $+ c_{qS2} \times$ (5.69c), we obtain,

$$\begin{aligned} \mathfrak{B}(\boldsymbol{\nu})^- \left[\left(c^-_{qP} - c^-_{qS1}\right)\mathbf{q}^{a-} + \left(c^-_{qS1} - c^-_{qS2}\right)\mathbf{q}^{b-}\right] &= c^-_{qP}\mathfrak{B}(\boldsymbol{\nu})^-\mathbf{q}^- - c^-_{qS2}\mathfrak{B}(\boldsymbol{\nu})^-\mathbf{q}^{\star-} \\ &+ \left[(c^-_{qS1})^2 - (c^-_{qP})^2\right]\mathbf{q}^{a-} + \left[(c^-_{qS2})^2 - (c^-_{qS1})^2\right]\mathbf{q}^{b-} - (c^-_{qS2})^2\mathbf{q}^{\star-} + (c^-_{qP})^2\mathbf{q}^-\,. \end{aligned} \tag{5.73}$$

Step 1b Using (5.72) to rewrite the left-hand side of equation (5.73), we have

$$\begin{aligned} \mathfrak{B}(\boldsymbol{\nu})^- \left(-\mathfrak{B}(\boldsymbol{\nu})^- \left(\mathbf{q}^{\star-} - \mathbf{q}^-\right) - c^-_{qS2}\mathbf{q}^{\star-} + c^-_{qP}\mathbf{q}^-\right) \;&=\; c^-_{qP}\mathfrak{B}(\boldsymbol{\nu})^-\mathbf{q}^- - c^-_{qS2}\mathfrak{B}^-(\boldsymbol{\nu})\mathbf{q}^{\star-} \\ \left(-(c^-_{qP})^2 + (c^-_{qS1})^2\right)\mathbf{q}^{a-} + \left(-(c^-_{qS1})^2 + (c^-_{qS2})^2\right)\mathbf{q}^{b-} &- (c^-_{qS2})^2\mathbf{q}^{\star-} + (c^-_{qP})^2\mathbf{q}^-\,. \end{aligned} \tag{5.74}$$

After simplification, we obtain,

$$\begin{aligned} -(\mathfrak{B}^-)^2\left(\mathbf{q}^{\star-} - \mathbf{q}^-\right) \;=\; &\left(-(c^-_{qP})^2 + (c^-_{qS1})^2\right)\mathbf{q}^{a-} + \left(-(c^-_{qS1})^2 + (c^-_{qS2})^2\right)\mathbf{q}^{b-} \\ &- (c^-_{qS2})^2\mathbf{q}^{\star-} + (c^-_{qP})^2\mathbf{q}^-\,. \end{aligned} \tag{5.75}$$

Equation (5.72) together with (5.75) give a linear system which determines uniquely $(\mathbf{q}^{a-}, \mathbf{q}^{b-})$ with a right-hand side containing only $\mathbf{q}^{\star-}$ and $\mathbf{q}-$,

$$\begin{pmatrix} \alpha & \beta \\ \alpha\tilde{\alpha} & \beta\tilde{\beta} \end{pmatrix} \begin{pmatrix} \mathbf{q}^{a-} \\ \mathbf{q}^{b-} \end{pmatrix} = \begin{pmatrix} -\mathfrak{B}(\mathbf{q}^{\star-} - \mathbf{q}^{-}) - \mathrm{c}^{-}_{q\mathrm{S}2}\mathbf{q}^{\star-} + \mathrm{c}^{-}_{q\mathrm{P}}\mathbf{q}^{-} \\ \mathfrak{B}^2(\mathbf{q}^{\star-} - \mathbf{q}^{-}) - (\mathrm{c}^{-}_{q\mathrm{S}2})^2\mathbf{q}^{\star-} + (\mathrm{c}^{-}_{q\mathrm{P}})^2\mathbf{q}^{-} \end{pmatrix}, \tag{5.76}$$

where

$$\alpha = \mathrm{c}^{-}_{q\mathrm{P}} - \mathrm{c}^{-}_{q\mathrm{S}1}, \quad \tilde{\alpha} = \mathrm{c}^{-}_{q\mathrm{S}1} + \mathrm{c}^{-}_{q\mathrm{P}}, \quad \beta = \mathrm{c}^{-}_{q\mathrm{S}1} - \mathrm{c}^{-}_{q\mathrm{S}2} \quad \tilde{\beta} = \mathrm{c}^{-}_{q\mathrm{S}1} + \mathrm{c}^{-}_{q\mathrm{S}2}. \tag{5.77}$$

Note that the determinant of the coefficient matrix in (5.76) is

$$\alpha\beta(\tilde{\beta} - \tilde{\alpha}) = \left(\mathrm{c}^{-}_{q\mathrm{P}} - \mathrm{c}^{-}_{q\mathrm{S}1}\right)\left(\mathrm{c}^{-}_{q\mathrm{S}1} - \mathrm{c}^{-}_{q\mathrm{S}2}\right)\left(\mathrm{c}^{-}_{q\mathrm{S}2} - \mathrm{c}^{-}_{q\mathrm{P}}\right). \tag{5.78}$$

This is invertible under assumption of distinct wave speeds (5.9), in which case, we obtain the expression of $\mathbf{q}^{a-}$ and $\mathbf{q}^{b-}$ in terms of $\mathbf{q}^{\star-}$ and $\mathbf{q}^{-}$.

$$\begin{pmatrix} \mathbf{q}^{a-} \\ \mathbf{q}^{b-} \end{pmatrix} = \frac{1}{\tilde{\beta} - \tilde{\alpha}} \begin{pmatrix} \frac{\tilde{\beta}}{\alpha} & -\frac{1}{\alpha} \\ -\frac{\tilde{\alpha}}{\beta} & \frac{1}{\beta} \end{pmatrix} \begin{pmatrix} -\mathfrak{B}(\mathbf{q}^{\star-} - \mathbf{q}^{-}) - \mathrm{c}^{-}_{q\mathrm{S}2}\mathbf{q}^{\star-} + \mathrm{c}^{-}_{q\mathrm{P}}\mathbf{q}^{-} \\ \mathfrak{B}^2(\mathbf{q}^{\star-} - \mathbf{q}^{-}) - (\mathrm{c}^{-}_{q\mathrm{S}2})^2\mathbf{q}^{\star-} + (\mathrm{c}^{-}_{q\mathrm{P}})^2\mathbf{q}^{-} \end{pmatrix}. \tag{5.79}$$

From here, we can proceed by working with either expression of $\mathbf{q}^{a-}$ and (5.69a) or with $\mathbf{q}^{b-}$ and (5.69c). The first option is chosen in the next step, for which it is useful to further simplify the expression of $\mathbf{q}^{a-}$ given in (5.79),

$$\begin{aligned} \alpha(\tilde{\beta} - \tilde{\alpha})\mathbf{q}^{a-} &= \tilde{\beta}\left(-\mathfrak{B}(\mathbf{q}^{\star-} - \mathbf{q}^{-}) - \mathrm{c}^{-}_{q\mathrm{S}2}\mathbf{q}^{\star-} + \mathrm{c}^{-}_{q\mathrm{P}}\mathbf{q}^{-}\right) \\ &\quad - \left(\mathfrak{B}^2(\mathbf{q}^{\star-} - \mathbf{q}^{-}) - (\mathrm{c}^{-}_{q\mathrm{S}2})^2\mathbf{q}^{\star-} + (\mathrm{c}^{-}_{q\mathrm{P}})^2\mathbf{q}^{-}\right) \\ &= -\left(\tilde{\beta}\mathfrak{B} + \mathfrak{B}^2\right)(\mathbf{q}^{\star-} - \mathbf{q}^{-}) + \mathrm{c}^{-}_{q\mathrm{S}2}\left(-\tilde{\beta} + \mathrm{c}^{-}_{q\mathrm{S}2}\right)\mathbf{q}^{\star-} + \mathrm{c}^{-}_{q\mathrm{P}}\left(\tilde{\beta} - \mathrm{c}^{-}_{q\mathrm{P}}\right)\mathbf{q}^{-} \\ &= -\left(\tilde{\beta}\mathfrak{B} + \mathfrak{B}^2\right)(\mathbf{q}^{\star-} - \mathbf{q}^{-}) - \mathrm{c}^{-}_{q\mathrm{S}2}\mathrm{c}^{-}_{q\mathrm{S}1}\mathbf{q}^{\star-} + \mathrm{c}^{-}_{q\mathrm{P}}\left(\tilde{\beta} - \mathrm{c}^{-}_{q\mathrm{P}}\right)\mathbf{q}^{-}. \end{aligned} \tag{5.80}$$

With some algebraic manipulation[18], we obtain

$$\mathrm{c}^{-}_{q\mathrm{P}}\left(\tilde{\beta} - \mathrm{c}^{-}_{q\mathrm{P}}\right) - \alpha(\tilde{\beta} - \tilde{\alpha}) = \mathrm{c}^{-}_{q\mathrm{S}1}\mathrm{c}^{-}_{q\mathrm{S}2}. \tag{5.82}$$

This gives us the useful expression,

$$\alpha(\tilde{\beta} - \tilde{\alpha})\left(\mathbf{q}^{a-} - \mathbf{q}^{-}\right) = -\left(\tilde{\beta}\mathfrak{B} + \mathfrak{B}^2 + \mathrm{c}^{-}_{q\mathrm{S}1}\mathrm{c}^{-}_{q\mathrm{S}2}\right)(\mathbf{q}^{\star-} - \mathbf{q}^{-}). \tag{5.83}$$

Step 2a Using (5.69a), we have,

$$\left(\mathfrak{B}^{-} + \mathrm{c}^{-}_{q\mathrm{P}}\right)\left(\mathbf{q}^{a-} - \mathbf{q}^{-}\right) = 0 \quad \Rightarrow \quad \left(\mathfrak{B}^{-} + \mathrm{c}^{-}_{q\mathrm{P}}\right)\alpha(\tilde{\beta} - \tilde{\alpha})\left(\mathbf{q}^{a-} - \mathbf{q}^{-}\right) = 0. \tag{5.84}$$

Substitute the difference given by (5.83) into the above expression:

$$\left(\mathfrak{B}^{-} + \mathrm{c}^{-}_{q\mathrm{P}}\right)\left(\tilde{\beta}\mathfrak{B} + \mathfrak{B}^2 + \mathrm{c}^{-}_{q\mathrm{S}1}\mathrm{c}^{-}_{q\mathrm{S}2}\right)(\mathbf{q}^{\star-} - \mathbf{q}^{-}) = 0. \tag{5.85}$$

[18] This is seen as,

$$\begin{aligned} &\left(\mathrm{c}^{-}_{q\mathrm{S}1} - \mathrm{c}^{-}_{q\mathrm{P}}\right)\left(\mathrm{c}^{-}_{q\mathrm{S}2} - \mathrm{c}^{-}_{q\mathrm{P}}\right) = \mathrm{c}^{-}_{q\mathrm{S}1}\mathrm{c}^{-}_{q\mathrm{S}2} - \mathrm{c}^{-}_{q\mathrm{P}}\left(\mathrm{c}^{-}_{q\mathrm{S}1} + \mathrm{c}^{-}_{q\mathrm{S}2} - \mathrm{c}^{-}_{q\mathrm{P}}\right) \\ \Rightarrow \quad &\mathrm{c}^{-}_{q\mathrm{P}}\left(\tilde{\beta} - \mathrm{c}^{-}_{q\mathrm{P}}\right) - \alpha(\tilde{\beta} - \tilde{\alpha}) = \mathrm{c}^{-}_{q\mathrm{P}}\left(\mathrm{c}^{-}_{q\mathrm{S}1} + \mathrm{c}^{-}_{q\mathrm{S}2} - \mathrm{c}^{-}_{q\mathrm{P}}\right) - \left(\mathrm{c}^{-}_{q\mathrm{P}} - \mathrm{c}^{-}_{q\mathrm{S}1}\right)\left(\mathrm{c}^{-}_{q\mathrm{S}2} - \mathrm{c}^{-}_{q\mathrm{P}}\right) = \mathrm{c}^{-}_{q\mathrm{S}1}\mathrm{c}^{-}_{q\mathrm{S}2}. \end{aligned} \tag{5.81}$$

We compute the left-hand side,

$$\begin{aligned}\left(\mathfrak{B}^- + \mathrm{c}_{qP}^-\right)\left(\tilde{\beta}\mathfrak{B} + \mathfrak{B}^2 + \mathrm{c}_{qS1}^-\mathrm{c}_{qS2}^-\right)&\\ = \tilde{\beta}\mathfrak{B}^2 + \mathfrak{B}^3 + \mathrm{c}_{qS1}^-\mathrm{c}_{qS2}^-\mathfrak{B} + \mathrm{c}_{qP}^-\tilde{\beta}\mathfrak{B} + \mathrm{c}_{qP}^-\mathfrak{B}^2 + \mathrm{c}_{qP}^-\mathrm{c}_{qS1}^-\mathrm{c}_{qS2}^-&\\ = \left(\mathfrak{B}^2 + \mathrm{c}_{qS1}^-\mathrm{c}_{qS2}^- + \mathrm{c}_{qP}^-\tilde{\beta}\right)\mathfrak{B} + \left(\tilde{\beta} + \mathrm{c}_{qP}^-\right)\mathfrak{B}^2 + \mathrm{c}_{qP}^-\mathrm{c}_{qS1}^-\mathrm{c}_{qS2}^-\,.&\end{aligned} \tag{5.86}$$

We thus arrive at,

$$\left[\left(\mathfrak{B}^2 + \mathrm{c}_{qS1}^-\mathrm{c}_{qS2}^- + \mathrm{c}_{qP}^-\tilde{\beta}\right)\mathfrak{B} + \left(\tilde{\beta} + \mathrm{c}_{qP}^-\right)\mathfrak{B}^2 + \mathrm{c}_{qP}^-\mathrm{c}_{qS1}^-\mathrm{c}_{qS2}^-\right]\left(\mathbf{q}^{\star-} - \mathbf{q}^-\right) = 0\,, \tag{5.87}$$

where we have introduced

$$\mathfrak{p}_3 := \mathrm{c}_{qS1}^-\mathrm{c}_{qS2}^-\mathrm{c}_{qP}^-\,, \quad \mathfrak{p}_2 := \mathrm{c}_{qS1}^-\mathrm{c}_{qS2}^- + \mathrm{c}_{qS1}^-\mathrm{c}_{qP}^- + \mathrm{c}_{qS2}^-\mathrm{c}_{qP}^-\,. \tag{5.88}$$

In noting that $\mathfrak{p}_2 = \mathrm{c}_{qS1}^-\mathrm{c}_{qS2}^- + \mathrm{c}_{qP}^-\tilde{\beta}$, we rewrite the above equation as

$$\left(\mathfrak{B}_-^3 + \mathfrak{p}_2^-\,\mathfrak{B}_- + \left(\mathrm{c}_{qS1}^- + \mathrm{c}_{qS2}^- + \mathrm{c}_{qP}^-\right)\mathfrak{B}_-^2 + \mathfrak{p}_3^-\,\mathbb{d}\right)\left(\mathbf{q}^{\star-} - \mathbf{q}^-\right) = 0\,. \tag{5.89}$$

Step 2b Recall from (5.13), we have

$$\begin{aligned}\mathbf{q} = \begin{pmatrix}\overrightarrow{\boldsymbol{\epsilon}}\\ \rho\mathbf{v}\end{pmatrix}\,, \qquad \mathfrak{B}(\boldsymbol{\nu})\mathbf{q} = -\begin{pmatrix}\mathbb{A}^t(\boldsymbol{\nu})\mathbf{v}\\ \boldsymbol{\sigma\nu}\end{pmatrix}&\\ \mathfrak{B}(\boldsymbol{\nu})^2\mathbf{q} = \begin{pmatrix}\rho^{-1}\mathbb{A}^t(\boldsymbol{\nu})\boldsymbol{\sigma\nu}\\ \boldsymbol{\Gamma}(\boldsymbol{\nu})\mathbf{v}\end{pmatrix}\,, \quad \mathfrak{B}(\boldsymbol{\nu})^3\mathbf{q} = -\frac{1}{\rho}\begin{pmatrix}\mathbb{A}^t(\boldsymbol{\nu})\,\boldsymbol{\Gamma}(\boldsymbol{\nu})\mathbf{v}\\ \boldsymbol{\Gamma}(\boldsymbol{\nu})\boldsymbol{\sigma\nu}\end{pmatrix}\,.&\end{aligned} \tag{5.90}$$

We substitute this into (5.89), and use the last three components of equation (5.89) to obtain,

$$\begin{aligned}&-\left(\frac{\boldsymbol{\Gamma}(\boldsymbol{\nu})}{\rho} + \mathfrak{p}_2^-\right)\left((\boldsymbol{\sigma\nu})^{\star-} - (\boldsymbol{\sigma\nu})^-\right) + \rho^-\left(\left(\mathrm{c}_{qSa} + \mathrm{c}_{qP}\right)\frac{\boldsymbol{\Gamma}(\boldsymbol{\nu})}{\rho} + \mathfrak{p}_3^-\right)\left(\mathbf{v}^{\star-} - \mathbf{v}^-\right) = 0\\ &\Rightarrow (\boldsymbol{\sigma\nu})^{\star-} - (\boldsymbol{\sigma\nu})^- = \rho^-\left(\frac{\boldsymbol{\Gamma}(\boldsymbol{\nu})}{\rho} + \mathfrak{p}_2^-\right)^{-1}\left(\left(\mathrm{c}_{qSa} + \mathrm{c}_{qP}\right)\frac{\boldsymbol{\Gamma}(\boldsymbol{\nu})}{\rho} + \mathfrak{p}_3^-\right)\left(\mathbf{v}^{\star-} - \mathbf{v}^-\right)\,.\end{aligned} \tag{5.91}$$

With some algebraic manipulation, we arrive at

$$(\boldsymbol{\sigma\nu})^{\star-} - (\boldsymbol{\sigma\nu})^- = \rho^-\left(\mathrm{c}_{qS1}^- + \mathrm{c}_{qS2}^- + \mathrm{c}_{qP}\right)\left(1 + \gamma\left(\frac{\boldsymbol{\Gamma}(\boldsymbol{\nu})}{\rho} + \mathfrak{p}_2\right)^{-1}\right)\left(\mathbf{v}^{\star-} - \mathbf{v}^-\right), \tag{5.92}$$

where

$$\gamma := \frac{\mathfrak{p}_3}{\mathrm{c}_{qS1}^- + \mathrm{c}_{qS2}^- + \mathrm{c}_{qP}} - \mathfrak{p}_2\,. \tag{5.93}$$

Derivation of HDG trace From this point, following the same hybridization procedure as done in isotropy, we employ the transmission condition (5.70),

$$\widehat{\mathbf{v}} := \mathbf{v}^{\star\pm}\,, \qquad \widehat{\boldsymbol{\sigma\nu}} = (\boldsymbol{\sigma\nu})^{\star-}\,, \tag{5.94}$$

and the relation (5.92) obtained from the Rankine–Hugoniot jump condition at an interface with normal vector $\boldsymbol{\nu}$, to arrive at the hybridized trace for displacement and traction,

$$\begin{cases}\widehat{\mathbf{v}} = \boldsymbol{\lambda}_{\mathbf{v}}\,; & \text{(5.95a)}\\ \widehat{\boldsymbol{\sigma\nu}} = (\boldsymbol{\sigma\nu})^- + M^{\mathrm{G-ani}}\left(\boldsymbol{\lambda}_{\mathbf{v}} - \mathbf{v}^-\right)\,, & \text{(5.95b)}\end{cases}$$

with

$$M^{\mathrm{G-ani}} := \rho^-\left(\mathrm{c}_{\mathrm{qS1}}^- + \mathrm{c}_{\mathrm{qS2}}^- + \mathrm{c}_{qP}^-\right)\left(1 + \gamma\left(\frac{\boldsymbol{\Gamma}(\boldsymbol{\nu})}{\rho^-} + \mathfrak{p}_2^-\right)^{-1}\right)\,. \tag{5.96}$$

6 Numerical experiments: elastic isotropy

The HDG method is implemented in the open-source parallel software `hawen`[19], [29]. We perform numerical experiments to evaluate the performance of the different choices of stabilization for the accuracy of the wave propagation. To evaluate the difference between a reference solution (either an analytic one or a numerical one computed with refined discretization) and simulations, we introduce the relative error defined for a wave field w such that

$$\widehat{\mathfrak{e}}(w;\,\mathbf{x}) \;=\; \frac{|\,w^{\mathrm{ref}}(\mathbf{x}) \;-\; w^{\mathrm{simu}}(\mathbf{x})\,|}{\|w^{\mathrm{ref}}(\mathbf{x})\|}\,. \tag{6.1}$$

In our experiments, w is either a component of the displacement field $\mathbf{u}$, velocity field $\mathbf{v}$ or of the stress tensor $\boldsymbol{\sigma}$. The mean errors $\mathfrak{e}$ and $\mathfrak{E}$ are defined such that

$$\begin{aligned}
&\mathfrak{e}(w) \;:=\; \frac{1}{n_x}\sum_{k=1}^{n_x}\widehat{\mathfrak{e}}(w,\mathbf{x}_k)\,;\\
&\mathfrak{E}(\mathbf{u}) \;:=\; \frac{1}{3}\sum_{j=\{x,y,z\}}\mathfrak{e}(u_j,\mathbf{x}_k)\,;\qquad \mathfrak{E}(\boldsymbol{\sigma}) \;:=\; \frac{1}{6}\sum_{j=\{xx,yy,zz,xy,xz,yz\}}\mathfrak{e}(\sigma_j,\mathbf{x}_k)\,,
\end{aligned} \tag{6.2}$$

where $\mathbf{x}_k$ corresponds to the k^{th} position where the solutions are evaluated, with a total of n_x positions. Typically, we use a Cartesian grid to select these positions in order to balance the contributions of each place. In all of the following experiments, we however exclude the positions near the boundaries, and the source position when a Dirac point-source is used.

The different stabilization analyzed In the experiments, we consider the formulations with displacement or velocity, respectively $(\mathbf{u},\boldsymbol{\sigma})_{\boldsymbol{S}}$ and $(\mathbf{v},\boldsymbol{\sigma})_{\boldsymbol{S}}$ in (2.8) and (2.9). Below we detail the main stabilizations tested, introduced in Table 1:

Formulation $(\mathbf{u},\boldsymbol{\sigma})_{\boldsymbol{S}}$ with $\widehat{\boldsymbol{\sigma}\boldsymbol{\nu}} = \boldsymbol{\sigma}_h - \boldsymbol{\tau}_{\mathbf{u}}(\mathbf{u}_h - \boldsymbol{\lambda}_{\mathbf{u}h})$:

$$\text{choices of } \boldsymbol{\tau}_{\mathbf{u}} \quad \begin{cases}
\boldsymbol{\tau}_{\mathbf{u}\mathrm{I}} := -\mathrm{i}\omega\,\mathrm{I}_d\,; \quad \boldsymbol{\tau}_{\mathbf{u}\mathrm{I}_s} := -\mathrm{i}\omega\,\rho\,\mathrm{c}_{\mathrm{qS2}}\,\mathrm{I}_d\,; & \text{identity based}\,;\\
\boldsymbol{\tau}_{\mathbf{u}\boldsymbol{\Gamma}} := -\mathrm{i}\omega\,\boldsymbol{\Gamma}\,; \quad \boldsymbol{\tau}_{\mathbf{u}\boldsymbol{\Gamma}_s} := \dfrac{-\mathrm{i}\omega}{\mathrm{c}_{\mathrm{qS2}}}\boldsymbol{\Gamma}\,; & \text{Kelvin–Christoffel based}\,;\\
\boldsymbol{\tau}_{\mathbf{u}\mathrm{G}} := -\mathrm{i}\omega\,M_{\mathrm{Godunov}}\,; & \text{Godunov stabilization}\,.
\end{cases} \tag{6.3a}$$

Formulation $(\mathbf{v},\boldsymbol{\sigma})_{\boldsymbol{S}}$ with $\widehat{\boldsymbol{\sigma}\boldsymbol{\nu}} = \boldsymbol{\sigma}_h - \boldsymbol{\tau}_{\mathbf{v}}(\mathbf{v}_h - \boldsymbol{\lambda}_{\mathbf{v}h})$:

$$\text{choices of } \boldsymbol{\tau}_{\mathbf{v}} \quad \begin{cases}
\boldsymbol{\tau}_{\mathbf{v}\mathrm{I}} := \mathrm{I}_d\,; & \boldsymbol{\tau}_{\mathbf{v}\mathrm{I}_s} := \rho\,\mathrm{c}_{\mathrm{qS2}}\,\mathrm{I}_d\,; & \text{identity based}\,;\\
\boldsymbol{\tau}_{\mathbf{v}\boldsymbol{\Gamma}} := \boldsymbol{\Gamma}\,; & \boldsymbol{\tau}_{\mathbf{v}\boldsymbol{\Gamma}_s} := \dfrac{1}{\mathrm{c}_{\mathrm{qS2}}}\boldsymbol{\Gamma}\,; & \text{Kelvin–Christoffel based}\,;\\
\boldsymbol{\tau}_{\mathbf{v}\mathrm{G}} := M_{\mathrm{Godunov}}\,; & & \text{Godunov stabilization}\,.
\end{cases} \tag{6.4a}$$

Here, the Kelvin–Christoffel matrix for elastic isotropy and vertical transverse isotropy are respectively given in Propositions 6 and 7. The Godunov matrices are respectively given in (4.64) and (5.96).

Remark 12. *Alternatives for (6.3) and (6.4) have been implemented and numerically compared, in particular replacing the wave-speed* $\mathrm{c}_{\mathrm{qS2}}$*. For the sake of conciseness, we only present on the most effective ones, which corresponds to taking the lowest velocity. We further refer to Subsections 6.2, 7.1 and 7.2 where the stabilizations based upon the identity are thoroughly analyzed, comparing real and imaginary choices and several orders of magnitude for the scalar coefficient.*

We start by considering an elastic isotropic medium in dimensions 2 or 3. In this case, the stiffness tensor $\boldsymbol{C}$ is defined from the two Lamé parameters λ and μ, see Subsection 3.5.1. The absorbing boundary conditions to approximate free-space propagation are given by, [37, 40],

$$\boldsymbol{\sigma}\cdot\boldsymbol{\nu} \;-\; \mathrm{i}\omega\Big(\sqrt{(\lambda+2\mu)\rho}\;\boldsymbol{\nu}\otimes\boldsymbol{\nu} \;+\; \sqrt{\mu\,\rho}\;(\mathbb{I}_{\mathbb{d}} \;-\; \boldsymbol{\nu}\otimes\boldsymbol{\nu})\Big)\mathbf{u} \;=\; 0\,, \qquad \text{on } \Gamma. \tag{6.5}$$

[19] https://ffaucher.gitlab.io/hawen-website/

6.1 2D homogeneous medium with point source (`benchmark2Diso-R5`)

We consider a disk of radius $R = 5$ with constant values of density, P- and S-wave speeds. This is our experiment `benchmark2Diso-R5` described as follows:

$$\texttt{benchmark2Diso-R5} \quad \begin{cases} \text{Disk of radius } R = 5 \text{ with Dirac source in } (0,0)\,, \\ \mathrm{c_P} \;=\; 2.5\times 10^{-3}\,, \quad \mathrm{c_S} \;=\; 10^{-3}\,, \quad \rho \;=\; 1\,, \\ \qquad \Rightarrow\; \lambda \;=\; 4.25\times 10^{-6} \quad \text{and} \quad \mu \;=\; 10^{-6}\,. \\ \text{Simulations with fixed mesh of about } 30\,000 \text{ triangles}, \\ \omega/(2\pi) \;\in\; (1,15) \text{ mHz}; \quad \text{polynomial orders between 1 and 7}\,. \end{cases} \tag{6.6}$$

Analytic solutions in two dimensions We consider here the solution $\mathbf{g}_\beta$ to the homogeneous isotropic elastic equation with Dirac source at position $\mathbf{y} = (y_1, y_2)$ having polarizations at $\mathbf{y}$ in direction $\mathbf{e}_1 = \mathbf{e}_x$ and $\mathbf{e}_2 = \mathbf{e}_y$, respectively,

$$\left(-\omega^2\rho - \mathcal{L}_{\lambda,\mu}\right)\mathbf{g}_I(\mathbf{x};\mathbf{y}) = \mathbf{e}_\beta\,\delta_{\mathbf{y}}(\mathbf{x})\,, \quad \text{with} \quad I = 1,2\,. \tag{6.7}$$

Here $\mathcal{L}_{\lambda,\mu}$ is the elastic problem (2.8) under elastic isotropy (3.114), in 2D space variable $\mathbf{x} = (x_1, x_2)$. The analytic expressions of the solutions are known for homogeneous background parameters λ, μ and ρ, and are given by the first and second column of the outgoing elastic Green's tensor whose expression can be found in, e.g., [1, Equations (1.24) and (1.25)],

$$\mathbf{u}_I^{\mathrm{ref2D}}(\mathbf{x};\mathbf{y}) = \mathbf{g}_I(\mathbf{x};\mathbf{y}) = \mathbf{g}_I^{\mathrm{P}}(\mathbf{x};\mathbf{y}) \;+\; \mathbf{g}_I^{\mathrm{S}}(\mathbf{x};\mathbf{y})\,, \tag{6.8}$$

where

$$\begin{cases} \mathbf{g}_I^{\mathrm{P}}(\mathbf{x},\mathbf{y}) = \dfrac{1}{\mu\,\mathsf{k}_{\mathrm{S}}^2}\nabla_{\mathbf{x}}\left(\partial_{x_I}\phi_{\mathrm{P}}\right)\,, & \text{with } \phi_{\mathrm{P}}(\mathbf{x},\mathbf{y}) = \frac{\mathrm{i}}{4}\mathrm{H}_0^{(1)}(\mathsf{k}_{\mathrm{P}}|\mathbf{x}-\mathbf{y}|)\,, \\ \mathbf{g}_I^{\mathrm{S}}(\mathbf{x},\mathbf{y}) = -\,\dfrac{1}{\mu}\left(\phi_{\mathrm{S}}\,\mathbf{e}_I \;+\; \dfrac{1}{\mathsf{k}_{\mathrm{S}}^2}\nabla_{\mathbf{x}}\left(\partial_{x_I}\phi_{\mathrm{P}}\right)\right)\,, & \text{with } \phi_{\mathrm{S}}(\mathbf{x},\mathbf{y}) = \dfrac{\mathrm{i}}{4}\mathrm{H}_0^{(1)}(\mathsf{k}_{\mathrm{S}}|\mathbf{x}-\mathbf{y}|)\,. \end{cases} \tag{6.9}$$

In the above expressions, $\mathrm{H}_n^{(1)}$ is the n-th Hankel function of the first kind[20], while $\nabla_{\mathbf{x}}$ is the gradient in variable $\mathbf{x}$. In the above expression, for $\mathbf{x} \neq 0$ and $\mathbf{y} = 0$, the term $\nabla_{\mathbf{x}}\partial_{x_I}\phi_\alpha$ with $\alpha =$ 'P','S' and $I = 1,2$, is the vector[21],

$$\nabla_{\mathbf{x}}\partial_{x_I}\phi_\alpha = \frac{\mathrm{i}\mathsf{k}_\alpha}{4}\left(\frac{\mathsf{k}_\alpha\,\mathrm{H}_1^{(1)}(\mathsf{k}_\alpha r)}{r} - \mathrm{H}_0^{(1)}(\mathsf{k}_\alpha r)\mathsf{k}_\alpha + \frac{\mathrm{H}_1^{(1)}(\mathsf{k}_\alpha r)}{r^2}\right)\frac{x_I}{r^2}\mathbf{x}\,, \quad \text{where } r := |\mathbf{x}|\,. \tag{6.12}$$

We also recall that $\mathsf{k}_{\mathrm{S}} = \frac{\omega}{c_{\mathrm{S}}} = \omega\sqrt{\frac{\rho}{\mu}}$ thus $\mu\mathsf{k}_{\mathrm{S}}^2 = \omega^2\rho^2$, while $\mathsf{k}_{\mathrm{P}} = \frac{\omega}{c_{\mathrm{P}}} = \omega\sqrt{\frac{\rho}{\lambda+2\mu}}$.

In Figure 3, we picture the real parts of the analytic solutions for the displacement and the stress tensor, respectively $\mathbf{u}^{\mathrm{ref}}$ and $\boldsymbol{\sigma}^{\mathrm{ref}}$, at frequency $\omega/(2\pi) = 2$mHz.

[20] cf. https://dlmf.nist.gov/10.2.

[21] This can be seen as follows. It is derived for generic $g = \mathrm{H}_0^{(1)}(\mathsf{k}|\mathbf{x}|)$ and $\mathbf{x} \neq 0$. We write $\partial_i := \partial_{x_i}$. Since $\mathrm{H}_0^{(1)\prime} = -\mathrm{H}_1^{(1)}$, we have,

$$\partial_i g = -\mathrm{H}_1^{(1)}(\mathsf{k}r)\,\mathsf{k}\frac{x_i}{r} \quad \Rightarrow \quad \partial_{ij}^2\phi = \left(-\mathrm{H}_1^{(1)\prime}(\mathsf{k}r)\mathsf{k}^2 \;+\; \frac{\mathsf{k}\,\mathrm{H}_1^{(1)}(\mathsf{k}r)}{r^2}\right)\frac{x_i x_j}{r}\,. \tag{6.10}$$

Next we use identity $\mathrm{H}_1^{(1)\prime}(z) = \mathrm{H}_0^{(1)}(z) - \frac{1}{z}\mathrm{H}_1^{(1)}(z)$

$$\partial_{ij}^2 g = \left(\frac{\mathrm{H}_1^{(1)}(\mathsf{k}r)\,\mathsf{k}^2}{\mathsf{k}|\mathbf{x}|} \;-\; \mathrm{H}_0^{(1)}(\mathsf{k}r)\,\mathsf{k}^2 + \frac{\mathsf{k}\,\mathrm{H}_1^{(1)}(\mathsf{k}r)}{r^2}\right)\frac{x_i x_j}{r^2}\,. \tag{6.11}$$

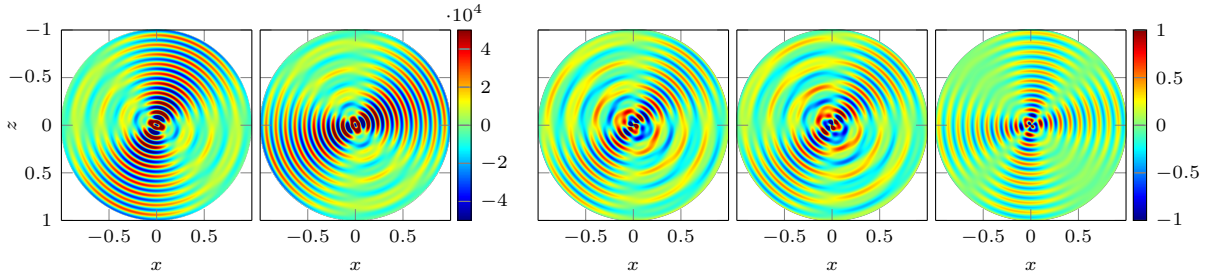

(a) $\mathrm{Re}(u_x^{\mathrm{ref}})$. (b) $\mathrm{Re}(u_z^{\mathrm{ref}})$. (c) $\mathrm{Re}(\sigma_{xx}^{\mathrm{ref}})$. (d) $\mathrm{Re}(\sigma_{zz}^{\mathrm{ref}})$. (e) $\mathrm{Re}(\sigma_{xz}^{\mathrm{ref}})$.

Figure 3: Analytic solutions at 2mHz for `benchmark2Diso-R5` (6.6), corresponding to (6.8) and (6.9).

6.1.1 HDG formulation $(\mathbf{u}, \boldsymbol{\sigma})_{\boldsymbol{S}}$

The analytical solution for free-space propagation is compared with the simulations with absorbing boundary conditions (6.5), and we use the different choices of stabilization coefficients (6.3). To avoid the singularity at the origin, and reduce the effect of the boundary conditions, the numerical errors $\mathfrak{e}$ and $\mathfrak{E}$ (6.1) and (6.2) that are plotted below are restricted to interval $6 \times 10^{-2} \leq \|\mathbf{x}\| \leq 4.90$. Using formulation $(\mathbf{u}, \boldsymbol{\sigma})_{\boldsymbol{S}}$, the mean of the relative error $\mathfrak{e}$ (6.1) with the frequency is pictured in Figure 4 where we compare the different wave fields independently. Here we compare the stabilization coefficients $\boldsymbol{\tau}_{\mathbf{uI}}$, $\boldsymbol{\tau}_{\mathbf{u\Gamma}}$ and $\boldsymbol{\tau}_{\mathbf{uG}}$, that is, the identity-based, Kelvin–Christoffel and Godunov stabilization respectively.

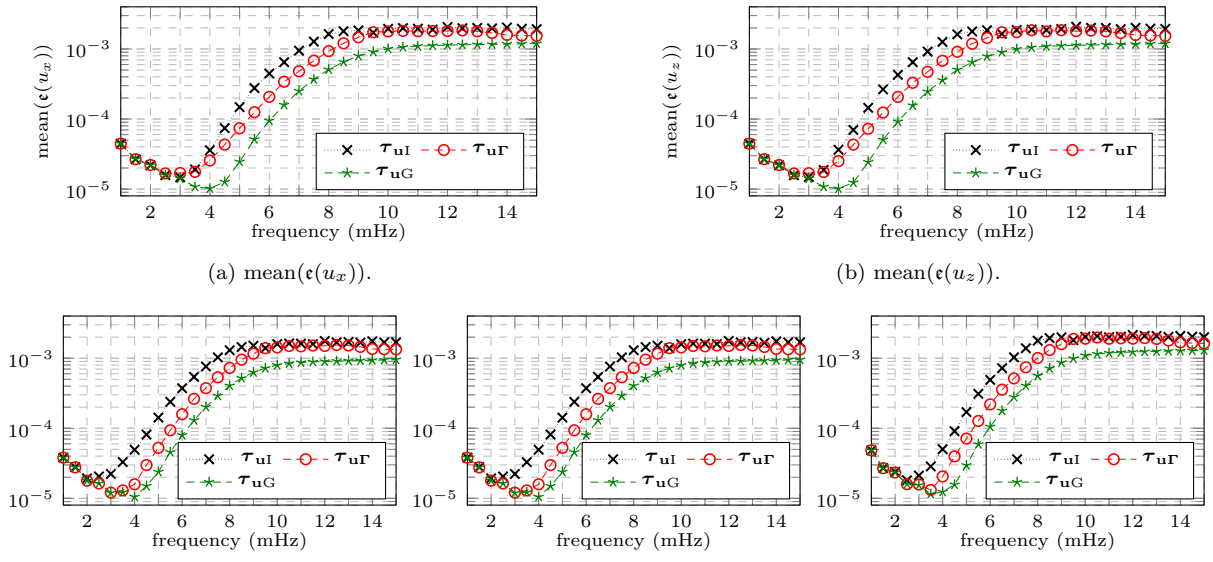

(a) $\mathrm{mean}(\mathfrak{e}(u_x))$. (b) $\mathrm{mean}(\mathfrak{e}(u_z))$.

(c) $\mathrm{mean}(\mathfrak{e}(\sigma_{xx}))$. (d) $\mathrm{mean}(\mathfrak{e}(\sigma_{zz}))$. (e) $\mathrm{mean}(\mathfrak{e}(\sigma_{xz}))$.

Figure 4: Evolution of the error $\mathfrak{e}$ of (6.2) with frequency for `benchmark2Diso-R5` (6.6) using HDG discretization formulation $(\mathbf{u}, \boldsymbol{\sigma})_{\boldsymbol{S}}$ for polynomial order 3 and stabilization (6.3).

Observation In the evolution of the relative error with frequency (Figure 4), we observe the similar behaviour and error level for all fields, whether it is displacement (u_x and u_z) or stress tensor (σ_{xx}, σ_{zz} and σ_{xz}). We observe three regions in the error plots that correspond to low, intermediate, and high frequencies.

– At low frequency (below 4 Hz), the relative error is minimal as we have the largest wavelength.

The error stays relatively stable, and all choices of stabilization provide similar results. We however note a slight increase for the smallest frequencies, which corresponds to the lack of accuracy of the absorbing boundary condition for large wavelength.

– For high frequencies, the error is the highest as we have smaller wavelengths; this is expected as there are less points per wavelength at fixed polynomial order. Regarding the different choices of stabilization coefficients, we see that the Godunov stabilization is the most accurate, reducing the relative error by a factor 2 compared to the other choices.

– In the intermediate region, the relative error increases with increasing frequencies, and we clearly see the improvement of the Godunov stabilization, by a factor 2 to 5, compared to the Kelvin–Christoffel and identity-based stabilizations respectively.

– We note that the minimal error for each stabilization is reached at different frequencies: for the Godunov stabilization, the minimal error is obtained at 4 Hz, while it is rather at 3 Hz for the two other stabilizations. Furthermore, for any frequency, the Godunov stabilization always gives the best result.

To further investigate the stabilization coefficient, we use a scaling parameter based upon the S-wave speed for the identity and Kelvin–Christoffel matrices, namely with $\boldsymbol{\tau}_{\mathbf{u}\mathrm{I}_s}$ and $\boldsymbol{\tau}_{\mathbf{u}\boldsymbol{\Gamma}_s}$ in (6.3). As the level of error is similar for both fields (Figure 4), we plot global relative error $\mathfrak{E}$ of (6.2) in Figure 5. In this picture we represent the error with frequency and with polynomial order. In the evolution of the error with frequency, Figures 5a and 5b, we see that using the scaled stabilization coefficients $\boldsymbol{\tau}_{\mathbf{u}\mathrm{I}_s}$ or $\boldsymbol{\tau}_{\mathbf{u}\boldsymbol{\Gamma}_s}$ provide similar error level compared to using $\boldsymbol{\tau}_{\mathbf{u}\mathrm{G}}$. This is confirmed by the evolution of error with the polynomial orders in Figures 5c and 5d. We further see the expected improvement with the use of higher order polynomials, and we have similar accuracy for the displacement $\mathbf{u}$ and stress tensor $\boldsymbol{\sigma}$.

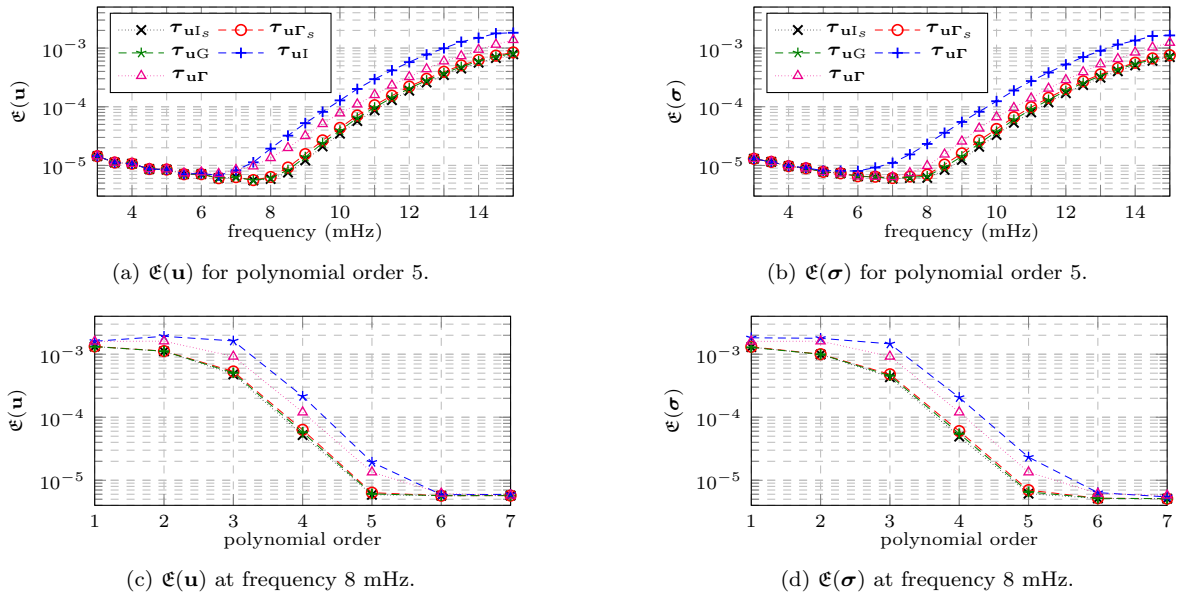

(a) $\mathfrak{E}(\mathbf{u})$ for polynomial order 5.

(b) $\mathfrak{E}(\boldsymbol{\sigma})$ for polynomial order 5.

(c) $\mathfrak{E}(\mathbf{u})$ at frequency 8 mHz.

(d) $\mathfrak{E}(\boldsymbol{\sigma})$ at frequency 8 mHz.

Figure 5: Evolution of the error $\mathfrak{E}$ of (6.2) with frequency (top) and polynomial order (bottom) for `benchmark2Diso-R5` (6.6) using HDG discretization formulation $(\mathbf{u}, \boldsymbol{\sigma})_{\boldsymbol{S}}$ and stabilization (6.3).

We see that the stabilization coefficient based upon the Godunov matrix, $\boldsymbol{\tau}_{\mathbf{u}\mathrm{G}}$ in (6.3), is the best choice in terms of accuracy of the solutions. The level of accuracy can be matched by other stabilization, however, by using empirical scaling factors, that we have found here in terms of the S-wave speed ($\boldsymbol{\tau}_{\mathbf{u}\mathrm{I}_s}$ and $\boldsymbol{\tau}_{\mathbf{u}\boldsymbol{\Gamma}_s}$). Nonetheless, one cannot guarantee that this scaling is optimal in all possible configurations, cf. Subsection 6.2, and the genuine option is to use the robustness of $\boldsymbol{\tau}_{\mathbf{u}\mathrm{G}}$ which does not involve a scaling parameter.

6.1.2 Comparisons of HDG formulations

We now compute the wave fields with the HDG discretization using the formulation in terms of the velocity, that is, $(\mathbf{v}, \boldsymbol{\sigma})_{\boldsymbol{S}}$. In Figure 6, we compare the relative error with frequency, for the stabilization coefficients of (6.4), and also compare the two HDG formulations $(\mathbf{u}, \boldsymbol{\sigma})_{\boldsymbol{S}}$ and $(\mathbf{v}, \boldsymbol{\sigma})_{\boldsymbol{S}}$. We see that the two formulations have similar accuracy, and the stabilization based upon the Godunov matrix, which is the most natural one, is the best choice as it does not need an extra parameter for scaling.

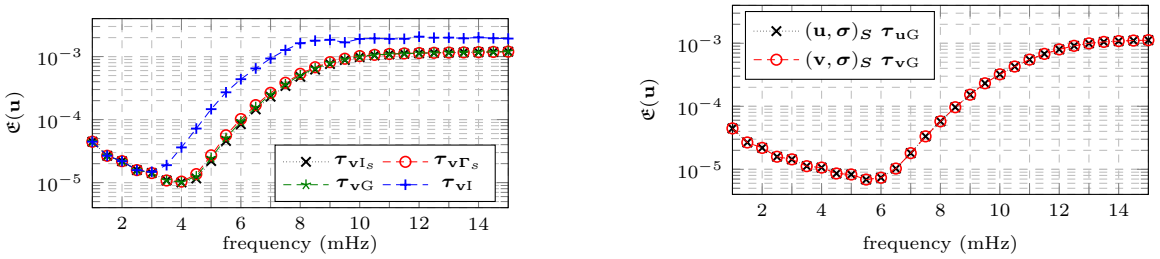

(a) $\mathfrak{E}(\mathbf{u})$ using polynomial order 3.

(b) $\mathfrak{E}(\mathbf{u})$ using polynomial order 4.

Figure 6: Evolution of the error $\mathfrak{E}(\mathbf{u})$ of (6.2) with frequency for `benchmark2Diso-R5` (6.6) using HDG discretization formulations $(\mathbf{u}, \boldsymbol{\sigma})_{\boldsymbol{S}}$ and $(\mathbf{v}, \boldsymbol{\sigma})_{\boldsymbol{S}}$ and stabilization coefficients (6.3) and (6.4).

6.1.3 Condition number of the global matrix

To further compare the formulations in terms of displacement or velocity, and with the choice of stabilization, we compute the condition number of the global matrix assembled with the HDG discretization. We provide in Figure 7 the evolution of the condition number with frequency for different orders of polynomials.

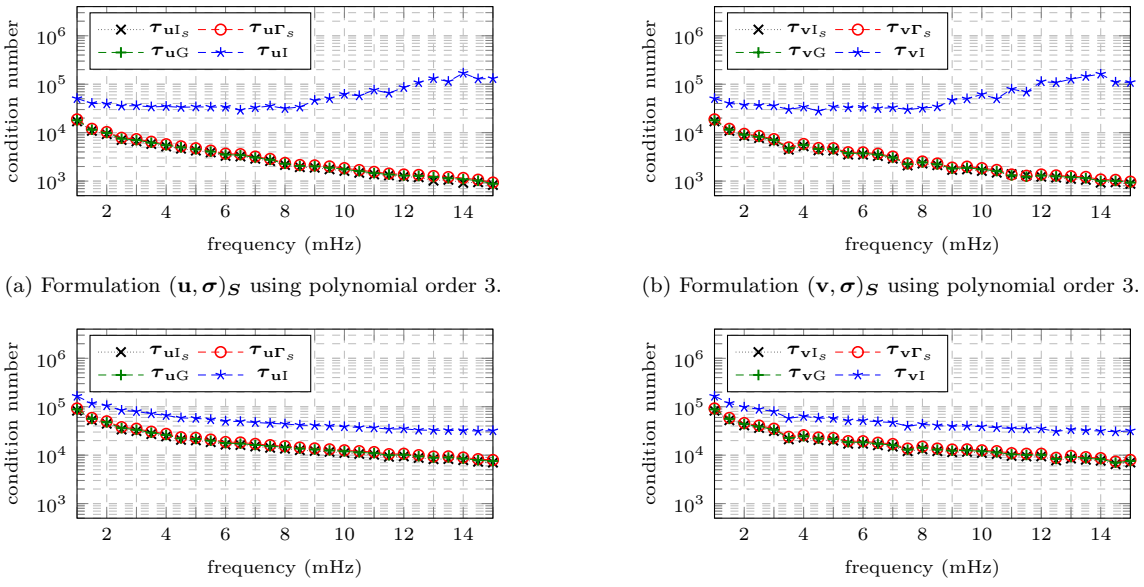

(a) Formulation $(\mathbf{u}, \boldsymbol{\sigma})_{\boldsymbol{S}}$ using polynomial order 3.

(b) Formulation $(\mathbf{v}, \boldsymbol{\sigma})_{\boldsymbol{S}}$ using polynomial order 3.

(c) Formulation $(\mathbf{u}, \boldsymbol{\sigma})_{\boldsymbol{S}}$ using polynomial order 6.

(d) Formulation $(\mathbf{v}, \boldsymbol{\sigma})_{\boldsymbol{S}}$ using polynomial order 6.

Figure 7: Condition number of the global discretization matrix using HDG for `benchmark2Diso-R5` (6.6).

We observe a drastic difference in the condition number between the identity-based stabilization coefficients ($\boldsymbol{\tau}_{\mathbf{uI}}$ and $\boldsymbol{\tau}_{\mathbf{vI}}$), while other choices show similar tendency. It indicates that the naive stabilization

not only reduces the accuracy as shown in Figures 4 and 6, but also deteriorates the condition number of the linear system. Moreover, even when the accuracy is acceptable (that is, for low frequencies), the condition number of the global matrix is still higher. We also observe that using high-order polynomials increases the condition number of the global matrix, while using higher frequencies does not, or even slightly reduces the condition numbers. Furthermore, we do not observe differences between the HDG formulations using the displacement or the velocity.

6.1.4 Concluding remarks on experiment `benchmark2Diso-R5`

With this first experiment considering isotropic elastic 2D homogeneous medium, we can draw the following comments.

- The HDG methods using displacement or velocity formulation, respectively $(\mathbf{u}, \boldsymbol{\sigma})_{\boldsymbol{S}}$ and $(\mathbf{v}, \boldsymbol{\sigma})_{\boldsymbol{S}}$, are equally accurate. Note that here we avoid the zero-frequency where only the formulation $(\mathbf{u}, \boldsymbol{\sigma})_{\boldsymbol{S}}$ is appropriate.
- The stabilizations using the identity and Kelvin–Christoffel matrices $\boldsymbol{\tau}_{\mathbf{uI}}$ and $\boldsymbol{\tau}_{\mathbf{u\Gamma}}$ are less accurate than using the Godunov matrix with $\boldsymbol{\tau}_{\mathbf{u}\mathrm{G}}$, cf. Figure 4. Those stabilization coefficients also lead to an increase of the condition number of the global matrix, even for low frequencies where it is accurate, Figure 7.
- The accuracy using stabilization coefficient based on identity and Kelvin–Christoffel matrices can be improved by using a well chosen scaling parameter, here related to the S-wave speed. In this case, using $\boldsymbol{\tau}_{\mathbf{u}\mathrm{I}_s}$ and $\boldsymbol{\tau}_{\mathbf{u}\Gamma_s}$ is equally accurate as $\boldsymbol{\tau}_{\mathbf{u}\mathrm{G}}$. However, this scaling coefficient is empirical and cannot be assumed to be universal.

6.2 3D homogeneous medium with planewave (`benchmark3Diso-Pw`)

We consider the propagation of planewaves in the three-dimensional domain $(-1,1)\times(-1,1)\times(-1,1)$. Following Appendix A (that simplifies with isotropy), we defined the P- and S-planewave as follow:

$$\text{P-planewave configuration: } \mathbf{u}(\mathbf{x},\omega) = \boldsymbol{p}(\mathbf{x})\, e^{\mathrm{i}\frac{\omega}{\mathrm{c_P}}(\boldsymbol{d}\cdot\mathbf{x})}\,. \tag{6.13a}$$

$$\text{S-planewave configuration: } u_x = u_z = 0\,,\quad u_y(\mathbf{x},\omega) = e^{\mathrm{i}\frac{\omega}{\mathrm{c_S}}(\boldsymbol{d}\cdot\mathbf{x})}\,, \tag{6.13b}$$

$$\text{with } \boldsymbol{p} = (1,0,1)^t \quad \text{and} \quad \boldsymbol{d} = \left(1/\sqrt{2},0,1/\sqrt{2}\right)^t. \tag{6.13c}$$

To emphasize the different behaviour of the stabilization, we further impose a strong contrast between the P- and S-wavespeeds, we use:

$$\texttt{benchmark3Diso-Pw} \quad \begin{cases} \text{Cube } (-1,1)^3 \text{ with planewave} \\ \mathrm{c_P} = 2.5\times10^{-3}\,,\quad \mathrm{c_S} = 10^{-4}\,,\quad \rho = 1\,, \\ \qquad \Rightarrow\ \lambda = 6.24\times10^{-6} \quad \text{and} \quad \mu = 10^{-8}\,. \\ \text{Simulations with fixed mesh of about } 40\,000 \text{ tetrahedra,} \\ \text{P-planewave at } \omega/(2\pi) = 8 \text{ mHz;} \quad \text{polynomial order4}\,, \\ \text{S-planewave at } \omega/(2\pi) = 0.4 \text{ mHz;} \quad \text{polynomial order4}\,, \end{cases} \tag{6.14}$$

We illustrate the analytic solutions of the experiment (6.14) in Figure 8. The consideration of planewaves results in having only one type of wave (P- or S-) propagating, allowing us to investigate the accuracy of the discretization with each one separately. As we have seen that scaling of the stabilization based upon the S-wavespeed improves the accuracy, this experiment serves in particular to investigate the case where only P-waves propagate.

In this experiment, the frequency and order of polynomial are fixed, and we vary the magnitude of the stabilization; we also consider purely real and imaginary coefficients. In Figures 9 and 10, we show the mean of the relative error $\mathfrak{e}$ of (6.1) for the non-zero components for the P- and S-planewave respectively.

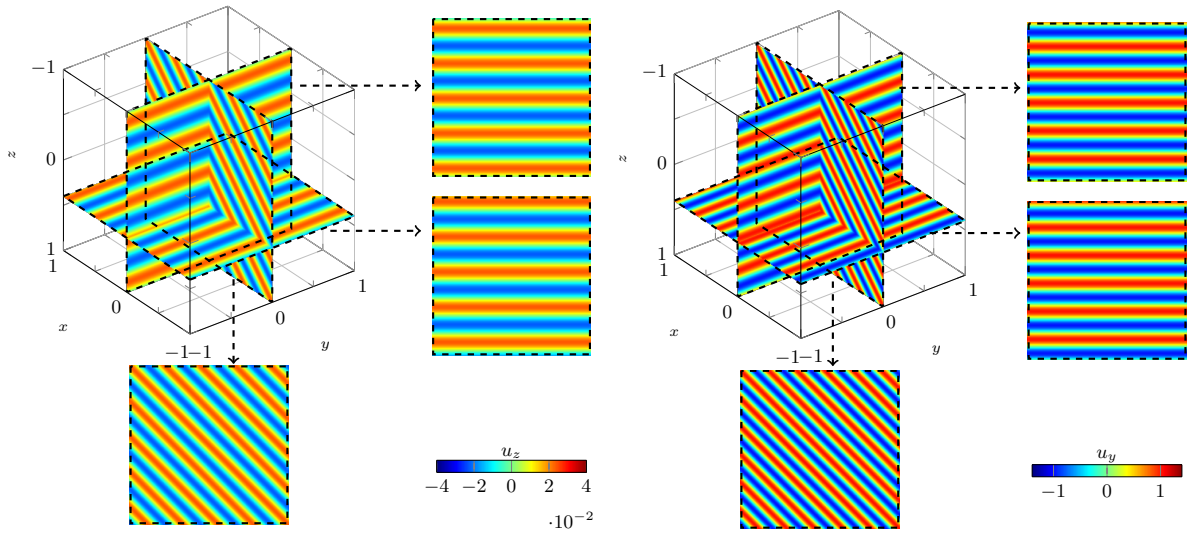

(a) Field u_z for the P-planewave at 8 mHz.

(b) Field u_y for the S-planewave at0.4 mHz.

Figure 8: Reference solution for the 3D planewave propagation of `benchmark3Diso-Pw` (6.14).

For the P-planewave, the non-zero components are u_x, u_z, σ_{xx}, σ_{yy}, σ_{zz} and σ_{xz}. For the S-planewave, the non-zero components are u_y, σ_{xy} and σ_{yz}. We consider the formulation $(\mathbf{u}, \boldsymbol{\sigma})_{\boldsymbol{S}}$, and investigate stabilization $\pm\tau \mathrm{I}_d$ and $\pm \mathrm{i}\tau \mathrm{I}_d$ with τ varying between several order of magnitude. In Figures 9 to 11, we also indicate the error level obtained with the Godunov and Kelvin–Christoffel stabilization $\boldsymbol{\tau}_{\mathbf{u}\mathrm{G}}$ and $\boldsymbol{\tau}_{\mathbf{u}\boldsymbol{\Gamma}}$ (horizontal lines) and the values of the P- and S-wavelength (vertical lines). We picture the results for the formulation $(\mathbf{v}, \boldsymbol{\sigma})_{\boldsymbol{S}}$ in Figure 11.

We observe that

- For the P-planewave, the accuracy for the different fields is similar (Figure 9), except for the component σ_{xz} which is slightly less accurate (6×10^{-6} relative error compared to 10^{-6} for the other components). In this experiment, the S-planewave is less accurate than the P-planewave because it has a smaller wavelength (0.25 compared to 0.31) at the selected frequencies.

- Comparing the formulations, we see that $(\mathbf{u}, \boldsymbol{\sigma})_{\boldsymbol{S}}$ and $(\mathbf{v}, \boldsymbol{\sigma})_{\boldsymbol{S}}$ are equally accurate. For best efficiency, the formulation $(\mathbf{u}, \boldsymbol{\sigma})_{\boldsymbol{S}}$ should use a purely imaginary stabilization while formulation $(\mathbf{v}, \boldsymbol{\sigma})_{\boldsymbol{S}}$ a real-valued one. This is explained by the $(\mathrm{i}\omega)$ factor appearing between the two formulations. Also we note that the accuracy is not affected by the sign of the stabilization, namely taking $\pm\tau$ does no change the results in these experiments.

- For the P-planewave, the Godunov stabilization $\boldsymbol{\tau}_{\mathbf{u}\mathrm{G}}$ gives the most accurate results, accuracy that is never reach by identity-based stabilization, nor by the Kelvin–Christoffel coefficient. The best performance with identity-based stabilization is obtained with scale $\rho\omega c_{\mathrm{P}}$ or ρc_{P}, for displacement and velocity formulations respectively.

- For the S-planewave, the accuracy of the Godunov stabilization can be improved with identity-based stabilization. However, the optimal scale is difficult to select as it is not exactly $\rho\omega c_{\mathrm{S}}$ (for displacement formulation, ρc_{S} for velocity formulation), but a lower value.

We see that the Godunov stabilization is the most versatile as it accurately treats the P-planewave and remains very efficient for the S-planewave. It seems that identity-based approach can be very efficient to treat the S-waves but there is no unifying scaling that can treat both P- and S-waves. In practical experiments of wave propagation, we would have a mix of P- and S-waves, and the Godunov stabilization

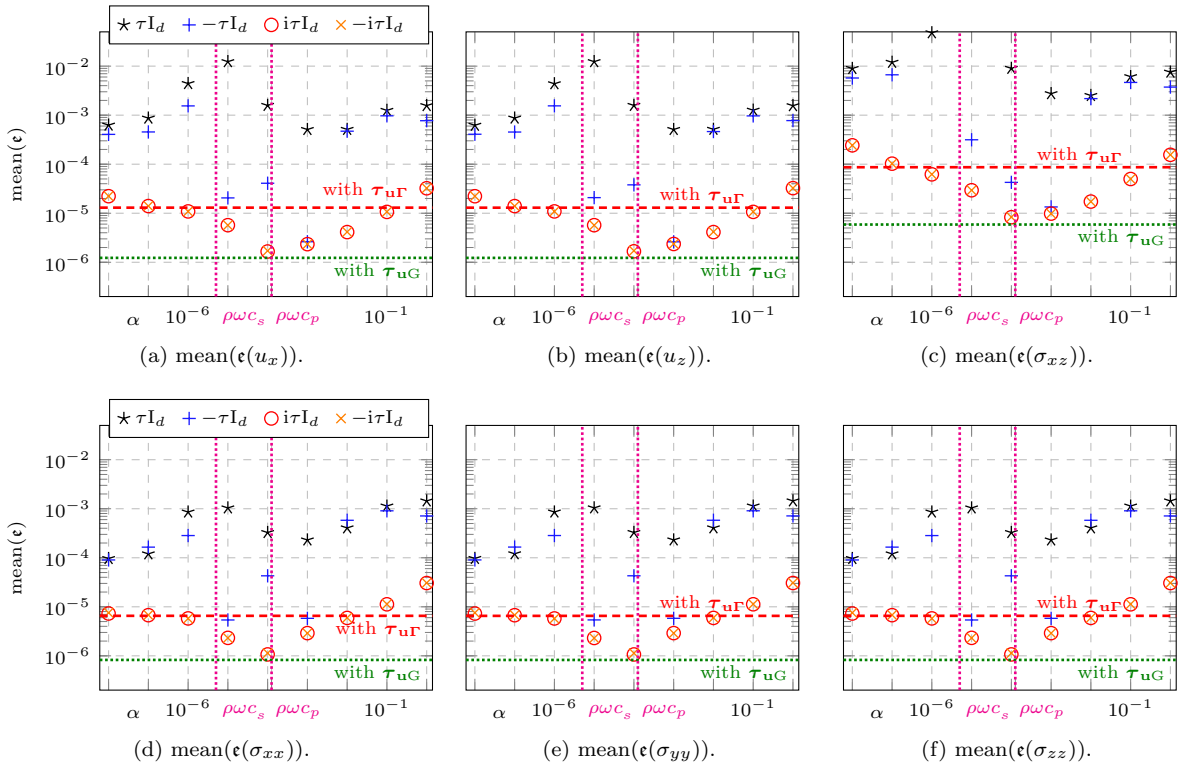

(a) mean($\mathfrak{e}(u_x)$). (b) mean($\mathfrak{e}(u_z)$). (c) mean($\mathfrak{e}(\sigma_{xz})$).

(d) mean($\mathfrak{e}(\sigma_{xx})$). (e) mean($\mathfrak{e}(\sigma_{yy})$). (f) mean($\mathfrak{e}(\sigma_{zz})$).

Figure 9: Mean of the relative error $\mathfrak{e}$ of (6.1) using the stabilization $\boldsymbol{\tau} := \tau\mathrm{I}_d$ and varying the magnitude of coefficient τ. It corresponds with `benchmark3Diso-Pw` (6.14) using HDG discretization of formulation $(\mathbf{u},\boldsymbol{\sigma})_{\boldsymbol{S}}$ for 8 mHz P-planewave propagation at polynomial order 4. The relative error obtained with the Godunov stabilization $\boldsymbol{\tau}_{\mathbf{uG}}$ is indicated with the horizontal dashed line, and the values of the P- and S-wavelength with the vertical lines.

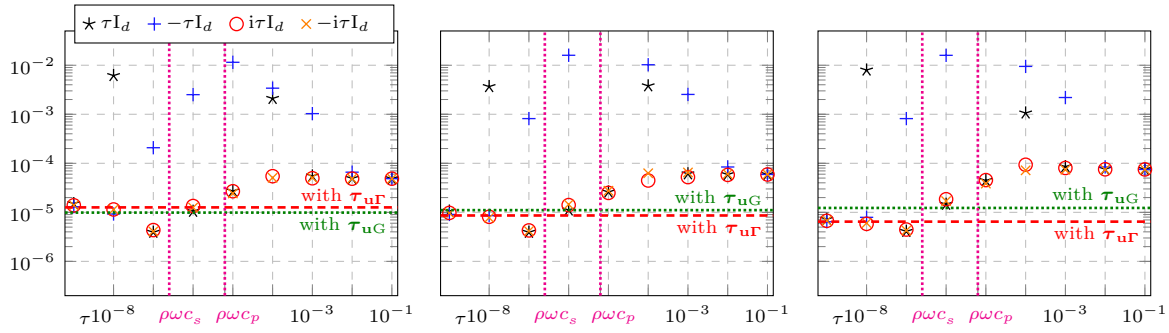

(a) $\mathfrak{e}(u_y)$. (b) $\mathfrak{e}(\sigma_{xy})$. (c) $\mathfrak{e}(\sigma_{yz})$.

Figure 10: Mean of the relative error $\mathfrak{e}$ of (6.1) using the stabilization $\boldsymbol{\tau} := \tau\mathrm{I}_d$ and varying the magnitude of coefficient τ. It corresponds with `benchmark3Diso-Pw` (6.14) using HDG discretization of formulation $(\mathbf{u},\boldsymbol{\sigma})_{\boldsymbol{S}}$ for 0.4 mHz S-planewave propagation at polynomial order 4. The relative error obtained with the Godunov stabilization $\boldsymbol{\tau}_{\mathbf{uG}}$ is indicated with the horizontal dashed line, and the values of the P- and S-wavelength with the vertical lines.

appears as the safest choice. Nonetheless, as S-waves tend to be more energetic than P-waves after equipartition time ([50, 51]), it explains why a stabilization based upon S-wavelength is performing well in the point-source experiment of Subsection 6.1.

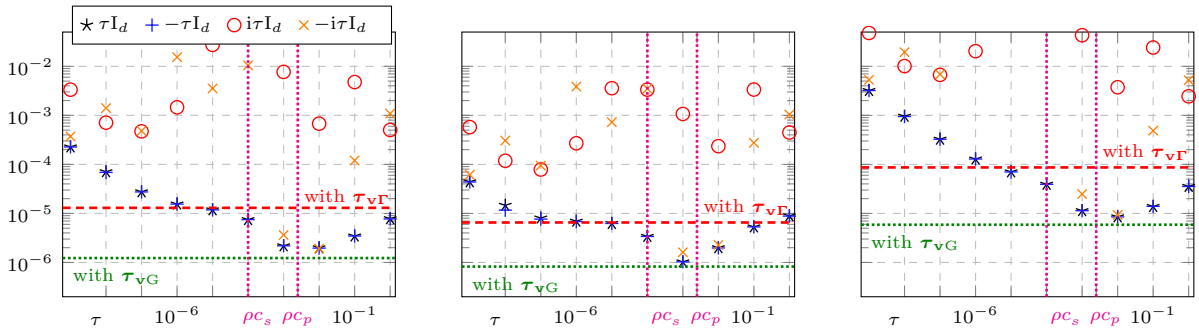

(a) P-planewave relative error $\mathfrak{e}(u_x)$ (left), $\mathfrak{e}(\sigma_{yy})$ (middle) and $\mathfrak{e}(\sigma_{xz})$ (right) for 8 mHz frequency.

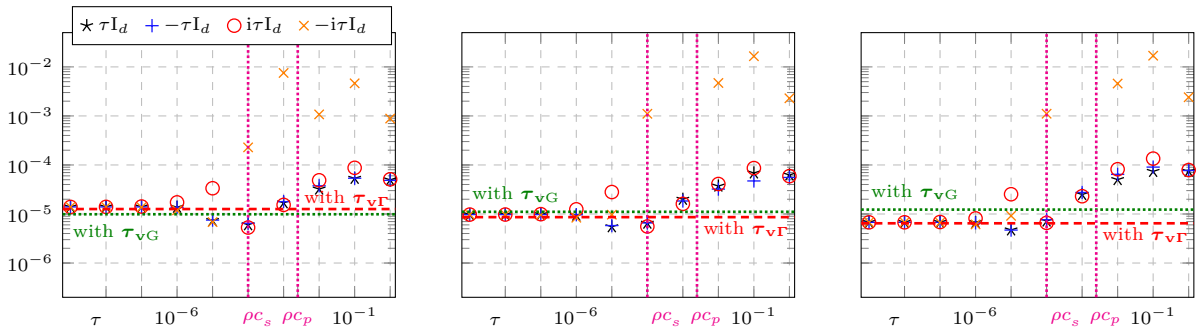

(b) S-planewave relative error $\mathfrak{e}(u_y)$ (left), $\mathfrak{e}(\sigma_{xy})$ (middle) and $\mathfrak{e}(\sigma_{yz})$ (right) for 0.4 mHz frequency.

Figure 11: Mean of the relative error $\mathfrak{e}$ of (6.1) using the stabilization $\dot{\boldsymbol{\tau}} := \tau\mathrm{I}_d$ and varying the magnitude of coefficient τ. It corresponds with `benchmark3Diso-Pw` (6.14) using HDG discretization of formulation $(\mathbf{v}, \boldsymbol{\sigma})_{\boldsymbol{S}}$ at polynomial order 4. The relative error obtained with the Godunov stabilization $\boldsymbol{\tau}_{\mathbf{v}\mathrm{G}}$ is indicated with the horizontal dashed line, and the values of the P- and S-wave speeds with the vertical lines.

6.3 2D experiment with highly varying properties (`benchmark2Diso-He`)

One advantage of writing the elastic system in terms of the compliance matrix $\boldsymbol{S}$ rather than the stiffness tensor $\boldsymbol{C}$ is to easily handle physical properties that are not constant per cell. To fully use this property, we design an experiment where the wave speeds and density are 'solar-like', that is, we follow the solar background given by model `S`, [12]. Model `S` provides us with radial profiles for the density and P-wave speed models, that we picture in Figure 12. For the purpose of this experiment, the S-wavespeed is selected as $\mathrm{c_S} = 0.70\mathrm{c_P}$. For this experiment, we consider a two-dimensional disk of radius 1 on which the radial profiles are applied.

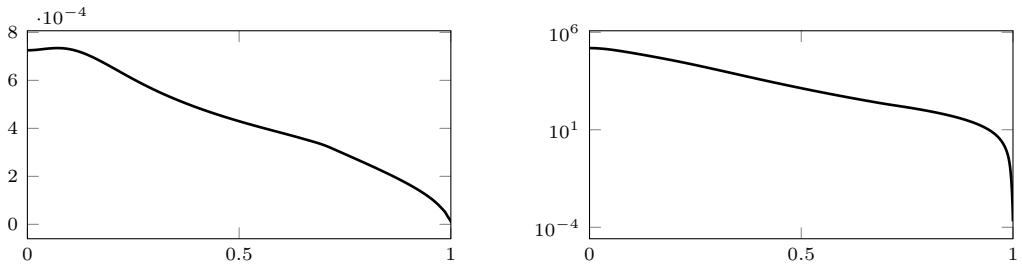

(a) Wave speed model.

(b) Density model on logarithmic scale.

Figure 12: Solar-like background wave speed and density extracted from model `S` for radial position between 0 and 1. In our elastic experiment, we use $\mathrm{c_S} = 0.70\mathrm{c_P}$.

The models of physical properties are particularly challenging because of the high variation in their amplitude, cf. Figure 12, where the density is pictured on a logarithmic scale. Namely, the density is exponentially decreasing near surface ([5, 4]) and the wave speed varies of about two orders of magnitude in the domain. Therefore, it is fundamental to correctly represent the models within the discretization, and using a piecewise-constant approximation would necessitate to design extremely small cells near radius 1. Using the flexibility of the discretization with the compliance tensor, we instead represent the physical parameters (wave speeds and density) using a basis of Lagrange functions on each cell. In Figure 13 we picture the mesh of the 2D disk that we used for the simulations, and compare the density model near surface when represented with piecewise-constant or with Lagrange basis of order 3, that is, with 10 coefficients per cell. The piecewise-constant representation looses the spherical nature of the medium, and shows some strong variations which will intrinsically lead to inaccurate simulations. The Lagrange polynomial representation preserves the spherical nature of the model which appears radial as expected.

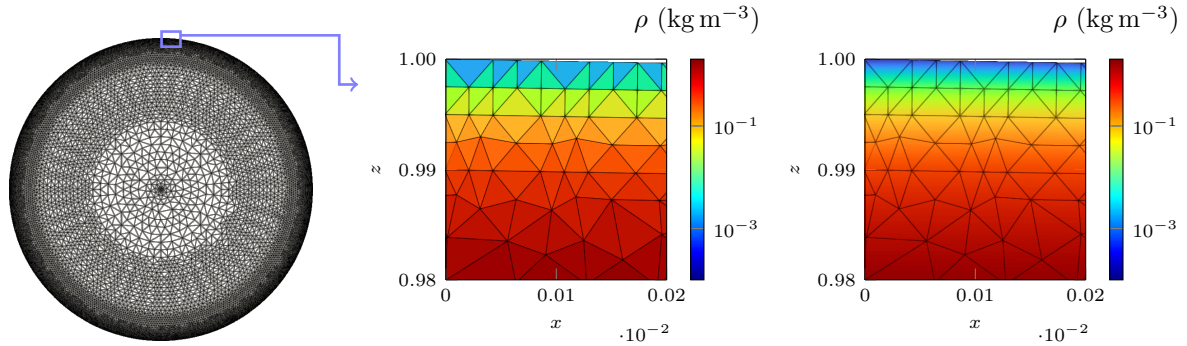

(a) Mesh with about 50 000 cells.

(b) Zoom near surface for piecewise-constant representation.

(c) Zoom near surface for representation with Lagrange basis of order 3.

Figure 13: Solar-like density near surface and computational mesh, considering a unitary disk.

In this case of (strongly) heterogeneous properties, there is no analytic solution for the elastic wave equation. To evaluate the accuracy depending on the stabilization coefficients, we build a reference solution which is computed with a refined mesh composed of 80 000 cells (while for the simulation we have 50 000 cells, Figure 13a), with a polynomial order of 7, and using $\boldsymbol{\tau}_{\mathbf{u}\mathrm{G}}$. The reference solutions are shown in Figure 14 where we also compare with the solution using a piecewise-constant representation. Due to the exponentially decreasing nature of the density, we scale the displacement fields by $\sqrt{\rho}$ to better visualize the solution, [4, 5]. For similar reason, the components of stress tensor are scaled by $1/\sqrt{\rho}$.

Comparing simulations using a piecewise-constant representation for the model parameters or allowing them to vary within the cell, we see drastic difference. Using a piecewise-constant representation, the solutions (both in terms of displacement $\mathbf{u}$ and stress tensor $\boldsymbol{\sigma}$) show wiggles and artifacts, while the radial nature is not preserved. On the contrary, the simulations using model represented in a Lagrange basis on each cell capture well the spherical pattern and provide smooth solutions. With such high variation in the background models, we see that it is mandatory to design an efficient representation, and that piecewise-constant is not appropriate, therefore, the HDG formulation based upon the compliance tensor $\boldsymbol{\sigma}$ is extremely useful as it allows us to vary the models within each cell, without having to compute their derivatives (as it would be the case using a formulation with the stiffness tensor $\boldsymbol{C}$).

In Figure 15, we plot the relative error $\mathfrak{E}$ depending on the frequency and polynomial orders, for the stabilization coefficients of (6.3). For some frequency and order, stabilization $\boldsymbol{\tau}_{\mathbf{u}\mathrm{I}}$ results in a ill-conditioned matrix that either cannot be factorized or lead to a particularly erroneous solutions, in particular at low and high orders. This confirms the high-increase in condition number observed in Figure 7. While stabilization $\boldsymbol{\tau}_{\mathbf{u}\Gamma}$ appears stable, it gives a higher error than the other stabilization.

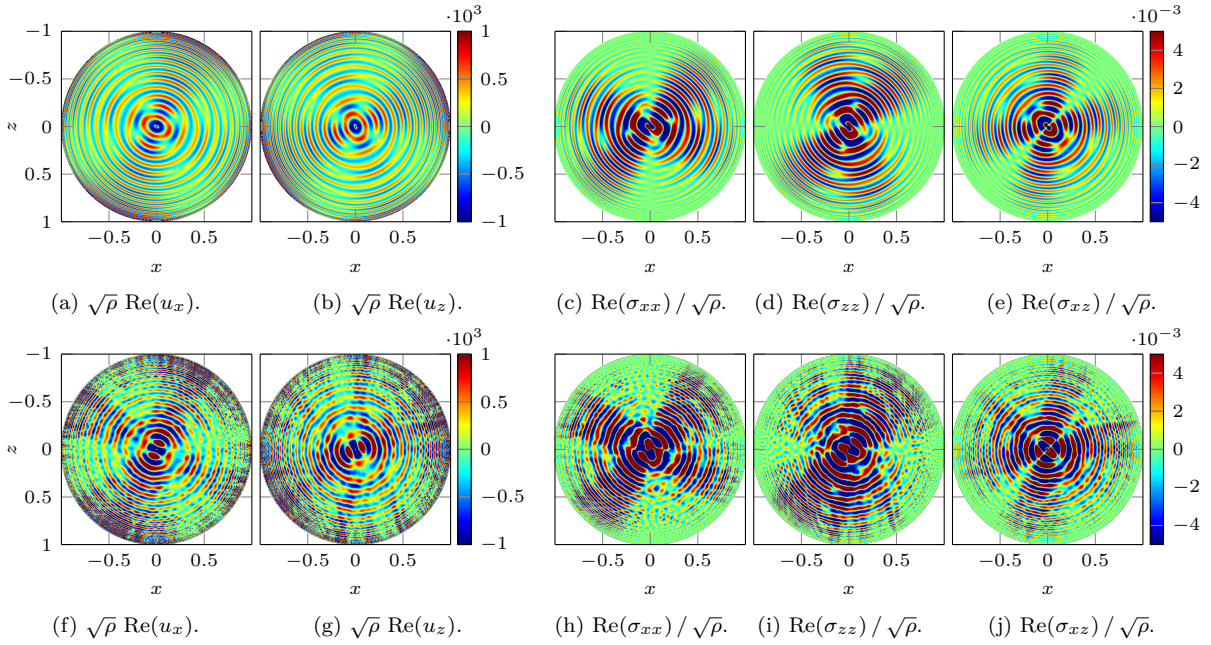

(a) $\sqrt{\rho}\,\mathrm{Re}(u_x)$. (b) $\sqrt{\rho}\,\mathrm{Re}(u_z)$. (c) $\mathrm{Re}(\sigma_{xx})\,/\,\sqrt{\rho}$. (d) $\mathrm{Re}(\sigma_{zz})\,/\,\sqrt{\rho}$. (e) $\mathrm{Re}(\sigma_{xz})\,/\,\sqrt{\rho}$.

(f) $\sqrt{\rho}\,\mathrm{Re}(u_x)$. (g) $\sqrt{\rho}\,\mathrm{Re}(u_z)$. (h) $\mathrm{Re}(\sigma_{xx})\,/\,\sqrt{\rho}$. (i) $\mathrm{Re}(\sigma_{zz})\,/\,\sqrt{\rho}$. (j) $\mathrm{Re}(\sigma_{xz})\,/\,\sqrt{\rho}$.

Figure 14: Comparison of the solution at 4 mHz of the elastic isotropic wave equation using the solar-like background models of Figure 12 using piecewise-constant representation (bottom) or allowing representations that vary within each cell (top). The computations use HDG formulation $(\mathbf{u},\boldsymbol{\sigma})_{\boldsymbol{S}}$ with stabilization $\boldsymbol{\tau}_{\mathbf{u}\mathrm{G}}$ and polynomial order 7.

Namely, this heterogeneous test enforces the results that $\boldsymbol{\tau}_{\mathbf{u}\mathrm{G}}$ is the safest and more robust choice, while scaling with the S-wave speed, with either $\boldsymbol{\tau}_{\mathbf{u}\mathrm{I}_s}$ or $\boldsymbol{\tau}_{\mathbf{u}\boldsymbol{\Gamma}_s}$, can provide good accuracy.

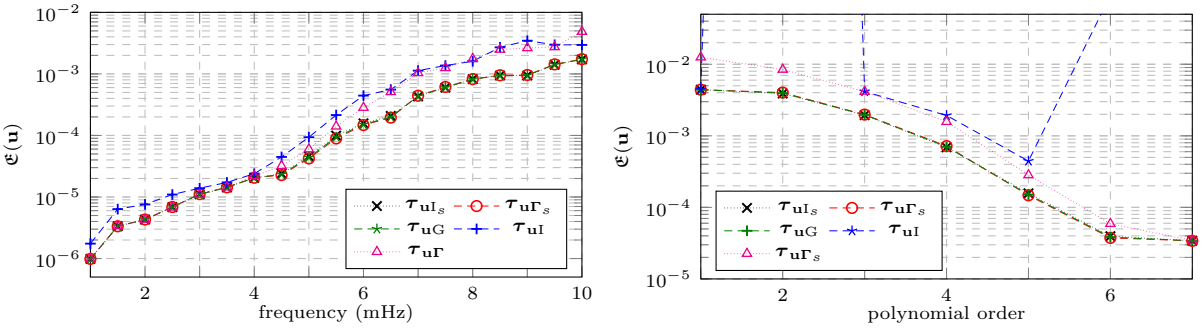

(a) $\mathfrak{E}(\mathbf{u})$ for polynomial order 5. (b) $\mathfrak{E}(\mathbf{u})$ at frequency 6 mHz.

Figure 15: Relative error $\mathfrak{E}$ of (6.2) with frequency (left) and the polynomial order (right) for `benchmark2Diso-He` using HDG discretization of formulation $(\mathbf{u},\boldsymbol{\sigma})_{\boldsymbol{S}}$ and stabilization coefficients of (6.3).

7 Numerical experiments: elastic transverse isotropy

In the context of vertical transverse isotropy (VTI), there are five parameters that define the stiffness tensor, see Subsection 3.5.2. These are the Lamé parameters λ and μ and the Thomsen's parameters, ϵ, δ and γ. In Subsection 7.3, we further consider the tilted case that introduces two angles, cf. Subsection 3.5.3.

7.1 3D homogeneous medium with planewave (`benchmark3Dvti-Pw`)

In this experiment, we start from the isotropic configuration of Subsection 6.2 to have a strong contrast between the wavespeeds, and add anisotropy with non-zero Thomsen's parameters such that we have,

$$\texttt{benchmark3Dvti-Pw} \quad \begin{cases} \text{Cube } (-1,1)^3 \text{ with planewave} \\ \lambda = 6.23 \times 10^{-6}\,, \quad \mu = 10^{-8}\,, \quad \rho = 1\,, \\ \epsilon = 1.12\,, \quad \delta = -0.235 \quad \gamma = 2.28\,. \\ \text{Simulations with fixed mesh of about } 40\,000 \text{ tetrahedra,} \\ \text{qP-planewave at } \omega/(2\pi) = 10 \text{ mHz;} \quad \text{polynomial order4}\,, \\ \text{sH-planewave at } \omega/(2\pi) = 0.7 \text{ mHz;} \quad \text{polynomial order4}\,, \end{cases} \tag{7.1}$$

Here the values of the anisotropic coefficients ϵ, δ and γ correspond to the muscovite crystal in [54]. This amounts to the following values of the stiffness tensor coefficients:

$$C_{11} = C_{22} = 2.025 \times 10^{-5}\,, \quad C_{33} = 6.25 \times 10^{-6}\,, \tag{7.2a}$$
$$C_{44} = C_{55} = 10^{-8}\,, \quad C_{66} = 5.56 \times 10^{-8}\,, \tag{7.2b}$$
$$C_{12} = C_{11} - 2C_{66} = 2.0139 \times 10^{-5}\,, \quad C_{23} = C_{23} = 4.5296 \times 10^{-6}\,. \tag{7.2c}$$

In Figure 16, we evaluate the accuracy of the solution depending on the stabilization for the HDG formulation $(\mathbf{u}, \boldsymbol{\sigma})_{\boldsymbol{S}}$. The qP-planewave is computed at frequency 10 mHz and the sH-planewave at frequency 0.7 mHz, leading to wavelength of size 0.329 and 0.259 respectively.

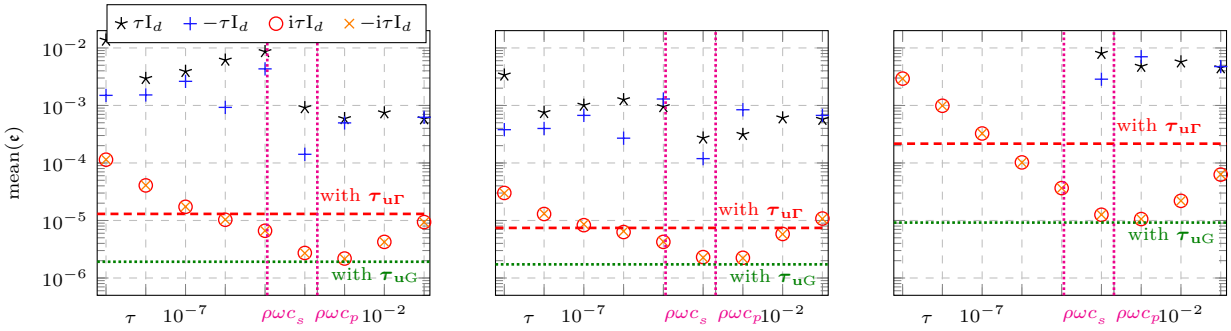

(a) qP-planewave relative error $\mathfrak{e}(u_x)$ (left), $\mathfrak{e}(\sigma_{yy})$ (middle) and $\mathfrak{e}(\sigma_{xz})$ (right) for 10 mHz frequency.

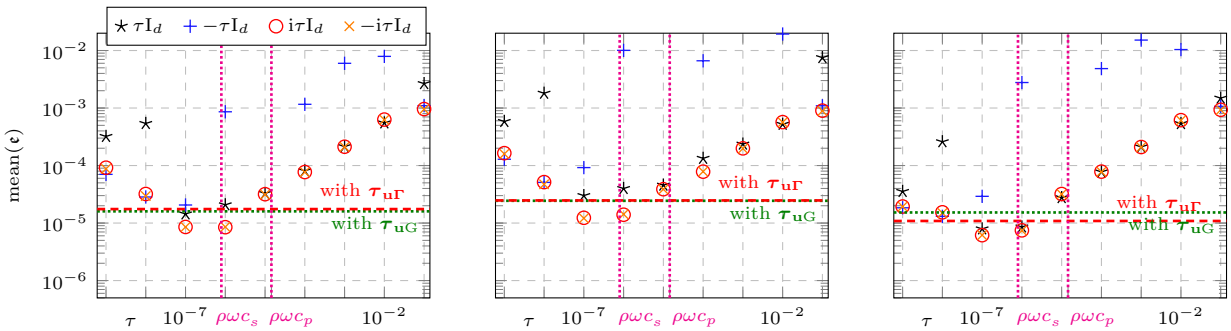

(b) sH-planewave relative error $\mathfrak{e}(u_y)$ (left), $\mathfrak{e}(\sigma_{xy})$ (middle) and $\mathfrak{e}(\sigma_{yz})$ (right) for 0.7 mHz frequency.

Figure 16: Mean of the relative error $\mathfrak{e}$ of (6.1) using the stabilization $\boldsymbol{\tau} := \tau \mathrm{I}_d$ and varying the magnitude of coefficient τ. It corresponds with `benchmark3Dvti-Pw` (7.1) using HDG discretization of formulation $(\mathbf{u}, \boldsymbol{\sigma})_{\boldsymbol{S}}$ at polynomial order 4. The relative error obtained with the Godunov stabilization $\boldsymbol{\tau}_{\mathbf{uG}}$ is indicated with the horizontal dashed line, and the values of the qP- and sH-wavelength with the vertical lines.

The observations in the context of an elastic VTI medium follow those of the elastic isotropic case of Subsection 6.2. For the qP-planewave propagation, the Godunov stabilization is the most accurate, accuracy that can only be approached by using a scaling in terms of the qP-wavespeeed for identity-based stabilization. For the sH-planewave propagation, the accuracy of Godunov can be improved by taking a low-valued coefficient for identity-based stabilization, however the precise value is not the qS-wavelength but below it. Therefore, the Godunov stabilization is most robust to treat both qP- and sH-waves.

7.2 3D unscaled homogeneous medium with planewave (`benchmark3Dvti-PwB`)

In this experiment, we use unscaled parameter values and select the ones of the Biotite crystal in [54], which gives us

$$\texttt{benchmark3Dvti-PwB} \quad \begin{cases} \text{Cube } (-1,1)^3 \text{ with planewave} \\ \lambda = 3.9157 \times 10^{10}\,, \quad \mu = 5.4848 \times 10^{9}\,, \quad \rho = 3050\,, \\ \epsilon = 1.222\,, \quad \delta = -0.388 \quad \gamma = 6.12\,. \\ \text{Simulations with fixed mesh of about } 40\,000 \text{ tetrahedra,} \\ \text{qP-planewave at } \omega/(2\pi) = 15 \text{ kHz;} \quad \text{polynomial order4}\,, \\ \text{sH-planewave at } \omega/(2\pi) = 10 \text{ kHz;} \quad \text{polynomial order4}\,, \end{cases} \tag{7.3}$$

This amounts to the following values of the stiffness tensor coefficients:

$$C_{11} = C_{22} = 1.7264 \times 10^{11}\,, \quad C_{33} = 5.0126 \times 10^{10}\,, \quad C_{44} = C_{55} = 5.4848 \times 10^{9}\,, \tag{7.4a}$$

$$C_{66} = 7.2618 \times 10^{10}\,, \quad C_{12} = C_{11} - 2C_{66} = 2.7399 \times 10^{10}\,, \tag{7.4b}$$

$$C_{23} = C_{23} = 1.0528 \times 10^{10}\,, \qquad \rho = 3050\,. \tag{7.4c}$$

Here the magnitude of the parameters is much higher than in our previous experiments (that can be seen as 'normalized' experiments), hence we have to adjust the frequency that is now to be selected in the kHz. We use frequencies 15 and 10 kHz for the qP- and sH-planewave, which leads to wavelength of size 0.362 and 0.358 respectively. The accuracy with the amplitude of the stabilization is pictured in Figure 17.

In this experiment the magnitude of the stabilization has to be adapted to the physical parameters and frequency that are much higher than in the previous experiments. Despite the qP- and sH-wavespeed being relatively close in this experiment, we still observe that the Godunov stabilization is the most efficient to handle qP-waves, while for sH-waves, a low-valued coefficient for an identity-based stabilization suffices.

7.3 2D experiment with highly varying properties (`benchmark2Dtti-He`)

We now consider a 2D experiment with a point-source, and start from the high-varying properties of the experiment presented in Subsection 6.3, that give us the Lamé parameters λ, μ, and the density ρ. Then we use constant Thomsen's parameters with $\epsilon = 0.25$, $\delta = 0.15$ and $\theta = 45°$. In Figure 18, we show the reference solutions at frequency 4 mHz, which is computed on a mesh with 80 000 triangles (while following simulations would use 50 000 elements), using polynomial order 7 and the Godunov stabilization. Compared to the isotropic case of Figure 14, we see that the solution is less smooth with more wiggles. Note that for the TTI absorbing boundary conditions, we follow [7]. It is out of the scope to investigate the accuracy of the anisotropic boundary conditions here.

In Figure 19, we plot the relative error $\mathfrak{E}$ depending on the frequency and polynomial orders, for the HDG formulation $(\mathbf{u}, \boldsymbol{\sigma})_{\boldsymbol{S}}$. We note that stabilization $\boldsymbol{\tau}_{\mathbf{uI}}$ can result in a ill-conditioned matrix hence not all cases can be computed with this choice of stabilization. The results confirm the behaviour observed in the isotropic case, that the Godunov stabilization gives the most accurate results, and the level accuracy can be met with other stabilization with a well-chosen scaling factor (in terms of the S-wavelength here). Namely, it appears that considering transverse isotropy does not modify the behaviour and efficiency of the discretization.

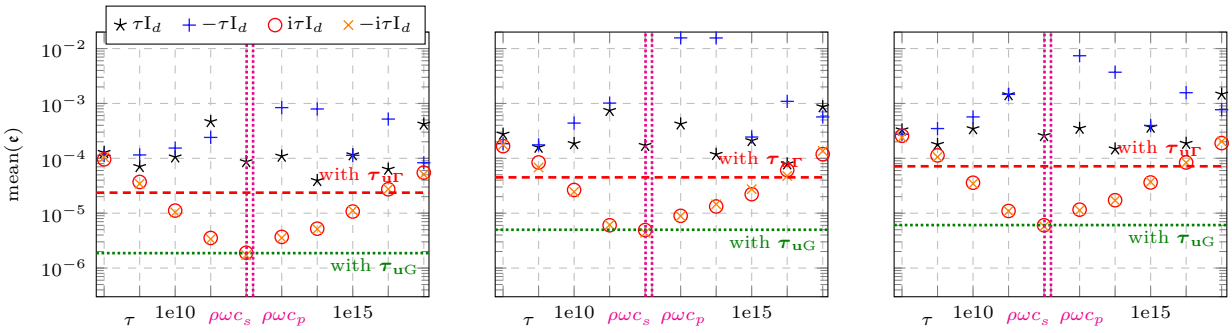

(a) qP-planewave relative error $\mathfrak{e}(u_x)$ (left), $\mathfrak{e}(\sigma_{yy})$ (middle) and $\mathfrak{e}(\sigma_{xz})$ (right) for 15 kHz frequency.

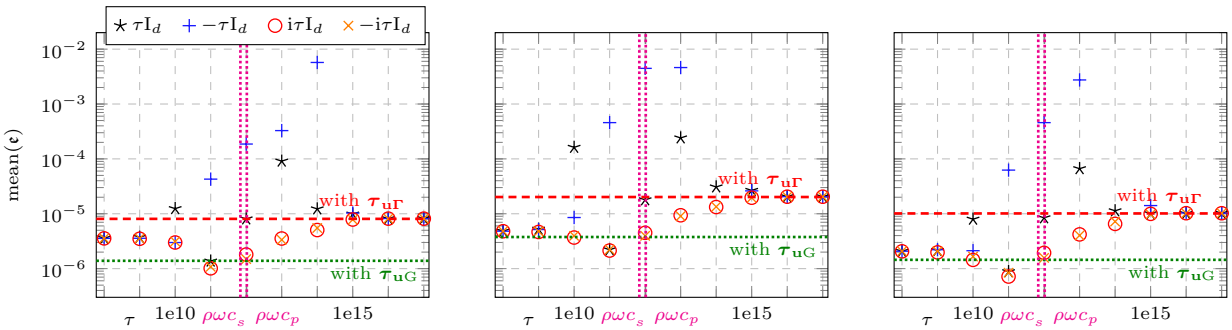

(b) sH-planewave relative error $\mathfrak{e}(u_y)$ (left), $\mathfrak{e}(\sigma_{xy})$ (middle) and $\mathfrak{e}(\sigma_{yz})$ (right) for 10 kHz frequency.

Figure 17: Mean of the relative error $\mathfrak{e}$ of (6.1) using the stabilization $\boldsymbol{\tau} := \tau\mathrm{I}_d$ and varying the magnitude of coefficient τ. It corresponds with `benchmark3Dvti-PwB` (7.3) using HDG discretization of formulation $(\mathbf{u},\boldsymbol{\sigma})_{\boldsymbol{S}}$ at polynomial order 4. The relative error obtained with the Godunov stabilization $\boldsymbol{\tau}_{\omega M^{\mathrm{aniso}}}$ is indicated with the horizontal dashed line, and the values of the qP- and sH-wavelength with the vertical lines.

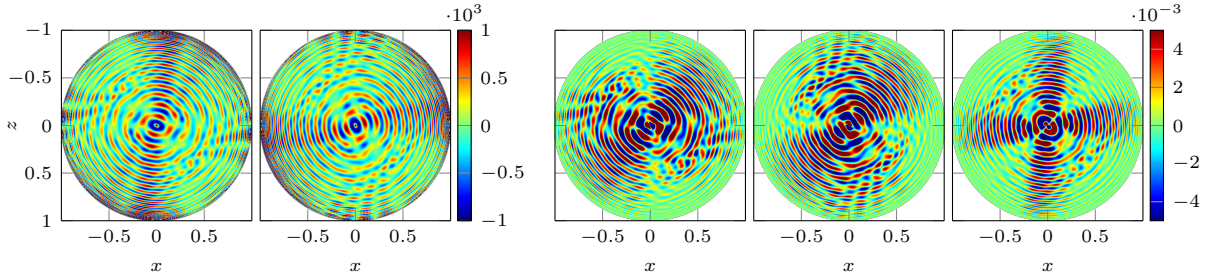

(a) $\sqrt{\rho}\,\mathrm{Re}(u_x)$. (b) $\sqrt{\rho}\,\mathrm{Re}(u_z)$. (c) $\mathrm{Re}(\sigma_{xx})\,/\,\sqrt{\rho}$. (d) $\mathrm{Re}(\sigma_{zz})\,/\,\sqrt{\rho}$. (e) $\mathrm{Re}(\sigma_{xz})\,/\,\sqrt{\rho}$.

Figure 18: Solutions at 4 mHz of the elastic TTI wave equation using the solar-like background models of Figure 12 with model representations that vary within each cell. The computations use HDG formulation $(\mathbf{u},\boldsymbol{\sigma})_{\boldsymbol{S}}$ with stabilization $\boldsymbol{\tau}_{\mathrm{uG}}$ and polynomial order 7.

8 Conclusion

In this work, we have employed Voigt's notation in the HDG method to describe compactly the discrete problem for anisotropic elasticity. Additionally, a first-order formulation with compliance tensor is used and allows for mesh-wise parameter variation. This, together with the Voigt's notation which provides efficient booking-keeping of physical parameters, form indispensable features in quantitative reconstruction of elastic parameters. Secondly, to determine an optimal choice of stabilization, we constructed the

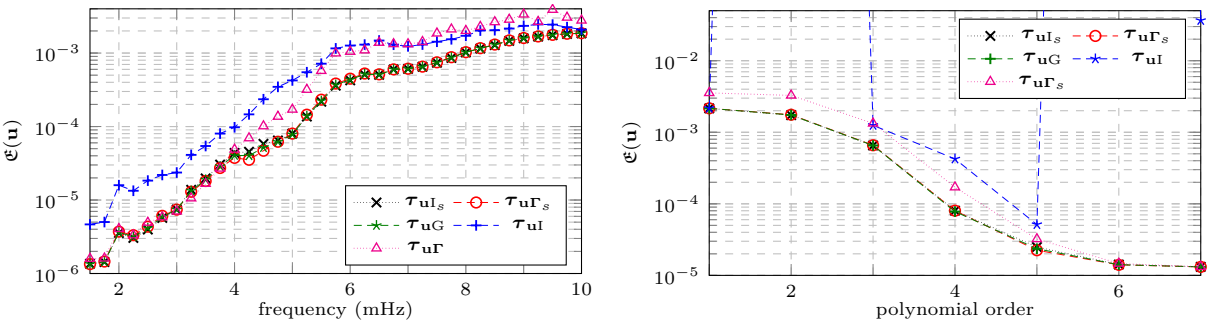

(a) $\mathfrak{E}(\mathbf{u})$ for polynomial order 4.

(b) $\mathfrak{E}(\mathbf{u})$ at frequency 5 mHz.

Figure 19: Relative error $\mathfrak{E}$ of (6.2) with frequency (left) the polynomial order (right) for `benchmark2Dtti-He` using HDG discretization of formulation $(\mathbf{u}, \boldsymbol{\sigma})_{\boldsymbol{S}}$.

hybridized Godunov-upwind flux for anisotropic elasticity, which offers a versatile choice and removes the need for scaling factor tuning. This problem concerns in particular identity-based stabilization, a popular choice due to its simple form, however one which lacks a universal scaling factor especially for geophysical material. We have carried out numerical experiments in two and three dimensions, considering isotropic elasticity and anisotropy, which highlight the performance and versatility of the Godunov stabilization.

A Planewave analysis for VTI

In this appendix, we provide the planewave analysis for vertical transverse isotropic media (VTI), following [11, Section 1.3]. Tilted transverse isotropy (TTI) refers to material having one direction of rotational symmetry. For VTI material, this direction is parallel to the z-axis, and the (x, y) becomes the plane of isotropy. Recall the VTI stiffness tensor given in (3.123),

$$\bar{\bar{\mathbf{C}}}_{\mathrm{VTI}} = \begin{pmatrix} \mathsf{c}_{11} & \mathsf{c}_{11}-2\mathsf{c}_{66} & \mathsf{c}_{13} & 0 & 0 & 0 \\ \mathsf{c}_{21} & \mathsf{c}_{11} & \mathsf{c}_{13} & 0 & 0 & 0 \\ \mathsf{c}_{13} & \mathsf{c}_{13} & \mathsf{c}_{33} & 0 & 0 & 0 \\ 0 & 0 & 0 & \mathsf{c}_{44} & 0 & 0 \\ 0 & 0 & 0 & 0 & \mathsf{c}_{44} & 0 \\ 0 & 0 & 0 & 0 & 0 & \mathsf{c}_{66} \end{pmatrix} \qquad \begin{matrix} z\text{-axis} \\ \text{rotational symmetry.} \end{matrix} \tag{A.1}$$

A.1 Dispersion relation

The generic form of planewave is given by

$$\mathbf{u}_{\mathrm{pw}} = \mathbf{p}\, e^{\mathrm{i}(\omega t - \mathbf{k}\cdot\mathbf{x})} = \mathbf{p}\, e^{\mathrm{i}\omega(t - s\,\widehat{\mathbf{k}}\cdot\mathbf{x})}, \qquad \text{with } |\hat{\mathbf{k}}| = 1\,. \tag{A.2}$$

Here, ω is the angular frequency, $\mathbf{p}$ the polarization, $\hat{\mathbf{k}}$ the direction of propagation, $\mathbf{k}$ the wave vector and s the slowness, which is the inverse of the phase velocity: $s = 1/v$. The wave vector, phase velocity vector, and slowness vector and their magnitudes satisfy,

$$\begin{gathered} \mathbf{k} = k\,\widehat{\mathbf{k}}\,; \qquad \mathbf{v} = v\,\hat{\mathbf{k}}\,; \qquad \mathbf{s} := \frac{\mathbf{k}}{\omega} = \frac{\hat{\mathbf{k}}}{v} = s\,\hat{\mathbf{k}}\,, \\ \text{and relation} \qquad k = \frac{\omega}{v}\,, \quad s = \frac{1}{v}\,. \end{gathered} \tag{A.3}$$

Substituting the planewave $\mathbf{u}_{\mathrm{pw}}$ of (A.2) into the wave equation (2.8), we obtain a relation for the

velocity and polarization, written in the 3 equivalent variants[22],

$$\begin{aligned}(\mathbf{\Gamma}(\mathbf{k}) - \rho\omega^2)\mathbf{p} = 0 \quad &\Leftrightarrow \quad (\mathbf{\Gamma}(\hat{\mathbf{k}}) - \rho v^2)\mathbf{p} = 0 \\ &\Leftrightarrow \quad (\mathbf{\Gamma}(\mathbf{s}) - \rho)\mathbf{p} = 0\,.\end{aligned} \tag{A.5}$$

• Using the first equation in (A.5), the eigenvalue is given by $\rho\omega^2$ satisfying the following relation, also called the *dispersion relation* between ω and the wave vector $\mathbf{k}$,

$$\det\left(\mathbf{\Gamma}(\mathbf{k}) \,-\, \rho\omega^2\,\mathbb{Id}\right) = 0\,. \qquad \text{Dispersion relation} \tag{A.6}$$

• Working with the second equation in (A.5), the eigenvalue is given by ρv and satisfies,

$$\det\left(\mathbf{\Gamma}(\hat{\mathbf{k}}) \,-\, \rho v^2\mathbb{Id}\right) = 0\,. \tag{A.7}$$

Recall from Assumption (4.62) that the Kelvin–Christoffel matrix $\mathbf{\Gamma}(\hat{\mathbf{k}})$ is diagonalizable with three distinct eigenvalues denoted by

$$\rho c_{\text{qP}}^2 \;>\; \rho c_{\text{qS1}}^2 \;>\; \rho c_{\text{qS2}}^2\,, \qquad \text{corresponding to direction } \hat{\mathbf{k}}\,. \tag{A.8}$$

The corresponding eigenvectors are $\mathbf{p}_i$ which gives polarization of the planewave.

• The third equation (A.5) implies the following relation which defines the *slowness surface*,

$$\det\left(\mathbf{\Gamma}(\mathbf{s}) \,-\, \rho\,\mathbb{Id}\right) = 0 \qquad \text{Equation of slowness surface} \tag{A.9}$$

A.2 Planewave with propagating direction in the symmetry plane (x, z)

The Kelvin–Christoffel matrix (4.61) for VTI material writes as,

$$\mathbf{\Gamma}_{\text{VTI}}(\hat{\mathbf{k}}) = \begin{pmatrix} C_{11}\hat{k}_x^2 + C_{66}\hat{k}_y^2 + C_{55}\hat{k}_z^2 & (C_{13}+C_{55})\hat{k}_y\hat{k}_z & (C_{13}+C_{55})\hat{k}_x\hat{k}_z \\ & C_{66}\hat{k}_x^2 + C_{11}\hat{k}_y^2 + C_{55}\hat{k}_z^2 & (C_{11}-C_{66})\hat{k}_x\hat{k}_y \\ & & C_{55}(\hat{k}_x^2+\hat{k}_y^2) + C_{33}\hat{k}_z^2 \end{pmatrix} \tag{A.10}$$

For direction of propagation only in (x, z) plane, we set $\hat{k}_y = 0$ in the above expression

$$\mathbf{\Gamma}_{\text{VTI}}(\hat{k}_x, 0, \hat{k}_z) = \begin{pmatrix} C_{11}\hat{k}_x^2 + C_{55}\hat{k}_z^2 & 0 & (C_{13}+C_{55})\hat{k}_x\hat{k}_z \\ 0 & C_{66}\hat{k}_x^2 + C_{55}\hat{k}_z^2 & 0 \\ (C_{13}+C_{55})\hat{k}_x\hat{k}_z & 0 & C_{55}\hat{k}_x^2 + C_{33}k_z^2 \end{pmatrix} \tag{A.11}$$

Writing the determinant by expanding second row (or second column), the dispersion relation for VTI material with $\hat{k}_y = 0$ gives,

$$\left(C_{66}\hat{k}_x^2 + C_{55}\hat{k}_z^2 - \rho v^2\right) \;=\; 0 \qquad \begin{array}{c}\text{SH dispersion relation, propagation} \\ \text{direction in the symmetry plane.}\end{array} \tag{A.12}$$

or

$$\left(c_{11}\hat{k}_x^2 + c_{55}\hat{k}_z^2 - \rho v^2\right)\left(c_{55}\hat{k}_x^2 + c_{33}k_z^2 - \rho v^2\right) - (c_{13}+c_{55})^2\hat{k}_x^2\hat{k}_z^2 = 0\,, \tag{A.13}$$

for inplane dispersion relation for propagation direction in the symmetry plane.

[22] For the second and third equation we use relation

$$\mathbf{\Gamma}(\mathbf{k}) \;=\; k^2\mathbf{\Gamma}(\hat{\mathbf{k}}) \;=\; \omega^2\mathbf{\Gamma}(\mathbf{s})\,. \tag{A.4}$$

The second equation is obtained by dividing both sides of the first equation by k^2 and using the fact that $\frac{\rho\omega^2}{k^2} = \rho v$. The third equation is obtained by dividing both sides (of the first equation) by ω^2 and the fact that $\mathbf{s} = \mathbf{k}/\omega$.

SH-planewave The dispersion relation (A.12) defines SH-wave speed and corresponding polarization (or eigenfunctions):

$$v_{\mathrm{SH}}^2(\hat{k}_x,0,\hat{k}_z)=\frac{c_{66}\hat{k}_x^2+c_{55}\hat{k}_z^2}{\rho}\,,\qquad \mathbf{p}_{\mathrm{SH}}(\hat{k}_x,0,\hat{k}_z)=\begin{pmatrix}0\\1\\0\end{pmatrix}\,, \tag{A.14}$$

Since the above polarization is perpendicular to the propagation direction, this defines a family of pure SH-waves,

$$\begin{pmatrix}0\\1\\0\end{pmatrix} e^{\mathrm{i}\omega\left(t\,-\,\mathrm{s}_{\mathrm{SH}}\,(\hat{k}_x x+\hat{k}_z z)\right)} \tag{A.15}$$

Note that the slowness surface associated with SH-waves is an ellipse, cf. [11, Figure 1.1].

Inplane planewaves The qSV- and qP-wave speeds are roots of dispersion relation (A.13), cf. also [11, Equation (1.79)],

$$\begin{aligned} v_{qSV}^2(\hat{k}_x,0,\hat{k}_z)&=\frac{1}{2\rho}\left(C_{11}\hat{k}_x^2+C_{33}\hat{k}_z^2+C_{55}-\mathcal{C}\right)\,,\\ v_{qP}^2(\hat{k}_x,0,\hat{k}_z)&=\frac{1}{2\rho}\left(C_{11}\hat{k}_x^2+C_{33}\hat{k}_z^2+C_{55}+\mathcal{C}\right)\,,\\ &\text{with}\quad \mathcal{C}^2=\Big((C_{11}-C_{55})\hat{k}_x^2+(C_{55}-C_{33})\hat{k}_z^2\Big)^2+4(C_{13}+C_{55})^2\hat{k}_x^2\,\hat{k}_z^2\,. \end{aligned} \tag{A.16}$$

The corresponding polarizations (eigenfunctions) are, for $\alpha=\mathrm{qP},\mathrm{qSV}$,

$$\mathbf{p}_\alpha(\hat{k}_x,0,\hat{k}_z)=\frac{1}{\sqrt{(c_{11}+c_{55})\hat{k}_x^2+(c_{55}+c_{33})k_z^2-2\rho\,v_\alpha}}\begin{pmatrix}\sqrt{c_{55}\hat{k}_x^2+c_{33}k_z^2-\rho v_\alpha^2}\\0\\\sqrt{c_{11}\hat{k}_x^2+c_{55}k_z^2-\rho\,v_\alpha^2}\end{pmatrix}\,. \tag{A.17}$$

Thus we obtain the family of inplane planewaves:

$$\mathbf{p}_\alpha\, e^{\mathrm{i}\omega\left(t\,-\,\mathrm{s}_\alpha\,(\hat{k}_x x+\hat{k}_z z)\right)}\,,\quad \text{for } \alpha=\mathrm{qP},\mathrm{qSV}\,. \tag{A.18}$$

Propagation along inplane axis We consider the following specific directions along x and z axis.

– Propagation along z-axis: substitute $\hat{k}_x=0$ in the expression of inplane polarization (A.17) and speeds (A.16), we obtain

$$\begin{aligned} &\mathbf{p}_\alpha(0,0,1)=\frac{1}{\sqrt{C_{55}+C_{33}}}\begin{pmatrix}\sqrt{C_{33}-\rho v_\alpha^2}\\0\\\sqrt{C_{55}-\rho v_\alpha^2}\end{pmatrix}\,,\\ &\text{and}\quad v_{qP}^2(0,0,1)=\frac{C_{33}}{\rho}\,,\quad v_{qSV}^2(0,0,1)=\frac{C_{55}}{\rho}\,. \end{aligned} \tag{A.19}$$

The polarization can be written more explicitly as

$$\begin{aligned} \mathbf{p}_{qP}(0,0,1)&=\frac{1}{\sqrt{C_{55}+C_{33}}}\begin{pmatrix}\sqrt{C_{33}-\rho v_{pP}^2}\\0\\0\end{pmatrix}\,,\\ \mathbf{p}_{qSV}(0,0,1)&=\frac{1}{\sqrt{C_{55}+C_{33}}}\begin{pmatrix}0\\0\\\sqrt{C_{55}-\rho v_{qSV}^2}\end{pmatrix}\,. \end{aligned} \tag{A.20}$$

We thus observe that, with $\mathbf{k} = (0,0,1)^t$, the above polarizations satisfy,

$$\mathbf{p}_{qP}(0,0,1) \parallel \hat{\mathbf{k}} = (0,0,1)^t\,, \qquad \mathbf{p}_{qSV}(0,0,1) \perp \hat{\mathbf{k}} = (0,0,1)^t \tag{A.21}$$

The two inplane planewaves propagating along z-axis are true P and S waves. In another word,

$$\begin{aligned} &\frac{C_{33}}{\rho}\left(= v_{qP}^2(0,0,1)\right) \text{ denotes the square speed of a pure P wave}\,,\\ &\frac{C_{55}}{\rho}\left(= v_{qSV}^2(0,0,1)\right) \text{ denotes the square speed of a pure S wave speod} \end{aligned} \tag{A.22}$$

– Propagation along x-axis: Substitute $\hat{k}_z = 0$ in the expression of inplane speeds (A.16) and polarization (A.17), we obtain

$$\begin{aligned} \mathbf{p}_\alpha(1,0,0) &= \frac{1}{\sqrt{C_{11}+C_{55}}}\begin{pmatrix}\sqrt{C_{55}-\rho v_\alpha^2}\\ 0\\ \sqrt{C_{11}-\rho v_\alpha^2}\end{pmatrix}\,, \quad \text{for } \alpha = \text{qP, qSV}\,,\\ v_{qP}^2(1,0,0) &= \frac{C_{11}}{\rho}\,, \qquad v_{qSV}^2(1,0,0) = \frac{C_{55}}{\rho} \end{aligned} \tag{A.23}$$

The polarization can be written more explicitly as

$$\begin{aligned} \mathbf{p}_{qP}(1,0,0) &= \frac{1}{\sqrt{C_{11}+C_{55}}}\begin{pmatrix}\sqrt{C_{55}-\rho v_\alpha^2}\\ 0\\ 0\end{pmatrix} \quad \Rightarrow \quad \begin{array}{c}\text{represents a pure P wave}\\ \text{with square speed } \frac{C_{11}}{\rho}\end{array}\,,\\ \mathbf{p}_{qSV}(1,0,0) &= \frac{1}{\sqrt{C_{11}+C_{55}}}\begin{pmatrix}0\\ 0\\ \sqrt{C_{11}-\rho v_\alpha^2}\end{pmatrix} \quad \Rightarrow \quad \begin{array}{c}\text{represents a pure S wave}\\ \text{with square speed } \dfrac{C_{55}}{\rho}\end{array}\,. \end{aligned} \tag{A.24}$$

We list below propagation speed along x and z-axis (i.e., with propagation in the symmetry plane), which defines speed of true P or S waves,

$$\begin{aligned} &\sqrt{\frac{C_{55}}{\rho}} \leftrightarrow \text{pure S-wave speed along } x \text{ or } z \text{ axis in the symmetry plane,}\\ &\sqrt{\frac{C_{11}}{\rho}} \leftrightarrow \begin{array}{c}\text{pure P-wave speed along } x \text{ axis}\\ \text{(also called squared horizontal P-wave speed)'}\end{array}\\ &\sqrt{\frac{C_{33}}{\rho}} \leftrightarrow \begin{array}{c}\text{pure P-wave speed along } z \text{ axis}\\ \text{(also called squared vertical P-wave speed)}\cdot\end{array} \end{aligned}$$

Remark 13 (In relation to Thomsen's parameters)**.** *The above computation explains the origin of wavespeed parameters (parameters α_0, β_0) in Thomsen's set of parameters for VTI, [54]. For wave propagation in (x,z) plane, the direction of propagation $\widehat{\mathbf{k}} = (\widehat{k}_x, 0, \widehat{k}_z)^t$ is now written in terms of the angle beween $\widehat{\mathbf{k}}$ and the symmetry axis $\hat{e}_z$,*

$$\hat{k}_z = \cos\theta, \qquad \hat{k}_x = \sin\theta\,. \tag{A.25}$$

The Thomsen's parameters [54] for VTI are,

$$\alpha_0 = \sqrt{C_{33}/\rho}\,, \quad \textit{vertical P wavespeed} \tag{A.26a}$$
$$\beta_0 = \sqrt{C_{55}/\rho}\,, \quad \textit{vertical (or horizontal) S wavespeed} \tag{A.26b}$$
$$\epsilon = \frac{C_{11}-C_{33}}{2C_{33}}\,, \tag{A.26c}$$
$$\gamma = \frac{C_{66}-C_{44}}{2C_{44}}\,, \tag{A.26d}$$
$$\delta = \frac{(C_{13}+C_{44})^2-(C_{33}-C_{44})^2}{2C_{33}\,(C_{33}-C_{44})}\,, \tag{A.26e}$$

The inplane and SH wave speeds (A.14) and (A.16) can be written in terms of θ as

$$v_{qP}(\theta)^2 = \alpha_0^2\left(1+\varepsilon\,\sin^2\theta+\mathfrak{D}\right)\,, \tag{A.27a}$$
$$v_{qSV}(\theta)^2 = \alpha_0^2\left(1+\frac{\alpha_0^2}{\beta_0^2}\left(\varepsilon\,\sin^2\theta-\mathfrak{D}\right)\right)\,, \tag{A.27b}$$
$$v_{sH}(\theta)^2 = \beta_0^2\left(1+\gamma\,\sin^2\theta\right)\,, \tag{A.27c}$$
$$\tag{A.27d}$$

where

$$\mathfrak{D} = \frac{1}{2}\left(1-\frac{\beta_0^2}{\alpha_0^2}\right)\left[\left(1+\frac{4(\varepsilon-2\delta)}{(1-\frac{\beta_0^2}{\alpha_0^2})}\sin^2\theta\cos^2\theta+4\varepsilon\frac{1-\frac{\beta_0^2}{\alpha_0^2}+\varepsilon}{(1-\frac{\beta_0^2}{\alpha_0^2})^2}\sin^4\theta\right)^{1/2}-1\right]\,. \tag{A.28}$$

B Formal derivation of Kelvin–Christoffel flux

Numerical trace of gradient of a scalar quantity We review the definitions of numerical trace of the gradient found in existing works on HDG method for second-order scalar equations, in particular for the Poisson equation (static regime) and Helmholtz equation (dynamic regime). These will be isotropic stabilization i.e. scalar scaling factor multiple of identity.

– Helmholtz equation : Consider Helmholtz equation, $-\Delta \mathsf{w}-\omega^2\mathsf{w}=\mathsf{f}$, written in first-order formulation (with respect to spatial derivatives) but second-order in frequency, cf. [25],

$$\mathbf{q} = -\nabla \mathsf{w}\,, \qquad -\omega^2\,\mathsf{w}+\nabla\cdot\mathbf{q}=\mathsf{f}\,. \tag{B.1}$$

In the HDG method applied to the above system, working with isotropic stabilization, the numerical trace for the first-order unknown $\mathbf{q}$ is given as, cf. [25, Equation (2.3)]

$$\widehat{\mathbf{q}} = \mathbf{q}_h \;+\; \mathrm{i}\,\omega\,\tau_{\text{dyn-scalar}}\,(\mathsf{w}_h-\widehat{\mathsf{w}})\,\boldsymbol{\nu}\,, \qquad \text{with positive}\;\; \tau_{\text{dyn-scalar}}=\mathsf{O}(1)\,. \tag{B.2}$$

Here $\boldsymbol{\nu}$ is the outward-pointing normal vector along ∂K.

Another equivalent approach is given by working with pure first order formulation (i.e. both in spatial derivatives and ω) unknown ($\tilde{\mathbf{q}}=-\frac{1}{\mathrm{i}\omega}\nabla\mathsf{w},\mathsf{w}$), with $\tilde{f}=\frac{1}{\mathrm{i}\omega}\mathsf{f}$, cf. [39, Equation (2)],

$$\mathrm{i}\omega\,\tilde{\mathbf{q}} \;+\; \nabla\mathsf{w}=0\,, \qquad \mathrm{i}\omega\,\mathsf{w} \;+\; \nabla\cdot\tilde{\mathbf{q}}=\tilde{f}\,, \tag{B.3}$$

with numerical trace, cf. [39, Equation (4e)],

$$\widehat{\tilde{\mathbf{q}}} = \tilde{\mathbf{q}}_h \;+\; \tau_{\text{dyn-scalar}}(\mathsf{w}_h-\widehat{\mathsf{w}})\,\boldsymbol{\nu}\,, \qquad \text{with}\;\; \tau_{\text{dyn-scalar}}>0\,. \tag{B.4}$$

In [39], numerical investigation is also carried out to compare different value for $\tau_{\text{Helmholtz}}=1,\frac{1}{h},h$ with optimal convergence for $\tau_{\text{Helmholtz}}=1$, additionally, second option slows down the convergence for w, and third one for ∇w, cf. discussion in [39, Figures 2 and 4].

The numerical traces in (B.2) and (B.4) are equivalent to,

$$\widehat{\nabla \mathsf{w}} = \nabla \mathsf{w} - \mathrm{i}\,\omega\,\tau_{\text{dyn-scalar}}(\mathsf{w}_h - \widehat{\mathsf{w}})\boldsymbol{\nu}\,, \qquad \text{with positive } \tau_{\text{dyn-scalar}} = \mathsf{O}(1)\,. \tag{B.5}$$

This is also found in [38, Table 1]. In [38], investigation on the effect of τ is extended to complex ones both for frequencies and scaling factor. Investigations therein are carried out to compare $\tau \in \mathbb{C}$, thus not just nonzero real. The conclusions of [38] is that for ω real then the HDG method remains uniquely solvable for $\operatorname{Re}\tau \neq 0$. Additionally, the HDG method results in small artificial dissipation which disappears for τ pure imaginary and ωh small enough, cf. [38, Page 21].

– Poisson equation : Another perspective is to work with static elliptic equation, specifically with a solution to the Poisson equation, cf e.g. [22] which considers the mixed boundary problem for the Poisson equation written in first-order formulation

$$\mathbf{q} = -\nabla w, \qquad \nabla \cdot \mathbf{q} = f\,,$$

with numerical trace defined by, cf. [22, Equation (1.3d)]

$$\widehat{\nabla w} = \nabla w_h + \tau_{\text{static-scalar}}\,(w_h - \lambda)\,\boldsymbol{\nu}\,, \qquad \text{with } \tau_{\text{static-scalar}} > 0\,. \tag{B.6}$$

In comparing $\tau_{\text{static-scalar}} = 1, h$ and $\frac{1}{h}$, numerical investigation in [22] observes optimal convergence rate for 1, cf. Table 4.1 therein.

Numerical trace of gradient of displacement vector In the HDG method, the displacement vector $\mathbf{u}$ is approximated by

$$\mathbf{u}\big|_{\mathring{K}} \text{ by } \mathbf{u}_h = \begin{pmatrix} u_{hx} & u_{hy} & u_{hz} \end{pmatrix}^t\,, \quad \mathbf{u}|_{\partial K} \text{ by } \boldsymbol{\lambda} = \begin{pmatrix} \lambda_x & \lambda_y & \lambda_z \end{pmatrix}^t\,. \tag{B.7}$$

Associated with $\mathbf{u}_h$, define

$$\boldsymbol{\varepsilon}_h := \frac{1}{2}\left(\nabla \mathbf{u}_h + (\nabla \mathbf{u}_h)^t\right)\,, \qquad \boldsymbol{\sigma}_h := \mathbf{C}\,\boldsymbol{\varepsilon}\,. \tag{B.8}$$

Starting from the definition (B.5) of numerical trace of the gradient of a scalar quantity, we obtain a relation for the numerical trace of a gradient of each Cartesian component of the displacement vector $\mathbf{u}$,

$$\widehat{\nabla u_I} = \nabla u_{hI} - \mathrm{i}\omega\,\tau_I\left(u_I^h - \lambda_I^h\right)\boldsymbol{\nu}\,, \quad \text{along } \partial K\,, \quad I = x, y, z \tag{B.9}$$

We denote by τ_I the HDG stabilization parameter, following (B.5), for direction I. In basis $\{\hat{\mathbf{e}}_x, \hat{\mathbf{e}}_y, \hat{\mathbf{e}}_z\}$, the gradient of $\mathbf{u}$ is the matrix,

$$\nabla \mathbf{u} = \begin{pmatrix} \nabla^t u_x \\ \nabla^t u_y \\ \nabla^t u_z \end{pmatrix},$$

expression (B.9) thus gives the I-row of $\widehat{\nabla \mathbf{u}}^h$ along ∂K,

$$\widehat{\nabla \mathbf{u}} = \nabla \mathbf{u}_h - \mathrm{i}\omega\, S_{\text{diag}}\,(\boldsymbol{u}_h - \boldsymbol{\lambda}) \otimes \boldsymbol{\nu}\,, \qquad \text{with } S_{\text{diag}} = \begin{pmatrix} \tau_x & 0 & 0 \\ 0 & \tau_y & 0 \\ 0 & 0 & \tau_z \end{pmatrix}. \tag{B.10}$$

Recall that $\otimes$ is the tensor product (2.3), with the stabilization matrix S_{diag} is diagonal in Cartesian basis. Note that the right-hand side of (B.10) for $\widehat{\nabla \mathbf{u}}^h$ holds in all coordinate basis.

Numerical trace of stress tensor The numerical trace of the strain and stress tensor $\boldsymbol{\sigma}$ is given by

$$\widehat{\boldsymbol{\varepsilon}} := \frac{\widehat{\nabla \mathbf{u}} + (\widehat{\nabla \mathbf{u}})^t}{2}\,, \qquad \widehat{\boldsymbol{\sigma}} = \mathbf{C}\,\widehat{\boldsymbol{\varepsilon}}\,. \tag{B.11}$$

We next substitute in the expression (B.10) for $\widehat{\nabla \mathbf{u}}$, and of $\boldsymbol{\varepsilon}$ in (B.8), the numerical trace for the stress tensor along ∂K is a symmetric matrix given by,

$$\widehat{\boldsymbol{\varepsilon}} \;=\; \boldsymbol{\varepsilon}_h \;-\; \mathrm{i}\omega\, S_{\mathrm{diag}}\,(\boldsymbol{u}_h - \boldsymbol{\lambda}) \odot \boldsymbol{\nu}\,. \tag{B.12}$$

Recall the symmetric tensor product $\odot$ is defined in (3.15) Applying the stiffness tensor $\mathbf{C}$ (which is defined on $\overline{\partial K}$), to both sides, we obtain an expression for numerical trace of $\boldsymbol{\sigma}$,

$$\widehat{\boldsymbol{\sigma}} \;=\; \boldsymbol{\sigma}_h - \mathrm{i}\omega\,\mathbf{C}\,(S_{\mathrm{diag}}\,(\boldsymbol{u}_h \;-\; \boldsymbol{\lambda}) \odot \boldsymbol{\nu}) = \boldsymbol{\sigma}_h - \mathrm{i}\omega\,\mathbf{C}\,(\boldsymbol{\nu} \otimes \boldsymbol{\tau}\,(\boldsymbol{u}_h \;-\; \boldsymbol{\lambda}))\;. \tag{B.13}$$

The second identity with $\otimes$ is due to the symmetry of stiffness tensor $\mathbf{C}$, $c_{ijkl} = c_{jikl} = c_{ijlk} = c_{klij}$. From this we obtain,

$$\widehat{\boldsymbol{\sigma}}\,\boldsymbol{\nu} \;=\; \boldsymbol{\sigma}_h\,\boldsymbol{\nu} \;-\; \mathrm{i}\omega\;\mathrm{M}^{\mathrm{stab}}\,(\mathbf{u}_h - \boldsymbol{\lambda})\;, \tag{B.14}$$

where $\mathrm{M}^{\mathrm{stab}} = [\boldsymbol{\nu}\cdot\mathbf{C}\cdot\boldsymbol{\nu}]\cdot S_{\mathrm{diag}} = \boldsymbol{\Gamma}(\boldsymbol{\nu})\cdot S_{\mathrm{diag}}$.

C Discussion of literature regarding stabilization employed in HDG method for elasticity

In this appendix we review HDG stabilizations that can be found in the literature which are concerned with time- and frequency-domain elastodynamics and elastostatics. The different stabilization are then equivalently written in our notation, for formulations $(\mathbf{u},\boldsymbol{\sigma})_{\boldsymbol{S}}$ and $(\mathbf{v},\boldsymbol{\sigma})_{\boldsymbol{S}}$. Note that most of the stabilization in the literature are identity-based.

C.1 Stabilizations for frequency-domain elastodynamics

C.1.1 Discussion in [42]

Our reference is the discussion given in [42] for identity-based stabilization (i.e., using a scalar multiple of the identity) for isotropic elasticity. Both formulations with first- and second-order in frequency are considered in [42], with unknowns $(\mathbf{u}, \frac{\mathrm{i}}{\omega}\boldsymbol{\sigma}, \widehat{\mathbf{u}})$ and $(\mathbf{u},\boldsymbol{\sigma},\widehat{\mathbf{u}})$, cf. Equations (2.5) and (2.6) therein. Below, by 'equivalent' we mean equivalent in our notation without the projection operator employed in [42], and under convention $\mathbf{v} = -\mathrm{i}\omega\mathbf{u}$. In particular, the numerical investigation in [42] is carried out with unknowns $(\mathbf{u},\boldsymbol{\sigma})$.

1. The first variant works with unknowns

$$\widehat{\frac{\mathrm{i}}{\omega}\boldsymbol{\sigma}_h\boldsymbol{\nu}} := \frac{\mathrm{i}}{\omega}\boldsymbol{\sigma}_h\boldsymbol{\nu} \;-\; \boldsymbol{\tau}_K(\widehat{\mathbf{u}_h} - P\mathbf{u}_h)\,, \tag{C.1}$$

with $\boldsymbol{\tau}_K : \partial K \to \mathbb{R}^{3\times 3}_{\mathrm{sym}}$ satisfying: $\forall \boldsymbol{\xi} \in L^2(\partial K)$ and $\forall K \in \mathcal{T}_h$,

$$\frac{c_1}{h_K}\|\boldsymbol{\xi}\|^2_{\partial K} \;\le\; \langle \boldsymbol{\tau}_K\boldsymbol{\xi}\,,\,\overline{\boldsymbol{\xi}}\rangle_{\partial K} \;\le\; \frac{c_2}{h_K}\|\mathbf{w}\|^2_{\partial K}\,, \tag{C.2}$$

for some constant c_1 and c_2, and h_K size of element K. In our notation, this is 'equivalent' to,

$$\widehat{\boldsymbol{\sigma}_h}\boldsymbol{\nu} = \boldsymbol{\sigma}_h\boldsymbol{\nu} \;+\; \mathrm{i}\omega\boldsymbol{\tau}_K(\widehat{\mathbf{u}_h} - \mathbf{u}_h)\,, \qquad \widehat{\boldsymbol{\sigma}_h}\boldsymbol{\nu} = \boldsymbol{\sigma}_h\boldsymbol{\nu} - \boldsymbol{\tau}_K(\widehat{\mathbf{v}_h} - \mathbf{v}_h)\,. \tag{C.3}$$

2. In [42], it is also indicated that the sign of $\boldsymbol{\tau}_K$ is not relevant, and a variant called 'time-reversal' is proposed therein,

$$\widehat{\frac{\mathrm{i}}{\omega}\boldsymbol{\sigma}_h\boldsymbol{\nu}} \;:=\; \frac{\mathrm{i}}{\omega}\boldsymbol{\sigma}_h\boldsymbol{\nu} + \boldsymbol{\tau}_K(\widehat{\mathbf{u}_h} - \mathbf{u}_h)\,. \tag{C.4}$$

In our notation, this is 'equivalent' to,

$$\widehat{\boldsymbol{\sigma}_h}\boldsymbol{\nu} = \boldsymbol{\sigma}_h\boldsymbol{\nu} \;-\; \mathrm{i}\omega\boldsymbol{\tau}_K(\widehat{\mathbf{u}_h} - \mathbf{u}_h)\,, \qquad \widehat{\boldsymbol{\sigma}_h}\boldsymbol{\nu} = \boldsymbol{\sigma}_h\boldsymbol{\nu} + \boldsymbol{\tau}_K(\widehat{\mathbf{v}_h} - \mathbf{v}_h)\,. \tag{C.5}$$

Note that in Subsection 6.2, we also investigate how the sign of the stabilization affects the accuracy.

3. A ω-scaled stabilization is also considered with,

$$\widehat{\frac{\mathrm{i}}{\omega}\boldsymbol{\sigma}_h\boldsymbol{\nu}} := \frac{\mathrm{i}}{\omega}\boldsymbol{\sigma}_h\boldsymbol{\nu} - \omega\,\boldsymbol{\tau}_K(\widehat{\mathbf{u}_h} - \mathbf{u}_h) \tag{C.6}$$

In our notation, this is 'equivalent' to, with P a projection operator,

$$\widehat{\boldsymbol{\sigma}_h}\boldsymbol{\nu} = \boldsymbol{\sigma}_h\boldsymbol{\nu} \;+\; \mathrm{i}\omega^2\boldsymbol{\tau}_K(\widehat{\mathbf{u}_h} - P\mathbf{u}_h)\,. \tag{C.7}$$

4. A fourth variant is also proposed in [47] for elastostatics. In our notation, this is 'equivalent' to,

$$\widehat{\boldsymbol{\sigma}_h}\boldsymbol{\nu} = \boldsymbol{\sigma}_h\boldsymbol{\nu} + \boldsymbol{\tau}_K(\widehat{\mathbf{u}_h} - P\mathbf{u}_h)\,, \qquad \widehat{\boldsymbol{\sigma}_h}\boldsymbol{\nu} = \boldsymbol{\sigma}_h\boldsymbol{\nu} + \frac{\mathrm{i}}{\omega}\boldsymbol{\tau}_K(\widehat{\mathbf{v}_h} - P\mathbf{v}_h)\,. \tag{C.8}$$

Summary for value of scaling factor discussed in [42] The above variants can be summarized as follows, cf. [42, Equation (6.3)],

$$\widehat{\boldsymbol{\sigma}_h}\boldsymbol{\nu} \;=\; \boldsymbol{\sigma}_h\boldsymbol{\nu} \;+\; \alpha_K\tau_K(\widehat{\mathbf{u}_h} - \mathbf{u}_h)\,, \tag{C.9}$$

with different implication for time-dependent problem, cf. [42, Proposition 6.3],

$$\tau_K = \frac{1}{h_K}\,, \quad \text{and} \quad \alpha_K = \underbrace{\mathrm{i}\omega}_{\text{dissipative}}\,, \quad \underbrace{-\mathrm{i}\omega}_{\substack{\text{energy}\\ \text{accumulating}}}\,, \quad \mathrm{i}\omega^2, \quad \text{or} \quad \underbrace{1}_{\text{conservative}}\,.$$

Here h_K is the characteristic length of the mesh cell K.

C.1.2 Other works on frequency-domain elasticity

In [7, 6], for both isotropy and anisotropy, formulation with first-order in frequency and unknowns $(\boldsymbol{\sigma}, \mathbf{v})$ is employed. The numerical trace is given by, cf. [7, Equation (9)],

$$\hat{\boldsymbol{\sigma}} = \boldsymbol{\sigma}_h - \mathcal{S}(\mathbf{v}_h - \lambda)\otimes\mathbf{n}\,, \qquad \hat{\boldsymbol{\sigma}}\boldsymbol{\nu} = \boldsymbol{\sigma}_h\boldsymbol{\nu} - \mathcal{S}(\mathbf{v}_h - \lambda)\,,$$

with $\mathcal{S}$ a local stabilization matrix. The above form was deduced from the numerical trace proposed in [44], see below discussion. For numerical implementation in [6], $\mathcal{S}$ is in fact taken to be multiple of the identity, for both isotropic and anisotropic elasticity.

C.2 Stabilizations for time-domain isotropic elasticity

• The work [31, Section 4.1] considers the isotropic elastic wave equation in the time domain, with unknowns $(F, \mathbf{v}, \widehat{\mathbf{v}})$ where $\partial_t F = \nabla\mathbf{v}$. The stabilization considered therein is, [31, Equation (35d)],

$$\widehat{\boldsymbol{\sigma}_h(t)}\,\boldsymbol{\nu} \;=\; \boldsymbol{C}F_h(t)\,\boldsymbol{\nu} \;+\; \mathtt{S}\,(\widehat{\mathbf{v}_h(t)} \;-\; \mathbf{v}_h(t))\,. \tag{C.10}$$

The choice for $\mathtt{S}$ is a multiple of the identity, cf. [31, Section 4.1.3], such that

$$\mathtt{S} = \rho\,\mathrm{c_P}\,\mathbb{I}\mathtt{d} \quad \text{or} \quad \rho\,\mathrm{c_S}\,\mathbb{I}\mathtt{d}. \tag{C.11}$$

In our notation, this is 'equivalent' to (with convention $\partial_t \leftrightarrow -\mathrm{i}\omega$, this corresponds to time-harmonic formulation $(\mathbf{v}, \nabla\mathbf{u}, \widehat{\mathbf{v}})$),

$$\widehat{\boldsymbol{\sigma}_h}\,\boldsymbol{\nu} = \boldsymbol{\sigma}_h\,\boldsymbol{\nu} \;+\; \mathtt{S}\,(\widehat{\mathbf{v}_h} \;-\; \mathbf{v}_h)\,, \qquad \widehat{\boldsymbol{\sigma}_h}\,\boldsymbol{\nu} \;=\; \boldsymbol{\sigma}_h\,\boldsymbol{\nu} - \mathrm{i}\,\omega\mathtt{S}\,(\widehat{\mathbf{u}_h} \;-\; \mathbf{u}_h)\,. \tag{C.12}$$

• In [44], the time-domain isotropic elastic equation[23] is considered, cf. their Equation (30) therein,

$$\rho\,\partial_t^2\mathbf{u} - \nabla\cdot(\mu\nabla\mathbf{u} \;+\; (\mu+\lambda)\,\nabla\cdot\mathbf{u}\,\mathbb{I}\mathtt{d}) = \mathbf{f}\,. \tag{C.13}$$

[23] Note that this equation is not exactly in the original elastic equation. It is obtained if we assume μ homogeneous and rewrite $\nabla\cdot\mu\nabla^t\mathbf{u} = \mu\nabla\cdot\nabla^t\mathbf{u} = \mu\nabla\nabla\cdot\mathbf{u} = \nabla\mu\nabla\cdot\mathbf{u}$.

Unknowns are the displacement gradient, the pressure, the velocity, and the trace of the velocity: ($H := \nabla\mathbf{u}, p := (\mu+\lambda)\nabla\cdot\mathbf{u}, \mathbf{v}, \widehat{\mathbf{v}}$). The numerical flux is, cf. [44, Equations (33) and (36)],

$$\begin{aligned}\widehat{\mu\nabla\mathbf{u}(t)+p(t)\,\mathbb{d}} = \mu H_h \,+\, p\,\mathbb{d} \,-\, \mathrm{S}_{[44]}(\mathbf{v}_h-\hat{\mathbf{v}})\otimes\boldsymbol{\nu}\,, \quad \text{with} \quad \mathrm{S}_{[44]} \text{ definite postive,}\\ \Rightarrow \quad \widehat{\boldsymbol{\sigma}(t)}\boldsymbol{\nu} = \boldsymbol{\sigma}_h(t)\boldsymbol{\nu} \,+\, \mathrm{S}_{[44]}(\hat{\mathbf{v}}-\mathbf{v}_h)\,.\end{aligned} \tag{C.14}$$

A common choice for stabilization matrix is, cf. [44, Equations (37)],

$$\mathrm{S}_{[44]} = \rho\,\omega_c\,\mathbb{d}\,, \quad \text{where } \omega_c \text{ is the characteristic frequency}\,. \tag{C.15}$$

In our notation, this is 'equivalent' to

$$\widehat{\boldsymbol{\sigma}}\boldsymbol{\nu} = \boldsymbol{\sigma}_h\boldsymbol{\nu} \,+\, \rho\,\omega_c(\boldsymbol{\lambda}_{\mathbf{v}}-\mathbf{v}_h)\,. \tag{C.16}$$

C.3 Stabilization for elastostatics

• The formulation and stabilization of [44] were also employed for elastostatics in [43, Equation (55e)] and [28, Equation (2.11)], with identity-based stabilization, $\frac{\mu}{h}\mathbb{d}$, with h characteristic length, cf. [43, Equation (5.6)].

• In [49], first-order formulation with unknown ($\mathbf{u}, \mathbf{L} := -\boldsymbol{C}^{1/2}\boldsymbol{\epsilon}$) is employed together with an isotropic stabilization such that, cf. Equation (29) therein,

$$\widehat{\mathbb{A}(\boldsymbol{\nu})\boldsymbol{C}^{1/2}\mathbf{L}} \,=\, \mathbb{A}(\boldsymbol{\nu})\,\mathbf{D}^{1/2}\,\mathbf{L}_h \,-\, \tau\,(\boldsymbol{\lambda}_{\mathbf{u}}-\mathbf{u}_h)\,, \qquad \tau>0\,. \tag{C.17}$$

Here we have identified their notation $\mathbf{D}$ with $\boldsymbol{C}^{1/2}$ and N in [43] can be related to $\mathbb{A}(\boldsymbol{\nu})$. In our notation, this is 'equivalent' to,

$$\widehat{\boldsymbol{\sigma}\boldsymbol{\nu}} \,=\, \boldsymbol{\sigma}_h\boldsymbol{\nu} \,+\, \tau(\boldsymbol{\lambda}_{\mathbf{u}}-\mathbf{u}_h)\,, \quad \tau>0\,. \tag{C.18}$$

Numerical investigations in [49, Section 5.3] use $\tau>0$ varying from 0.1 to 1000. Their conclusion is that the optimal value of the stabilization is not the same depending on if one looks at the accuracy of the primal or mixed unknowns, cf. Figures 13 and 14 (ignoring the effect of post-processing) therein.

• Stabilization containing the symmetric stiffness tensor was introduced in [52, 33], working with unknowns ($\boldsymbol{\sigma}, \mathbf{u}$) and numerical trace, cf. [52, Equation (3f)] and [33, Equation (5f)], and a fourth-order tensor $\mathbf{T} = (\tau_{ijkl})$,

$$\begin{aligned}\widehat{\sigma_{ij}} \,&=\, \sigma_{h,ij} \,+\, \tau_{ijkl}\,(\lambda_k-u_{h,k})\nu_l\,, && \text{for } \boldsymbol{\nu}\cdot\mathbf{T}\cdot\boldsymbol{\nu} \text{ positive definite}\,,\\ \text{or}\quad \widehat{\boldsymbol{\sigma}\boldsymbol{\nu}} \,&=\, \boldsymbol{\sigma}_h\boldsymbol{\nu} \,+\, \boldsymbol{\tau}\,(\boldsymbol{\lambda}_{\mathbf{u}}-\mathbf{u}_h)\,, && \text{for symmetric positive definite } \boldsymbol{\tau}\,.\end{aligned} \tag{C.19}$$

The well-posedness of the HDG formulation was given in [52] under the assumption that $\boldsymbol{\nu}\cdot\mathbf{T}\cdot\boldsymbol{\nu}$ is positive definite. In the second form of numerical trace, $\boldsymbol{\tau} = \alpha\boldsymbol{\Gamma}(\boldsymbol{\nu})$ with α a scaling constant, and the Kelvin–Christoffel matrix $\boldsymbol{\Gamma}$, (4.61). Numerical investigations in [52, Section 5.2] consider $\alpha = \{1, 10^5, h, \frac{1}{h}\}$ with h the characteristic length of the mesh cell. As a follow-up to these results, in [33, Section 5], a comparison between Kelvin-Christoffel stabilization (i.e., using $\alpha=1$) and identity-based stabilization was carried out, with the conclusion that both stabilizations give similar performance.

References

[1] H. Ammari, E. Bretin, J. Garnier, H. Kang, H. Lee, and A. Wahab, *Mathematical methods in elasticity imaging*, in Mathematical Methods in Elasticity Imaging, Princeton University Press, 2015.

[2] D. N. Arnold and F. Brezzi, *Mixed and nonconforming finite element methods: implementation, postprocessing and error estimates*, ESAIM: Mathematical Modelling and Numerical Analysis, 19 (1985), pp. 7–32.

[3] D. N. Arnold, F. Brezzi, B. Cockburn, and L. D. Marini, *Unified analysis of discontinuous Galerkin methods for elliptic problems*, SIAM journal on numerical analysis, 39 (2002), pp. 1749–1779.

[4] H. Barucq, F. Faucher, D. Fournier, L. Gizon, and H. Pham, *Efficient and accurate algorithm for the full modal Green's kernel of the scalar wave equation in helioseismology*, SIAM Journal on Applied Mathematics, 80 (2020), pp. 2657–2683, https://doi.org/10.1137/20M1336709.

[5] H. Barucq, F. Faucher, and H. Pham, *Outgoing solutions and radiation boundary conditions for the ideal atmospheric scalar wave equation in helioseismology*, ESAIM: Mathematical Modelling and Numerical Analysis, 54 (2020), pp. 1111–1138, https://doi.org/10.1051/m2an/2019088.

[6] M. Bonnasse-Gahot, *High order discontinuous Galerkin methods for time-harmonic elastodynamics*, PhD thesis, Université Nice Sophia Antipolis, 2015.

[7] M. Bonnasse-Gahot, H. Calandra, J. Diaz, and S. Lanteri, *Hybridizable discontinuous Galerkin method for the 2-d frequency-domain elastic wave equations*, Geophysical Journal International, 213 (2018), pp. 637–659.

[8] T. Bui-Thanh, *From Godunov to a unified hybridized discontinuous Galerkin framework for partial differential equations*, Journal of Computational Physics, 295 (2015), pp. 114–146.

[9] T. Bui-Thanh, *From Rankine-Hugoniot condition to a constructive derivation of HDG methods*, in Spectral and High Order Methods for Partial Differential Equations ICOSAHOM 2014, Springer, 2015, pp. 483–491.

[10] T. Bui-Thanh, *Construction and analysis of HDG methods for linearized shallow water equations*, SIAM Journal on Scientific Computing, 38 (2016), pp. A3696–A3719.

[11] J. M. Carcione, *Wave fields in real media: Wave propagation in anisotropic, anelastic, porous and electromagnetic media*, Elsevier, 2007.

[12] J. Christensen-Dalsgaard, W. Däppen, S. V. Ajukov, E. R. Anderson, H. M. Antia, S. Basu, V. A. Baturin, G. Berthomieu, B. Chaboyer, S. M. Chitre, A. N. Cox, P. Demarque, J. Donatowicz, W. A. Dziembowski, M. Gabriel, D. O. Gough, D. B. Guenther, J. A. Guzik, J. W. Harvey, F. Hill, G. Houdek, C. A. Iglesias, A. G. Kosovichev, J. W. Leibacher, P. Morel, C. R. Proffitt, J. Provost, J. Reiter, E. J. Rhodes, F. J. Rogers, I. W. Roxburgh, M. J. Thompson, and R. K. Ulrich, *The current state of solar modeling*, Science, 272 (1996), pp. 1286–1292, https://doi.org/10.1126/science.272.5266.1286.

[13] G. Ciarlet Philippe, *The finite element method for elliptic problems*, Studies in Mathematics and its Aplications. North-Holland Publishing Company Amsterdam. New York-Oxford, (1978), https://doi.org/10.1137/1.9780898719208.

[14] B. Cockburn, *The hybridizable discontinuous Galerkin methods*, in Proceedings of the International Congress of Mathematicians 2010 (ICM 2010) (In 4 Volumes) Vol. I: Plenary Lectures and Ceremonies Vols. II–IV: Invited Lectures, World Scientific, 2010, pp. 2749–2775.

[15] B. Cockburn, *Static condensation, hybridization, and the devising of the HDG methods*, Building bridges: connections and challenges in modern approaches to numerical partial differential equations, (2016), pp. 129–177.

[16] B. Cockburn, *The pursuit of a dream, Francisco Javier Sayas and the HDG methods*, SeMA Journal, 79 (2022), pp. 37–56.

[17] B. Cockburn, *Hybridizable discontinuous Galerkin methods for second-order elliptic problems: overview, a new result and open problems*, Japan Journal of Industrial and Applied Mathematics, (2023), pp. 1–40.

[18] B. Cockburn, D. A. Di Pietro, and A. Ern, *Bridging the hybrid high-order and hybridizable discontinuous Galerkin methods*, ESAIM: Mathematical Modelling and Numerical Analysis, 50 (2016), pp. 635–650.

[19] B. Cockburn, B. Dong, and J. Guzmán, *A superconvergent ldg-hybridizable Galerkin method for second-order elliptic problems*, Mathematics of Computation, 77 (2008), pp. 1887–1916.

[20] B. Cockburn and J. Gopalakrishnan, *A characterization of hybridized mixed methods for second order elliptic problems*, SIAM Journal on Numerical Analysis, 42 (2004), pp. 283–301.

[21] B. Cockburn, J. Gopalakrishnan, and R. Lazarov, *Unified hybridization of discontinuous Galerkin, mixed, and continuous Galerkin methods for second order elliptic problems*, SIAM Journal on Numerical Analysis, 47 (2009), pp. 1319–1365.

[22] B. Cockburn, J. Guzmán, S.-C. Soon, and H. K. Stolarski, *An analysis of the embedded discontinuous Galerkin method for second-order elliptic problems*, SIAM journal on numerical analysis, 47 (2009), pp. 2686–2707.

[23] B. Cockburn, G. E. Karniadakis, and C.-W. Shu, *The development of discontinuous Galerkin methods*, in Discontinuous Galerkin methods: theory, computation and applications, Springer, 2000, pp. 3–50.

[24] B. Cockburn and K. Shi, *Superconvergent HDG methods for linear elasticity with weakly symmetric stresses*, IMA Journal of Numerical Analysis, 33 (2013), pp. 747–770.

[25] J. Cui and W. Zhang, *An analysis of HDG methods for the helmholtz equation*, IMA Journal of Numerical Analysis, 34 (2014), pp. 279–295.

[26] D. A. Di Pietro and A. Ern, *A hybrid high-order locking-free method for linear elasticity on general meshes*, Computer Methods in Applied Mechanics and Engineering, 283 (2015), pp. 1–21.

[27] S. Du and F.-J. Sayas, *New analytical tools for HDG in elasticity, with applications to elastodynamics*, Mathematics of Computation, 89 (2020), pp. 1745–1782.

[28] M. S. Fabien, *A GPU-accelerated hybridizable discontinuous Galerkin method for linear elasticity*, Commun Comput Phys, 27 (2020), pp. 513–545.

[29] F. Faucher, ***hawen**: time-harmonic wave modeling and inversion using hybridizable discontinuous Galerkin discretization*, Journal of Open Source Software, 6 (2021), https://doi.org/10.21105/joss.02699.

[30] F. Faucher and O. Scherzer, *Adjoint-state method for Hybridizable Discontinuous Galerkin discretization, application to the inverse acoustic wave problem*, Computer Methods in Applied Mechanics and Engineering, 372 (2020), p. 113406, https://doi.org/10.1016/j.cma.2020.113406.

[31] P. Fernandez, A. Christophe, S. Terrana, N. C. Nguyen, and J. Peraire, *Hybridized discontinuous Galerkin methods for wave propagation*, Journal of Scientific Computing, 77 (2018), pp. 1566–1604.

[32] S. Fernández-Méndez, *An introduction to the hybridizable discontinuous Galerkin method*, in Efficient High-Order Discretizations for Computational Fluid Dynamics, Springer, 2021, pp. 261–275.

[33] G. Fu, B. Cockburn, and H. Stolarski, *Analysis of an HDG method for linear elasticity*, International Journal for Numerical Methods in Engineering, 102 (2015), pp. 551–575.

[34] M. Giacomini and R. Sevilla, *Discontinuous Galerkin approximations in computational mechanics: hybridization, exact geometry and degree adaptivity*, SN Applied Sciences, 1 (2019), p. 1047.

[35] M. Giacomini, R. Sevilla, and A. Huerta, *HDGlab: An open-source implementation of the hybridisable discontinuous Galerkin method in matlab*, Archives of Computational Methods in Engineering, 28 (2021), pp. 1941–1986.

[36] G. Giorgiani, D. Modesto, S. Fernández-Méndez, and A. Huerta, *High-order continuous and discontinuous Galerkin methods for wave problems*, International Journal for numerical methods in Fluids, 73 (2013), pp. 883–903.

[37] D. Givoli and J. B. Keller, *Non-reflecting boundary conditions for elastic waves*, Wave motion, 12 (1990), pp. 261–279, https://doi.org/10.1016/0165-2125(90)90043-4.

[38] J. Gopalakrishnan, S. Lanteri, N. Olivares, and R. Perrussel, *Stabilization in relation to wavenumber in HDG methods*, Advanced Modeling and Simulation in Engineering Sciences, 2 (2015), pp. 1–24.

[39] R. Griesmaier and P. Monk, *Error analysis for a hybridizable discontinuous Galerkin method for the helmholtz equation*, Journal of Scientific Computing, 49 (2011), pp. 291–310.

[40] R. L. Higdon, *Absorbing boundary conditions for elastic waves*, Geophysics, 56 (1991), pp. 231–241, https://doi.org/10.1190/1.1443035.

[41] A. Huerta, A. Angeloski, X. Roca, and J. Peraire, *Efficiency of high-order elements for continuous and discontinuous Galerkin methods*, International Journal for numerical methods in Engineering, 96 (2013), pp. 529–560.

[42] A. Hungria, D. Prada, and F.-J. Sayas, *HDG methods for elastodynamics*, Computers & Mathematics with Applications, 74 (2017), pp. 2671–2690.

[43] N. C. Nguyen and J. Peraire, *Hybridizable discontinuous Galerkin methods for partial differential equations in continuum mechanics*, Journal of Computational Physics, 231 (2012), pp. 5955–5988.

[44] N. C. Nguyen, J. Peraire, and B. Cockburn, *High-order implicit hybridizable discontinuous Galerkin methods for acoustics and elastodynamics*, Journal of Computational Physics, 230 (2011), pp. 3695–3718.

[45] N. C. Nguyen, J. Peraire, and B. Cockburn, *An implicit high-order hybridizable discontinuous Galerkin method for the incompressible navier–stokes equations*, Journal of Computational Physics, 230 (2011), pp. 1147–1170.

[46] M. Paipuri, S. Fernández-Méndez, and C. Tiago, *Comparison of high-order continuous and hybridizable discontinuous Galerkin methods for incompressible fluid flow problems*, Mathematics and computers in simulation, 153 (2018), pp. 35–58.

[47] W. Qiu, J. Shen, and K. Shi, *An HDG method for linear elasticity with strong symmetric stresses*, Mathematics of Computation, 87 (2018), pp. 69–93.

[48] W. H. Reed and T. R. Hill, *Triangular mesh methods for the neutron transport equation*, tech. report, Los Alamos Scientific Lab., N. Mex.(USA), 1973.

[49] R. Sevilla, M. Giacomini, A. Karkoulias, and A. Huerta, *A superconvergent hybridisable discontinuous Galerkin method for linear elasticity*, International Journal for Numerical Methods in Engineering, 116 (2018), pp. 91–116.

[50] N. M. Shapiro, M. Campillo, L. Margerin, S. K. Singh, V. Kostoglodov, and J. Pacheco, *The Energy Partitioning and the Diffusive Character of the Seismic Coda*, Bulletin of the Seismological Society of America, 90 (2000), pp. 655–665, https://doi.org/10.1785/0119990021.

[51] R. Snieder, *Coda wave interferometry and the equilibration of energy in elastic media*, Phys. Rev. E, 66 (2002), p. 046615, https://doi.org/10.1103/PhysRevE.66.046615, https://link.aps.org/doi/10.1103/PhysRevE.66.046615.

[52] S.-C. Soon, B. Cockburn, and H. K. Stolarski, *A hybridizable discontinuous Galerkin method for linear elasticity*, International journal for numerical methods in engineering, 80 (2009), pp. 1058–1092.

[53] S. Terrana, J.-P. Vilotte, and L. Guillot, *A spectral hybridizable discontinuous Galerkin method for elastic–acoustic wave propagation*, Geophysical Journal International, 213 (2018), pp. 574–602.

[54] L. Thomsen, *Weak elastic anisotropy*, Geophysics, 51 (1986), pp. 1954–1966.

[55] B. Tie and A.-S. Mouronval, *Systematic development of upwind numerical fluxes for the space discontinuous Galerkin method applied to elastic wave propagation in anisotropic and heterogeneous media with physical interfaces*, Computer Methods in Applied Mechanics and Engineering, 372 (2020), p. 113352.

[56] B. Tie, A.-S. Mouronval, V.-D. Nguyen, L. Series, and D. Aubry, *A unified variational framework for the space discontinuous Galerkin method for elastic wave propagation in anisotropic and piecewise homogeneous media*, Computer Methods in Applied Mechanics and Engineering, 338 (2018), pp. 299–332.

[57] E. F. Toro, *Riemann solvers and numerical methods for fluid dynamics: a practical introduction*, Springer Science & Business Media, 2013.

[58] P.-H. Tournier, P. Jolivet, V. Dolean, H. S. Aghamiry, S. Operto, and S. Riffo, *3d finite-difference and finite-element frequency-domain wave simulation with multilevel optimized additive schwarz domain-decomposition preconditioner: A tool for full-waveform inversion of sparse node data sets*, Geophysics, 87 (2022), pp. T381–T402.

[59] J. Vila-Pérez, M. Giacomini, R. Sevilla, and A. Huerta, *Hybridisable discontinuous Galerkin formulation of compressible flows*, Archives of Computational Methods in Engineering, 28 (2021), pp. 753–784.

[60] R. Wang and R. Zhang, *A weak Galerkin finite element method for the linear elasticity problem in mixed form*, Journal of Computational Mathematics, 36 (2018), p. 469.

[61] L. C. Wilcox, G. Stadler, C. Burstedde, and O. Ghattas, *A high-order discontinuous Galerkin method for wave propagation through coupled elastic–acoustic media*, Journal of Computational Physics, 229 (2010), pp. 9373–9396.

[62] S. Yakovlev, D. Moxey, R. M. Kirby, and S. J. Sherwin, *To CG or to HDG: a comparative study in 3D*, Journal of Scientific Computing, 67 (2016), pp. 192–220.

[63] Q. Zhan, Q. Ren, M. Zhuang, Q. Sun, and Q. H. Liu, *An exact Riemann solver for wave propagation in arbitrary anisotropic elastic media with fluid coupling*, Computer Methods in Applied Mechanics and Engineering, 329 (2018), pp. 24–39.

RESEARCH CENTRE
BORDEAUX – SUD-OUEST

200, avenue de la Vieille Tour
33405 Talence Cedex

Publisher
Inria
Domaine de Voluceau - Rocquencourt
BP 105 - 78153 Le Chesnay Cedex
inria.fr

ISSN 0249-6399